NUREG/CR-6008
ORNL/TM-12131

Constraint Effects on Fracture Toughness for Circumferentially Oriented Cracks in Reactor Pressure Vessels

Prepared by
B. R. Bass, D. K. Shum, J. Keeney-Walker

Oak Ridge National Laboratory

Prepared for
U.S. Nuclear Regulatory Commission

NUREG/CR-6008
ORNL/TM-12131
RF

Constraint Effects on Fracture Toughness for Circumferentially Oriented Cracks in Reactor Pressure Vessels

Manuscript Completed: June 1992
Date Published: August 1992

Prepared by
B. R. Bass, D. K. Shum, J. Keeney-Walker

Oak Ridge National Laboratory
Operated by Martin Marietta Energy Systems, Inc.

Oak Ridge National Laboratory
Oak Ridge, TN 37831-6285

Prepared for
Division of Engineering
Office of Nuclear Regulatory Research
U.S. Nuclear Regulatory Commission
Washington, DC 20555
NRC FIN B0119
Under Contract No. DE-AC05-84OR21400

Abstract

Pressurized-thermal-shock (PTS) loading produces biaxial stress fields in a reactor pressure vessel (RPV) wall with one of the principal stresses aligned parallel to postulated surface cracks in either longitudinal or circumferential welds. The limited quantity of existing biaxial test data suggests a significant decrease of fracture toughness under out-of-plane (i.e., parallel to the crack front) biaxial loading conditions when compared with toughness values obtained under uniaxial conditions. Any increase in crack-tip constraint resulting from these out-of-plane biaxial stresses would act in opposition to the in-plane constraint relaxation that has been previously demonstrated for shallow cracks. Consequently, understanding of both in-plane and out-of-plane crack-tip constraint effects is necessary to a refined analysis of fracture initiation from shallow cracks under PTS transient loading. This report is the second in a series investigating the potential impact of far-field out-of-plane stresses and strains on fracture initiation toughness. Selected fracture prediction models, previously validated for small-scale fracture specimens under nearly plane strain conditions, were applied to additional large-scale data with the objective of validating models in the plane stress-to-plane strain domain before applying them to positive out-of-plane strain conditions. The general finding was that applications of the models resulted in predictions of fracture behavior that conflicted with existing experimental data considered relevant to the problem. Because of the conflicting results, it is apparent that testing of RPV steels is required (1) to determine the magnitude of out-of-plane biaxial loading effects on fracture toughness and (2) to provide a basis for development of predictive models. This course of action is necessary to support a refined treatment of in-plane and out-of-plane constraint effects in PTS analysis. Proposed in this report are criteria for a biaxial specimen that would form the basis of a testing program designed to provide data to explain differences between theoretical predictions and measured material behavior. Results of design studies on the biaxial specimen will be presented in a future report from the Heavy-Section Steel Technology Program.

Contents

List of Figures

List of Tables

Executive Summary

Pressurized-thermal-shock (PTS) loading produces biaxial stress fields in a reactor pressure vessel (RPV) wall with one of the principal stresses aligned parallel to postulated surface cracks in either longitudinal or circumferential welds. The limited quantity of existing biaxial test data suggest a significant decrease in crack-initiation toughness under out-of-plane biaxial loading conditions when compared with toughness values obtained under uniaxial conditions. Any increase in crack-tip constraint resulting from these out-of-plane biaxial stresses would act in opposition to the in-plane constraint relaxation that has been previously demonstrated for shallow cracks. Consequently, understanding of both in-plane and out-of-plane crack-tip constraint effects is necessary to a refined analysis of fracture initiation from shallow cracks under PTS transient loading. This report is the second in a series investigating the potential impact of far-field out-of-plane stresses and strains on fracture initiation toughness.

A summary of existing biaxial test data indicating a significant decrease in fracture toughness under out-of-plane biaxial loading conditions is given in Table ES.1.

Table ES.1 Summary of experimental data exhibiting a decrease in toughness for out-of-plane biaxial stresses

Experiment(s)	Crack geometry	Biaxiality ratio	Reduction in K_c (%)
Shallow-crack and thermal-shock data (HSST/ORNL)	Through-crack	1:1 (equibiaxial)	~40
Biaxial/tensile specimen data (BAM, Germany)	Through-crack	1:0.3	25
Spinning-disk data (CNITMASH, Russia)	Finite-length surface crack	1:1 (equibiaxial)	37

Comparisons of measured data from thermal-shock experiments and shallow-crack beam tests conducted in the Heavy-Section Steel Technology (HSST) Program at Oak Ridge National Laboratory (ORNL) provide insight into the impact of biaxial far-field stress distributions on fracture toughness. The thermal-shock experiments employed shallow cracks having initial depths comparable to those in the shallow-crack beam tests, but with a very long crack front. Results from these thermal-shock tests show an increase in toughness relative to the American Society of Mechanical Engineers lower bound curve, but not of a magnitude that would have been inferred from the shallow-crack data. It has been suggested that the biaxial stress field produced by the thermal-shock loading had the effect of reducing fracture toughness well below (~40%) those values associated with uniaxial loading of the shallow-crack beams.

Experimental and analytical studies at Bundesanstalt für Materialprüfung (BAM), Germany, examined the influence of biaxial stress states on fracture toughness of pressure vessel steels. A nominal biaxial stress state was generated in small tensile specimens via a transverse bending stress that develops in conjunction with tensile loading. The ratio of tensile to transverse components of stress had maximum and mean values of 1:0.3 and 1:0.15, respectively. BAM reported that fracture toughness (K) values of the biaxially loaded specimens were ~25% lower than those of single-edge notched specimens.

Unpublished data were reported from CNITMASH, Russia, concerning fracture toughness measurements under biaxial loading conditions produced in a spinning-disk facility. These tests utilized circular disks having a diameter 450 to 600 mm, thickness 150 mm, and surface cracks of maximum depth 40 mm and length 200 mm. In these experiments, an estimated 37% reduction in toughness (K_c) was reported for the biaxially loaded spinning disks, as compared with data from uniaxially loaded specimens.

The scarcity of experimental data addressing the effects of biaxial far-field stress distribution on fracture toughness provides part of the motivation for studying the issue from an analytical perspective. Two different analytical approaches to the problem are presented in this report. The first approach addresses crack initiation by focusing on the near-crack-tip fields within a region extending a few crack-tip-opening displacements directly ahead of the crack tip. Two-parameter fracture characterization methods, which incorporate the higher-order T-stress and Q-stress terms, are used to provide the technical basis for addressing the shortcomings of conventional one-parameter methods based on the K and J parameters. The near-crack-tip results are then interpreted within the context of a selected number of micromechanical fracture models for the prediction of crack initiation. The Ritchie-Knott-Rice (RKR) model is adopted for the prediction of cleavage fracture, and the McClintock-Hancock-MacKenzie (MHM) model is adopted for the prediction of ductile fracture. These two models are chosen because they have been applied to

A 533 B material, in the lower-transition and upper-shelf regions, respectively, with some success under nonirradiated and irradiated conditions.

The second approach focuses on the development of correlation parameters that relate fracture toughness with a volume of material loaded above nominal stress threshold states. Candidate correlation parameters include, but are not limited to, those based on a critical maximum principal stress contour methodology. This methodology relates cleavage-crack initiation to the attainment of a critical area enclosed within a selected maximum principal stress contour surrounding the crack tip. A correlation between fracture toughness and this numerically determined area parameter is provided through applications to measured data. This approach is applied to the analysis of existing fracture toughness data obtained from compact-tension (CT) specimens having a common planform, but with varying thicknesses.

The fracture prediction models described above were applied to additional measured data with the objective of validating the models in the plane stress-to-plane strain domain before applying them to positive out-of-plane strain conditions. Results from these applications are summarized in Table ES.2. The RKR model was applied to fracture-initiation toughness data generated in the HSST Program from large-scale wide-plate experiments and shallow-crack beam tests. Finite-element analyses of these experiments were performed using loading conditions measured in the test. Full-field finite strain solutions based on the plane strain assumption were generated from models having a highly refined crack-tip region. Correlations of measured and predicted toughness for the WP-1 and -2 series of wide-plate experiments based on the Q-stress parameter indicate that the RKR model predictions fall substantially below the toughness values determined from analysis of the measured data. Fracture toughness predictions from the RKR model for the shallow-crack beam specimens were compared with measured toughness values for four values of critical stress. Again, the RKR model predictions were below measured values, but not to the extent observed in the wide-plate specimens.

Inconsistencies between measured and predicted toughnesses for the wide-plate and shallow-crack beam experiments could result from one or more factors. One possible difficulty may be the presence of three-dimensional (3-D) effects in the wide-plate specimens due to chevroned notches that cannot be represented in the two-dimensional (2-D) plane strain models employed in the present analyses. It is unclear what modifications may be required to the J-Q methodology to represent these 3-D effects should they be present. Also, previous applications of the RKR prediction model to measured data have been confined to small-scale laboratory specimens. There may be difficulties with

Table ES.2 Summary of applications of fracture prediction models to measured data in plane stress-to-plane strain domain

Fracture prediction model	Test specimen configuration	Analysis objective	Analysis assessment
RKR cleavage initiation model	Wide plate	Comparison of model toughness predictions with measured values	No agreement (model substantially underpredicts measured values)
	Shallow-crack beam	Comparison of model toughness predictions with measured values	Marginal agreement (model underpredicts measured values)
	Thermally shocked cylinder	Comparison of model toughness predictions with measured values	(Analyses in progress)
Critical area/maximum principal stress contour model	CT specimens with 4T planform (thicknesses 25.4, 50.8, and 101.6 mm)	Determination of unique critical maximum principal stress at initiation	No calibration of model (no unique critical stress for three specimens)
MHM ductile initiation model	(No applications to existing measured data were performed in this study)		

applications of this model to large-scale structures that have not yet been identified.

Correlations based on the stress contour method indicate that development of the methodology depends on establishing the existence of critical σ_{pj} stress values that correlate fracture toughness behavior over a range of transverse strain values. In analyses designed to validate and calibrate the model in the plane stress-to-plane strain domain, the stress contour method was applied to fracture toughness data for A 533 B steel previously generated by McCabe and Landes for a study of thickness effects in the transition region. Analyses of 3-D finite-element models of compact specimens having a common planform of a 4T specimen and thicknesses ranging from 10.16 to 101.5 mm were performed in an attempt to estimate critical σ_{pj} stress values in the negative transverse strain domain. The results were inconclusive because a critical σ_{pj} value common to three different thicknesses (25.4, 50.8, and 101.6 mm) of the specimens could not be established. However, the data set utilized in these analyses included only one cleavage-initiation toughness value for each specimen thickness. Also, the experimental data were not reported in sufficient detail to permit resolution of substantial differences between measured and computed curves representing load vs load-line displacements for the test specimens. Because of these difficulties with the experimental data, the viability of the stress contour methodology for correlating fracture toughness in the plane stress-to-plane strain domain cannot be judged on the basis of the above application.

The fracture models employed herein must be considered unvalidated for predicting the effects of biaxial out-of-plane stress on cleavage fracture toughness, because applications to small- and large-specimen fracture data did not produce consistent results in predicting fracture behavior. Notwithstanding these general findings, toughness predictions implied by these models for out-of-plane strain effects were provided herein for reference purposes. Within the assumptions of the various models and analyses presented here, tensile transverse strains are predicted to produce a relatively small decrease in effective cleavage fracture toughness when compared to that of identical specimens loaded uniaxially. Applications of the RKR model (described in Appendix C) and the stress contour methodology (described in Appendix D) support a reduction of ~9% to 20% due to positive strains. The MKM model (described in Appendix C) predicted a minimal ductile toughness deviation. However, because the fracture methodologies considered in this study produced results that conflict with existing data considered relevant to this problem, these estimates cannot be applied with confidence in addressing questions that affect licensing and regulatory issues for RPVs.

Studies currently under way in the HSST Program are using methodologies described in this report to better understand the substantial differences in measured fracture toughness from the thermal-shock experiments and the shallow-crack beam tests. It is clear that several different competing mechanisms affecting fracture toughness are present in these experiments. In addition to the biaxial stress field, other factors include shallow-crack effects, methods of structural loading, structural and crack geometries, and material properties. A *definitive* conclusion regarding biaxial effects requires an understanding of the factors affecting toughness that is sufficient to permit an unambiguous separation of the individual contributions.

From these studies, it is apparent that testing of RPV steels is required (1) to determine the magnitude of out-of-plane biaxial loading effects on fracture toughness, and (2) to provide a basis for development of predictive models. The most desirable program would involve suitable test specimens and loading conditions for which the only variables are imposed biaxial loading components. This course of action is necessary to support a refined treatment of in-plane and out-of-plane constraint effects on crack initiation from shallow cracks under PTS loading conditions. As a consequence, criteria for a biaxial specimen proposed in this report would form the basis of a testing program designed to explain differences between theoretical predictions and measured material behavior. Design studies are currently under way in the HSST Program to develop a set of geometric parameters, material and fracture properties, and loading conditions for the specimen satisfying these design criteria. Results of the design studies on the biaxial specimen will be presented in a future report from the HSST Program.

1 Introduction

This report describes work undertaken to develop and validate analytical methods for estimating the potential impact of out-of-plane biaxial far-field stresses on crack initiation toughness of shallow inner surface cracks in nuclear reactor pressure vessels (RPVs). Motivation for this study comes from the observation that, while existing fracture toughness data are largely obtained under nearly plane strain conditions in compact test specimens, far-field stresses that act in a direction parallel to the crack front for both axial and circumferential flaws are present in RPVs. Figure 1 depicts a configuration of particular concern in this study, that is, a shallow circumferential crack in the weld of a ring-forged RPV experiencing positive strain parallel to the crack front due to the hoop component of biaxial loading. The components of a typical far-field stress distribution in a RPV wall during a pressurized-thermal-shock (PTS) transient are shown in Fig. 2 (from Ref. 1). The thermal, pressure, and residual stresses are all biaxial, with both in-plane and out-of-plane components. This biaxial stress distribution occurs both during the normal operation of an RPV and under postulated PTS conditions. In Fig. 3* tensile out-of-plane stresses acting parallel to a shallow longitudinal crack in an RPV are on the order of 350 MPa in a PTS transient. These far-field out-of-plane stresses have no equivalent in compact specimens used in conventional fracture toughness testing. Any increase in crack-tip constraint resulting from these out-of-plane biaxial stresses would act in opposition to the in-plane constraint relaxation that has been previously demonstrated for shallow cracks.[2] Consequently, understanding of both in-plane and out-of-plane crack tip constraint effects is necessary to a refined analysis of fracture initiation from shallow cracks under PTS transient loading.

Pennell* has suggested that results from thermal-shock cylinder experiments[3] and shallow-crack beam tests[2] conducted in the Heavy-Section Steel Technology (HSST) Program at Oak Ridge National Laboratory (ORNL) provide insight into the impact of biaxial far-field stress distributions on fracture toughness. The shallow-crack beam tests[2] were conducted to generate fracture toughness data that characterize the relaxation of crack-tip constraint associated with shallow-crack geometries. Crack depths typical of those associated with postulated distributions in an RPV were utilized in the beam tests. Results from the shallow-crack testing program, shown in Fig. 4, indicate that the lower bound to the uniaxial shallow-crack beam fracture data is ~60% greater than that of the deep-crack data in the lower-transition region. [Analyses[4] of PTS transients have shown that crack initiation is most likely to

*W. E. Pennell, "Aging Impact on the Safety and Operability of Nuclear Reactor Pressure Vessels."

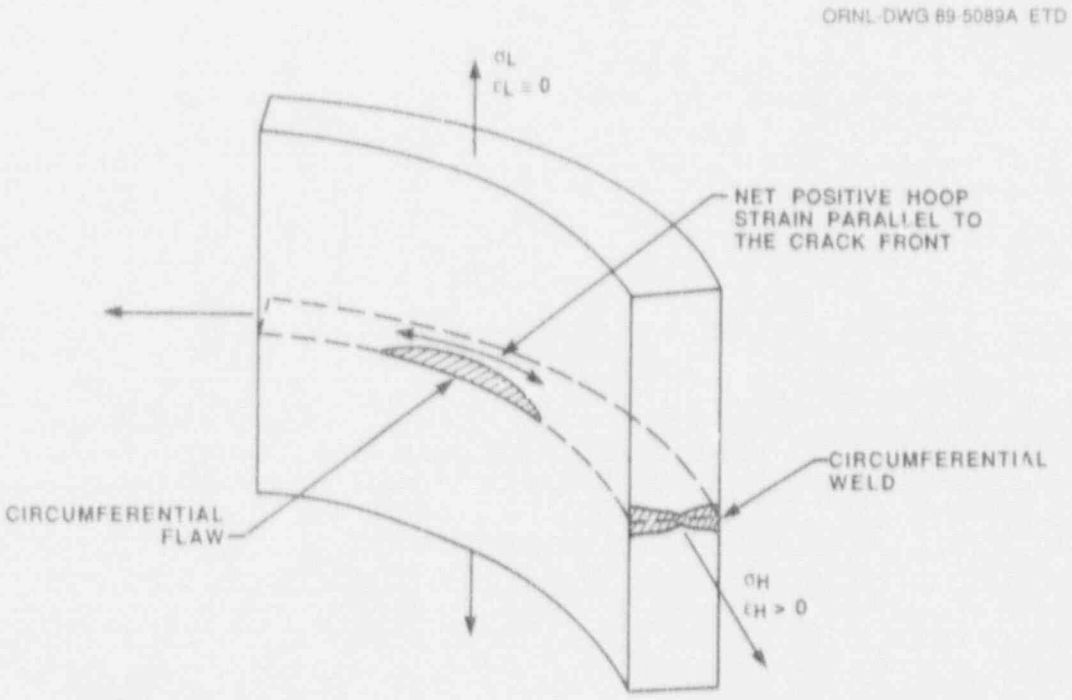

Figure 1 Configuration of circumferential flaw in weld of ring-forged reactor vessel showing positive tensile loop strains parallel to crack front

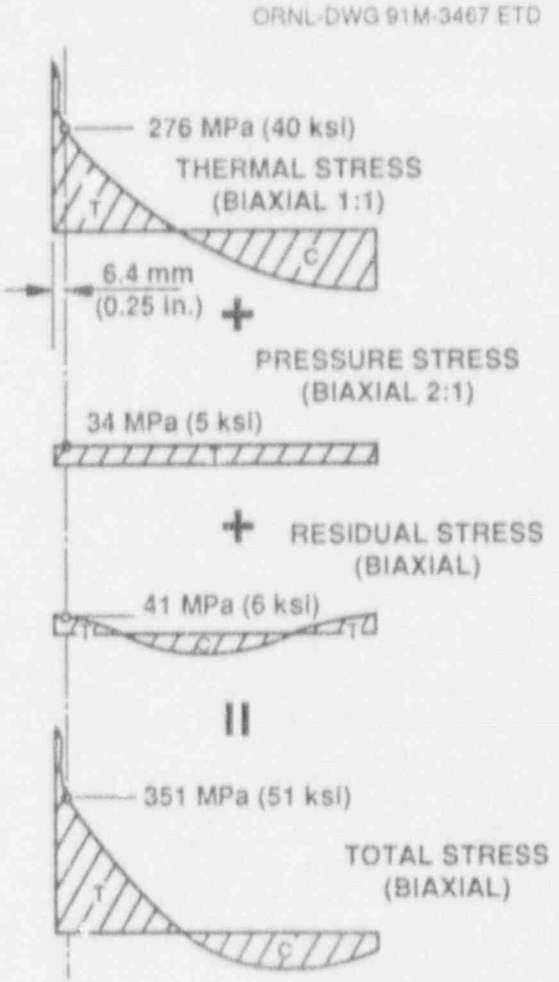

Figure 2 Components of far-field stress distribution existing in reactor vessel wall during PTS transient

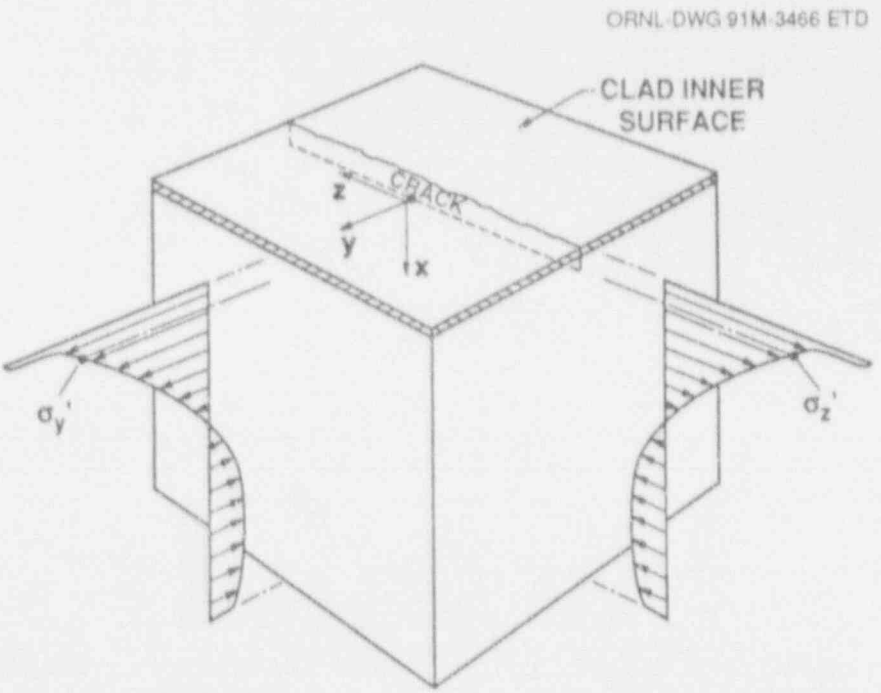

Figure 3 Vessel wall biaxial far-field stresses during PTS transient with one component aligned parallel to front of longitudinal crack

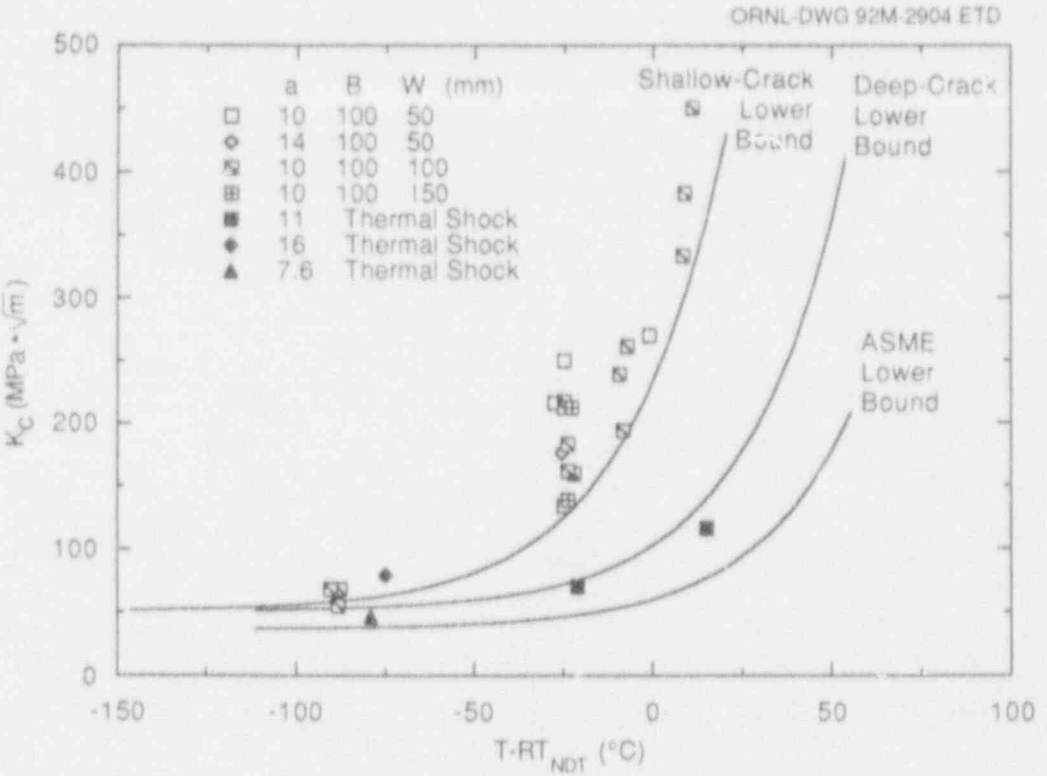

Figure 4 Comparison of cleavage initiation toughness data from shallow-crack beam tests and from thermal-shock experiments

occur at a temperature relative to the reference nil-ductility transition temperature (RT_{NDT}) associated with the lower-transition region of the fracture toughness curve.] The thermal-shock experiments[3] also employed shallow cracks having depths comparable to those in the shallow-crack beam tests, but with a very long crack front. In Fig. 4, results from these tests show crack initiation toughness values from the thermal-shock experiments that are substantially lower in magnitude than toughness values that would have been inferred from the shallow-crack data. It is postulated that the biaxial stress field produced by the thermal-shock loading may have the effect of reducing fracture toughness well below those values associated with uniaxial loading of the shallow-crack beams.*

Experimental and analytical studies[5–10] were performed at Bundesanstalt für Materialprüfung (BAM), Germany, to determine the influence of nominal stress states of higher multiaxiality than plane strain on fracture toughness of engineering structures. The program at BAM utilized several different test specimens, beginning with a double-T shaped geometry loaded in uniaxial tension. A biaxial nominal stress state was attained in the 50- by 80-mm cross section of the specimen via a transverse bending stress that develops in conjunction with the uniaxial tension component. The ratio of the tensile component to the transverse component of stress along the crack front had a maximum value of 1:0.3 and a mean value of 1:0.15. For comparison purposes, single-edge notched (SEN) specimens of the same cross section as the double-T specimens were fabricated from the same material (a 22 NiMoCr37 steel) and tested. Aurich et al.[6] reported that fracture toughness (K) values of the biaxially loaded specimen were ~25% lower than those of the SEN specimen.

A later study reported by Aurich et al.[10] focused on a plate-shaped specimen having dimensions 1000 × 1000 × 140 mm with an approximate semielliptical surface crack of depth a = 83 mm and length 2c = 480 mm. The plates were loaded in eight-point bending to produce a biaxial stress state along portions of the crack front. Also, compact tension (CT) specimens from the same material as the plates were tested over the same temperature range as the plates. Because cleavage toughness values for the biaxially loaded plates were lower than those for CT specimens, Aurich et al.[10] asserted that uniaxially loaded specimens tested under plane strain conditions will not necessarily give a lower bound toughness. However, fracture in these specimens evidently initiated at points on the end radius of the surface crack where the far-field stress components were oblique (or normal), rather than parallel, to the crack front.

Introduction

Unpublished data from CNITMASH, Russia, concerning fracture toughness under biaxial loading conditions were reported by M. Brumovsky.* Biaxial loading was produced in a spinning-disk facility that utilized circular disks with a diameter 450 to 600 mm, a thickness of 150 mm, and surface cracks of 40-mm maximum depth and 200-mm length. In these experiments, an estimated 37% reduction in toughness (K_c) was reported for the biaxially loaded spinning disks, as compared with data from uniaxially loaded specimens.

*M. Brumovsky, Skoda Works, Czechoslovakia, personal communication to W. E. Pennell, Oak Ridge National Laboratory, May 11, 1992.

2 Objectives, Scope, and Structure of the Study

This report represents the second in a series that describes an investigation of the potential impact of far-field out-of-plane stresses and strains on fracture initiation toughness. The specific objectives of the investigation are embodied in the following elements:

1. identification and evaluation of existing biaxial fracture toughness data,
2. selection of fracture parameters suitable for characterizing the fracture process,
3. selection of fracture prediction models potentially capable of incorporating the effects of out-of-plane stresses on fracture initiation,
4. applications of the fracture prediction models to existing measured data in the plane stress-to-plane strain domain and comparisons between the predicted and measured results, and
5. applications of fracture prediction models from element (4) to the prediction of positive out-of-plane stress and strain effects on fracture initiation toughness.

Results from investigations devoted to each of these elements are presented in the subsequent sections of this report.

The scarcity of experimental data (with companion high-quality analytical interpretation) addressing the effects of biaxial far-field stress distribution on fracture toughness provides the motivation for studying these issues from an analytical perspective. Two different analytical approaches to the problem are presented in this report. The first approach addresses crack initiation by focusing on the near-crack-tip fields, along the crack plane, within a region extending a few crack-tip-opening displacements (CTODs) directly ahead of the crack tip. Two-parameter fracture characterization methods, which incorporate the higher-order T-stress and Q-stress terms, are used to provide the technical basis for addressing the shortcomings of conventional one-parameter methods based on the K and J parameters. The near-crack-tip results are then interpreted within the context of selected micromechanical fracture models for the prediction of crack initiation. The Ritchie-Knott-Rice (RKR) model is adopted for the prediction of cleavage fracture, and the McClintock-Hancock-MacKenzie (MHM) model is adopted for the prediction of ductile fracture. These two models are chosen because they have been applied to A 533 grade B class 1 steel, in the lower-transition and upper-shelf regions, respectively, with some success under nonirradiated and irradiated conditions. Detailed results for these near-crack-tip fields are obtained using the boundary-layer method. A boundary-layer method does not involve explicit consideration of loading and geometry. Instead, the method incorporates prescribed in-plane and out-of-plane loading and geometry considerations in a general manner.

The second approach focuses on the development of correlation parameters that relate fracture toughness with a volume of material loaded above threshold values of nominal stress states. Candidate correlation parameters include, but are not limited to, those based on a critical maximum principal stress contour methodology. This methodology relates cleavage crack initiation with the attainment of a critical area enclosed within a selected maximum principal stress contour surrounding the crack tip. A correlation between fracture toughness and this numerically determined area parameter is obtained through applications to measured data. In this study, the approach is applied to analyses of existing fracture toughness data obtained from CT specimens having a common planform, but with varying thickness.

This report is organized to provide the reader with a summary overview of results from each element of the investigation, as well as overall conclusions and recommended plans for further development and validation. More detailed information supporting these results and conclusions is provided in Appendixes A–G of this report.

Beginning in Chap. 3, licensing issues that were previously identified in the first phase of this work are outlined as they pertain to crack initiation toughness predictions for circumferential flaws. A summary of results from the first report[11] in this series is given in Chap. 4. Chapter 5 follows with a brief review of the concept of plane strain fracture toughness and the relationship between generalized plane strain (GPS) and the effects on fracture toughness of positive straining along a crack front. The assumption of GPS conditions is central to the application of the various analytical models presented in this study.

In Chap. 6, candidate fracture prediction models for cleavage and ductile modes of fracture are presented. Results from applications of these models to measured data generated in the plane stress-to-plane strain domain are given in Chap. 7. The potential for correlating fracture toughness with postfracture measurements of thickness reduction (TR) induced by in-plane loading is evaluated.

In Chap. 8, results from this study concerning the effects of applied transverse strains on fracture toughness are summarized. The motivation and scope of a proposed large-

scale biaxial testing program are presented. Finally, conclusions from this study and recommendations for future work are summarized in Chap. 9.

3 Licensing Issues Pertaining to Fracture Toughness

Application of linear-elastic and elastic-plastic fracture mechanics (LEFM, EPFM) theories to the analysis of RPVs, as in the case of the Nuclear Regulatory Commission (NRC) ORNL Integrated Pressurized-Thermal Shock (IPTS) studies,[4] has traditionally assumed plane strain constraint. It is well-known from small-specimen testing that loss of plane strain constraint results in an increase in apparent fracture toughness.[12,13] While a satisfactory explanation of the observed correlation between constraint and toughness is still lacking, evolution of the controlling failure mechanism and near-crack-tip stress and strain states are thought to play important roles in the observed transition as loading progresses from plane strain-to-plane stress conditions.

Furthermore, it is noted that toughness elevation due to loss of plane strain constraint is accompanied by an increase in the magnitude of negative transverse strain induced along the crack front. Because a state of induced negative strain parallel to the crack front is associated with a greater resistance to crack initiation, the question arose as to whether a state of prescribed positive strain parallel to the crack front may be associated with an enhanced tendency toward crack initiation. It is further observed that, while existing fracture toughness data are largely obtained under nearly plane strain conditions, the state of transverse strain along the crack front of a circumferential crack is positive in magnitude (see Fig. 1). This state of positive transverse or out-of-plane straining occurs both during the normal operations of an RPV and under postulated thermal-shock conditions. Issues thus arise relative to the degree of conservatism inherent to the application of shallow-crack plane strain fracture toughness to the evaluation of circumferential shallow cracks, particularly to those in ring-forged vessels that have no longitudinal welds.[14] The need for early resolution of these issues is accentuated by the fact that four out of five reactor vessels that currently do not meet the minimum Charpy upper-shelf requirement, given in Ref. 15, are of ring-forged construction.[16]

The formation of distinct vertical plumes of cooling water beneath the inlet nozzles during a safety-injection transient, sometimes referred to as thermal streaming, provides an additional motivation for reconsidering the methodology used for evaluating circumferentially oriented shallow cracks in a pressure vessel. In the NRC/ORNL IPTS studies,[4] the occurrence of thermal streaming was considered analytically only to the extent of using the centerline temperature of the plume within the height of the core in an axisymmetric calculation of the radial temperature and stress distributions. Consequently, the axial stress component arising from the circumferential variation in vessel temperature was not considered.

The possible necessity for including this axial stress component, which would contribute to a more severe loading situation with respect to a circumferentially oriented shallow crack, was emphasized by recent thermal streaming experiments performed in the HDR reactor vessel for the case of loop-flow stagnation.[17,18] These studies indicate that, for the particular HDR configuration considered, the magnitude of the total axial thermal stress at the center of the plume is higher than the corresponding circumferential thermal stress. Loop-stagnation, thermal-hydraulic analyses performed for U.S. pressurized-water reactor (PWR) vessels suggest that the axial stress caused by thermal streaming would be much lower for U.S. vessels than the axial stress calculated from the HDR studies.[19] While current understanding of the effects of thermal streaming on pressure vessel fracture behavior is far from complete, resolution of this issue will most certainly require a better understanding of the fracture behavior of a pressure vessel with circumferentially oriented shallow cracks.

4 Summary of Previous Results

The first report[11] in this series described the development of analysis methods for estimating the decrease in crack-initiation toughness, from a reference plane strain value, due to positive straining along the crack front for a circumferential shallow crack in an RPV. The analysis methods are based on two different approaches that were developed to analyze and explain the effects of transverse strain and stress states on fracture toughness. The first approach, relating crack initiation with material failure at points within a few CTODs directly ahead of the crack tip, was used to examine ductile crack initiation. This micromechanical approach provides a relation between fracture toughness and effective stress and strain values at failure that can be determined experimentally. The second approach focuses on the correlation parameter defined in terms of a critical area enclosed within a critical maximum principal stress contour and described in Chap. 2.

In the first phase of this investigation, the scope was limited to crack front constraint conditions that can be described in terms of conventional one-parameter (K or J), in-plane, near-tip fields and the transverse strain. Validation checks of the analysis methods under study were made through applications to some large-scale fracture data. For magnitudes of the transverse strain up to a few times the yield strain, preliminary estimates on the change in crack-initiation toughness associated with either negative or positive straining along a crack front were made for conditions of contained crack-tip yielding. Results from the validation checks were judged to be promising but incomplete. The primary problem encountered in the validation checks is the absence of experimental data on the magnitude of the transverse strain attendant with the generation of the small-specimen fracture data. In addition, it is thought that two-parameter in-plane approaches may be needed to characterize crack initiation in some of these tests. For contained crack-tip yielding, the preliminary estimates indicated that the change in crack-initiation toughness from a reference plane strain value due to transverse strain probably does not exceed a few percent in either direction. However, analyses performed subsequent to the evaluation (and described in the following sections) indicate that applications of the fracture models to some large-specimen fracture data generated in the plane stress-to-plane strain domain predicted fracture behavior that conflicts with trends of existing data judged to be relevant to the problem.

In the absence of definitive experimental data in the area of crack-initiation toughness under positive out-of-plane straining conditions, the observations from the analytical study were considered tentative. Recommendations for additional work necessary to provide more precise estimates on the effects of positive out-of-plane straining on the crack-initiation toughness of circumferentially oriented flaws are given as follows:

1. formulation of an experimental program to determine the crack-initiation toughness of pressure vessel materials under directly comparable uniaxial and biaxial loading conditions,
2. generation of experimental material failure stress-strain data that are central to the application of the near-tip toughness prediction model,
3. performance of detailed finite-element analyses that can provide accurate descriptions of the near-tip stress and strain fields associated with the generation of some of the existing fracture data,
4. determination of the applicability of one- and two-parameter fracture analysis approaches for examining existing fracture data,
5. performance of detailed finite-element analyses to compare toughness predictions from both the micromechanical and correlation parameter approaches with existing toughness data for temperatures extending into the transition region, and
6. performance of detailed finite-element analyses for the stress and strain distributions ahead of a circumferential flaw in an RPV under postulated loading conditions including severe accident scenarios involving thermal-streaming considerations.

5 Plane Strain and GPS Concepts

5.1 Plane Strain Fracture Toughness

Current pressure vessel fracture-prevention technology relies on the use of correlation fracture parameters such as the stress intensity factor K[20,21] and the Hutchinson, Rice, and Rosengren (HRR) intensity parameter J[22-24] to characterize both the applied load and the resistance of material to crack initiation. These fracture parameters serve as convenient one-parameter descriptions of the stress and strain distributions within two distinct annular regions surrounding a crack tip.

The strains are entirely elastic within the annular region characterized by K; a combination of elastic and plastic strains exist within the annular region characterized by J. The existence and/or extent of these one-parameter annular regions is dependent on both the loading and geometry of the structure under consideration. The magnitude of the crack-tip stress and strain intensity parameter at the onset of crack initiation is often determined from an experimental load vs crack-mouth opening displacement record of a laboratory-size fracture specimen. Provided that the near-tip stress and strain fields do indeed display an annular region characterizable by K or J and that this annular region is of sufficient size so that a continuum description based on K or J is physically meaningful, the magnitude of this parameter at crack initiation is assumed to be a material property. The constant value of K at crack initiation under mode I conditions is denoted as K_{Ic} and is referred to as the plane strain fracture toughness of a given material.

Within the context of these one-parameter fracture analysis approaches, it is well-known that the magnitude of K and J at crack initiation decreases with increasing specimen thickness when all other test variables are held constant.[12,13] As specimen thicknesses are increased beyond a minimum value, these parameters reach an essentially constant value. Associated with the minimum specimen thickness is a strain parallel to the crack front that is much smaller in magnitude than the yield strain of the test material, except in regions where the crack front meets the specimen sides. This state of crack front constraint is denoted as a state of plane strain in the terminology of fracture mechanics.

Shortcomings of these conventional one-parameter fracture correlations methods, which also include problems associated with transferability of small-specimen toughness data to large-scale structural applications, are being addressed through development of various two-parameter methods. Applications in this report consider two-parameter descriptions (K-T or J-Q) of the near-crack-tip fields that incorporate effects of the higher-order T-stress[25] for LEFM conditions or the Q-stress[26] for more general EPFM conditions. It has been proposed that the conventional concept of fracture toughness in terms of a critical *value* of K or J can be extended, in a two-parameter approach, in the form of a fracture *locus* involving combinations of K or J and T or Q. Details of these two-parameter formulations are given in Appendix A.

Current fracture analysis methods do not provide a straightforward procedure to estimate the effects of positive out-of-plane straining on crack-initiation toughness based on existing plane stress-to-plane strain crack-initiation data. Current capability to estimate crack-initiation toughness under conditions of minor relaxation from plane strain is empirical, and methods such as Irwin's β_{Ic} approach[27,28] are physically plausible only for limited deviations from plane strain toward plane stress conditions. Prediction of crack initiation requires a detailed understanding of how the attainment of a critical value of either K or J corresponds to more basic material properties, an understanding that is currently being sought as part of the objective of this study. Without a better understanding of the correlation between a given value of K or J at crack initiation and the associated through-thickness straining conditions in the vicinity of a crack tip, it is difficult to justify the use of an extrapolation scheme to estimate effects of positive out-of-plane straining on crack initiation. The fundamental uncertainty in any extrapolation scheme thus concerns the basis for choosing the independent extrapolation variable.

5.2 GPS

The GPS concept allows for a unified description of crack front conditions from positive out-of-plane straining toward plane stress in this study. Consider a Cartesian coordinate system located within a three-dimensional (3-D) body where (x_1, x_2) are the "in-plane" coordinates and (x_3) is the "out-of-plane" coordinate. The in-plane displacement components along the x_1 and x_2 directions are denoted as u_1 and u_2, while the out-of-plane displacement component along the x_3 direction is denoted as u_3. A state of plane strain is said to exist when (1) the in-plane displacement components depend only on the in-plane coordinates (x_1, x_2) and are independent of (x_3), and (2) the out-of-plane displacement component $u_3 = 0$.

Plane

For the purpose of this discussion, a state of GPS is said to exist when u_1 and u_2 are again dependent only on (x_1, x_2), while the nonzero out-of-plane displacement component u_3 is defined by the relation

$$u_3 = \varepsilon_3 x_3 \ , \qquad (1)$$

where ε_3 is a scalar such that the out-of-plane strain component is uniform and has a magnitude equal to ε_3.

As indicated earlier, one of the motivations for this study is to explore the unknown effects of positive transverse straining on fracture toughness of a circumferential crack in an RPV. Figure 2 indicates the components of far-field stress distribution present in the vessel wall during a PTS transient, with the thermal stress identified as the primary contributor to out-of-plane effects. The limiting case is that of a fully circumferential crack. Under axisymmetric loading (pressure is always axisymmetric; thermal-shock can be axisymmetric or nonaxisymmetric), the crack-tip fields for the fully circumferential situation represent the "cleanest" and simplest deviation from conventional two-dimensional (2-D) plane strain constraint. While the fully circumferential case may appear "artificial" to some at first glance, it must be noted that the fully circumferential case is in fact the circumferential flaw geometry of interest in current probabilistic fracture assessment of RPVs under PTS conditions.[4] Consequently, the fully circumferential case has immediate application and, fortuitously, is also the simplest to examine from the perspective of departure from plane strain constraint. Note that while the discussion has thus far focused on transverse strain and circumferential flaws, the effects of positive transverse stress in relation to axial flaws can be considered in a similar fashion.

As one attempts more "realism" in modeling the circumferential crack situation, one can contemplate circumferential flaws with large aspect ratios. With reference to Fig. 1, assume that 3-D effects are confined to portions of the crack front that intersect with the inner surface of the vessel. For large-aspect-ratio circumferential flaws, it appears reasonable to expect that the crack-tip fields would also be essentially 2-D GPS in nature over a substantial portion of the crack front. In the limit as one contemplates a "thumb-nail" inner-surface circumferential flaw, the 2-D viewpoint breaks down, and the situation is inherently 3-D in nature. The general applicability of 2-D (GPS) or 3-D assumptions in an RPV analysis, which involves a combination of variables such as vessel and flaw geometry and loading conditions, cannot be determined in an a priori fashion. As an example, current guidelines on RPV pressure-temperature limits use a 6-to-1 flaw as the reference flaw shape, and it is unclear under what conditions a 6-to-1 flaw would be considered 2-D or 3-D in nature.

Finally, in this study, it will prove convenient to regard moderate departure from plane strain constraint in laboratory-size specimens as characterized by a state of GPS. In these situations, the magnitude of the out-of-plane strain induced by the in-plane loading is negative. Similarly, it will also prove convenient to consider positive out-of-plane straining in the vicinity of part-circumferential flaws in a pressure vessel to be characterized by a state of GPS. This idealization becomes more meaningful as the ratio of a circumferential flaw's depth to its circumferential dimension decreases. The magnitude of the prescribed out-of-plane strain in these situations is then positive. Use of GPS in either context is thus necessarily approximate, and more precise descriptions of the crack front strain state will be employed as the need arises.

6 Fracture Prediction Models

6.1 Micromechanical Models for Cleavage and Ductile Fracture

The RKR model[29] is adopted for the prediction of cleavage fracture, and the MHM model[30,31] is adopted for the prediction of ductile fracture. These two models are chosen because they have been applied to A 533 B material, in the lower-transition and upper-shelf regions, respectively, with some success under nonirradiated and irradiated conditions.[32–34] Successful application of the RKR model to the analysis of fracture in the lower-shelf and in the ductile to brittle transition region for a German RPV-grade steel is also noted.[35] On the other hand, some recent investigations appear to cast doubt on the applicability of the RKR model to A 508 Class 3, another RPV-grade steel, in the lower-shelf and transition regions.[36]

A key simplifying feature of these predictive fracture models is that they are "one-dimensional" in nature. That is, the attainment of a critical condition for fracture is phrased in terms of stress and strain quantities evaluated directly ahead of a 2-D crack front along the crack plane. Another key simplifying feature is that the statistical nature of fracture, which is particularly evident under cleavage failure conditions, is not considered. These models are also phenomenological in nature because they describe the conditions necessary for crack initiation in continuum terms without providing an explanation for the underlying micromechanical process for fracture.

The RKR and the MHM fracture models hypothesize that crack initiation can be expressed in terms of the attainment of critical values of global stress and strain measures determined from a continuum elastic-plastic fracture analysis. The RKR model hypothesizes that cleavage fracture under Mode I conditions is governed by the attainment of a temperature-independent critical level of opening-mode stress over a minimum physical distance ahead of the crack front. The minimum physical distance necessary for cleavage fracture is often identified with the distance from the original crack front to cleavage initiation sites. It has been suggested in Ref. 35 that both the steep gradient and the scatter in fracture toughness that are characteristic of the transition region can be attributed to the experimentally observed scatter in cleavage initiation sites, thereby providing further justification for using the RKR model for examining cleavage fracture. However, available data suggest that both the nature and location of the cleavage initiation sites vary considerably for nominally identical RPV-grade materials.[35,36] Consequently, a proper consideration of the micromechanics of fracture is an integral element in the application of this fracture model.

The MHM model hypothesizes that ductile fracture is governed by the attainment of a critical level of Mises effective plastic strain ε_e subject to an associated critical level of stress state expressed in terms of the hydrostatic to effective stress ratio σ_m/σ_e. Similar to the RKR model, the MHM model also requires that this critical condition be achieved over a minimum physical distance ahead of the crack front. The minimum physical distance necessary for ductile fracture is less well defined. This minimum distance has been identified with the minimum size of a region that could accommodate the micromechanical processes of void nucleation, coalescence, and growth that are associated with ductile fracture or plastic-flow localization.

The common requirement of a minimum physical distance over which the failure criterion is met for both the RKR and the MHM models is a consequence of the observation that a critical value of stress or strain measure can usually be achieved ahead of a crack front, even for infinitesimal load levels. This observation is a consequence of the self-similar nature of crack-tip fields with respect to a given combination of loading and nondimensional distance ahead of the crack front. The self-similar nature of the crack-tip fields is observed for both LEFM and EPFM fields under one-parameter (K, J) or two-parameter (K-T, J-Q) dominance conditions. In addition, this self-similarity is observed under small-strain (sharp crack) as well as large-strain (finite initial root radius) assumptions. Additional discussion concerning these models is given in Appendix B.

6.2 Stress Contour Correlation Model

A second approach is employed to investigate the effect of prescribed transverse and in-plane stress states on fracture toughness. The methodology employed here is based on a correlation procedure constructed by Anderson and Dodds[37] to remove the geometry dependence of cleavage fracture toughness values for single-edge-notched bend (SENB) specimens of A 3C steel for a range of crack depths. This procedure utilizes a local stress-based criterion for cleavage fracture and detailed finite-element analysis. From Ref. 37, dimensional analysis for small-scale yielding (SSY) implies that the principal stress ahead of the crack tip can be written as

$$\frac{\sigma_{p1}}{\sigma_o} = f\left(\frac{J^2}{\sigma_o^2 A}\right) , \qquad (2)$$

where σ_o is the 0.2% offset yield strength derived from a uniaxial stress-strain curve, σ_{p1} is the maximum principal stress at a point, and A is the area enclosed by the contour on which σ_{p1} is a constant. The strategy employed in Ref. 37 utilizes a fracture criterion dependent upon achieving a critical volume V_{CR} within which the principal stress is $>\sigma_{p1}$. For a specimen subjected to GPS conditions, the volume is essentially equal to the specimen thickness B times the area within the σ_{p1} contour on the midplane ($V_{CR} = B \cdot A_{CR}$). Equation (2) is the appropriate normalization for SSY solutions when using the latter fracture criterion based on volume or area. This technique was successfully employed by Keeney-Walker et al.[38] to correlate cleavage initiation toughness data from CT specimens with data from the large-scale WP-1 series of HSST wide-plate specimens.[39] Additional discussion concerning this model appears in Appendix D.

6.3 Correlation Between Induced TR and Fracture Toughness

It has been proposed recently that postfracture measurements of TR induced by in-plane loading can be correlated with fracture toughness.[40] An assessment was performed in this study to determine whether a TR model could be used to verify the previously described analytical models in the negative out-of-plane strain domain. The TR correlation examined herein was originally formulated for plate-type fracture specimens for which the loading is "in-plane" in nature, and which results in Mode I or opening-mode separation of the crack faces under the applied load.[40] For the specified "in-plane" loading conditions, the transverse displacement along the crack front must necessarily be negative, and "TR" is identified with this type of transverse displacement. The premise of the TR correlation is simply that TR can be used as an approximate measure of the CTOD under the prescribed in-plane loading conditions.

The starting point of the TR correlation is a CTOD vs J-integral relation of the form

$$\text{CTOD} = J/\sigma_{f1} , \qquad (3)$$

where the flow properties of the material are specified via the parameter σ_{f1}, which is the average value of the uniaxial yield and ultimate stress in tension. A correlation between TR and toughness follows by substituting TR for CTOD in Eq. (3). For the present purpose, this correlation is generalized to take the form

$$\text{TR} = J/(m\sigma_y) , \qquad (4)$$

where m should be regarded as an empirical adjustment factor. The extent to which Eq. (4) can be demonstrated to hold at some distance ahead of the crack front would demonstrate the merits of the proposed TR correlation for the determination of toughness.

7 Validation Experiences with J-Q Methodology and Fracture Prediction Models

7.1 Comparison of Unirradiated A 533 B $J_c(Q)$ Toughness Loci from Shallow-Flaw and WP-1 Testing Programs

Detailed posttest 2-D plane strain analysis results for two specimen geometries are presented in this section. The primary objectives of these analyses are to evaluate the utility of the recently proposed two-parameter J-Q concept to characterize the crack-tip fields up to the onset of crack initiation in specimens with different flaw depths and to provide a framework for interpreting and ordering the observed toughness differences between the deep- and shallow-flaw geometries. Specifically, detailed 2-D finite-strain, finite-element analyses were performed for

1. seven specimens from the series-1 HSST wide-plate experiments, and
2. six specimens from the production phase of the HSST shallow-flaw fracture toughness testing program. (Three of the specimens are deep-flaw specimens with nominal crack depth to specimen width ratio a/W = 0.5, while the remaining three are shallow-flaw specimens with nominal a/W = 0.1.)

The ORNL wide-plate series-1 (WP-1) tests[39,41] provide a set of crack-initiation data against which comparison can be made with the deep- and shallow-flaw data obtained in the shallow-flaw[2] study. The WP-1 specimens were of SEN geometry and fabricated from A 533 grade B class 1 steel plate (HSST-13A). The WP-1 specimens were 1 m wide, ~10.8 m long, and 0.1 to 0.15 m (4 to 6 in.) thick. Each side of the specimens was side-grooved to a depth equal to 12.5% of the specimen thickness, and in most cases the crack front was cut into a truncated chevron configuration.

The shallow-crack beam tests[2] were performed to produce fracture toughness data that would quantify the relaxation of crack-tip constraint associated with shallow-crack geometries. Beam specimens were fabricated from A 533 grade B class 1 steel plate (HSST 13B and WP-CE), with dimensions that varied from 40.6- to 86-cm (16- to 34-in.) length, 10.2-cm (4-in.) depth, and thicknesses of 5, 10, and 15 cm (2, 4, and 6 in.). Sharp cracks of depths 1 and 5 cm (0.4 and 2.0 in.) (a/W = 0.1 and 0.5) were installed in the beams, which were then tested in three-point bend loading at temperatures corresponding to the lower-shelf and the lower-transition region of the plate material.

Finite-element analyses of the wide-plate and shallow-crack beam experiments were performed using loading conditions measured in the test. Full-field finite-strain solutions based on plane strain assumptions were generated from models having a highly refined crack-tip region and a crack-tip profile with an initial root radius. As described in Appendixes B and C, the finite initial root radius, which is much smaller than the outer dimensions of the mesh, facilitates numerical convergence of the solution. The full-field mesh and crack-tip profile used in analyses of the wide-plate specimens are depicted in Fig. B.1.

Crack initiation for the WP-1 specimens occurred over a narrow temperature range that envelops the test temperature of the deep- and shallow-flaw specimens. Current understanding of the J-Q approach would suggest that the $J_c(Q)$ toughness loci from the WP-1 and the deep- and shallow-flaw specimens should be very similar. Instead, recent reanalysis of the ORNL WP-1 tests using the (2-D) J-Q approach indicates a very different $J_c(Q)$ toughness locus for the WP-1 tests as compared to the deep- and shallow-flaw locus. A comparison of the WP-1 and the deep- and shallow-flaw $J_c(Q)$ toughness loci is presented in Fig. 5. Toughness values are expressed in terms of K, and they are further normalized by the plate 13-A small-specimen characterization toughness K_{Ic}. In Fig. 5, the WP-1 results based on two sets of analysis assumptions are presented. The open-square symbols correspond to analysis results based on 2-D plane strain assumptions. The filled-square symbols correspond to analysis results based on an approximate correction of the same 2-D plane strain results to account for the inherently 3-D nature of the WP-1 crack fronts.

When the wide-plate and shallow-crack beam results are evaluated separately, each set of crack-initiation toughness data appears to support a J-Q interpretation. That is, higher toughness values correspond to more negative Q-stresses, which imply a decrease in triaxiality and crack-tip constraint. Collectively, however, results in Fig. 5 indicate that the WP-1 $J_c(Q)$ toughness locus is much steeper than that for the deep- and shallow-flaw specimens. The presence of 3-D effects in the WP-1 specimens is hypothesized to provide at least a partial explanation for the observed differences between the two $J_c(Q)$ toughness loci. (Tests were performed on three different thicknesses of the shallow-crack beams, and no 3-D effects were detected in the toughness data.)

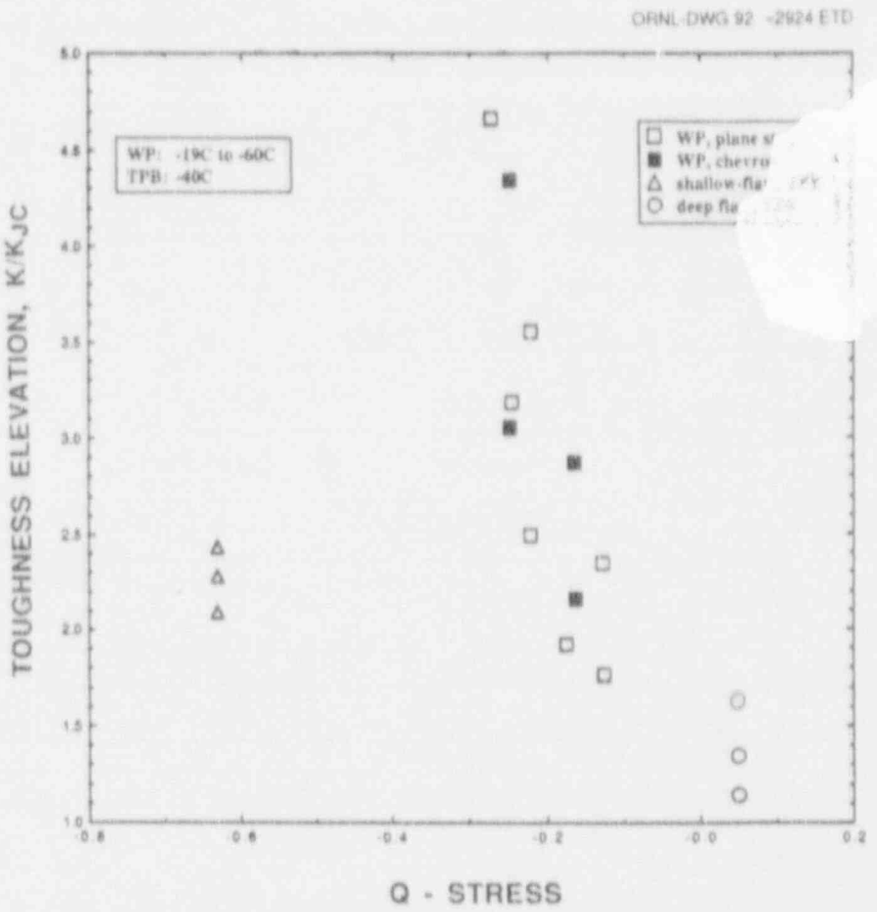

Figure 5 Comparison of shallow-crack and wide-plate crack initiation toughness data

7.2 Applications of Fracture Models to Fracture Toughness Data

In this section, various fracture prediction models are applied to available measured data with the objective of validating the models in the plane stress-to-plane strain domain before applying them to positive out-of-plane strain conditions. Additional details of these studies are provided in Appendixes B to F.

7.2.1 Small-Specimen Toughness Data

Validation of the RKR model and the MHM model through applications to conventional small-specimen toughness data has been discussed in Chap. 6. With reference to the objective of this study, namely, determining the potential toughness deviation due to out-of-plane biaxial stress effects, it is noted that "validation" of the RKR and the MHM models is in the sense that these models have been successfully applied toward predicting the overall temperature dependence of small-specimen fracture toughness data. Scatter of both the toughness data and the magnitude of the induced transverse strain at a given temperature is not explicitly considered. A discussion on this scatter and its relevance toward the validation of a predictive fracture model is presented in Appendix F.

However, it is noted that the experimental data employed in these validations were obtained using small-scale specimens that range in size from 1T-CT to 11T-CT specimens. Based on the results to be presented in Appendixes E and F, the magnitude of the induced transverse contraction strain at fracture associated with 1T-CT specimens is on the order of the yield strain. In the absence of toughness data obtained under prescribed negative transverse straining, these studies could be viewed as providing validation of the RKR and the MHM models under moderate relaxation from plane strain constraint conditions. Because the state of tensile transverse straining appropriate to RPV discussions is on the order of the yield strain, it appears reasonable to employ these models to evaluate the effect on fracture toughness of transverse strain (positive or negative) on the order of the yield strain.

7.2.2 Large-Scale Specimen Toughness Data

Results from application of the RKR prediction model to the WP-1 series of experiments are given in Fig. 6. Correlations of measured and predicted toughness for the experiments based on the Q-stress parameter are expressed in terms of K-factors normalized by SSY values corresponding to initial conditions. For the WP-1 series (Fig. 6), toughness predictions are given for three values of the critical stress ratio, σ_c/σ_o = 2.2, 2.6, and 3.4, where σ_o = 465 MPa. Results for the WP-2 series of experiments are given in Appendix B. For both series of experiments, the RKR-model predictions fall substantially below the toughness values determined from the measured data. Fracture toughness predictions from the RKR model for the shallow-crack beam specimens are compared with measured toughness values in Fig. 7. Predictions are given for four values of the critical stress ratio, σ_c/σ_o = 2.7, 3.0, 3.4, and 4.0. Again, the RKR model predictions fall below measured values, but not to the extent indicated for the wide-plate specimens. Note that these results were obtained based on 2-D plane strain assumptions, which were the basis for development of the J-Q methodology. It has not been established to what extent these differences are due to problems associated with representing 3-D stress states in the wide plates by a 2-D model or to problems with the RKR prediction model. As discussed previously, applications of the RKR prediction model to measure data have been confined to small-scale laboratory specimens. There may be difficulties with applications of the model to large-scale structures subjected to nominal 3-D stress states that have not yet been identified.

7.2.3 Stress Contour Correlation Methodology

The development of the critical maximum principal stress contour methodology described in Sect. 6 depends on establishing the existence of a critical σ_{p1} stress value that correlates fracture toughness behavior over a range of transverse strain values. In analyses designed to validate and calibrate the model in the plane stress-to-plane strain domain, the stress contour method was applied to fracture toughness data for A 533 B steel previously generated by McCabe and Landes[42] for a study of thickness effects in the transition region. Analyses of 3-D finite-element models of compact specimens having a common planform of a

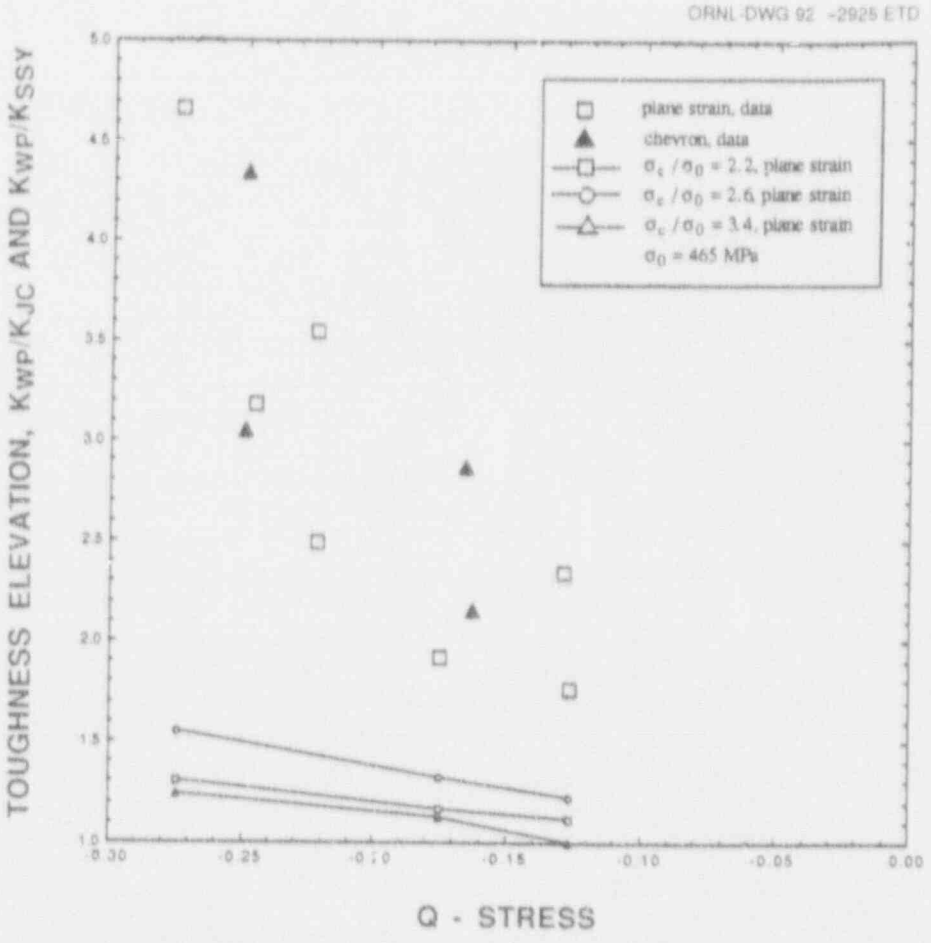

Figure 6 Correlation of measured and predicted toughness for WP-1 wide-plate series based on Q-stress parameter

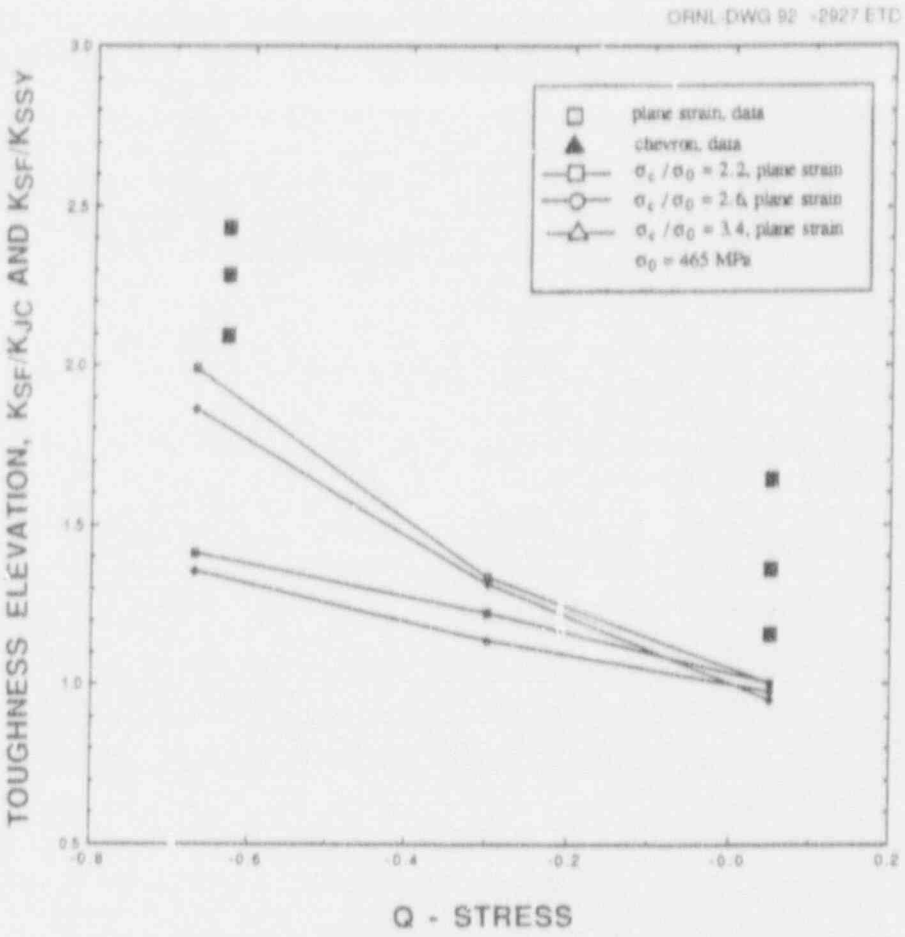

Figure 7 Correlation of measured and predicted toughness for shallow-crack beam specimens based on Q_c-stress parameter

4T specimen and thicknesses ranging from 10.16 to 101.6 mm were performed in an attempt to estimate a critical σ_{p1} stress value in the negative transverse strain domain. This estimate of a critical σ_{p1} value is necessary to provide input to toughness correlations in the positive transverse strain domain and, thereby, to provide estimates of reductions in fracture toughness associated with these strains. Four specimen thicknesses were analyzed: (1) Model A - 101.6 mm; (2) Model B - 50.8 mm; (3) Model C - 25.4 mm; and (4) Model D - 10.16 mm. The analyses used an incremental elastic-plastic constitutive model, and a small strain formulation. A multilinear stress-strain curve was generated from wide-plate data corresponding to a temperature of 0°C (yield stress of 434.8 MPa); the curve was then elevated to the yield stress of 482.6 MPa reported in Ref. 42.

The load vs load-line displacements (normalized by specimen width W) from the finite-element analysis of Model D were compared with experimental data[42] in Fig. 8 to determine if the structural response could be reproduced in the model. From the analysis, the model yielded and became nonlinear at a lower load than that implied by the experimental data. To reproduce the linear part of the load/displacement curve in Fig. 8, an artificially high yield stress of 610 MPa (determined from a parametric study) was required.

The critical area parameter A_{CR} was evaluated at initiation for each model over a range of σ_{p1} values corresponding to cleavage initiation. From Fig. 9, the correlations for Models A and B do not intersect; Model C intersects Model A at ~1250 MPa and coincides with Model B between 1360 and 1400 MPa. Model D intersects Model A at ~1340 MPa and Model B at 1500 MPa. This correlation proved to be unsuccessful in establishing a critical σ_{p1} parameter. It should be noted that the data set utilized in these analyses included only one cleavage initiation toughness value for each specimen thickness. Also, the experimental data were not reported in sufficient detail to permit resolution of substantial differences between measured and computed curves representing load vs load-line displacements for the test specimens. Because of these difficulties with the experimental data, the viability of the stress contour methodology for correlating fracture toughness in the plane stress-to-plane strain domain cannot be judged on the basis of the above application.

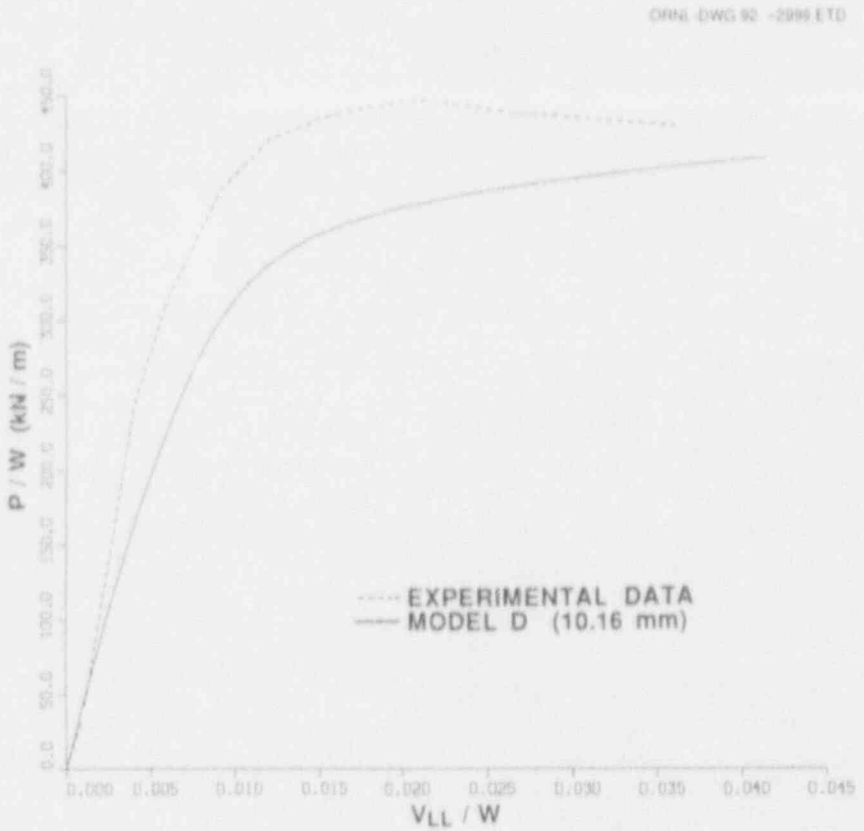

Figure 8 Load vs load-line displacement (both normalized by W) for Model D, which is 10.16 mm thick, and experimental data

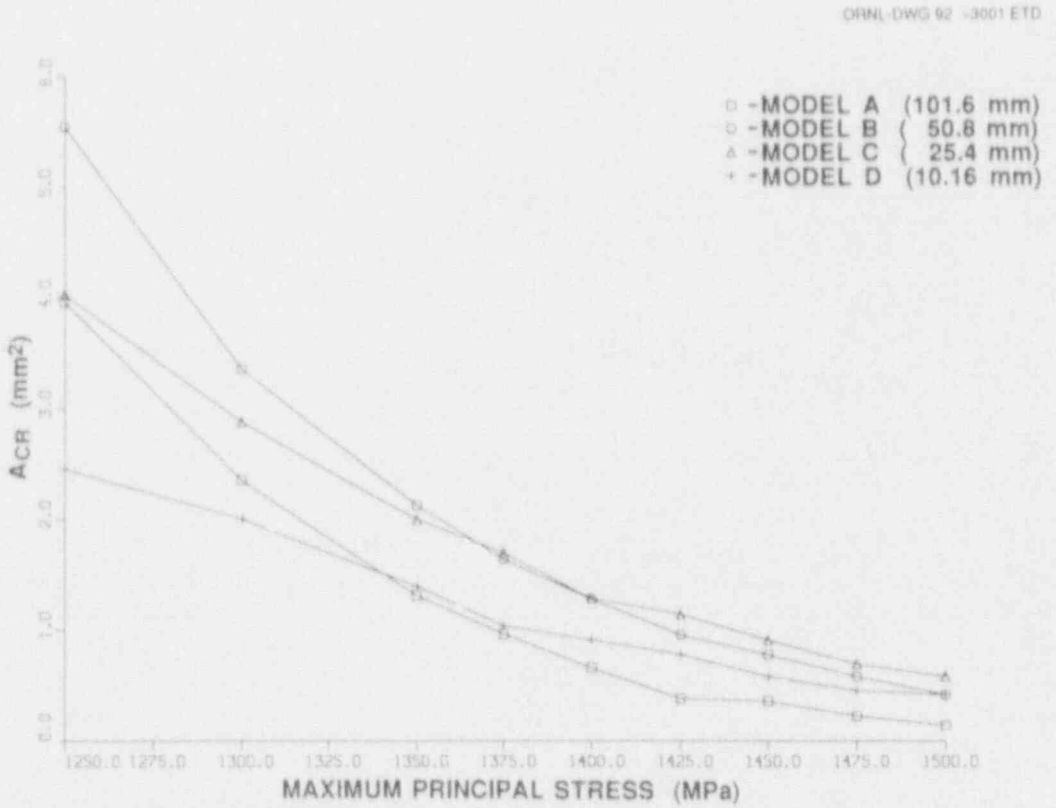

Figure 9 A_{CR} vs maximum principal stress for the four 4T-CT models at initiation

The analysis results are compared with the SSY solution in Fig. 10 to investigate Q-stress effects. It can be observed that when the opening-mode stress, normalized by the yield stress, is plotted vs the normalized distance from the crack tip [$r/(J/\sigma_0)$], Model A is close to the SSY solution as expected, but Model B begins to diverge at a value of $r/(J/\sigma_0) \approx 3$; Models C and D are even more divergent. Additional details concerning these analyses are given in Appendix D.

7.2.4 Status Assessment of Fracture Prediction Models

In Sect. 7.2.2, fracture toughness predictions from the RKR model for the large-scale HSST wide-plate specimens were shown to be substantially below values determined from analysis of measured data from two different materials employed in the series of tests. Some possible reasons for the discrepancies were noted in the discussion of these results. Similarly, attempts described in Sect. 7.2.3 to calibrate the fracture correlation model based on a critical area A_{CR} within a contour of critical maximum principal stress, based on a very limited set of measured data, were unsuccessful. In the latter case, the experimental data were not reported in sufficient detail to permit adequate modeling of the load vs load-line displacement curves of the test specimens. The general finding is that applications of these fracture models to existing small- and large-scale fracture test results did not produce consistent results in predicting fracture behavior. Thus, the effects of biaxial out-of-plane stresses on fracture toughness cannot be predicted here on the basis of validated models.

Toughness estimates from these models in the positive transverse strain domain are given in Appendixes C and D of this report. However, capabilities of these models for predicting out-of-plane stress and strain effects on fracture toughness remain unvalidated, and confidence cannot be placed in applications of these results to questions that arise from licensing and regulatory issues. Estimates are given herein to provide a reference for toughness predictions implied by a specific interpretation of these models, as outlined in the previous sections.

7.3 Correlation Between Induced TR and Fracture Toughness

7.3.1 Wide Plates

It has been reported that postfracture TR measurements have been successfully correlated with cleavage crack

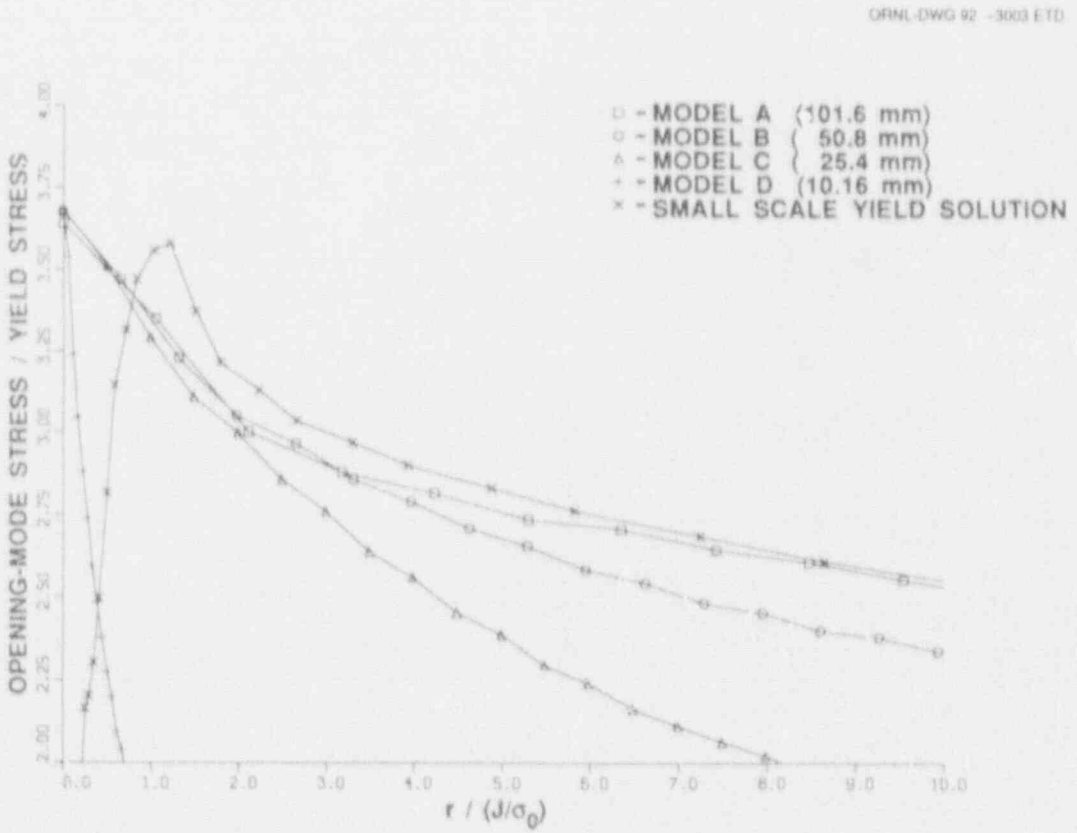

Figure 10 Comparison of normalized stress vs normalized distance from the crack-tip for the 4T-CT models and SSY solution

initiation, arrest, and reinitiation toughness values for the ORNL/NIST wide-plate specimens.[40,43] In the wide-plate studies, postfracture thickness-averaged transverse strain contours for each of the wide-plate specimens are reported, along with specimen thickness, temperature-dependent material properties, and the temperature distributions ahead of the crack front for each of the specimens. Based on this information and the proposed TR correlation, crack-arrest and reinitiation toughness values have been calculated and reported in Ref. 40 for WP-2 series and in Ref. 43 for WP-1, WP-CE, and WP-2 series of experiments. The results employ temperature as the independent variable such that the comparison is made across a temperature range, whereas Eq. (3) is formulated for isothermal conditions. It is thought that validation of the TR correlation for the wide-plate tests can be better accomplished by presenting TR-toughness results at a fixed temperature with toughness expressed in terms of J-integral values. By fixing the test temperature, the temperature dependence of various constraint effects in the wide-plate tests is eliminated. For the WP-1 series of tests, at least one crack-arrest event occurred in each specimen within a relatively narrow temperature range of 53 to 62°C. The associated crack-tip locations also fall within a narrow range between 49 and 56 cm. Consequently, it is possible to evaluate the TR correlation for the WP-1 specimens with six data points obtained at essentially the same temperature and crack length.

The results of such a comparison are presented in Fig. 11, along with three straight lines that correspond to the predicted relationship between TR and J as indicated by Eq. (4). The experimental data and finite-element results used to generate Fig. 11 are presented in Appendix F. The predicted TR-J relations are for WP-1 material at 60°C with an associated yield stress σ_y = 412 MPa. The three straight lines are based on three values of the empirical adjustment factor, m. If values of TR are identical to values of CTOD, then the straight line denoted as m = 1 corresponds to the limiting, nonhardening, plane stress CTOD vs J relation. Similarly, the line denoted as m = 2 corresponds to the plane strain relation for a Ramberg-Osgood material with a hardening exponent of 10. In Ref. 43, validation of the TR correlation for the wide-plate tests was performed based on

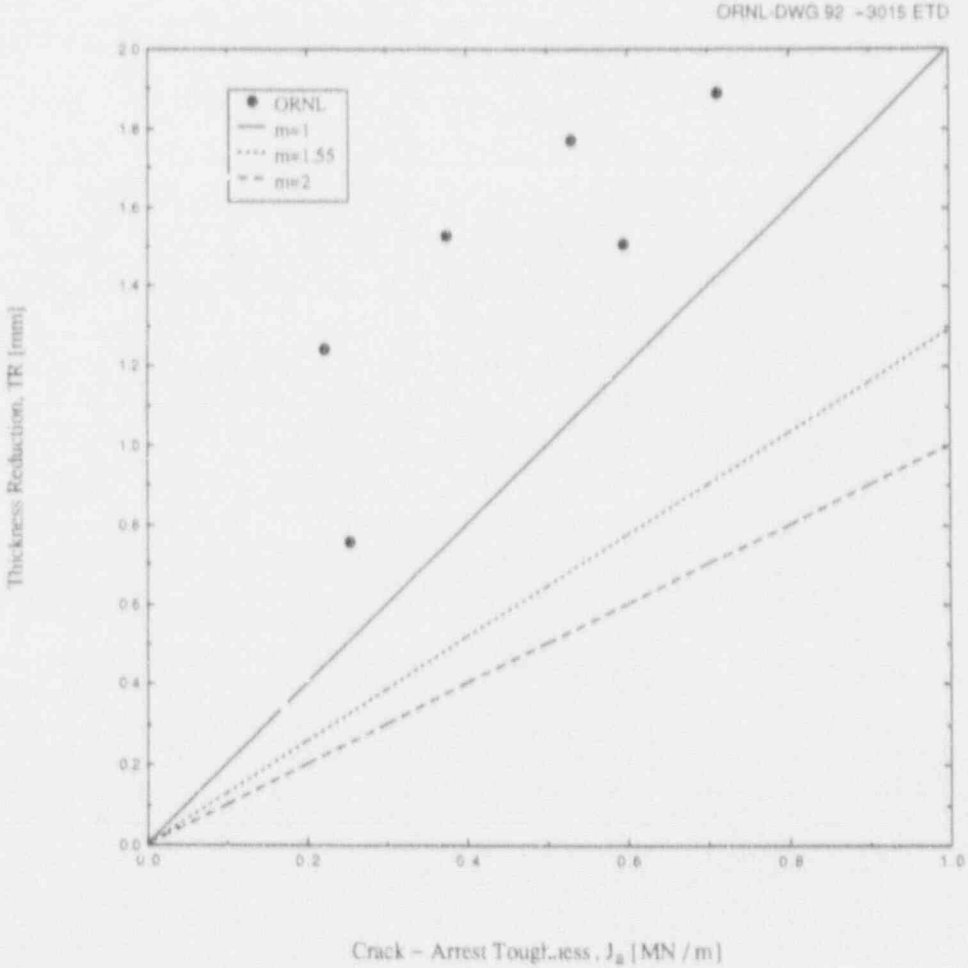

Figure 11 Comparison of measured and predicted crack-arrest toughness values based on Eq. (4) for six of WP-1 specimens

a value of flow stress adjusted for rate effects, with the adjustment corresponding to m = 1.55.

When comparison of TR predictions and the WP-1 results are cast in the form shown in Fig. 11, the proposed TR correlation for the WP-1 tests does not appear to be valid. This interpretation is based on the observation that the existence of a TR correlation involves not only a linear relationship between TR and toughness, but also this linear relationship needs to be "anchored" at the origin of the plot in Fig. 11. In addition, the TR-J data should be to the right of the m = 1 line due to the assumption of minimum constraint associated with the static, plane stress condition.

7.3.2 Compact Specimens

Postfracture TR measurements from three sizes of CT specimens have been obtained for the purpose of correlating with the associated crack-initiation fracture toughness values. These specimens are standard CT specimens (1/2T, 1T, 2T) with a crack length to width ratio of 0.5 and were also taken from HSST plate 13A. A total of 17 specimens that were tested at a lower-shelf temperature of –75°C are considered. Postfracture TR measurements have been taken along the specimen surface at two locations ahead of the fatigue crack front using a microscope-micrometer setup. The measurement locations are denoted as t_o. The two choices of t_o are as follows: (1) a distance of 5 J/σ_o ahead of the crack front, where J is equal to $J_{cleavage}$ and σ_o is the uniaxial yield stress in tension at the test temperature, and (2) a location denoted as t_{max} that appears to have the most TR based on visual examination of the specimen with a microscope.

The average values of TR at the two measurement locations t_o for each specimen are plotted in Fig. 12, against the reported toughness values. Three straight lines are drawn for three values of the empirical adjustment factor m that correspond to the predicted relationship between TR and J as indicated by Eq. (4). Rate adjustment of the type employed in Ref. 43 corresponds to m = 1.47, based on yield stress σ_y = 500 MPa and flow stress σ_{fl} = 598 MPa at –75°C, and a rate-adjusted flow stress elevation of 138 MPa. The m = 1 line will be taken as indicative of the lowest constraint conditions, while the m = 2 line is taken

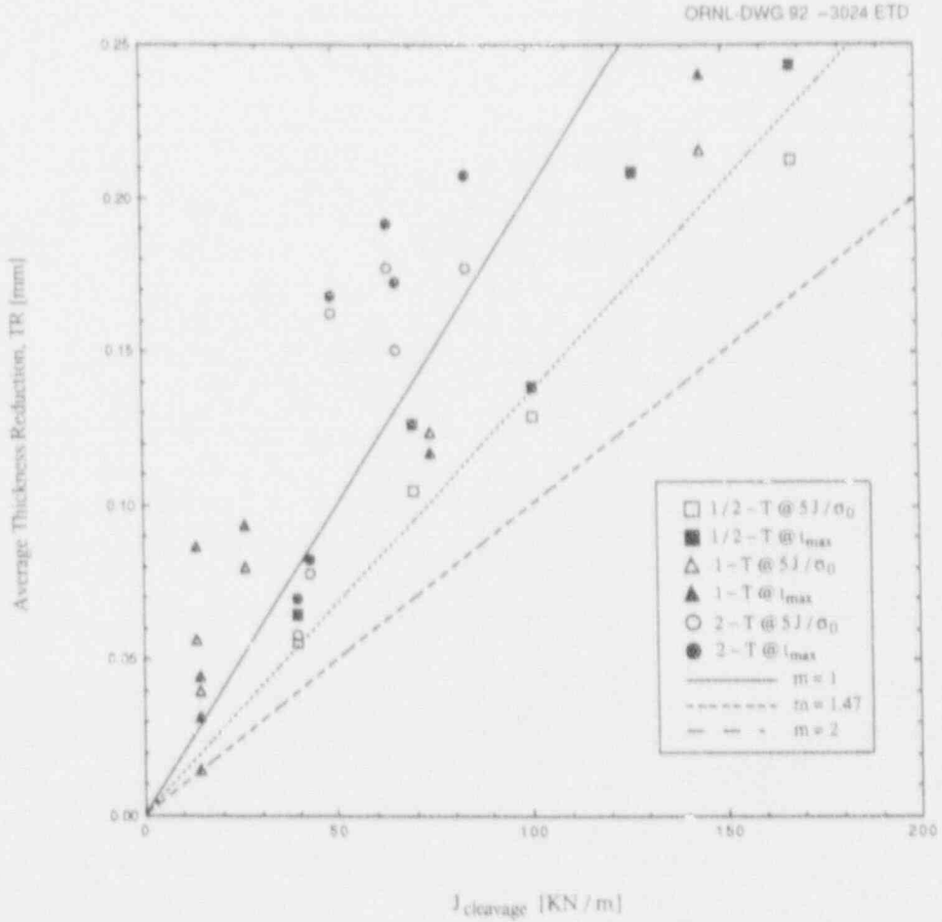

Figure 12 Comparison of measured and predicted toughness based on Eq. (4) for CT specimens

as indicative of plane strain constraint conditions. Results shown in Fig. 12 indicate that aside from the 1/2T specimens, it does not appear that a correlation of the type suggested by Eq. (4) applies to the 1T and 2T specimens. Magnitudes of the transverse strain for the various specimens are as follows: 0.4% to 1.6% for the 1/2-CT, 0.2% to 1% for the 1T-CT, and 0.1% to 0.4% for the 2T-CT specimens. For the 1/2T specimens, the TR correlation appears to be validated for both large and small values of induced TR, provided one assumes an adjustment factor less than that suggested in Ref. 43.

In view of the apparent lack of correlation between the measured TR and toughness values for the CT specimens, analyses were performed for a 3-D finite element model of a 1T-CT specimen in an attempt to gain further insights. Specifically, the question concerns to what extent post-fracture TR measurements can be related to the amount of TR just before crack initiation or to the amount of residual TR after crack initiation. Details of these finite-element analyses are described in Appendix E.

The load histories for three of the 1T-CT specimens considered in Fig. 12 were examined. The finite-element analyses predict substantially lower values of residual TR than those determined experimentally for two specimens, while the prediction for the third specimen is nearly identical to the corresponding experimental measurement. It is thought that this observation can be understood by recognizing that the experimental postfracture TR measurements represent the total plastic contribution from crack-initiation and crack-propagation effects. In contrast, the finite-element results represent in situ predictions of TR values due to the application of maximum load and subsequent unloading. Consequently, it would appear that the contribution to TR resulting from shear-lip formation due to crack propagation may at times overwhelm the contribution due to crack initiation.

The utility of a correlation based on induced TR toward determination of the effects of prescribed transverse displacement on fracture toughness may be limited. That is, even if the validity of a correlation between induced TR and toughness such as Eq. (4) can be established, it does not follow that this correlation can be used to determine toughness as a function of TR, nor that this correlation can be extrapolated into the positive straining regime, whether the positive straining is induced or prescribed.

8 Development and Validation Plans

8.1 Motivation for Biaxial Testing Program

In the previous sections, analysis methodologies for estimating the potential impact of biaxial far-field stresses on crack-initiation toughness of inner surface cracks in RPVs were presented. A modified boundary-layer approach that focuses on the near stress/strain fields directly ahead of the crack tip was introduced. This approach, combined with K-T or J-Q dual-parameter fracture characterization methodology, was employed to examine fracture initiation within the context of the RKR and MHM micromechanical fracture models. A fracture correlation parameter based on a stress contour method was used to relate cleavage crack initiation to the attainment of a critical area enclosed within a selected maximum principal stress contour ahead of the crack tip. Studies were also performed to determine whether a correlation between fracture toughness and TR induced by in-plane loading can be used to verify the analytical models of this report in the negative transverse strain regime.

The RKR and MHM fracture prediction models described above have been validated previously for small-scale fracture specimens under nearly plane strain constraint conditions. In this study, the RKR model was applied to fracture initiation toughness data generated in the HSST Program from large-scale wide-plate experiments and shallow-crack beam tests. Correlations of measured and predicted toughness for the WP-1 and -2 series of wide-plate experiments based on the Q-stress parameter indicate that the RKR model predictions fall substantially below the toughness values determined from analysis of the measured data. Fracture toughness predictions from the RKR model for the shallow-crack beam specimens were compared with measured toughness values for four values of critical stress. Again, the RKR model predictions were below measured values, but not to the extent observed in the wide-plate specimens. Possible reasons for the discrepancies were noted in the discussion of these results. The stress contour methodology was applied to fracture toughness data for A 533 grade B class 1 steel to establish the existence of a critical σ_{p1} stress value that correlates fracture toughness behavior over a range of transverse strain values. The results were unsuccessful because a critical σ_{p1} value common to three different thicknesses of the specimens could not be established.

Notwithstanding these general findings, toughness predictions implied by these models for out-of-plane strain effects were provided herein for reference purposes. Within the assumptions of the various models and analyses presented here, tensile transverse strains are predicted to produce a relatively small decrease in effective cleavage fracture toughness when compared with that of identical specimens loaded uniaxially. Applications of the RKR model (described in Appendix C) and the stress contour methodology (described in Appendix D) support a reduction in cleavage toughness of ~9% to 20% due to positive strains. The MKM model (described in Appendix C) predicted minimal ductile toughness deviation. However, because the fracture methodologies considered in this study have not been successfully validated using fracture data that involve out-of-plane straining, uncertainties remain with these estimates such that they cannot be applied with confidence in addressing questions that affect licensing and regulatory issues for RPVs.

Experimental evidence was compiled from three different testing programs that suggest a significant decrease in fracture toughness due to out-of-plane biaxial stress effects. Figure 13 depicts the reduction in fracture toughness (in percent of K_c) expressed as a function of biaxiality ratio (out-of-plane stress/normal stress) inferred from the testing programs described in Chap. 1. Estimates of reduced toughness for the thermally shocked, shallow-crack cylinders (equibiaxial loading) are as high as 40%, when compared to the shallow-crack beams (uniaxial loading). It is noted that detailed finite-element analyses employing the methodologies described in this report have not been performed to provide updated interpretations of these biaxial test results.

Studies currently under way in the HSST Program are using methodologies described in this report to better understand the substantial differences in measured fracture toughness from the thermal-shock experiments and the shallow-crack beam tests. It is clear that several different competing mechanisms affecting fracture toughness are presented in these two experiments. In addition to the biaxial stress field, other factors include shallow-crack effects, methods of structural loading, structural and crack geometries, and material properties. A definitive conclusion regarding biaxial effects requires an understanding of these factors affecting toughness that is sufficient to permit an unambiguous separation of the individual contributions.

From these studies, it is apparent that testing of RPV steels is required (1) to determine the magnitude of out-of-plane biaxial loading effects on fracture toughness, and (2) to provide a basis for development of predictive models. The most desirable program would involve suitable test

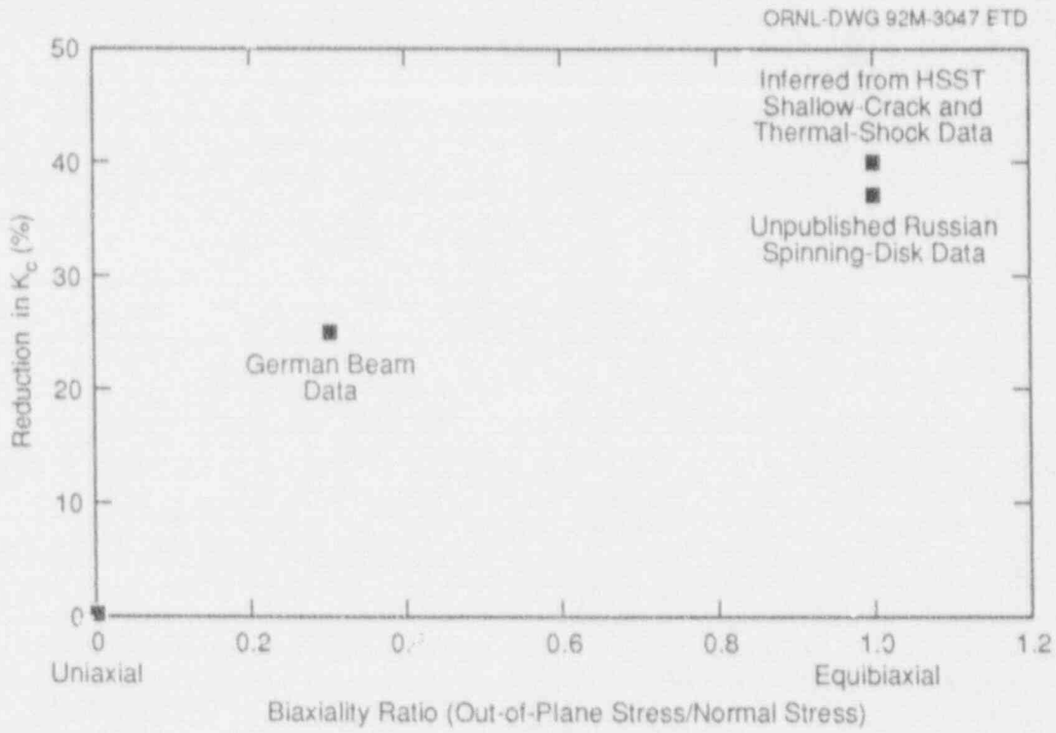

Figure 13 Experimental data indicating decrease in fracture toughness due to effects of out-of-plane biaxial stresses

...ns and loading conditions for which the only vari... are imposed biaxial loading components. This course ...ction is necessary to support a refined treatment of in-plane and out-of-plane constraint effects on crack initiation from shallow cracks under PTS loading conditions. As a consequence, criteria for a biaxial specimen are proposed in the next section that would form the basis of a testing program designed to provide data to explain differences between theoretical predictions and measured material behavior.

8.2 Design Criteria for Biaxial Specimen

The objective of the proposed biaxial fracture testing program is to obtain fracture toughness data under conditions of uniform far-field biaxial stresses that are selected to (1) produce prototypic crack-driving forces and out-of-plane stress and (2) provide the simplest loading conditions for analysis. In addition, the experimental data from the proposed testing program will provide much needed data for the purpose of verifying and refining the fracture prediction methodologies that form the basis of the analytical predictions described in previous chapters. Tests would be conducted on uniaxially and biaxially loading specimens for comparative purposes.

Design of the biaxial test specimen is based on the following criteria:

1. Test specimen must remain elastic in the throat (i.e., LEFM conditions must apply).
2. Tests must only be influenced by out-of-plane biaxial loading (i.e., shallow-flaw effects, metallurgical gradients, etc., must be minimized).
3. Yield strength of material should be representative of irradiated conditions and achievable through heat treatment.
4. Test temperature relative to RT_{NDT} should be representative of PTS temperatures (i.e., in lower-transition region).
5. Flaw must be long to enhance crack initiation.
6. Biaxial loading ratio should be representative of that experienced by circumferential flaw under PTS loading (i.e., equibiaxial or 1:1 ratio).
7. Stress at failure should be representative of that in the vessel wall during PTS event.
8. Sufficient driving force should be present at the crack tip to reasonably ensure crack initiation within the loading capacity of candidate testing machines, taken herein to be 27 MN.

A preliminary set of parameters was selected to initiate the design process and to meet these eight criteria. Criterion 2 may be satisfied by requiring a normalized crack depth, a/W, varying between 0.3 and 0.6 to minimize any shallow-crack effects. Additionally, to eliminate influence of metallurgical gradients, test specimens should be cut such that the majority of the crack-tip region is located in the center region of the source plate. To satisfy criterion 3, all analyses presented here are based on a yield strength level of 620 MPa. This strength level is both prototypic of irradiated A 533 grade B class 1 steel and is attainable in unirradiated A 533 B through heat treatment.

A geometry based on a double-tension specimen and the material characterization of HSST Plate 13A was assumed for these studies.[39] Examination of IPTS studies[4] reveals that many crack initiations occur within a temperature range of $T - RT_{NDT}$ from -25°C to 0°C. Testing at a temperature above RT_{NDT} would likely violate criterion 1. To ensure crack initiation and to satisfy criteria 4 and 8, the test temperature has been tentatively set at $T - RT_{NDT} = -25°C$. The initiation fracture toughness at this temperature is taken to be 72.5 MPa•$\sqrt{m}$. Further evidence that $T - RT_{NDT} = -25°C$ is a suitable temperature is provided by data from shallow-crack toughness tests.[3]

An essential test requirement is that the crack-driving force be sufficient to initiate the crack. However, scatter of the toughness data in the transition region often exceeds a factor of 2 (Ref. 39). In addition, some increase in toughness may be present in the biaxial specimens, because SEN tension specimens generally are less constrained than CT or SENB specimens. The loss of constraint for tension loading should be minor if linear elastic conditions are met. Also, the long flaw length dictated in criterion 5 provides more opportunities for crack initiation and should tend to bring about a lower initiation value. Based partly on the WP-1 series of wide-plate experiments,[39] a load ratio of $K_I/K_{Ic} = 2.5$ is assumed to be a requirement for these tests, satisfying part of criterion 8. This ratio implies that, at $T - RT_{NDT} = -25°C$, K_I must exceed 181 MPa•$\sqrt{m}$.

Design studies are currently under way in the HSST Program to develop a set of geometric parameters, material and fracture properties, and loading conditions for the specimen satisfying the above design criteria. Detailed near-crack-tip field analyses for one of several previously studied specimen geometries are presented in Appendix G to illustrate an application of the fracture methodology described in Chaps. 5 and 6 to the design process.

9 Summary and Conclusions

This report describes work that was undertaken to develop analytical methods for estimating the potential impact of biaxial far-field stresses on crack-initiation toughness of inner surface cracks in nuclear RPVs. A concern exists that the biaxial stress distribution could have an adverse impact on material fracture toughness under PTS loading conditions due to an increase in crack-tip constraint conditions. This report is the second in a series investigating the potential impact of far-field out-of-plane stresses and strains on fracture initiation toughness. The specific objectives of the investigation are embodied in the following elements: (1) identification and evaluation of existing biaxial fracture toughness data, (2) selection of fracture parameters suitable for characterizing the fracture process, (3) selection of fracture prediction models potentially capable of simulating the effects of out-of-plane stresses on fracture initiation toughness, (4) applications of the fracture prediction models to existing measured data in the plane stress-to-plane strain domain and comparisons between the predicted and measured results, and (5) applications of fracture prediction models in element (4) to the prediction of positive out-of-plane stress and strain effects on fracture initiation toughness.

Two different analytical approaches to the problem were presented in the report. The first utilizes two-parameter fracture characterization methods, which incorporate the higher-order T-stress and Q-stress terms, to provide the technical basis for addressing the shortcomings of conventional one-parameter methods. The near-crack-tip fields are interpreted within the context of the RKR model for prediction of cleavage fracture, and the MHM model for ductile fracture. The second approach focuses on the development of a stress contour correlation parameter that relates fracture toughness with a volume of material loaded above nominal stress threshold states. The stress contour method correlates cleavage crack initiation with the attainment of a critical area enclosed within a selected maximum principal stress contour surrounding the crack tip.

These fracture models were applied to existing measured data with the objective of validating the models in the plane stress-to-plane strain domain before applying them to positive out-of-plane strain conditions. The general finding was that applications of these two fracture models to small- and large-specimen fracture data did not produce consistent results in predicting fracture behavior. Notwithstanding these findings, toughness predictions implied by these models for out-of-plane strain effects were provided for reference purposes. Because the fracture methodologies considered in this study predict fracture behavior that conflicts with some of the existing data considered relevant to the problem, these estimates cannot be applied with confidence in addressing questions that affect licensing and regulatory issues for RPVs.

Limited experimental evidence from three testing programs implied a substantial decrease in fracture toughness from out-of-plane biaxial stress effects, with estimates of reduction in K_c as high as 40% for equibiaxial loading conditions. Proposed in this report are criteria for a biaxial specimen that would form the basis of a testing program designed to provide data to explain differences between theoretical predictions and measured material behavior. Testing of RPV steels is required to (1) determine the magnitude of out-of-plane biaxial loading effect on fracture toughness, and (2) provide a basis for development of predictive models. This course of action is necessary to support a refined treatment of in-plane and out-of-plane constraint effects on crack initiation from shallow cracks under PTS loading conditions. Any increase in crack-tip constraint resulting from out-of-plane stresses would act in opposition to the in-plane crack-tip constraint relaxation that has been previously demonstrated for shallow cracks.

Recommendations for additional work necessary to provide validated estimates of out-of-plane stress and strain effects on crack initiation toughness include the following:

1. formulation of an experimental program to determine the effects of far-field biaxial vs uniaxial loading conditions on the initiation toughness of shallow cracks in RPV steels;
2. determination of the applicability of two-parameter fracture analysis approaches (e.g., J-Q) to inherently 3-D stress states in the vicinity of the crack tip;
3. performance of detailed finite-element analyses that can provide accurate descriptions of the 3-D near-tip stress and strain fields associated with the generation of existing fracture data from the wide-plate experiments, thermal-shock experiments, and shallow-crack beam tests;
4. resolution of the observed differences between the two $J_C(Q)$ toughness loci for the wide-plate and the shallow-crack beam data;
5. resolution of the observed differences between fracture toughness from measured data and from predictions provided by the RKR model for the wide-plate tests and the shallow-crack beam tests;
6. resolution of the observed differences in measured fracture toughness from the uniaxiality loaded shallow-crack beam tests and the biaxially loaded thermal-shock experiments;

7. determination of the viability of the stress contour methodology for correlating fracture toughness in the out-of-plane stress/strain domain based on measured data; and
8. validation of a fracture prediction model for estimating out-of-plane stress/strain effects on cleavage fracture initiation toughness through applications to measured data.

References

1. W. E. Pennell, Martin Marietta Energy Systems, Inc., Oak Ridge Natl. Lab., "Heavy-Section Technology Program: Recent Developments in Crack Initiation and Arrest Research," *Proceedings of the U.S. Nuclear Regulatory Commission Nineteenth Water Reactor Safety Information Meeting*, USNRC Proceeding NUREG/CP-0019, October 1991.*

2. T. J. Theiss, D. K. M. Shum, and S. T. Rolfe, Martin Marietta Energy Systems, Inc., Oak Ridge Natl. Lab., "Interim Report on the HSST Shallow-Crack Program and Implications for Reactor Pressure Vessel Analyses," USNRC Report NUREG/CR-5886 (ORNL/TM-12115), June 1992.*

3. R. D. Cheverton et al., Martin Marietta Energy Systems, Inc., Oak Ridge Natl. Lab., "Review of Pressurized-Water-Reactor-Related Thermal-Shock Studies," ASTM Special Technical Publication No. 969, 752–766 (1988).

4. D. L. Selby et al., Martin Marietta Energy Systems, Inc., Oak Ridge Natl. Lab., "Pressurized Thermal Shock Evaluation of the H. B. Robinson Unit 2 Nuclear Power Plant," USNRC Report NUREG/CR-4183 (ORNL/TM-9567/V1 and V2), September 1985.*

5. D. Aurich, "The Influence of the Stress State on the Plastic Zone Size," *Eng. Frac. Mech.* 7, 761–765 (1975).†

6. D. Aurich et al., "The Influence on the Stress State of K_{Ic}," Paper G 5/2 in *Proceedings of the 4th International Conference on Structural Mechanics in Reactor Technology, San Francisco, CA, August 15-19, 1977.*

7. D. Aurich et al., "The Influence of Stress State on Fracture Toughness—Further Results," Paper G 2/3 in *Transactions of the 5th International Conference on Structural Mechanics in Reactor Technology, Berlin, Germany, August 13-17, 1979.*

8. J. Olschewski et al., "The Influence of Biaxial Loading on Fracture Toughness—Further Results," Paper G/F 3/3 in *Transactions of 7th International Conference on Structural Mechanics in Reactor Technology, Chicago, IL, August 1983.*

9. D. Aurich, *Übertragbarkeit von Bruchkennwerten von Proben auf Bauteile im Hinblick auf die Sicherheitsanalyse von Kernkraftwerks-komponenten*, Report RS 275, BAM, Berlin, Germany, September 14, 1984 (text in German).

10. D. Aurich et al., "The Influence of Multiaxial Stress States on Characteristic Parameters for Cleavage Fracture in the Elastic-Plastic Range," pp. 345–356 in *Proceedings International Conference Applied Fracture Mechanics to Materials and Structures*, 1984.

11. D. M. Shum et al., Martin Marietta Energy Systems, Inc., Oak Ridge Natl. Lab., "Analytical Studies of Transverse Strain Effects on Fracture Toughness for Circumferentially Oriented Cracks," USNRC Report NUREG/CR-5592 (ORNL/TM-11581), April 1991.*

12. S. T. Rolfe and J. M. Barsom, *Fracture and Fatigue Control in Structures: Applications of Fracture Mechanics*, Prentice-Hall, Inc., Englewood, N.J., 1977.

13. M. F. Kanninen and C. H. Popelar, *Advanced Fracture Mechanics*, Oxford University Press, New York, 1985.

14. W. E. Pennell, Martin Marietta Energy Systems, Inc., Oak Ridge Natl. Lab., "Heavy Section Steel Technology Program Fracture Issues," pp. 1-26 in *Proceedings of the USNRC Seventeenth Water Reactor Safety Information Meeting*, USNRC Conference Proceedings NUREG/CP-0105, Vol. 3, March 1990.*

15. *Code of Federal Regulations*, Title 10, Part 50, Section 50.61 and Appendix G.‡

16. J. G. Merkle, Martin Marietta Energy Systems, Inc., Oak Ridge Natl. Lab., "An Overview of the Low-Upper-Shelf Toughness Safety Margin Issue," USNRC Report NUREG/CR-5552 (ORNL/TM-11314), August 1990.*

17. M. Kuna, H. Kordisch, and A. Ockewitz, "Thermoelastic-Plastic FEM-Analysis of a Semi-Elliptical Surface Crack in a Cylinder Under Non-Axial-Symmetric Cooling," in *Proceedings of the*

European Symposium on Elastic-Plastic Fracture Mechanics: Elements of Defect Assessment, October 9–12, 1989, Freiburg, FRG [also to appear in *J. Mech. E.*, 1991].†

18. K. Kussmaul et al., "Cyclic and Transient Thermal Loading of the HDR Reactor Pressure Vessel with Respect to Crack Initiation with Crack Propagation," in *Proceedings of the Sixth International Seminar on Assuring Structural Integrity of Steel Reactor Pressure Boundary Components: SMIRT-10 Post Conference Seminar No. 2, 1989.*

19. T. G. Theofanous and K. Iyer, "Mixing Phenomena of Interest to SBLOCAs," *Nucl. Eng. Des.* 102, 91–103 (1987).†

20. M. L. Williams, "On the Stress Distribution at the Base of a Stationary Crack," *J. Appl. Mech.* 24, 109–114 (1957).†

21. G. R. Irwin, "Fracture Mechanics," in *Structural Mechanics*, Pergamon Press, New York, 1960.

22. J. Hutchinson, "Singular Behavior at the End of a Tensile Crack in a Hardening Material," *J. Mech. Phys. Solids* 16, 13–31 (1968).†

23. J. R. Rice and G. F. Rosengren, "Plane Strain Deformation Near a Crack Tip in a Power- Law Hardening Material," *J. Mech. Phys. Solids* 16, 1–12 (1968).†

24. J. A. Begley and J. D. Landes, "The J Integral as a Fracture Criterion," in *Fracture Toughness*, ASTM STP 514, 1–23 (1972).†

25. S. G. Larsson and A. J. Carlsson, "Influence of Non-Singular Stress Terms and Specimen Geometry on Small-Scale Yielding at Crack Tips in Elastic-Plastic Materials," *J. Mech. Phys. Solids* 21, 263–277 (1973).†

26. N. P. O'Dowd and C. F. Shih, "Family of Crack-Tip Fields Characterized by a Triaxiality Parameter: Part I—Structure of Fields," *J. Mech. Phys. Solids* 39, 989–1015 (1991).†

27. G. R. Irwin, "Fracture Mode Transition for a Crack Traversing a Plate," *J. Basic Eng.* 82(2), 417–425 (1960).†

28. J. G. Merkle, Martin Marietta Energy Systems, Inc., Oak Ridge Natl. Lab., "An Examination of the Size Effects and Data Scatter Observed in Small-Specimen Cleavage Fracture Toughness Testing," USNRC Report NUREG/CR-3672 (ORNL/TM-9088), August 1984.*

29. R. O. Ritchie, J. F. Knott, and J. R. Rice, "On the Relationship Between Critical Tensile Stress and Fracture Toughness in Mild Steel," *J. Mech. Phys. Solids* 21, 395-410 (1973).†

30. A. McClintock, "A Criterion for Ductile Fracture by the Growth of Holes," *J. Appl. Mech.* 35, 363-371 (1968).†

31. J. W. Hancock and A. C. MacKenzie, "On the Mechanisms of Ductile Fracture in High-Strength Steels Subjected to Multi-Axial Stress-States," *J. Mech. Phys. Solids* 24, 147–169 (1976).†

32. D. M. Parks, "Interpretation of Irradiation Effects on the Fracture Toughness of a Pressure Vessel Steel in Terms of Crack Tip Stress Analysis," *Journal of Engineering Materials and Technology* 98, 30–36 (1976).†

33. R. O. Ritchie, W. L. Server, and R. A. Wullaert, "Critical Fracture Stress and Fracture Strain Models for the Prediction of Lower and Upper Shelf Toughness in Nuclear Pressure Vessel Steels," *Met. Trans. A*, 10A, 1557–1570 (1979).†

34. R. A. Wullaert and W. L. Server, "Small Specimen Predictions of Fracture Toughness for Nuclear Pressure Vessel Steels," *Nucl. Eng. Des.* 57, 153–173 (1980).†

35. J. Heerens and D. T. Read, "Fracture Behavior of a Pressure Vessel Steel in the Ductile to Brittle Transition Region," National Institute of Standards and Technology, NISTIR 88/3099 (PB89-189195/AS), December 1988.

36. S. G. Druse, G. P. Gibson, and M. Capel, "Microstructural Control of Cleavage Fracture in an A508 Class 3 Pressure Vessel Steel," paper presented at the 22nd National Symposium on Fracture Mechanics, Atlanta, Georgia, June 26-28, 1990.

37. T. L. Anderson and R. H. Dodds, Jr., "Specimen Size Requirements for Fracture Toughness Testing in the Transition Region," Report MM-6585-90-5, Mechanics and Materials Center, Texas A&M University, College Station, Texas, May 1990.

38. J. Keeney-Walker, B. R. Bass, and J. D. Landes, Martin Marietta Energy Systems, Inc., Oak Ridge Natl. Lab., "An Investigation of Crack-Tip Stress-Field Criteria for Predicting Cleavage-Crack Initiation," USNRC Report NUREG/CR-5651 (ORNL/TM-11692), September 1991.*

39. D. J. Naus et al., Martin Marietta Energy Systems, Inc., Oak Ridge Natl. Lab., *Crack-Arrest Behavior in SEN Wide Plates of Quenched and Tempered A 533 Grade B Steel Tested Under Nonisothermal Conditions*, USNRC Report NUREG/CR-4930 (ORNL-6388), August 1987.*

40. G. R. Irwin, University of Maryland for Martin Marietta Energy Systems, Inc., Oak Ridge Natl. Lab., "Use of Thickness Reduction to Estimate Values of K," USNRC Report NUREG/CR-5697 (ORNL/TM-11581), October 1991.*

41. D. J. Naus et al., Martin Marietta Energy Systems, Inc., Oak Ridge Natl. Lab., "High-Temperature Crack-Arrest Behavior in 152-mm-Thick SEN Wide Plates of Quenched and Tempered A 533 Grade B Class 1 Steel," USNRC Report NUREG/CR-5330 (ORNL/TM-11083), April 1989.*

42. D. E. McCabe and J. D. Landes, "The Effect of Specimen Plan View Size and Material Thickness on the Transition Temperature Behavior of A533B Steel," Research Report 80-1D3-REVEM-R2, Westinghouse R&D Center, November 1980.

43. R. deWit, R. J Fields, and G. R. Irwin, "Use of Thickness Reduction to Estimate Fracture Toughness," paper presented at the ASTM Symposium on Constraint Effects in Fracture, Indianapolis, Ind., May 8–9, 1991.

---

*Available for purchase from National Technical Information Service, Springfield, VA 22161.

†Available in public technical libraries.

‡Available from American National Standards Institute, 1430 Broadway, New York, NY 10018. Copyrighted.

APPENDIXES

Appendix A

Two-Parameter Fracture Methods Involving T-Stress and Q-Stress

D. K. M. Shum

A.1 Introduction

A growing consensus within the fracture-mechanics community is that two-parameter methods, which incorporate the higher-order term T-stress and Q-stress, may provide the technical basis for addressing the shortcomings of conventional one-parameter fracture correlation methods. These shortcomings include apparent size effects on fracture toughness and the limited success associated with the transferability of small-specimen toughness data to large-scale structural applications. In this appendix the motivations and fundamentals of two-parameter methods involving the higher-order term T-stress and Q-stress are briefly reviewed. In this report two-parameter methods have been applied to the prediction of crack initiation in Appendix C and to the analysis of the proposed biaxial fracture specimen in Appendix G.

A.2 Current Status of One-Parameter Methods

Application of linear-elastic and elastic-plastic fracture mechanics (LEFM and EPFM) theories to the analysis of RPVs has traditionally been focused on the evaluation of the J-integral associated with a particular flaw geometry under specified loading conditions. Under LEFM conditions, well-known relations exist between J and the stress-intensity factor K for both plane strain and plane stress conditions. From theoretical considerations it is known that in cases for which J is an appropriate correlation parameter, the crack-tip-opening displacement (CTOD) can also be used in an interchangeable fashion. Thus, the parameters K, J, and CTOD form the basis of conventional one-parameter fracture correlation methods.[1,2]

Fundamental to the development of one-parameter methods is the understanding that restrictions in terms of geometry, loading conditions, and material properties exist to limit their general applicability. This understanding forms part of the motivation behind the establishment of various standardized small-specimen testing methods from which experimental data are obtained for structural applications. Research efforts have been devoted toward the determination of testing conditions that would ensure that small-specimen test results are obtained within the domain appropriate to the application of the one-parameter theories.[3–5] These efforts include detailed finite-element calculations of the crack-tip fields in various small-scale specimens and rather precise definitions of "valid" test conditions with respect to the determination of plane strain fracture toughness. Consideration of three-dimensional (3-D) effects in small-scale specimens is similarly phrased in terms of "nearness" to plane strain or plane stress "constraint" conditions describable by one-parameter theories.

In contrast to the research efforts focused on small-scale specimens, it is significant to note that the appropriateness of using one-parameter approaches in structural applications has generally been taken for granted. There have been very limited attempts to determine accurately the crack-tip fields in structural applications and to assess the utility of conventional one-parameter concepts in light of the structural application. Existing analysis methods postulate that one-parameter methods provide sufficient information for correlating or determining the fracture response of an engineering structure such as an RPV. This assumption has resulted in the acceptance of fracture data obtained from small-scale fracture specimens as generally appropriate in evaluating the fracture behavior of an RPV. Constraint effects, or possible deviation of RPV fracture responses from those of small-scale fracture specimens, are considered only in the context of attempts to characterize this deviation as a phenomenon between plane strain to plane stresslike crack front conditions within one-parameter theories.

A.3 Motivation for Two-Parameter Fracture Mechanics Approaches

Apparently potential deviation of RPV constraint from that of small-scale specimens under nominally plane strain conditions may be the manifestation of a more general phenomenon in which the cause of deviation is "in-plane" in nature. More to the point, it has been analytically demonstrated that, for a wide range of flaw geometries under nominally plane strain conditions, substantial variation in constraint can still result due to in-plane effects.[6–8] This type of deviation can also occur under conditions of plane stress. These in-plane effects have been referred to as T-stress or Q-stress effects, and the parameters T and Q, along with K and J, have been proposed as the basis of

emerging two-parameter fracture methods. Two example applications for which one-parameter methods may not uniquely characterize fracture are briefly described in the following sections.

A.3.1 Shallow-Flaw Fracture Toughness

Current attempts to determine "shallow-flaw" fracture toughness, from both theoretical and experimental standpoints, in part grow out of the recognition that one-parameter methods are inadequate in this instance. Available experimental data suggest that, for some materials, initiation of shallow flaws may occur under conditions of "enhanced" shallow-flaw toughness; magnitude of K or J necessary to initiate a shallow flaw can be, on average, up to a few times larger than the conventional small-specimen toughness value.[9–10] This size effect can take the form of crack length to remaining ligament ratio effect, the a/W effect, for a specimen of fixed plane form. An example of a shallow flaw in this context is one with a ratio of a/W = 0.1. Alternately, this size effect can take the form of a scaling effect for a given specimen type where all length dimensions of a specimen are fixed in their ratios to one another. An apparent increase in fracture toughness would then occur as the *absolute* dimension of the specimen is decreased.

An issue in the experimental determination of shallow-flaw fracture toughness is whether this shallow-flaw effect is dependent on the absolute crack size or the relative crack size. Limited analytical studies suggest that it might be necessary to consider a two-parameter description of the near-crack-tip fields that incorporates the effects of the higher-order term (T- or Q-stress, where appropriate) in an approximate description of the full-field solution associated with a shallow-flaw geometry. It is recognized that for some combination of flaw size and material behavior the near-crack-tip fields are not amendable to even a two-parameter characterization.

In view of the potential toughness enhancement due to shallow-flaw effects, an example structural application is given next for which two-parameter methods may be applicable. The structural application is in the area of probabilistic fracture mechanics safety assessment of an RPV subject to a hypothetical pressurized-thermal-shock (PTS) transient.[11]

A.3.2 Safety Assessment Under PTS Conditions

The prediction of vessel failure probability is dependent on a large number of parameters such as vessel geometry, loading conditions, and material properties.[11] A particularly significant analysis variable is the assumed initial flaw size distribution. Current probabilistic fracture mechanics analysis procedures assume an initial flaw population that is predominantly comprised of short flaws of lengths <13 mm (0.5 in.), relative to typical wall thicknesses on the order of 200 mm (8 in.) for an RPV. In the terminology of small-specimen testing, this corresponds to an a/W ratio of ~0.06. Analysis results suggest that when the loading conditions simulate the occurrence of a small-break loss-of-coolant accident (SBLOCA), the population of flaw sizes most susceptible to initiation that lead directly to failure are those that congregate near the inner surface of an RPV and are of a depth <13 mm. However, the majority of vessel failure scenarios are due to the arrest and reinitiation of initially shallow flaws that lead to ultimate vessel failure.

Prediction of the probability of vessel failure is based in part on the use of the ASME lower-bound K_{Ic} and K_{Ia} curves to represent the toughness of the RPV material.[12] The ASME lower-bound curves are based primarily on small-specimen data that were generated under essentially one-parameter dominant conditions. For the type of shallow flaws considered in the above example, the existence of K- or J-dominant, one-parameter crack-tip fields would be dependent on the elastic-plastic behavior of the vessel material. Based on available experimental and analytical results, shallow-flaw effects cannot be ruled out. Currently, the potential benefits of enhanced shallow-flaw toughness that would act to prevent initiation of shallow flaws that (1) lead directly to vessel failure and (2) lead eventually to vessel failure are not considered. A refined treatment of RPV safety assessment is likely to involve improved understanding of two-parameter effects from both analytical and experimental perspectives.

A.4 Definition of T-Stress

Within the context of LEFM, the asymptotic two-dimensional (2-D) near-crack-tip fields, as a function of position relative to the crack tip, can be expressed in the form of an infinite series. Let (r,θ) denote the position of a material point relative to the crack tip in polar coordinates. The infinite series denoting the Mode I stress components then takes the form

$$\sigma_{ij} = \frac{K_I}{\sqrt{2\pi r}} \tilde{\sigma}_{ij}(\theta) + T\,\delta_{1j}\,\delta_{i1} + \ldots . \quad (A.1)$$

where $\tilde{\sigma}_{ij}(\theta)$ are functions dependent on the angular coordinate θ only. These infinite series are commonly referred to as the Irwin-Williams series.[13,14] The first terms in these series become unbounded as the crack tip is

approached. The stress-intensity factor K is the amplitude of the first term in these series, and its value is undetermined from the asymptotic expansion.

The T-stress term is merely the next higher-order term in the series expansion for the opening-mode stress component. The T-stress term describes a stress field that is independent of position relative to the crack front and represents a uniform stress field parallel to the plane of the idealized 2-D crack. Within the context of 3-D LEFM, the Irwin-Williams asymptotic expansion concept can be generalized, resulting in three T-stresslike terms.[15,16]

A.5 Definition of Q-Stress

Within the context of EPFM, the counterpart to the Irwin-Williams series in 2-D is the HRR solution for deformation-theory material, for which the uniaxial stress-strain relation is of the Ramberg-Osgood form.[17,18] The infinite series denoting the Mode I stress components have the form

$$\sigma_{ij} = \sigma_o \left(\frac{J}{\alpha \sigma_o \varepsilon_o I_n r} \right)^{\frac{1}{n+1}} \tilde{\sigma}_{ij}(\theta) + \ldots , \quad (A.2)$$

where $\tilde{\sigma}_{ij}(\theta)$ are again functions dependent on the angular coordinate θ only. In the HRR solution, the first terms are also singular with an amplitude undetermined from the asymptotic analysis. In this case the undetermined amplitude corresponds to the value of the J-integral. Since the J-integral is path-independent for all deformation-theory material, its value can be evaluated from locations remote from the crack front. It is the path-independence of the J-integral, and its identification with the amplitude of the HRR field, that forms the basis of conventional one-parameter EPFM theory.

In a manner somewhat analogous to T-stress, the Q-stress term[7] plays the role of a higher-order term in the HRR expansion in the sense that the Mode I stress components in these series are assumed to take the form

$$\sigma_{ij} = \sigma_o \left(\frac{J}{\alpha \sigma_o \varepsilon_o I_n r} \right)^{\frac{1}{n+1}} \tilde{\sigma}_{ij}(\theta) + Q \sigma_o \delta_{ij} + \ldots$$

$$\text{for } |\theta| < \pi/2 \ . \quad (A.3)$$

Unlike the T-stress term, the Q-stress term is not an analytic consequence of the asymptotic expansion. Instead, use of the Q-stress term in the context of Eq. (A.3) follows from the following numerical observation. Detailed finite-element analyses performed for power-law hardening materials indicate that the near-crack-tip solutions appear to be consistent with the assumed expansion indicated in Eq. (A.3).[7] This assumed form generally applies only to the forward sectors symmetric about the crack plane ahead of the crack tip, extending approximately 90° to either side of the crack plane. Consequently, the utility of a Q-stress description of the near-crack-tip fields requires that the physical micromechanisms of fracture be confined within the forward sectors. The Q-stress term is readily understood as a state of 2-D hydrostatic stress superimposed on the HRR solution. Under conditions for which the T-stress can be defined, the Q-stress is related to the T-stress. Figure A.1 (from Ref. 7) illustrates this relationship for two values of the exponent in the definition of a power-law hardening material. The methodology for extending the Q-stress concept into 3-D fracture analysis is still an open issue.

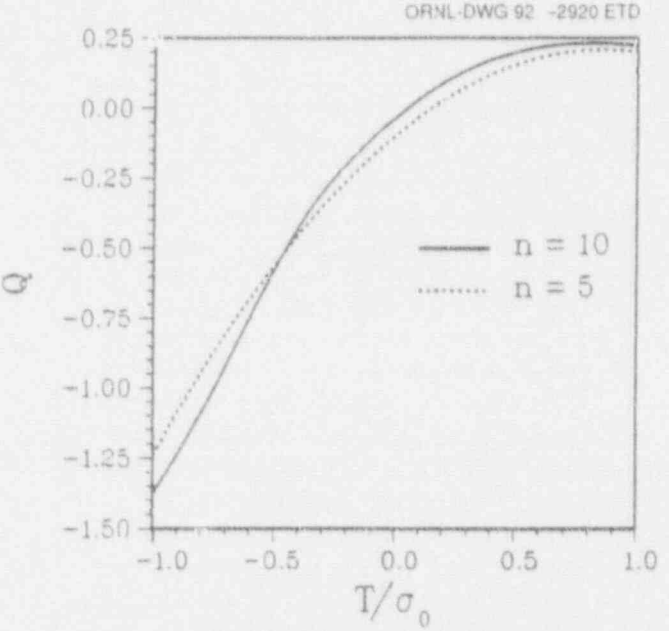

Figure A.1 Relationship between Q-stress and T-stress for two power-law hardening materials

Due to the numerical nature of its definition, determination of the Q-stress term is not without ambiguity. In its original development, the Q-stress term was defined as the difference between the full-field stress solution (to be explained shortly) of a given problem and the reference HRR stress solution along the crack plane. The stress solutions are obtained using finite-strain theory. It is observed that the Q-stress parameter thus determined is nearly constant over a distance up to 5 J/σ_o ahead of the original crack tip for the various stress components. Definition of the Q-stress term is made more precise by identifying Q-stress as the difference between the opening-mode stress component of the full-field and reference solutions at a distance of 2 J/σ_o

ahead of the crack front. A limitation with this approach is that HRR solutions are available only for cases of idealized pure power-law material models.

A more recent approach[19] is to define a second form for the Q family of fields using the Q = 0 solution as the reference solution:

$$\sigma_{ij} = \left(\sigma_{ij}\right)_{Q=0} + Q\sigma_0\delta_{ij} \quad \text{for } |\theta| < \frac{\pi}{2} \quad . \qquad (A.4)$$

Here, the Q = 0 solution is the small-scale yielding (SSY) solution (to be explained). The Q-stress term is then defined as the difference between the opening-mode stress component of the full-field distribution and the corresponding quantity in the associated SSY problem at a distance of $2\,J/\sigma_0$ ahead of the crack front using finite-strain theory. This approach has the advantage that it admits a more general representation of a material's stress-strain behavior.

Shih* has presented an interpretation of the two-parameter J-Q theory that spans the range of stress states extending from linear-elastic through elastic-plastic conditions. In this interpretation, J is a measure of the deformation that scales the size of the process zone, while Q scales the triaxiality level ahead of the crack tip. For essentially LEFM conditions, the deformation fields and triaxiality are tightly coupled, so that the imposition of tensile or compressive out-of-plane stresses can affect triaxiality. Under conditions of substantial plastic deformation, however, the deformation fields and stress triaxiality are independent parameters, with triaxiality being affected only by the imposition of a state of pure hydrostatic stress.

A.6 Full-Field and Modified-Boundary-Layer Solutions

The concepts of modified-boundary-layer (MBL) and full-field solutions provide the basis for understanding the relationship between conventional one-parameter fracture correlation methods and the two-parameter methods discussed previously. In addition, these concepts provide the framework for understanding the relationship between T-stress and Q-stress, and the conditions under which T-stress and/or Q-stress can be rigorously applied to the analysis of a fracture problem. Furthermore, these concepts can be used to gage the merits of various T-stress and Q-stress estimation schemes. In the following discussion, these concepts are first illustrated in the context of conventional one-parameter methods. Extension of these concepts in the context of two-parameter methods would then be self-evident.

A.6.1 Full-Field Solutions

Implicit to the application of one-parameter fracture methods to engineering structures containing finite-length flaws is the assumption concerning the existence of either a K- or J-annulus surrounding the crack-tip region. This assumption is equivalent to the idea that an annular region surrounding the crack tip can be located for which the totality of the influence of geometry, material behavior, and loading conditions can be adequately expressed in terms of an applied K or J value that characterizes the magnitude of the near-crack-tip fields acting upon this region. In addition, the size of the annular region needs to be sufficiently large, in comparison to relevant microstructural parameters such as the grain size, to ensure that a continuum, homogeneous description using the parameter K or J is physically meaningful. These fundamental assumptions form the basis of transferability of fracture toughness data obtained in small-scale fracture specimens to large-scale structural applications.

Inherent to these assumptions is the fact that limitations exist regarding the utility of these one-parameter approaches. For a given application, the full-field solutions are defined to be the stress and strain distributions within the structure obtained by explicitly considering the influence of the finite geometry of the structure and the flaw. Only to the extent that the full-field solution in the neighborhood of the crack tip can be adequately approximated by an asymptotic one-term description of the crack-tip fields would the use of one-parameter concepts be meaningful. In general, however, the validity of this approximation is often not quantitatively verified due to the prohibitive numerical requirements associated with modeling both the near-crack-tip region and the global behavior of the structure. Instead, the path-independence of the J-integral is used to determine its value in a generally rough model of the structure, without verifying the existence of the assumed K- or J-annulus.

A.6.2 MBL Solutions

The numerical difficulties associated with a quantitative determination of both the near-crack-tip and the global stress and strain fields are resolved via the concept of a boundary-layer analysis.[20] In a boundary-layer analysis, one focuses on the near-crack-tip fields that result as a consequence of the global response of the structure. In the classic boundary-layer approach, the global effects are wholly accounted for via the imposition of a "remote" K-field on the associated fracture problem of a "semifinite"

*C. F. Shih, "J-Q Fracture Methodology," presented at the Workshop on Constraint Effects in Fracture, sponsored by U.S. Nuclear Regulatory Commission, Rockville, Md., March 3, 1992.

crack within an "infinite" continuum. The boundary-layer problem with remote K-field loading is also known as the SSY problem and is discussed in Appendix C of Ref. 21.

Because the establishment of various standardized small-specimen testing methods is motivated in part by the observation that, under some combination of material behavior, loading conditions, and specimen geometry, the near-crack-tip fields cannot be adequately described using one-parameter K- and J-annulus concepts. The hypothesis that the observed deviation from one-parameter fields can be explained by incorporating an elastic T-stress contribution to the one-parameter approximation was first verified using the MBL approach.[15,16,22]

In an MBL approach, the remote loading of the SSY boundary-layer method is modified to include both K- and T-stress contributions. It is observed that, for a given material, the imposition of a nonzero value of the T-stress results in near-crack-tip fields that differ from the SSY fields in a predictable manner, regardless of the associated value of K. The near-crack-tip fields are dependent on the value of T only and are independent of the value of K specified in the analysis; on the other hand, value of the J-integral is dependent on the applied value of K only.

It has since been reported[6–8] that for a wide range of small-specimen geometries and loading conditions for which one-parameter methods have long been recognized to be inadequate, the observed deviations from SSY solutions can be characterized in terms of the T-stress and the Q-stress term. Consequently, it has been proposed that the conventional concept of fracture toughness in terms of a critical *value* of K or J can be extended, in a two-parameter approach, in the form of a fracture *locus* involving combinations of K or J and T or Q (see Fig. A.2).

In view of the full-field discussion, it is emphasized that the utility of these two-parameter approaches is also limited. Only to the extent that the full-field solutions in the neighborhood of the crack tip can be adequately approximated by an asymptotic two-term description of the crack-tip fields would the use of two-parameter concepts be meaningful. Additionally, it is necessary to ensure that the two-parameter annular region extends over a physically significant region surrounding the crack tip. For example, use of the elastic K-T concept in a structural application is strictly meaningful only if a K-T annulus surrounds the crack tip. With the onset of plasticity and its interaction with the geometry of the structure, the elastic K-T annulus would eventually be replaced by the elastic-plastic J-Q annulus under increasing applied load. Presumably, for some combination of material behavior and geometry, the J-Q annulus would cease to exist beyond some critical loading conditions.

A.7 Intensity vs Energy Approach

It is evident from the above discussion that one- and two-parameter fracture methods are based on the concept of characterizing the "intensity" of the near-crack-tip fields; therefore, it is inappropriate to suggest that these methods can also be understood in terms of an "energy" approach.

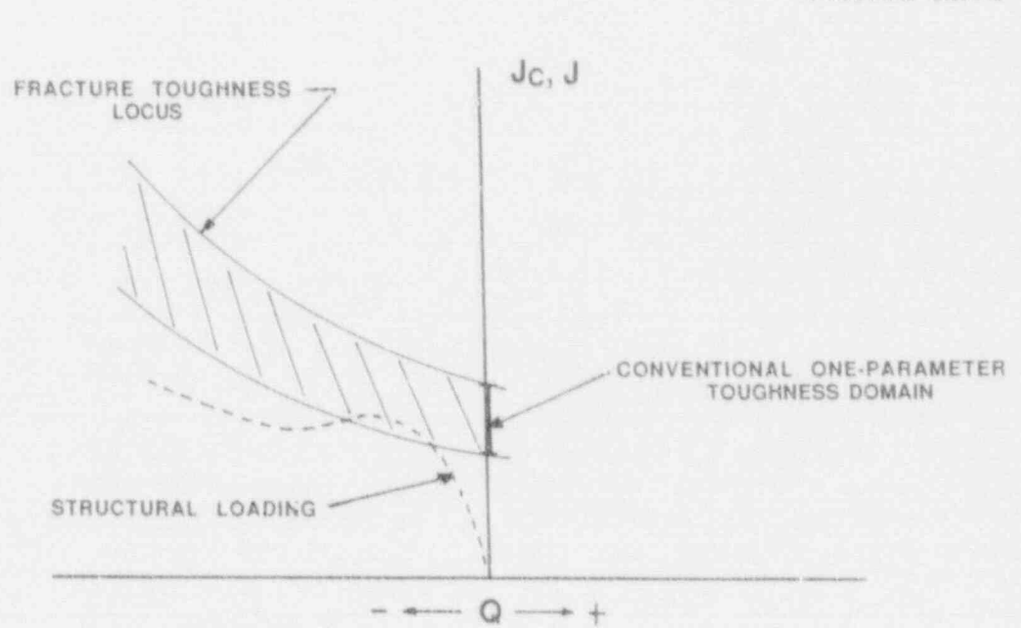

Figure A.2 Representation of J-Q fracture toughness locus

Two-Parameter

The distinction between an intensity vs an energy approach is not a matter of semantics, but is of a fundamental nature relating to the concept of fracture toughness and its transferability to structural application.

A general framework for examining an energy-balance approach in the context of continuum fracture mechanics was presented in Ref. 23. In Ref. 23 many erroneous ideas concerning energy-balance approaches are also discussed. The need to clearly understand that an energy-balance idea is inappropriate in the context of these one- and two-parameter fracture methods is also clearly expressed by Hutchinson.[24]

> Tempting though it may be, to think of the criterion for initiation of crack growth based on J as an extension of Griffith's energy-balance criterion, it is nevertheless incorrect to do so. This is not to say that an energy balance does not exist, just that it cannot be based on the deformation theory J.

A.8 References

1. S. T. Rolfe and J. M. Barsom, *Fracture and Fatigue Control in Structures: Applications of Fracture Mechanics*, Prentice-Hall Inc., Englewood, N.J., 1977.

2. M. F. Kanninen and C. H. Popelar, *Advanced Fracture Mechanics*, Oxford University Press, New York, 1985.

3. J. A. Begley and J. D. Landes, "The J Integral as a Fracture Criterion," in *Fract. Tough.*, ASTM STP 514, 1–23 (1972).*

4. R. M. McMeeking and D. M. Parks, "On Criteria for J Dominance of Crack Tip Fields in Large Scale Yielding," ASTM STP 668, 175–194 (1979).*

5. C. F. Shih and M. D. German, "Requirements for a One Parameter Characterization of Crack Tip Fields by the HRR Singularity," *Int. J. Fract.* 17, 27–43 (1981).*

6. A. M. Al-Ani and J. W. Hancock, "J-Dominance of Short Cracks in Tension and Bending," *J. Mech. Phys. Solids* 39, 23–43 (1991).*

7. N. P. O'Dowd and C. F. Shih, "Family of Crack-Tip Fields Characterized by a Triaxiality Parameter: Part I—Structure of Fields," *J. Mech. Phys. Solids* 39, 989–1015 (1991).*

8. W. A. Sorem, R. H. Dodds, Jr., and S. T. Rolfe, The University of Kansas, "An Analytical Comparison of Short Crack and Deep Crack CTOD Fracture Specimens of an A36 Steel," WRC Bulletin 351, Welding Research Council (1990).*

9. J. D. G. Sumpter and J. W. Hancock, "Shallow Crack Toughness of HY80 Welds: An Analysis based on T Stresses," *Int. J. Pres. Ves. & Piping* 45, 207–221 (1991).*

10. T. J. Theiss and J. W. Bryson, "Influence of Crack Depth on the Fracture Toughness of Reactor Pressure Vessel Steel," paper presented at the *ASTM Symposium on Constraint Effects in Fracture*, Indianapolis, Ind., May 8–9, 1991.

11. D. L. Selby et al., Martin Marietta Energy Systems, Inc., Oak Ridge Natl. Lab., "Pressurized Thermal Shock Evaluation of the H.B. Robinson Unit 2 Nuclear Power Plant," USNRC Report NUREG/CR-4183 (ORNL/TM-9567/V1 and V2), September 1985.†

12. 1989 ASME Boiler and Pressure Vessel Code, Section XI, "Rules for Inservice Inspection of Nuclear Power Plant Components."‡

13. M. L. Williams, "On the Stress Distribution at the Base of a Stationary Crack," *J. Appl. Mech.* 24, 109–114 (1957).*

14. G. R. Irwin, "Fracture Mechanics," in *Structural Mechanics*, Pergamon Press, New York, 1960.

15. J. R. Rice, "Limitations to the Small Scale Yielding Approximation for Crack Tip Plasticity," *J. Mech. Phys. Solids* 22, 17–26 (1974).*

16. D. M. Parks, "Three-Dimensional Aspects of HRR-Dominance, Defect Assessment in Components—Fundamentals and Applications," pp. 205–231 in *Proceedings of the European Symposium on Elastic-Plastic Fracture Mechanics*, ESIS/EGF Publication 9, 1968.*

17. J. W. Hutchinson, "Singular Behavior at the End of a Tensile Crack in a Hardening Material," *J. Mech. Phys. Solids* 16, 13–31 (1968).*

18. J. R. Rice and G. F. Rosengren, "Plane Strain Deformation Near a Crack Tip in a Power-Law Hardening Material," *J. Mech. Phys. Solids* 16, 1–12 (1968).*

19. N. P. O'Dowd and C. F. Shih, "Family of Crack-Tip Fields Characterized by a Triaxiality Parameter: Part II—Fracture Applications," *J. Mech. Phys. Solids* 39 (1991).

20. J. R. Rice, "Mathematical Analysis in the Mechanics of Fracture," in *Fracture: An Advanced Treatise*, H. Liebowitz, Ed. (Academic Press, New York, 1968), Vol. II, pp. 191–311.

21. T. J. Theiss, D. K. M. Shum, and S. T. Rolfe, Martin Marietta Energy Systems, Inc., Oak Ridge Natl. Lab., "Interim Report on the HSST Shallow-Crack Program and Implications for Reactor Pressure Vessel Analyses," USNRC Report NUREG/CR-5886 (ORNL/TM-12115), June 1992.

22. S. G. Larsson and A. J. Carlsson, "Influence of Non-Singular Stress Terms and Specimen Geometry on Small-Scale Yielding at Crack Tips in Elastic-Plastic Materials," *J. Mech. Phys. Solids* 21, 263–277 (1973).*

23. J. R. Rice, "An Examination of the Fracture Mechanics Energy Balance from the Point of View of Continuum Mechanics," pp. 309–340 in *Proceedings of the 1st International Congress on Fracture (Sendai, 1965)*, (T. Yokobori et al., Eds.), *Japanese Society for Strength and Fracture*, Tokyo, Vol. 1, 1966.*

24. J. W. Hutchinson, "Fundamentals of the Phenomenological Theory of Nonlinear Fracture Mechanics," *J. App. Mech.* 50, 1042–1051, 1983.*

*Available in public technical libraries.
†Available for purchase from National Technical Information Service, Springfield, VA 22161.
‡Available from American National Standards Institute, 1430 Broadway, New York, NY 10018, copyrighted.

Appendix B

Fracture Model Development

D. K. M. Shum

The development of predictive fracture models is complementary to the gathering of experimental fracture data. Validation of proposed fracture models within an accepted data base provides the necessary means for understanding the causes of fracture behavior in small-scale fracture specimens and, by extension, to structural applications. More importantly, validated fracture models can then, in turn, be used to provide fracture predictions in cases where experimental data are unavailable or impractical to obtain. A validated fracture model can be used to determine an appropriate testing matrix by identifying the relevant test parameters. The focus of the present investigation, namely determining the effects of transverse strain on crack initiation is a good example of the role that predictive fracture models can play in reactor pressure vessel (RPV) safety evaluation.

B.1 Candidate Fracture Toughness Prediction Models

In the following discussion, the Ritchie-Knott-Rice (RKR) model[1] is adopted for the prediction of cleavage fracture, and the McClintock-Hancock-MacKenzie (MHM) model[2,3] is adopted for the prediction of ductile fracture. These two models are chosen because they have been applied to A 533 B material with some success in the lower-transition and upper-shelf regions, respectively, under nonirradiated and irradiated conditions.[4–6] Successful application of the RKR model to the analysis of fracture in the lower-shelf and in the ductile-to-brittle transition region for 20MnMoNi55, an RPV-grade steel, is also noted.[7] On the other hand, some recent investigations appear to cast doubt on the applicability of the RKR model to A 508 Class 3, another RPV-grade steel, in the lower-shelf and transition regions.[8]

A key simplifying feature of these predictive fracture models is that they are one-dimensional (1-D) in nature. That is, the attainment of a critical condition for fracture is phrased in terms of stress and strain quantities evaluated directly ahead of a two-dimensional (2-D) crack front along the crack plane. Another key simplifying feature is that the statistical nature of fracture, which is particularly evident under cleavage failure conditions, is not considered. These models are also phenomenological in nature because they describe the conditions necessary for crack initiation in continuum terms, without providing an explanation for the underlying micromechanical process for fracture. Fracture models that incorporate, to varying degrees of sophistication, statistical and micromechanical aspects of cleavage and ductile failure are available in the literature.[9–16] However, in view of the limited validation of fracture models with respect to RPV-grade materials, adoption of the simple RKR and MHM models in the present study is deemed justified.

With reference to the objective of this study (namely, determining the potential toughness deviation due to transverse straining), it is noted that validation of the RKR and the MHM models in the references cited above is in the sense that these models have been successfully applied toward predicting the overall temperature dependence of small-specimen fracture toughness data. Scatter of both the toughness data and the magnitude of the induced transverse strain at a given temperature is not explicitly considered. A discussion on this scatter and its relevance toward the validation of a predictive fracture model is presented in Appendix F.

However, it is noted that the experimental data employed in these validations were obtained using small-scale specimens, such as 1T compact-tension (CT) specimens in the case of Refs. 1 and 7, and a range of 1T-CT to 11T-CT specimens in Refs. 4–6. Based on the results to be presented in Appendixes E and F, the magnitude of the induced transverse contraction strain at fracture associated with 1T-CT specimens is on the order of the yield strain. In the absence of toughness data obtained under prescribed negative transverse straining, these studies could be viewed as providing validation of the RKR and the MHM models under moderate relaxation from plane strain constraint conditions. Because the state of tensile transverse straining appropriate to RPV discussions is on the order of the yield strain, it appears reasonable to employ these models to evaluate the effects of transverse strain (positive or negative) on the order of the yield strain on fracture toughness.

The RKR and the MHM fracture models hypothesize that crack initiation can be expressed in terms of the attainment of critical values of global stress and strain measures determined from a continuum elastic-plastic fracture analysis. The RKR model hypothesizes that cleavage fracture under Mode I conditions is governed by the attainment of a temperature-independent critical level of opening-mode stress over a minimum physical distance ahead of the crack front.

The minimum physical distance necessary for cleavage fracture is often identified with the distance from the original crack front to cleavage-initiation sites. It has been suggested in Ref. 7 that both the steep gradient and the scatter in fracture toughness that are characteristic of the transition region can be attributed to the experimentally observed scatter in cleavage-initiation sites, thereby providing further justification for using the RKR model for examining cleavage fracture. However, available data suggest that both the nature and location of the cleavage-initiation sites, for example, vary considerably for nominally identical RPV-grade materials.[7,8] Consequently, a proper consideration of the micromechanics of fracture is an integral element in the application of this fracture model. Again, it must be emphasized that the statistical nature of cleavage fracture is not explicitly considered by the present application of the RKR model.

The MHM model hypothesizs that ductile fracture is governed by the attainment of a critical level of Mises effective plastic strain ε_e subject to an associated critical level of stress state expressed in terms of the hydrostatic to effective stress ratio σ_m/σ_e. Similar to the RKR model, the MHM model also requires that this critical condition be achieved over a minimum physical distance ahead of the crack front. The minimum physical distance necessary for ductile fracture is less well defined. This minimum distance has been identified with the minimum size of a region that could accommodate the micromechanical processes of void nucleation, coalescence, and growth that are associated with ductile fracture or plastic-flow localization.

Within the context of these two simple models of fracture, experimental observations of a transition from brittle to ductile failure mode, either as a function of test temperature or constraint, is presumed to be a consequence of the competing micromechanisms for fracture expressed by these two fracture models. Analytical prediction of this transition that takes into account T-stress effects has been attempted with some success.[17]

As discussed above, the RKR and MHM predictive fracture models provide a relation between experimentally obtained fracture toughness values, such as a critical value of K or J, with more "fundamental" material failure parameters in terms of global stress and strain measures and a critical material distance. The utility of these more fundamental material parameters is that they can, in principle, be determined experimentally, so that these parameters provide the basis for "fine-tuning" a predictive model to fit observed fracture toughness data. While much work has been devoted to the development of these fracture models, and to the identification of the associated fundamental material parameters, a surprising lack of activity has been related to the experimental determination of the magnitude of these critical material parameters. As will be evident shortly, the uncertainty regarding the critical values of these material parameters is reflected in the necessity to assume values for these parameters in the application of various fracture models in this study. Clearly, further development of the fracture models employed in this study awaits the experimental determination of the critical values associated with the various material failure criteria.

B.2 Requirement for Critical Distance Parameter

The common requirement of a minimum physical distance over which the failure criterion is met for both the RKR and the MHM models is a consequence of the observation that, in fracture problems, a critical value of stress or strain measure can usually be achieved ahead of a crack front, even for infinitesimal load levels. This observation is a consequence of the self-similar nature of crack-tip fields with respect to a given combination of loading and nondimensional distance ahead of the crack front. The self-similar nature of the crack-tip fields is observed for both linear-elastic fracture mechanics (LEFM) and elastic-plastic fracture mechanics (EPFM) fields under one-parameter (K,J) or two-parameter (K-T,J-Q) dominance conditions. In addition, this self-similarity is observed under small-strain assumptions (sharp crack), as well as large-strain (finite initial root radius) assumptions. The requirement of a minimum distance thus precludes the use, in fracture applications, of ductile failure models (such as the ones discussed in Refs. 18 and 19) that express the material failure conditions solely in terms of stress and strain measures.

B.3 Sample Calculations for Irradiation-Induced Toughness Degradation

The methodology to use the RKR and MHM models to examine the effects of out-of-plane strain on crack initiation, to be discussed in Appendixes C and G, is illustrated by the following example. Quantitative predictions of cleavage fracture for an irradiated RPV-grade material are obtained for conditions of small-scale yielding (SSY) based on reported critical values of the various material parameters in the lower-transition region.[4–6] Limited experimental data for Heavy-Section Steel Technology (HSST) Plate 02 (A 533 B) suggest that the critical cleavage stress is on the order of 1700 to 1800 MPa. The corresponding minimum critical distance to cleavage-initiation sites that best fits small-specimen data is on the order of 50 to 100 μm. It is assumed that irradiation does not affect the critical value of these material failure parameters.

Therefore, it is emphasized that these critical values need to be viewed as approximate in nature.

For an assumed lower-shelf irradiation-elevated yield stress of 620 MPa, a critical cleavage stress of 1800 MPa normalized with respect to the yield stress is ~2.9.* In the context of the RKR model, it is that portion of the stress distribution that decreases with increasing distance from the notch tip that is relevant to the prediction of fracture. Based on a range of critical distance parameters of 50 to 100 μm, the irradiation-degraded fracture toughness is predicted to be between 10.3 to 20.6 kN/m in terms of J, or between 44.7 and 63.2 MPa•$\sqrt{m}$ in terms of K, based on a Young's modulus of 193 GPa (28,000 ksi). This predicted irradiation-induced toughness degradation is consistent with experimental observations. Consequently, it is seen that the RKR model, while exceedingly simple in its present form, appears to provide toughness predictions that are consistent with observed toughness data.

As evident from the above example, quantitative determination of fracture toughness values using these simple fracture toughness prediction models requires that experimental data on critical material parameters be available for the material of interest. However, in predicting the amount of toughness *deviation* from standard ASTM-valid values due to out-of-plane strain or T-stress effects, for example, the reliance on the availability of experimental data for the various critical material parameters is lessened.

B.4 Application of the RKR Model to Fracture-Toughness Data from Large-Scale Experiments

The RKR model described in the previous sections was applied to fracture-initiation toughness data generated in the HSST Program from large-scale wide-plate experiments[20–24] and shallow-cracked beam tests.[25] One objective of these analyses was to validate the RKR model against specimens that are much larger than conventional laboratory specimens and more representative of RPV structural dimensions.

The HSST wide-plate experiments[20–24] utilized large plates with planar dimensions of 1 by 1 m and thicknesses of 0.1 or 0.15 m, to which long pull plates were welded to produce an assembly ~10 m long. The plate assembly was tested as a single-edge notched (SEN) tension specimen containing a sharp crack having a normalized depth of a/W ≈ 0.2. The WP-1 series[20,21] of experiments utilized plate specimens fabricated from good quality A 533 B steel (HSST Plate 13 A), while the WP-2 series[23–24] was based on a 2-1/4 Cr 1-Mo steel that had been specially heat treated to produce a low charpy upper-shelf energy. For most of the wide-plate specimens, the crack front region was cut into a chevron configuration to reduce the axial load required to achieve cleavage initiation in the lower transition region of the materials.

The shallow-crack beam tests[25] were performed to produce fracture toughness data that would quantify the relaxation of crack-tip constraint associated with shallow-crack geometries. Beam specimens were fabricated from A 533 grade B class 1 steel plate (HSST 13 B and WP-CE) with dimensions that varied from 40.6- to 86-cm (16- to 34-in.) length, 10.2-cm (4-in.) depth, and thicknesses of 5, 10, and 15 cm (2, 4, and 6 in.). Sharp cracks of depths 1 and 5 cm (0.4 and 2.0 in.) (a/W ≈ 0.1 and 0.5) were installed in the beams, which were then tested in three-point bend loading at temperatures corresponding to the lower shelf and the lower transition region of the plate material.

Finite-element analyses of the wide-plate and shallow-crack beam experiments were performed using loading conditions measured in the test. Full-field finite-strain solutions based on the plane strain assumptions were generated from models having a highly refined crack-tip region and a crack-tip profile with an initial root radius. As described in Appendix C, the finite initial root radius, which is much smaller than the outer dimensions of the mesh, facilitates numerical convergence of the solution. The full-field mesh and crack-tip profile used in analyses of the wide-plate specimens are depicted in Fig. B.1.

Results from application of the RKR prediction model to the WP-1 and -2 series of experiments are given in Figs. B.2 and B.3, respectively. Correlations of measured and predicted toughness for the two series of experiments based on the Q-stress parameter are expressed in terms of K-factors normalized by SSY values corresponding to initiation conditions. For the WP-1 series (Fig. B.2), toughness predictions are given for three values of the critical stress ratio, σ_c/σ_o = 2.2, 2.6, and 3.4, where σ_o = 465 MPa. For the WP-2 series (Fig. B.3), predictions are given for σ_c/σ_o = 3.6, 4.8, and 5.6, where σ_o = 250 MPa. For both series of experiments, the RKR model predictions fall substantially below the toughness values determined from analysis of the measured data.

Fracture toughness predictions from the RKR model for the shallow-cracked beam specimens are compared with measured toughness values in Fig. B.4. Predictions are given for four values of the critical stress ratio, σ_c/σ_o = 2.7, 3.0,

*With reference to Fig. C.8, the critical cleavage stress is exceeded over a distance $\leq 3J/\sigma_o$ for the case of $\varepsilon_z = 0$ (plain strain, SSY).

ORNL-DWG 92-2880 ETD

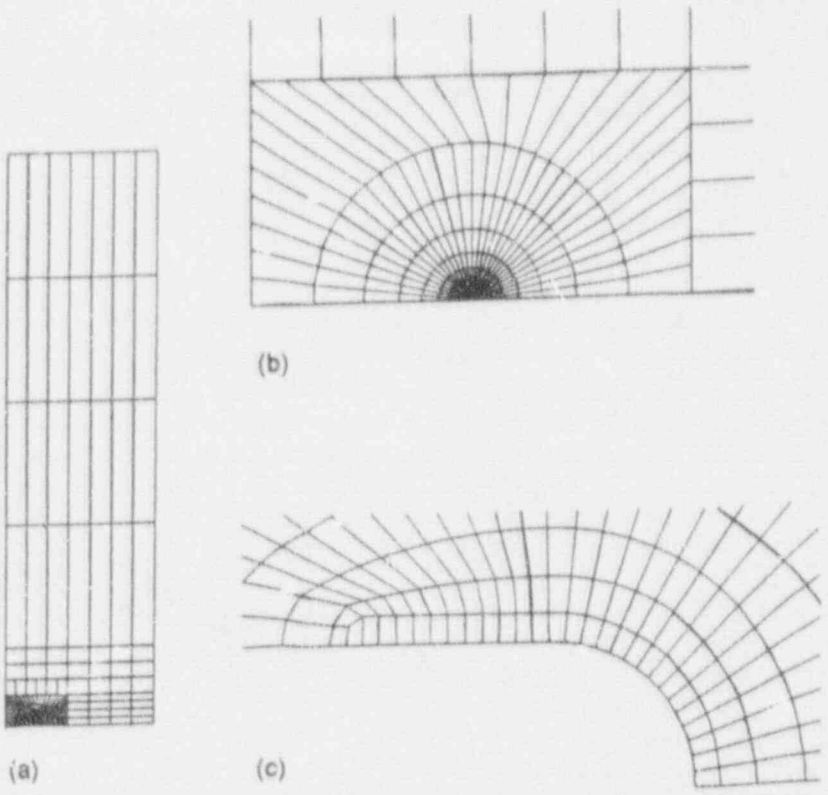

Figure B.1 Finite-element model for plane-strain full-field analysis of wide-plate specimens

ORNL-DWG 92-2925 ETD

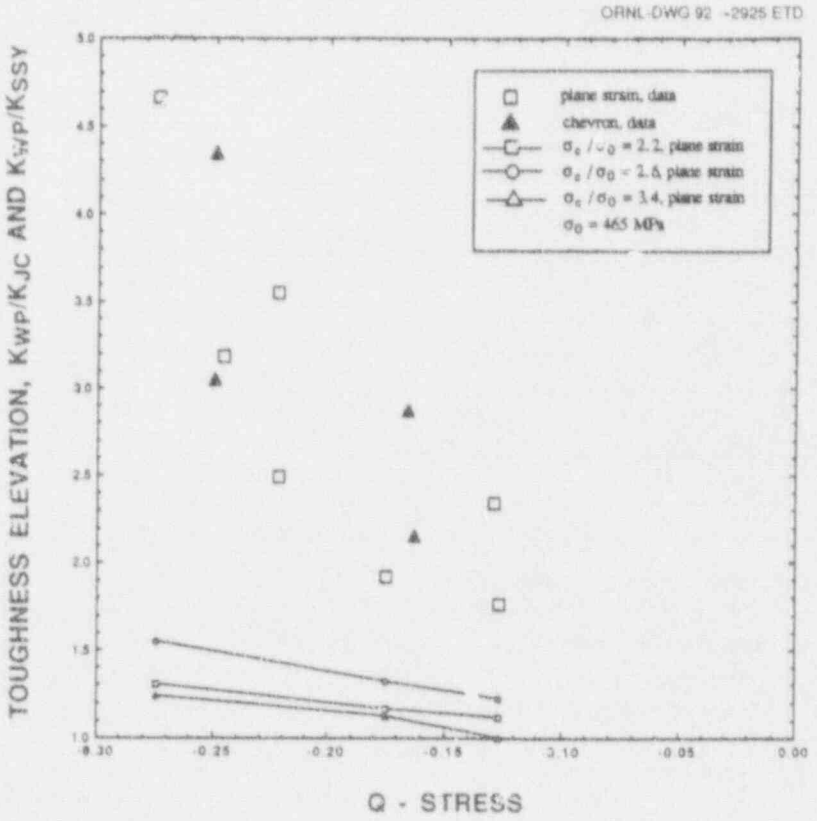

Figure B.2 Correlation of measured and predicted toughness for WP-1 wide-plate series based on Q-stress parameter

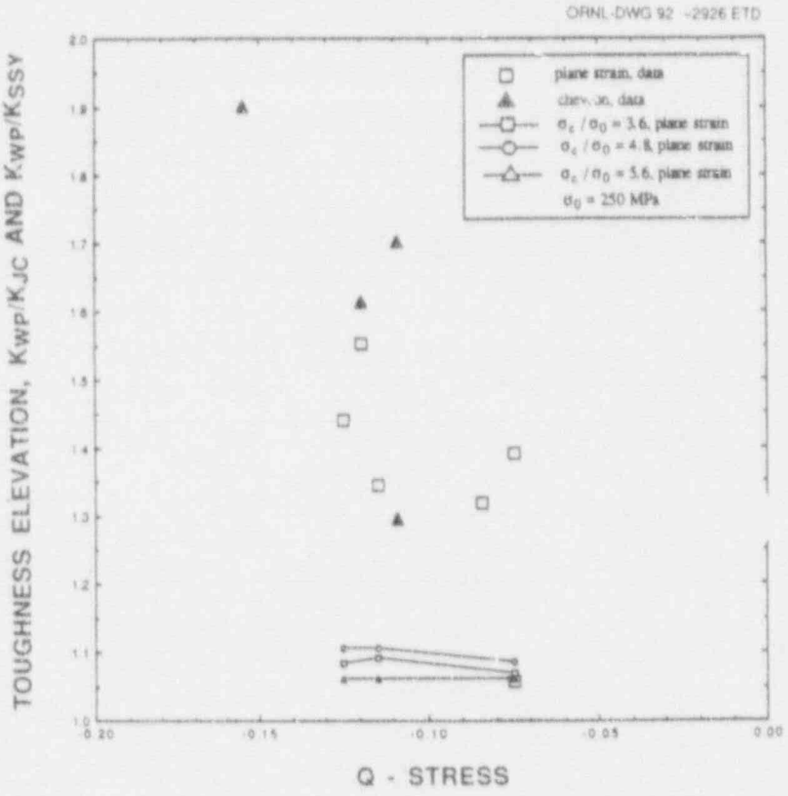

Figure B.3 Correlation of measured and predicted toughness for WP-2 wide-plate series based on Q-stress parameter

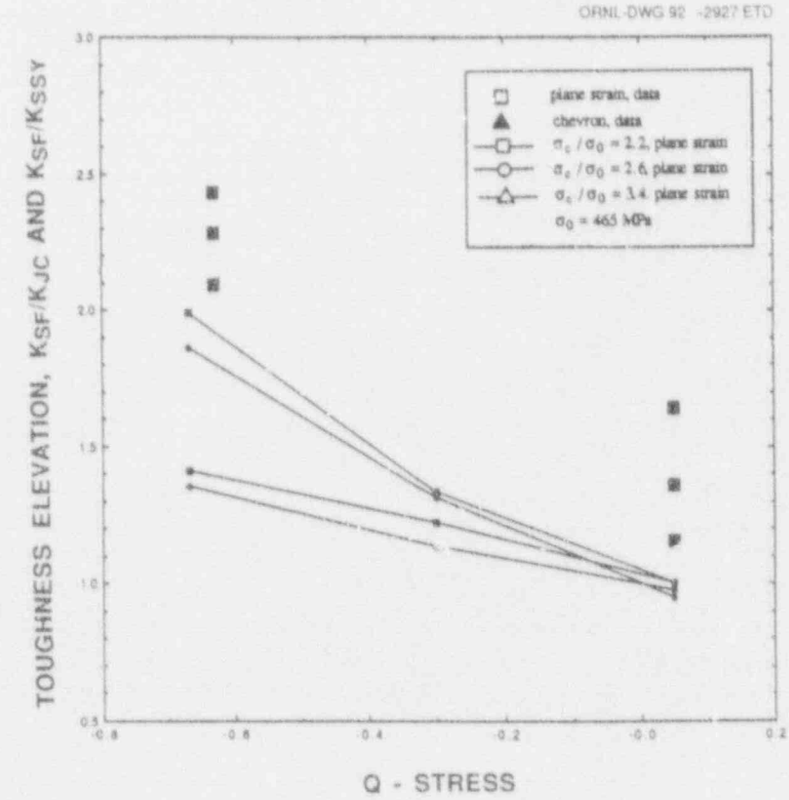

Figure B.4 Correlation of measured and predicted toughness for shallow-crack beam specimens based on Q-stress parameter

3.4, and 4.0. Again, the RKR model predictions fall below measured values, but not to the extent indicated in Figs. B.3 and B.4 for the wide-plate specimens.

Inconsistencies between measured and predicted toughnesses for the wide-plate experiments could be due to one or more factors. One possible difficulty may be the presence of three-dimensional (3-D) effects in the chevroned wide-plate specimens that cannot be represented in the 2-D plane strain models employed in the present analyses. Also, prior applications of the RKR prediction model to measure data have been confined to small-scale laboratory specimens. There may be difficulties with applications of the model to large-scale structures that have not yet been identified. Notwithstanding these difficulties in applying the RKR predictive model, predictions of toughness deviations under GPS conditions will be presented in the following appendix based on the same model.

B.5 References

1. R. O. Ritchie, J. F. Knott, and J. R. Rice, "On the Relationship Between Critical Tensile Stress and Fracture Toughness in Mild Steel," *J. Mech. Phys. Solids* 21, 395–410 (1973).*

2. F. A. McClintock, "A Criterion for Ductile Fracture by the Growth of Holes," *J. Appl. Mech.* 35, 363–371 (1968).*

3. J. W. Hancock and A. C. MacKenzie, "On the Mechanisms of Ductile Failure in High-Strength Steels Subjected to Multi-Axial Stress-States," *J. Mech. Phys. Solids* 24, 147–169 (1976).*

4. D. M. Parks, "Interpretation of Irradiation Effects on the Fracture Toughness of a Pressure Vessel Steel in Terms of Crack Tip Stress Analysis," *J. Eng. Mat. Tech.* 98, 30–36 (1976).*

5. R. O. Ritchie, W. L. Server, and R. A. Wullaert, "Critical Fracture Stress and Fracture Strain Models for the Prediction of Lower and Upper Shelf Toughness in Nuclear Pressure Vessel Steels," *Met. Trans. A* 10A, 1557–1570 (1979).*

6. R. A. Wullaert and W. L. Server, "Small Specimen Predictions of Fracture Toughness for Nuclear Pressure Vessel Steels," *Nucl. Eng. Des.* 57, 153–173 (1980).*

7. J. Heerens and D. T. Read, "Fracture Behavior of a Pressure Vessel Steel in the Ductile to Brittle Transition Region," National Institute of Standards and Technology NISTIR 88/3099 (PB89-189195/AS), December 1988.†

8. S. G. Druse, G. P. Gibson, and M. Capel, "Microstructural Control of Cleavage Fracture in an A508 Class 3 Pressure Vessel Steel," paper presented at the *22nd National Symposium on Fracture Mechanics, Atlanta, Georgia*, June 26–28, 1990.

9. T. Lin, A. G. Evans, and R. O. Ritchie, "A Statistical Model of Brittle Fracture by Transgranular Cleavage," *J. Mech. Phys. Solids* 34, 477–497 (1986).*

10. T. Lin, A. G. Evans, and R. O. Ritchie, "Statistical Analysis of Cleavage Fracture Ahead of Sharp Cracks and Round Notches," *Acta. Metall.* 34, 2205–2216 (1986).*

11. T. Lin, A. G. Evans, and R. O. Ritchie, "Stochastic Modelling of the Independent Roles of Particle Size and Grain Size in Transgranular Cleavage Fracture," *Metall. Trans.* 18A, 641–651 (1987).*

12. K. Wallin, "Statistical Modelling of Fracture in the Ductile-to-Brittle Transition Region, Defect Assessment in Components—Fundamentals and Applications," *Proceedings of the European Symposium on elastic-Plastic Fracture Mechanics*, ESIS/EGF Publication 9, 415–445 (1991).

13. K. Wallin, "Statistical Aspects of Constraint with Emphasis to Testing and Analysis of Laboratory Specimens in the Transition Region," paper presented at the *ASTM Symposium on Constraint Effects in Fracture, Indianapolis, Ind.*, May 8–9, 1991.

14. Y. Huang and J. W. Hutchinson, "A Model Study of the Role of Nonuniform Defect Distribution on Plastic Shear Localization," Harvard University Report MECH-140, April 1989.

15. Y. Huang and J. W. Hutchinson, "Cavitation Instabilities in Elastic-Plastic Solids," Harvard University Report MECH0-153, November 1989.

16. Yong-Yi Wang, "A Two-Parameter Characterization of Elastic-Plastic Crack Tip Fields and Applications to Cleavage Fracture," Ph.D Thesis, Dept. of Mechanical Engineering, Massachusetts Institute of Technology, May 1991.

17. G. Harlin and J. R. Willis, "The Influence of Crack Size on the Ductile-Brittle Transition," *Proc. R. Soc. Lond.* A415, 197–226 (1988).

18. V. Weiss, "Material Ductility and Fracture Toughness of Metals," pp. 458–474 in *Proceedings of the International Conference on Mechanical Behavior of Materials, Kyoto, Japan, August 15–20, 1971, The Society of Materials Science*, Japan (1972).

19. R. J. Dexter and S. Roy, "The Conditions of Ductile Fracture in Tensile Tests," paper presented at the *23rd National Symposium on Fracture Mechanics, College Station, Tex.*, 1991.

20. D. J. Naus et al., Martin Marietta Energy Systems, Inc., Oak Ridge Natl. Lab., "Crack-Arrest Behavior in SEN Wide Plates of Quenched and Tempered A533/Grade B Steel Tested Under Nonisothermal Conditions," USNRC Report NUREG/CR-4930 (ORNL-6388), August 1987.‡

21. D. J. Naus et al., Martin Marietta Energy Systems, Inc., Oak Ridge Natl. Lab., "High-Temperature Crack-Arrest Behavior in 152-mm-Thick SEN Wide Plates of Quenched and Tempered A533 Grade B Class 1 Steel," USNRC Report NUREG/CR-5330 (ORNL/TM-11083), April 1989.‡

22. D. J. Naus et al., Martin Marietta Energy Systems, Inc., Oak Ridge Natl. Lab., "SEN Wide-Plate Crack-Arrest Tests Using A533 Grade B Class 1 Material: WP-CE Test Series," USNRC Report NUREG/CR-5408 (ORNL/TM-11269), November 1989.‡

23. D. J. Naus et al., Martin Marietta Energy Systems, Inc., Oak Ridge Natl. Lab., "High-Temperature Crack-Arrest Tests Using 152-mm-Thick SEN Wide Plates of Low-Upper-Shelf Base Material: Tests WP-2.2 and WP-2.6," USNRC Report NUREG/CR-5450 (ORNL/TM-11352), February 1990.‡

24. D. J. Naus et al., Martin Marietta Energy Systems, Inc., Oak Ridge Natl. Lab., "Crack-Arrest Behavior in SEN Wide Plates of Low-Upper-Shelf Base Metal Tested Under Nonisothermal Conditions: WP-2 Series," USNRC Report NUREG/CR-5451 (ORNL/TM-6584), August 1990.‡

25. T. J. Theiss, D. K. M. Shum, and S. T. Rolfe, Martin Marietta Energy Systems, Inc., Oak Ridge Natl. Lab., "Interim Report on the HSST Shallow-Crack Program and Implications for Reactor Pressure Vessel Analyses," USNRC Report NUREG/CR-5886 (ORNL/TM-12115), June 1992.†

---

*Available in public technical libraries.

†Available from National Institute of Standards and Technology, 1430 Broadway, New York, NY 10018, Copyrighted.

‡Available for purchase from National Technical Information Service, Springfield, VA 22161.

Appendix C

Micromechanical/Boundary-Layer Approach to Crack-Initiation Prediction

D. K. M. Shum

C.1 Introduction

Evaluation of the potential toughness degradation, from a reference plane strain value, due to positive transverse straining along a crack front requires resolution of the following two issues. The first issue pertains to the extent that the near-crack-tip fields are perturbed from their reference plane strain distributions due to positive transverse straining. When the effects of transverse straining on the near-crack-tip fields are quantified, the perturbed fields can then be interpreted within the context of a postulated failure or crack-initiation model to provide estimates of potential toughness deviation. Toughness estimates provided in this manner are premised upon the assumption that transverse straining does not alter the fundamental micromechanism of crack initiation relative to the plane strain condition. The second issue pertains to whether the perturbation of the plane strain near-crack-tip fields due to transverse straining is sufficient to result in a change in the micromechanics of crack initiation (e.g., from a cleavage to a ductile failure mechanism).

Advanced continuum mechanics analysis methods can be applied toward the evaluation of the near-crack-tip fields due to various degrees of transverse straining, within which the plane strain condition is a special case. Crack-initiation models of varying sophistication and validity are available to provide a framework for assessing the effects of transverse straining on the near-crack-tip fields and fracture toughness. However, current understandings of the micromechanics of fracture are such that prediction of the micromechanism of fracture associated with a given set of loading conditions cannot be provided with confidence.

Consequently, the focus of this appendix is on the first issue outlined—namely, to present a method for estimating the potential toughness deviation from a reference plane strain value due to transverse straining, assuming that transverse straining does not alter the micromechanism of fracture associated with the plane strain condition. This method addresses crack initiation under generalized-plane-strain (GPS) conditions by focusing on the near-crack-tip fields, along the crack plane, within a region extending a few crack-tip-opening displacements (CTODs) directly ahead of the crack tip. The near-crack-tip results are then interpreted within the context of available micromechanical fracture models for the prediction of crack initiation. Detailed results for these near-crack-tip fields are obtained using the boundary-layer method. A boundary-layer method does not involve explicit consideration of loading and geometry. Instead, this method incorporates prescribed in-plane and out-of-plane loading and geometry considerations in a general manner. The concepts underlying the boundary-layer method, and the companion modified-boundary-layer (MBL) method, are discussed in Appendix A.

The essential difference between the present formulation and traditional small geometry change (SGC) linear-elastic fracture mechanics (LEFM) and elastic-plastic fracture mechanics (EPFM) formulations is that large geometry change (LGC) effects in the vicinity of the crack tip are considered. Consideration of LGC effects means that the traditional mathematically sharp crack is now replaced with a blunted notch under load, which is the physically more meaningful crack-tip representation when one is interested in events within a distance of a few CTODs from the deforming crack tip. Inclusion of LGC effects results in near-tip features that are quite different from those obtained under SGC approximations. These near-tip features are used to relate results from continuum stress analyses to microstructural failure mechanisms.

In the first phase of this work, an analytical description of the near-crack-tip region was developed based on GPS slip-line theory.[1] The loading conditions considered corresponded to small-scale yielding (SSY) for which the remote stress fields are characterized by the parameter K only. The analysis focused on the effects of out-of-plane straining on ductile crack initiation by interpreting the predicted near-crack-tip fields in light of a postulated ductile failure criterion. The slip-line model was used to provide near-term estimates on the change in crack-initiation toughness, relative to plane strain toughness, associated with either negative or positive straining on the order of the yield strain along a crack front.

In this appendix refined estimates on the change in crack-initiation toughness associated with a state of GPS along the crack front are presented. This refinement is accomplished by constructing a detailed, finite-element-based

Micromechanical

description of the near-crack-tip region, along with an elastic-plastic description of material behavior. The loading conditions to be considered also correspond to SSY. However, within the context of SSY, two classes of in-plane loading conditions will be considered. The first in-plane loading condition is one for which the remote stress fields are characterized by the parameter K only; the near-crack-tip fields that result under plane strain conditions will henceforth be referred to as the *reference* SSY results. The second in-plane loading condition is the MBL problem for which the remote stress fields are characterized by the parameters K and T. Details concerning the parameter T are discussed in Appendix A, which outlines the essential features of two-parameter approaches based on T-stress and Q-stress.

Analysis results are presented first for the case of single-parameter remote K-field loading. Comparison of present results with predictions based on the slip-line approach, where appropriate, are presented. Analysis results are then presented for the case where the remote in-plane loading conditions are characterized by both K and the higher-order parameter T. Analysis results are interpreted alternately in light of a postulated cleavage or ductile failure criterion. Finally, implications of these results toward crack initiation under GPS conditions are discussed.

A qualitative discussion on the anticipated effects of transverse strain on crack-tip fields is appropriate at this point. Beyond the near-tip region characterized by large-strain effects, magnitudes of the in-plane stress and strain components decrease with increasing distance from the crack tip. Consequently, the effects of transverse strain on the crack-tip fields in a GPS analysis are expected to become significant with increasing distance from the crack tip. A prescribed magnitude of the transverse strain, on the order of the yield strain, is expected to greatly perturb both the shape and size of the plastic zone. Perturbations of the distributions of stress and strain components from the reference plane strain distributions are also expected to be sensitive to transverse strain. Both of these effects have been observed in the analysis results to be presented. However, the critical question with respect to possible deviation from plane strain fracture toughness due to transverse straining is whether the perturbing effects of transverse strain are significant over the near-crack-tip region within which the micromechanisms of crack initiation take place. The analyses to be presented here are aimed toward a resolution of this question.

C.2 Material Models

Two material models will be considered in this appendix. The first material model is one that is linear-elastic below the yield point as characterized by the yield strain $\varepsilon_o = \sigma_o/E$, where σ_o is the uniaxial yield stress in tension and E is Young's modulus. Poisson's ratio is equal to 0.3. Beyond yield the material is of the power-law type with the hardening exponent denoted as n. The uniaxial true stress–true plastic strain curve in tension is of the form

$$\frac{\varepsilon}{\varepsilon_o} = \alpha\left(\frac{\sigma}{\sigma_o}\right)^n \quad . \tag{C.1}$$

The above material model is used to examine effects of out-of-plane straining on the near-crack-tip fields under single-parameter remote loading conditions. Various combinations of ε_o, α, and n have been considered in this study. While the reference SSY results are sensitive to the magnitude of these material parameters, the predicted deviations of the near-crack-tip fields from the SSY results due to transverse strain are remarkably similar for all cases considered. Consequently, numerical results are presented only for the case where $\alpha = 1$, $\varepsilon_o = 1/400$, and $n = 10$. These numerical values correspond to a material description often used to model the uniaxial stress-strain response in tension of a reactor pressure vessel (RPV)-grade material in the unirradiated condition.

The second material model is adopted to model the uniaxial stress-strain response in tension of an RPV-grade material subject to irradiation effects. This material model is used to examine alternately the effects of out-of-plane straining (only) and combined effects of T-stress and out-of-plane straining on the reference SSY near-crack-tip fields. The elastic portion of the uniaxial stress-strain curve is characterized by $\varepsilon_o = 1/311$, and Poisson's ratio is equal to 0.3. The uniaxial true stress–true plastic strain curve in tension is assumed to be bilinear. The plastic portion of the uniaxial stress-strain curve becomes nonhardening at a normalized stress level of $\sigma/\sigma_o = 1.3$ with an associated true plastic strain of 0.075.

C.3 Finite-Element Description of Near-Crack-Tip Region

In a boundary-layer approach the near-crack-tip region, over which the CTOD sets the size scale of the problem, is modeled by constructing a finite-element mesh with a suitably large outer boundary as indicated in Fig. C.1(*a*). A unique feature of the finite-element mesh is the highly refined crack-tip region. The high degree of refinement is necessary to obtain an accurate determination of the crack-tip fields within a distance of a few CTODs ahead of the blunting notch tip. Furthermore, the mathematically sharp crack-tip profile associated with small-strain fracture analysis is replaced, in the present finite-strain context, with an

initial root radius before the imposition of external loading. The assumption of a finite value of initial root radius is necessary to facilitate numerical convergence of the finite-element results. The outer radius of the mesh in Fig. C.1(*a*) is 1,000,000 times the initial root radius indicated in Fig. C.1(*b*).

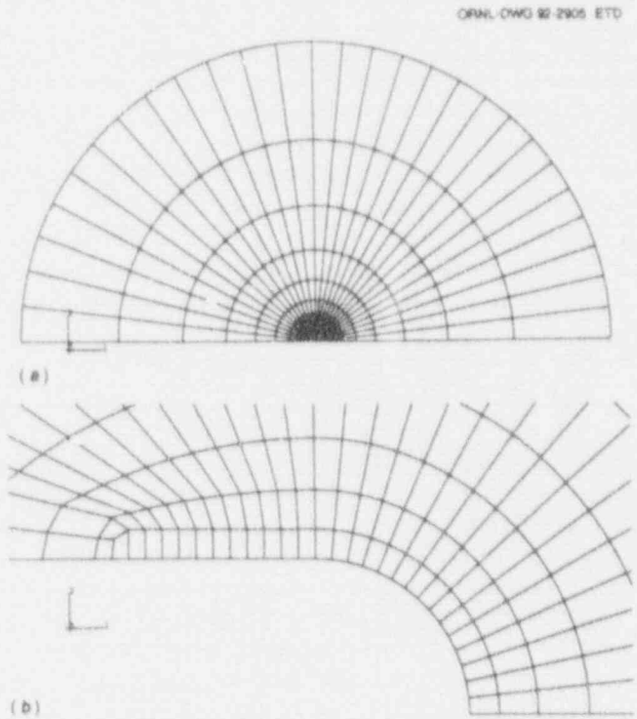

Figure C.1 **(*a*) Finite-element model of near-crack-tip region in boundary-layer approach. Near-crack-tip region is comprised of 40 rings of elements. Unique feature of finite-element mesh is highly refined crack-tip region. (*b*) Closeup of near-crack-tip finite-element model. Outer radius of mesh in (*a*) is ~1,000,000 times initial root radius indicated in this figure. High degree of refinement is necessary to obtain accurate determination of crack-tip fields within distance of few CTODs ahead of blunting notch tip**

The finite-strain, elastic-plastic, GPS nature of the present problem is examined using the finite-element code ABAQUS.[2] The analyses assume a rate-independent J_2 (isotropic-hardening) incremental plasticity theory as implemented in ABAQUS. The finite-element mesh in Fig. C.1(*a*) and (*b*) is made up of 1119 GPS elements and 3494 nodes. These elements behave as conventional 8-node isoparametric elements, except for an extra degree-of-freedom that allows for uniform straining in a direction perpendicular to the plane of the mesh.[2] The integration order for these elements is 2×2.

C.3.1 Boundary Conditions

The remote Mode I in-plane *stress* fields due to K and T are applied as *displacement* boundary conditions on the outer boundary of the finite-element mesh. The transverse strain ε_z is imposed as uniform displacement on the out-of-plane degree-of-freedom. Specifically, with Poisson's ratio denoted as ν, the in-plane displacement boundary conditions in polar coordinates are imposed via a relation of the form,

$$u_i = \frac{K\sqrt{2\pi r}}{E}\,\tilde{u}_i(\theta,\nu) + \frac{Tr}{E}\,\tilde{T}_i(\theta,\nu) + \varepsilon_z r\,\tilde{\varepsilon}_i(\theta,\nu) \quad . \tag{C.2}$$

The universal functions $\tilde{u}_i(\theta,\nu)$, $\tilde{T}_i(\theta,\nu)$, and $\tilde{\varepsilon}_i(\theta,\nu)$ are dependent on the angular coordinate θ and Poisson's ratio ν only.

The GPS problem examined in this study, as expressed by Eq. (C.2), is somewhat similar to a load-controlled biaxial test. From Eq. (C.2), it is seen that the in-plane displacement fields are perturbed from their classic K-dependence due to Poisson's ratio-induced in-plane displacements as a function of the applied values of T and ε_z.

In this study the parameters K, T, and ε_z are allowed to increase in fixed proportion from zero to their target values. The adoption of proportional in-plane and out-of-plane loading is motivated by the observation that, during the normal operation of an RPV, the pressure-induced axial and circumferential strains occur under proportional loading conditions. Note that under a postulated accident scenario, such as a pressurized-thermal-shock (PTS) transient, the in-plane and out-of-plane loading may not be proportional in nature.

C.3.2 Numerical Convergence Requirements

For a given target value of T-stress or transverse strain, increase in the target value of the parameter K increases the resolution of the near-crack-tip fields. An upper limit to the allowable target value of the parameter K exists for the following computational reasons. The requirement of contained crack-tip yielding requires the spread of plasticity to be confined within the elastic far field of the finite-element mesh; in this study this requirement is accomplished by limiting the maximum extent of the plastic zone to be <10% of the outer mesh dimension. Convergence requirements of the finite-element results are accomplished by limiting the maximum value of the residual nodal force per unit thickness at any node. Specifically, the maximum value is required to be <0.1% of the product between the

yield stress and the smallest element dimension in the finite-element mesh.

When considering finite-strain effects on the near-crack-tip fields, there are two common measures of CTOD for the case where the initial notch opening is semicircular in nature. The first measure of CTOD corresponds to the Mode I or opening-mode displacement of point B evaluated at the intersection of the straight crack flank with the semicircular notch, as indicated in Fig. C.2. The ratio of current CTOD to the initial notch opening is denoted as b/b_o. This measure of CTOD corresponds to the definition of CTOD employed in previous slip-line analyses.[3] The second measure of CTOD corresponds to the 45° intercept definition originally formulated for small-strain fracture analysis.[3] The ratio of current CTOD to the initial notch opening is denoted as δ/δ_o. As indicated in Fig. C.2, $b_o = \delta_o$ for the case of an initially semicircular notch opening.

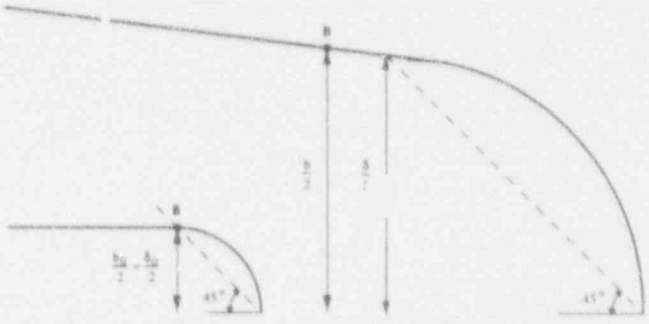

Figure C.2 Schematic illustrating two measures of CTOD employed in this study. First measure of CTOD corresponds to the Mode I or opening-mode displacement of point B. Second measure of CTOD corresponds to 45° intercept definition originally formulated for small strain fracture analysis

There is an aspect of numerical convergence associated with boundary-layer-type calculations that is distinct from consideration of force equilibrium. Specifically, this aspect of convergence concerns the minimum load level in a plane strain analysis, expressed in terms of b/b_o or δ/δ_o, that is necessary to achieve the self-similar crack-tip fields characteristic of K-dominant SSY. Previous investigators[4,5] have found that self-similarity of the SSY results is achieved for values of b/b_o or δ/δ_o, approximately >3 to 5. However, it is found that for the present calculations, self-similarity of the SSY results is achieved for b/b_o or δ/δ_o approximately >6 to 10, depending on the material model adopted. It is believed that this observation of a slower convergence may be specific to the finite-strain formulation employed in ABAQUS. In this study the value of the CTOD upon reaching a target K value is at least 10 times the initial notch opening, so that self-similarity of the SSY results is guaranteed.

Another observation that is perhaps related to ABAQUS requirement for self-similarity for the SSY results is that, when the 8-node (quadratic) finite-element mesh indicated in Fig. C.1(*a*) and (*b*) is replaced with 4-node (linear) GPS isoparametric elements, the numerically convergent value for the maximum opening-mode stress is ~5 to 10% lower than that obtainable with 8-node elements. The maximum value obtained with 8-node elements does agree with published results. This discrepancy in convergent values, depending on element type, does not appear to be due to mesh refinement effects in the usual finite-element sense.

C.4 Remote K-Field Loading Finite-Element Results

In this section, analysis results are presented for a material whose uniaxial stress-strain curve in tension is constructed to model the material response of an unirradiated RPV-grade material. The uniaxial true stress–true plastic strain curve in tension is of the power-law form as discussed previously. The single-parameter (T = 0) opening-mode stress distribution directly ahead of the blunting notch is presented in Fig. C.3(*a*) and (*b*) for three values of transverse strain $\varepsilon_z/\varepsilon_o$ = –0.95, 0, and 0.68. Plane strain conditions correspond to the case $\varepsilon_z/\varepsilon_o = 0$. The degree of positive out-of-plane straining is considered to be severe with respect to the normal operations of an RPV. In Fig. C.3(*a*) the stress distributions are shown within the region of finite-strain effects $[r/(J/\sigma_o) \le 1]$ where the opening-mode stress component decreases with decreasing distance from the notch tip. In Fig. C.3(*b*) the stress distributions in Fig. C.3(*a*) are redrawn to encompass both the finite-strain region and a portion of the small-strain region ahead of the blunting notch. Within the region of small strain, the stress distributions decrease with increasing distance from the notch tip. The influence of a given magnitude of ε_z is evidently not symmetric, as indicated in Fig. C.3(*b*). The implication of this asymmetry to fracture toughness prediction will be addressed later in this appendix.

In Fig. C.3(*a*) and (*b*) and subsequent figures, the stress and strain quantities are average nodal values based on extrapolated values from integration points of surrounding elements. In a boundary-layer analysis, the relevant dimensional length variable is the quantity J/σ_o, where J corresponds to the magnitude of the J-integral. For the finite-element results, the undeformed dimensional distance ahead of the blunted notch r is therefore expressed in a normalized form in terms of $r/(J/\sigma_o)$. Magnitude of the J-integral can be obtained using the standard plane strain

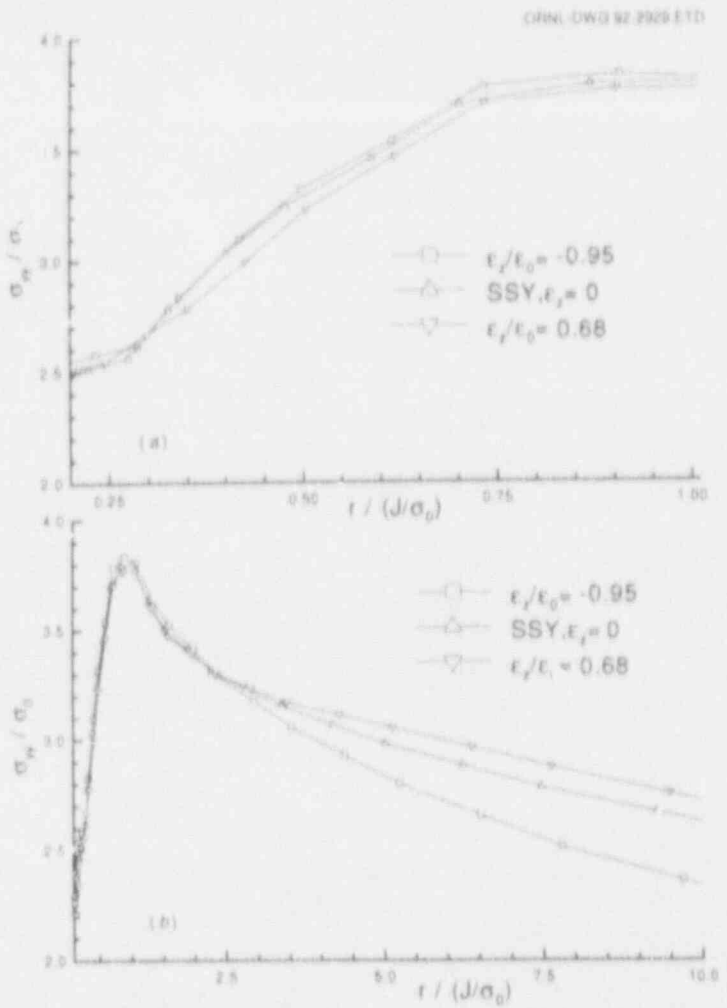

Figure C.3 (*a*) Distribution of opening-mode stress directly ahead of blunting notch for power-law hardening material and three values of transverse strain $\varepsilon_z/\varepsilon_0 = -0.95$, 0, and 0.68 under remote K-field loading (T = 0) conditions. Stress distributions are shown within region of "finite strain" effects r[(J/σ_0) ≤ 1] where opening-mode stress component decreases with decreasing distance from notch tip. Degree of positive out-of-plane straining is considered to be severe with respect to RPV normal operations. (*b*) Stress distributions in (*a*) are redrawn to encompass both finite strain region and portion of small strain region ahead of blunting notch. Within region of small strain, stress distributions decrease with increasing distance from notch tip. Influence of given magnitude of ε_z is evidently not symmetric with respect to plane strain distribution

conversion between J and K based on the applied value of K specified in Eq. (C.2). Alternately, J can be obtained using the J-integral option provided by ABAQUS. Excellent agreement is found between these two methods for evaluating J, thus providing another avenue for verifying the numerical accuracy of the finite-element results.

Interpretation of the finite-element results in terms of CTOD is readily accomplished by making use of the results presented in Fig. C.4(*a*) and (*b*). In Fig. C.4(*a*) the J-CTOD relation for the power-law hardening material being considered based on the Mode I displacement of point B is indicated as a function of transverse strain. The magnitudes of $\varepsilon_z/\varepsilon_0$ indicated in these results correspond to the maximum values of transverse strain employed in the analyses. In Fig. C.4(*b*) the J-CTOD relation based on the 45° intercept definition is indicated as a function of transverse strain. It is observed that over the range of transverse strain considered, the J-CTOD relation based on either definition of CTOD is relatively insensitive to the magnitude of the transverse strain. In addition, the J-CTOD relation itself is insensitive to either choice of the definition of CTOD. In Fig. C.4(*b*) it is observed that the 45° intercept J-CTOD relation has the form $\delta = 0.43\ J/\sigma_0$ for the range of transverse strain considered.

In Fig. C.5(*a*) to (*c*) the effective plastic strain distribution ε_e directly ahead of the blunting notch is indicated for three

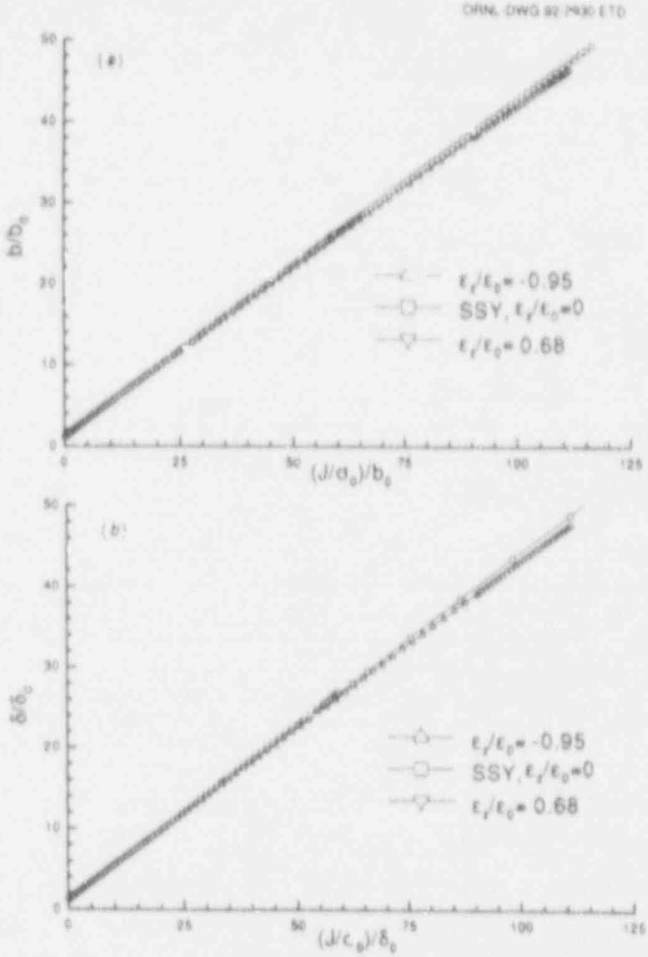

Figure C.4 (*a*) J-CTOD relation for power-law hardening material based on Mode I displacement of point B indicated in Fig. C.2 and as function of transverse strain under remote K-field loading (T = 0) conditions. Magnitudes of $\varepsilon_z/\varepsilon_0$ indicated in this figure correspond to maximum values of transverse strain employed in the analyses. (*b*) J-CTOD relation for power-law hardening material based on 45° intercept definition indicated in Fig. C.2 and as function of transverse strain under remote K-field loading (T = 0) conditions. For range of transverse strain considered, J-CTOD relation is insensitive to definition of CTOD employed and the magnitude of transverse strain

values of transverse strain $\varepsilon_z/\varepsilon_0 = -0.95$, 0, and 0.68 under remote K-field loading (T = 0) conditions. In Fig. C.5(*a*) the strain distributions are shown within the region of finite-strain effects [$r/(J/\sigma_0) \leq 1$]. In Fig. C.5(*b*) the strain distributions in Fig. C.5(*a*) are redrawn to encompass both the finite-strain region and a portion of the small-strain region ahead of the blunting notch. The scale along the vertical axis is chosen to highlight the effects of transverse strain on the extent of the plastic zone ahead of the blunting notch. The maximum extent of the plastic zone in terms of the normalized parameter $r/(J/\sigma_0)$ is associated with $\varepsilon_e = 0$. It is observed that the maximum extent of the plastic zone for magnitude of positive transverse strain $\varepsilon_e = 0.68$ is ~3.5 J/σ_0. This value is approximately one-third that of the plane strain analysis. While not evident in this figure, the maximum extent of the plastic zone for magnitude of negative transverse strain $\varepsilon_e = -0.95$ is more than twice that associated with the plane strain analysis. Analysis results also indicate that the shape of the plastic zone is very much affected by the magnitude of the prescribed transverse strain. In Fig. C.5(*c*) the strain distributions in Fig. C.5(*a*) are redrawn to encompass a larger portion of the finite-strain region.

Figure C.6(*a*) and (*b*) presents the distribution of effective plastic strain and the associated stress state, as characterized by the ratio of hydrostatic stress to effective stress σ_m/σ_e directly ahead of the blunting notch. Note that ε_e is not a unique function of σ_m/σ_e as indicated by the elbows in Fig. C.6(*a*). As will be discussed shortly, it is that portion of the ε_e distribution that decreases with increasing value of σ_m/σ_e that is relevant to the ductile failure model to be presented. In Fig. C.5(*b*) the strain distributions in Fig. C.6(*a*) are redrawn to encompass a larger portion of the finite-strain region. It is observed that only for that region ahead of the crack tip for which the magnitude of ε_e is less than ~5% are the effects of transverse straining apparent.

C.4.1 Comparison of Finite-Element and Slip-Line Results

Comparison of the present finite-element results with the analysis results obtained in the first phase of this work[1] is accomplished in the following manner. The slip-line analysis also assumed a material description of the form indicated in Eq. (C.1). The strain-hardening exponent N employed in the slip-line analysis can be identified with 1/n in the present finite-element analysis. The parameter α is also equal to unity in the slip-line analysis.

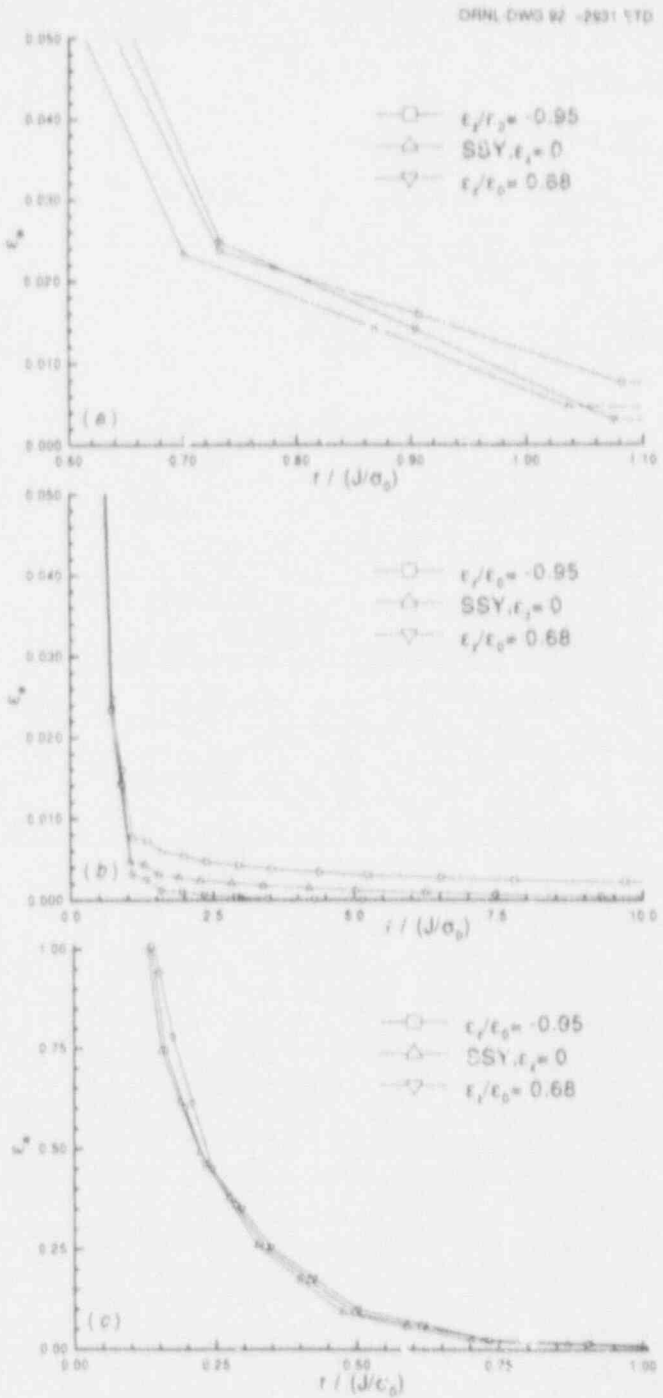

Figure C.5 (*a*) Distribution of effective plastic strain directly ahead of blunting notch for power-law hardening material and three values of transverse strain $\varepsilon_z/\varepsilon_0 = -0.95$, 0, and 0.68 under remote K-field loading (T = 0) conditions. Strain distributions are shown within region of finite strain effects $r/[(J/\sigma_0) \leq 1]$. Scale along vertical axis is chosen to highlight the effects of transverse strain and to facilitate comparison with slip-line results presented in Fig. C.7(*b*). (*b*) Strain distributions redrawn to encompass both finite strain region and portion of small strain region ahead of blunting notch. Scale along the vertical axis is chosen to highlight effects of transverse strain on extent of plastic zone ahead of blunting notch. Maximum extent of plastic zone in terms of normalized distance parameter $r/(J/\sigma_0)$ is associated with $\varepsilon_e = 0$. (*c*) Strain distributions redrawn to encompass larger portion of finite strain region. Scale along vertical axis is chosen to facilitate comparison with slip-line results presented in Fig. C.7(*c*)

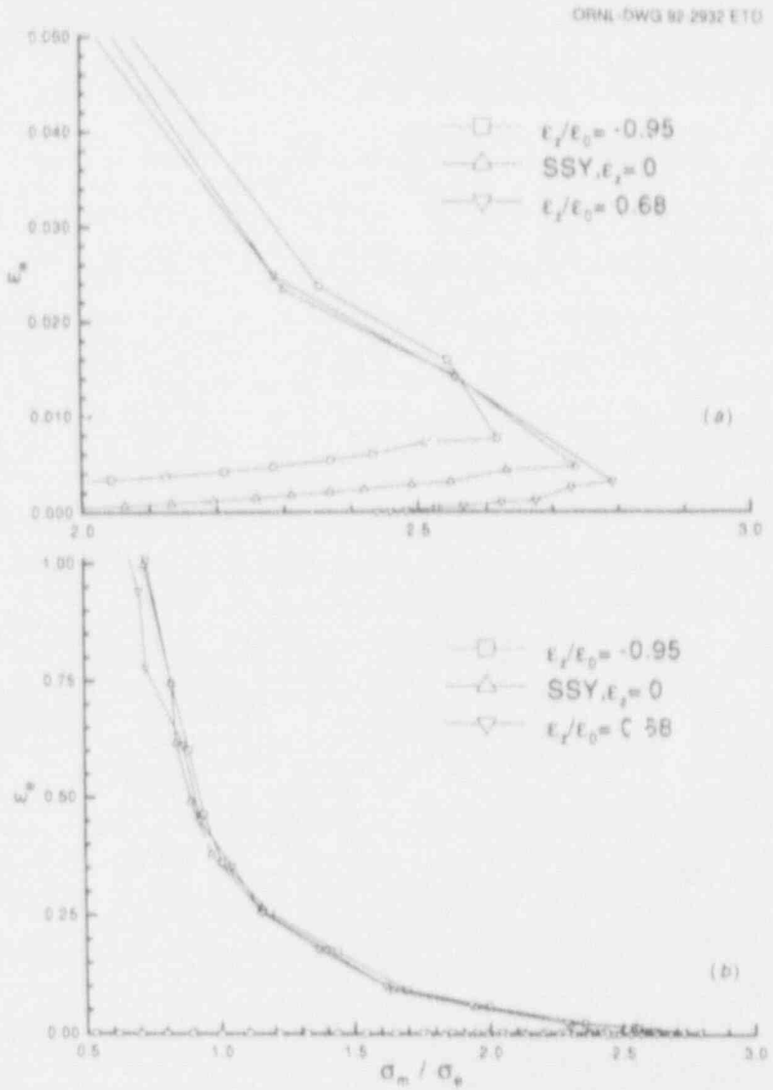

Figure C.6 (*a*) Distribution of effective plastic strain as function of stress ratio σ_m/σ_e for power-law hardening material and three values of transverse strain $\varepsilon_z/\varepsilon_0$ = –0.95, 0, and 0.68 under remote K-field loading (T = 0) conditions. Scale along vertical axis is chosen to highlight effects of transverse strain and to facilitate comparison with slip-line results presented in Fig. C.7(*d*). (*b*) Strain distributions redrawn to encompass larger portion of finite strain region. Scale along vertical axis is chosen to facilitate comparison with slip-line results presented in Fig. C.7(*e*)

However, a unique feature of the GPS slip-line analysis is that the magnitude of the shear strain ahead of the crack tip in the outer extent of the finite-strain region, referred to as the apex strain ε_a in the slip-line analysis, is undetermined from the slip-line analysis. In the first phase of this work, near-crack-tip fields were predicted using the slip-line approach based on an assumed value of the apex strain ($\varepsilon_a/\varepsilon_0$ = 4) that did not vary with respect to the magnitude of the transverse strain. In addition, the stipulation that the slip-line result be such that the out-of-plane stress component σ_z remains the intermediate principal stress component results in the "reality condition" that admissible values of ε_z, as a function of the assumed state of strain at the apex, must obey the inequality

$$|\varepsilon_z/\varepsilon_a| < 2/3 \quad . \tag{C.3}$$

In the following comparison, values of the apex strain determined from the finite-element analyses, as a function of transverse strain, are incorporated into the slip-line analysis. The location at which the finite-element apex strain is taken corresponds to ~2.4 δ or 1 J/σ_0. In the slip-line analysis, the apex strain is related to the principal plastic strain components at the apex via the relations,

$$\varepsilon_x = -\frac{\varepsilon_z}{2} - \varepsilon_a \quad , \tag{C.4a}$$

and

$$\varepsilon_y = -\frac{\varepsilon_z}{2} + \varepsilon_a \quad . \qquad \text{(C.4b)}$$

In view of the nodal average nature of the finite-element results, the apex strain is determined from the finite-element results based on the average value from Eqs. (C.4a) and (C.4b). The values of the apex strain thus determined are $\varepsilon_a/\varepsilon_o$ = 2.28, 1.36, and 1.88 for the range of transverse strain $\varepsilon_z/\varepsilon_o$ = –0.98, 0, and 0.68. Note that Eq. (C.3) is satisfied in all three cases.

In the slip-line analyses all length parameters are normalized with respect to the CTOD. For ease of comparison with the finite-element results, the relation CTOD = 0.43 J/σ_o, as determined from Fig. C.4(*a*) and (*b*), is used. The slip-line results thus determined are presented in Fig. C.7(*a*) to (*e*). The slip-line results are remarkably similar to their finite-element counterparts presented in Figs. C.3(*a*), C.5(*a*) and (*c*), and C.6(*a*) and (*b*). Consequently, these results provide mutual confirmation of both the validity and accuracy of these two methods for determining the crack-tip fields under GPS conditions.

C.5 Remote K-T Loading Finite-Element Results

In this section analysis results are presented for a material whose uniaxial stress-strain curve in tension is constructed to model the material response of an RPV-grade material subject to irradiation effects. The uniaxial true stress–true plastic strain curve in tension is bilinear in nature, as previously discussed. The in-plane loading conditions are characterized by K and various degrees of T-stress, while the transverse strain considered spans the range $-0.56 < \varepsilon_z/\varepsilon_o < 0.56$. Plane strain conditions correspond to the case $\varepsilon_z/\varepsilon_o$ = 0. The degree of positive out-of-plane straining is considered to be severe with respect to the normal operations of an RPV.

The single-parameter remote K-field loading (T = 0) opening-mode stress distribution directly ahead of the blunting notch is presented in Fig. C.8 for three values of $\varepsilon_z/\varepsilon_o$ = –0.56, and 0, 0.56. Similar to the findings for the unirradiated material model, the effects of a given magnitude of the transverse strain on the near-crack-tip fields are nonsymmetric in the present case also. In Fig. C.9 the effective plastic strain distribution ε_e directly ahead of the blunting notch is indicated. In Fig. C.10 the distribution of effective plastic strain and the associated stress state, as characterized by the ratio of hydrostatic stress to effective stress σ_m/σ_e directly ahead of the blunting notch is presented.

Figures C.11–C.13 show results analogous to those presented in Figs. C.8–C.10, except now for the case of plane strain (ε_z = 0) and various degrees of K and the second parameter down to T/σ_o = –0.45. The choice of negative T-stress values is motivated by the observations that the near-crack-tip fields associated with a short circumferential crack within an RPV appear to exhibit negative T-stress effects. In Fig. C.14(*a*) and (*b*) the J-CTOD relations associated with the plane strain, K-T analyses are presented. The J-CTOD results alternately employ a definition of CTOD based on the Mode I displacement of point B, or the 45° intercept as indicated in Fig. C.2. These results indicate that the J-CTOD relation is insensitive to the definition of CTOD employed, but is sensitive to the magnitude of the T-stress.

Figures C.15–C.17 present results for combined T-stress and transverse strain loading. The range of T-stress and transverse strain considered are those discussed previously. The results in Figs. C.15–C.17, when compared to those presented in Figs. C.8–C.13, permit a quantitative evaluation of the influence of T-stress and transverse strain on the crack-tip fields.

C.6 Crack Initiation Under GPS Conditions

The finite-element results presented in Figs. C.8–C.17 will now be taken as input to the RKR and the MHM models. A simplified view is adopted where a material will fail either in a cleavage or in a ductile manner in response to the loading conditions. The question being addressed is simply the magnitude of toughness deviation that can be expected under GPS conditions, assuming that the failure mechanism is either cleavage or ductile in nature. No attempt will be made to determine which failure mechanism is appropriate for the assumed material model. For the purpose of estimating the effects of out-of-plane straining on fracture toughness, it is further assumed that the range of critical material parameters necessary for brittle or ductile fracture is not affected by the magnitude of the out-of-plane strain or the T-stress. This is equivalent to assuming that the introduction of out-of-plane strain or T-stress does not alter the micromechanics governing cleavage or ductile fracture.

C.6.1 Cleavage Fracture

In Table C.1 estimates of toughness deviation from a reference plane strain K-dominant (ε_z = T = 0) value, based on

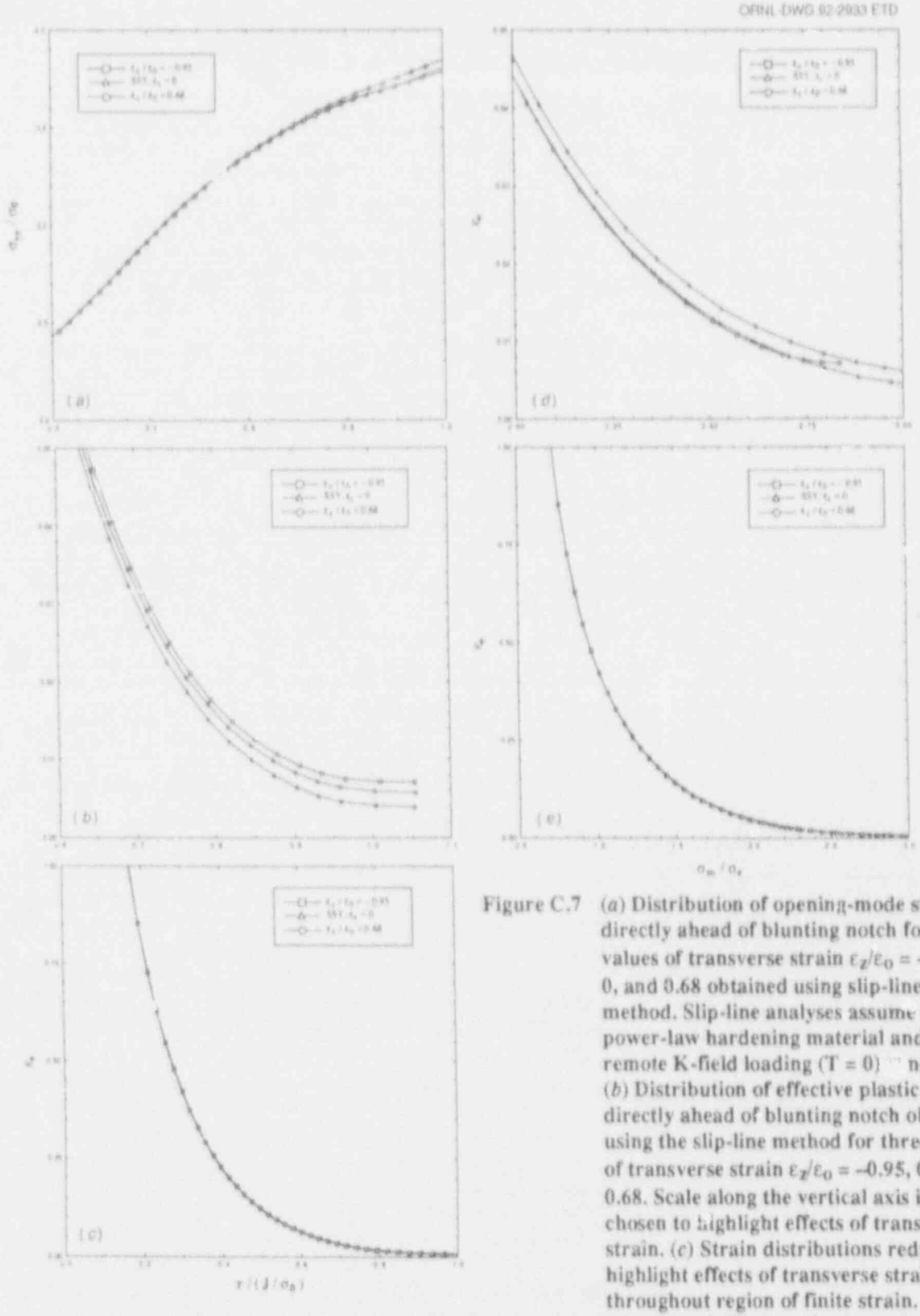

Figure C.7 (*a*) Distribution of opening-mode stress directly ahead of blunting notch for three values of transverse strain $\varepsilon_Z/\varepsilon_0 = -0.95$, 0, and 0.68 obtained using slip-line method. Slip-line analyses assume a power-law hardening material and remote K-field loading (T = 0) conditions. (*b*) Distribution of effective plastic strain directly ahead of blunting notch obtained using the slip-line method for three values of transverse strain $\varepsilon_Z/\varepsilon_0 = -0.95$, 0, and 0.68. Scale along the vertical axis is chosen to highlight effects of transverse strain. (*c*) Strain distributions redrawn to highlight effects of transverse strain throughout region of finite strain. (*d*) Distribution of effective plastic strain as function of stress ratio σ_m/σ_e obtained using slip-line method for three values of transverse strain $\varepsilon_Z/\varepsilon_0 = -0.95$, 0, and 0.68. Scale along vertical axis is chosen to highlight effects of transverse strain. (*e*) Strain distributions redrawn to highlight effects of transverse strain throughout region of finite strain

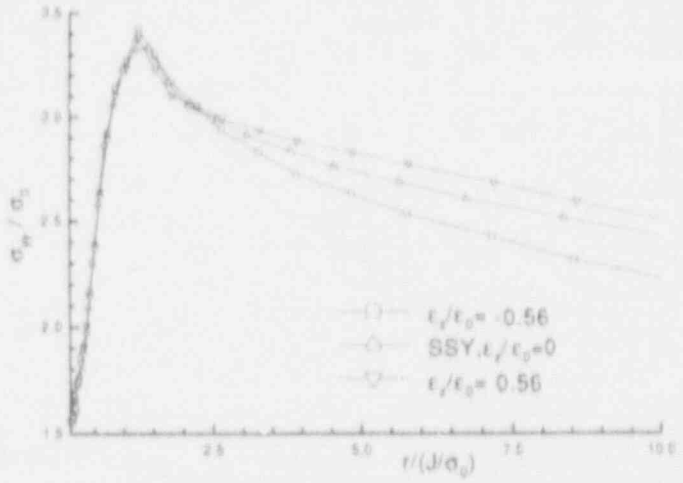

Figure C.8 Distribution of opening-mode stress directly ahead of blunting notch for irradiation-degraded (simulated) material and three values of transverse strain $\varepsilon_Z/\varepsilon_0$ = –0.56, 0, and 0.56 under remote K-field (T = 0) conditions. Degree of positive out-of-plane straining is considered to be severe with respect to RPV normal operations

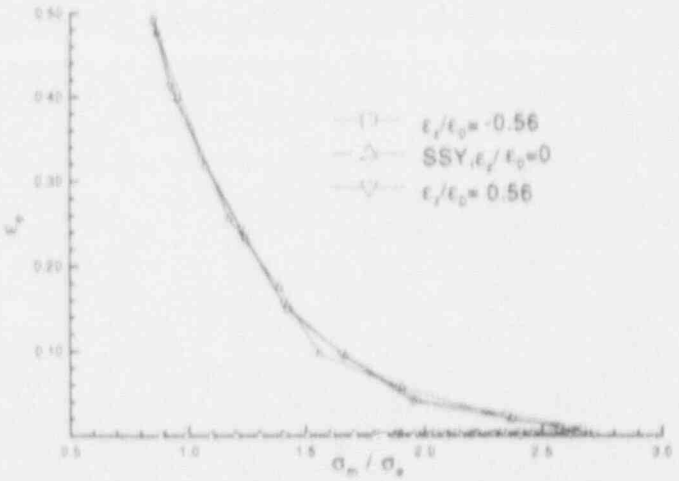

Figure C.10 Distribution of effective plastic strain as function of stress ratio σ_Z/σ_0 for irradiation-degraded (simulated) material and three values of transverse strain $\varepsilon_Z/\varepsilon_0$ = –0.56, 0, and 0.56 under remote K-field loading (T = 0) conditions

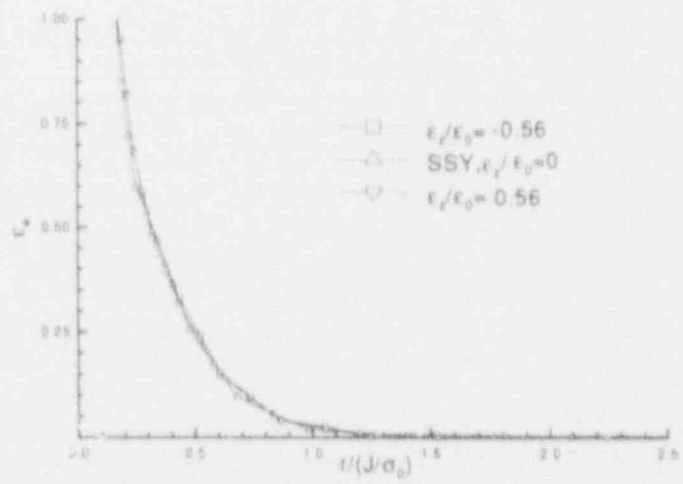

Figure C.9 Distribution of effective plastic strain directly ahead of blunting notch for irradiation-degraded (simulated) material and three values of transverse strain $\varepsilon_Z/\varepsilon_0$ = –0.56, 0, and 0.56 under remote K-field loading (T = 0) conditions

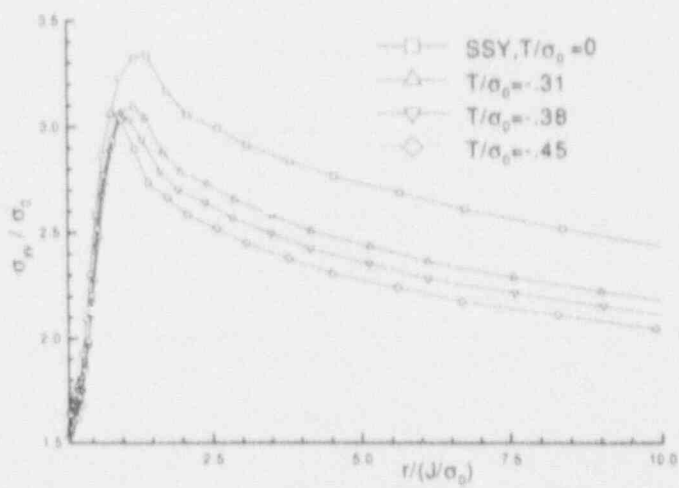

Figure C.11 Plane-strain distribution of opening-mode stress directly ahead of blunting notch for irradiation-degraded (simulated) material and various degrees of K and second parameter down to T/σ_0 = –0.45. Choice of negative T-stress values is motivated by shallow-flaw effects associated with RPV geometry

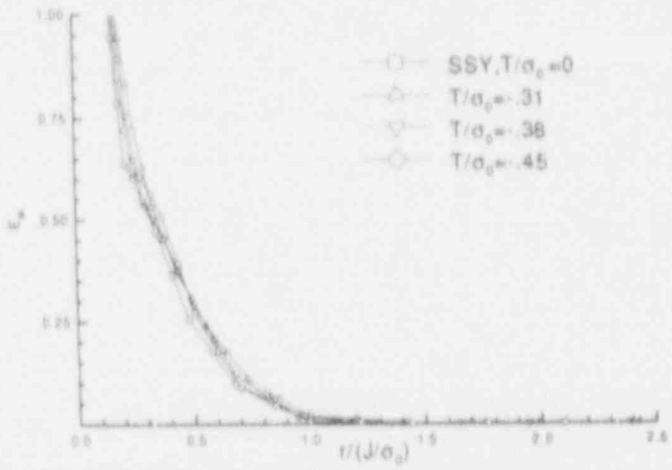

Figure C.12 Plane-strain distribution of effective plastic strain directly ahead of blunting notch for irradiation-degraded (simulated) material and various degrees of K and second parameter down to T/σ_0 = –0.45

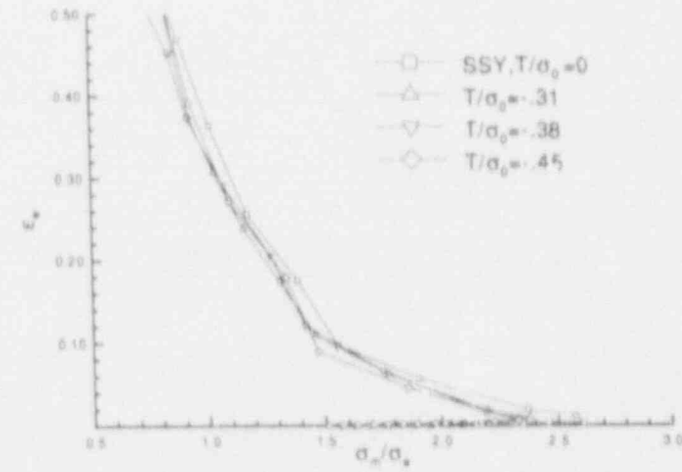

Figure C.13 Plane-strain distribution of effective plastic strain as function of stress ratio σ_m/σ_e for irradiation-degraded (simulated) material and various degrees of K and second parameter down to T/σ_0 = –0.45

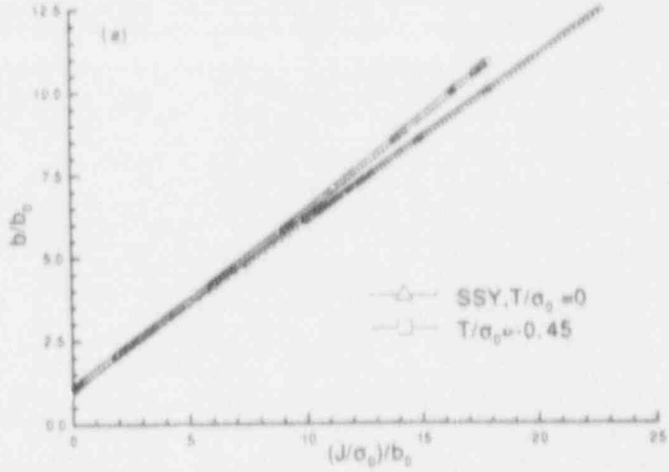

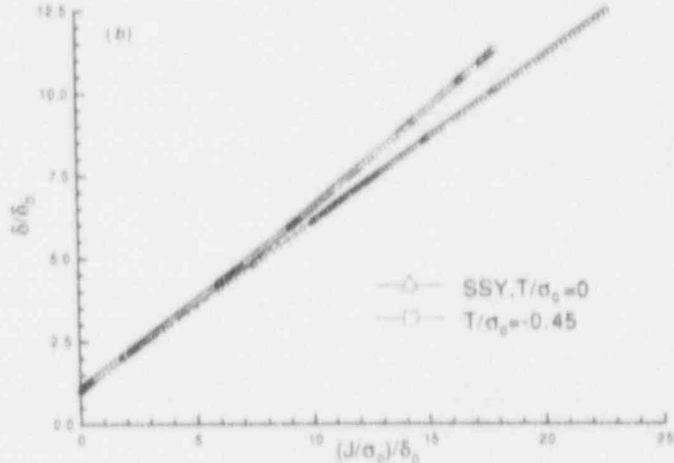

Figure C.14 (*a*) Plane-strain J-CTOD relation for irradiation-degraded (simulated) material based on Mode I displacement of point B indicated in Fig. C.2 and as function of second parameter T-stress. Magnitudes of T/σ_0 indicated in this figure correspond to maximum values of T-stress employed in specified analysis. (*b*) Plane-strain J-CTOD relation for irradiation-degraded (simulated) material based on 45° intercept definition indicated in Fig. C.2 and as function of second parameter T-stress. For range of T-stress considered, J-CTOD relation is insensitive to definition of CTOD employed but is sensitive to magnitude of T-stress

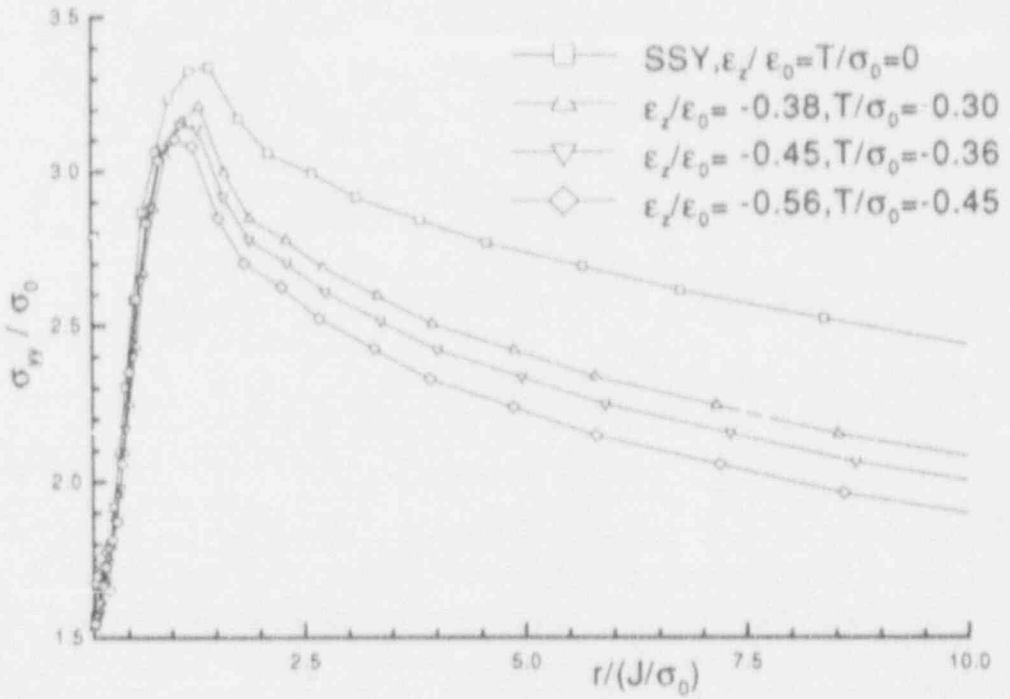

Figure C.15 Distributions of opening-mode stress directly ahead of blunting notch for irradiation-degraded (simulated) material under combined T-stress and transverse strain loading

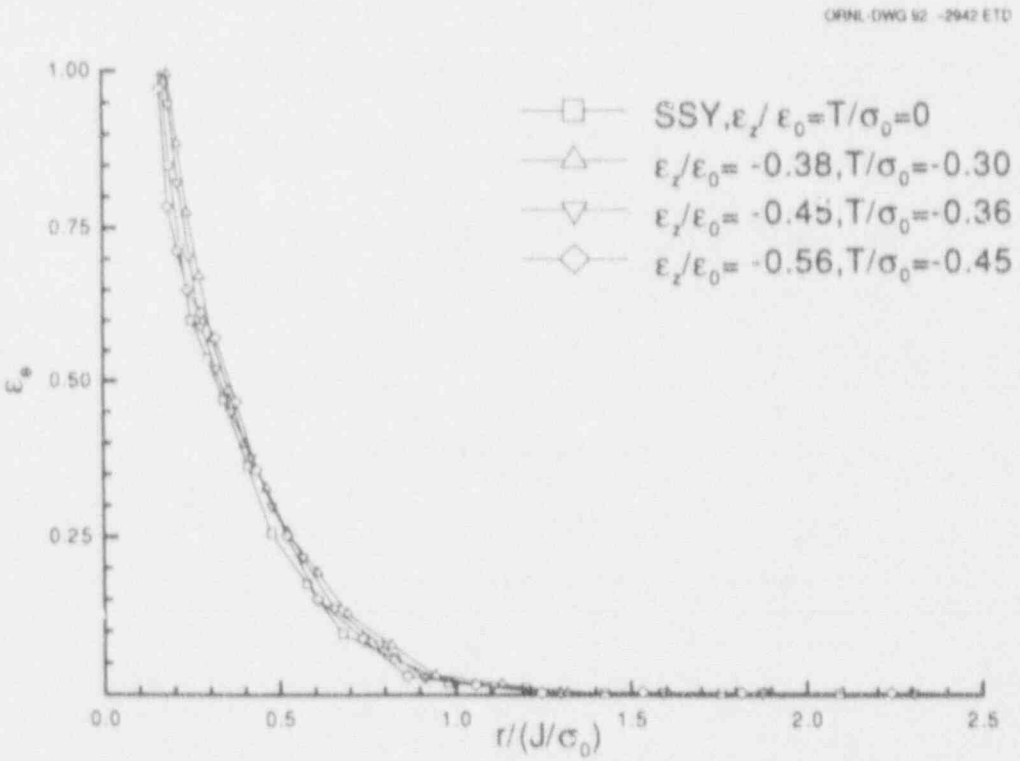

Figure C.16 Plane-strain distributions of effective plastic strain directly ahead of blunting notch for irradiation-degraded (simulated) material under combined T-stress and transverse strain loading

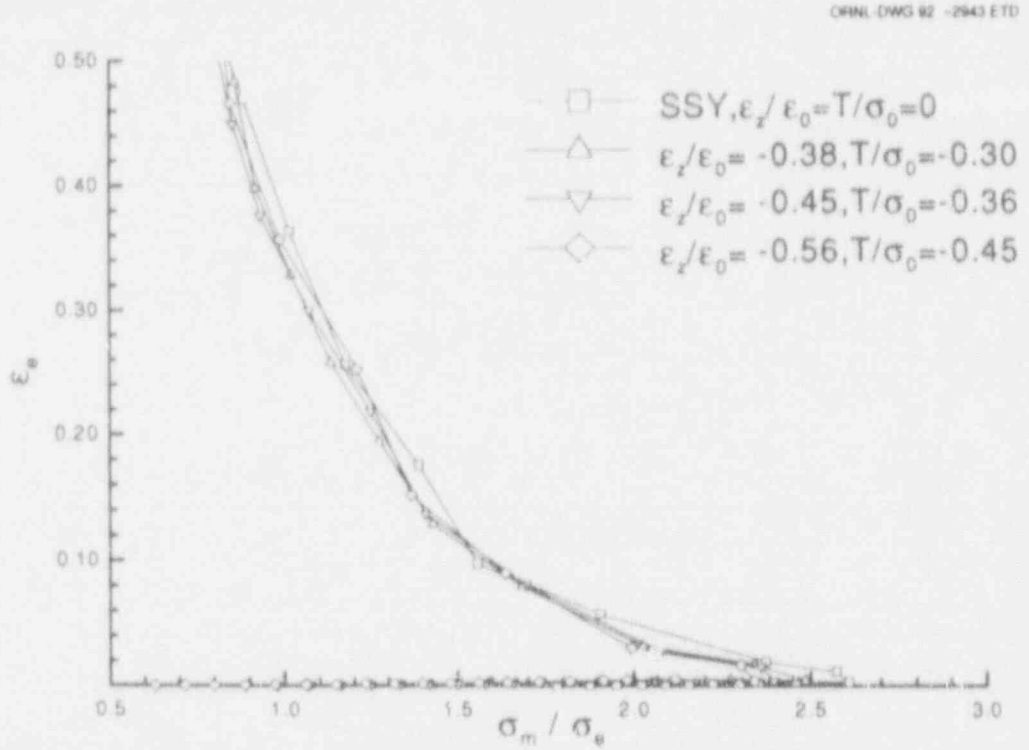

Figure C.17 Plane-strain distributions of effective plastic strain as function of stress ratio σ_m/σ_e for irradiation-degraded (simulated) material under combined T-stress and transverse strain loading

Table C.1 Estimates of toughness deviation, from a reference plane strain, K-dominant ($\varepsilon_z = T = 0$) value, based on the RKR model and a range of assumed cleavage fracture stress. These estimates are obtained based on results from Fig. C.8 for an irradiation-degraded (simulated) material and two values of transverse strain $\varepsilon_z/\varepsilon_0 = -0.56$ and 0.56. The predicted toughness deviations are relatively insensitive to the range of assumed critical cleavage stress. Magnitudes of the predicted toughness deviations are limited

	Critical value of $r/(J/\sigma_0)$			$J_{\varepsilon_z}/J_{SSY}$		$K_{\varepsilon_z}/K_{SSY}$	
σ_c/σ_o	$\varepsilon_z/\varepsilon_0 = 0.56$	SSY	$\varepsilon_z/\varepsilon_0 = -0.56$	$\varepsilon_z/\varepsilon_0 = 0.56$	$\varepsilon_z/\varepsilon_0 = -0.56$	$\varepsilon_z/\varepsilon_0 = 0.56$	$\varepsilon_z/\varepsilon_0 = -0.56$
2.5	10.10	8.60	6.20	0.85	1.39	0.92	1.18
2.6	8.50	6.85	5.15	0.81	1.33	0.90	1.15
2.7	6.90	5.45	4.15	0.79	1.31	0.89	1.15
2.8	5.35	4.15	3.45	0.78	1.20	0.88	1.10
2.9	3.70	3.20	2.85	0.87	1.12	0.93	1.06
3.0	2.60	2.50	2.40	0.96	1.04	0.98	1.02

the RKR model[6] and results from Fig. C.8, are presented for two values of out-of-plane strain and a range of assumed cleavage fracture stress. Results in Table C.1 indicate that toughness degradation due only to out-of-plane straining, with the T-stress parameter remaining equal to zero, is expected to be at most on the order of 20% in terms of K for the assumed set of analysis conditions. The limited range of predicted cleavage toughness deviations is qualitatively consistent with the near-term estimates provided in the first phase of this work.

In Table C.2 estimates of toughness deviation, from a reference plane strain, SSY ($\varepsilon_z = T = 0$) value, based on the RKR model and results from Fig. C.11 are presented for a range of plane strain T-stress conditions and a range of assumed cleavage fracture stress. Results from Fig. C.11 indicate that significant perturbation of the near-tip stress field from the reference plane strain distribution occurs under $T < 0$ conditions. Results in Table C.2 indicate that toughness deviations under negative T-stress conditions can be significant.

Table C.2 Estimates of toughness deviation, from a reference plane strain, K-dominant (ε_z = T = 0) value, based on the RKR model and a range of assumed cleavage fracture stress. These estimates are obtained based on results from Fig. C.11 for an irradiation-degraded (simulated) material and range of plane strain T-stress conditions. The predicted toughness deviations are relatively insensitive to the range of assumed critical cleavage stress. These results suggest that toughness deviations under negative T-stress conditions can be significant

	Critical value of $r/(J/\sigma_o)$			J_T/J_{SSY}			K_T/K_{SSY}		
σ_c/σ_o	T/σ_o = –0.45	T/σ_o = –0.38	T/σ_o = –0.31	T/σ_o = –0.45	T/σ_o = –0.38	T/σ_o = –0.31	T/σ_o = –0.45	T/σ_o = –0.38	T/σ_o = –0.31
2.5	2.7	3.45	4.20	3.19	2.49	2.05	1.79	1.58	1.43
2.6	2.05	2.65	3.35	3.34	2.59	2.05	1.83	1.61	1.43
2.7	1.60	1.95	2.60	3.41	2.80	2.10	1.85	1.67	1.45
2.8	1.35	1.65	1.95	3.07	2.52	2.13	1.75	1.59	1.46
2.9	1.20	1.45	1.65	2.67	2.21	1.94	1.63	1.49	1.39
3.0	1.05	1.20	1.45	2.38	2.08	1.72	1.54	1.44	1.31

In Table C.3 estimates of toughness deviation, from a reference plane strain, SSY (ε_z = T = 0) value, based on the RKR model and results from Fig. C.15, are presented for a range of T-stress and transverse strain conditions and a range of assumed cleavage fracture stress. From Figs. C.11 and C.15, it is observed that where T < 0 and $\varepsilon_z \neq 0$, the T-stress effects are primarily responsible for the observed deviation from the plane strain SSY distributions. The observation that T-stress effects dominate over transverse strain effects is reflected in the toughness estimates in Table C.3.

Finally, the toughness estimates presented in Tables C.1 to C.3 are plotted in Fig. C.18. It is observed that the predicted toughness deviations are relatively insensitive to the range of assumed critical cleavage stress. That is, while use of the RKR model to provide *quantitative* cleavage fracture toughness predictions is limited by the availability of material parameters relevant to the model, prediction of toughness *deviation* is, over the range of analysis conditions considered in this study, not very dependent on a quantitative knowledge of these parameter values.

C.6.2 Ductile Fracture

The results presented in Figs. C.8–C.17 pertain to an RPV-grade material with simulated irradiation effects on the uniaxial stress-strain behavior. The material failure curves for unirradiated A 533 B appropriate to the MHM ductile fracture model for three upper-shelf temperatures of 24, 77, and 177°C are indicated in Fig. C.19.[7] In the absence of material data under irradiated conditions, these failure curves will be adopted for the present analysis.

With respect to the prediction of ductile fracture, it is observed that the MHM failure criterion is exceeded by the results indicated in Figs. C.10, C.13, and C.17 for the

Table C.3 Estimates of toughness deviation, from a reference plane strain, K-dominant (ε_z = T = 0) value, based on the RKR model and a range of assumed cleavage fracture stress. These estimates are obtained based on results from Fig. C.15 for an irradiation-degraded (simulated) material and a range of T-stress and transverse strain conditions. The predicted toughness deviations are relatively insensitive to the range of assumed critical cleavage stress. These results suggest that T-stress effects dominate over transverse strain effects with respect to the predicted toughness deviations

	Critical value of $r/(J/\sigma_o)$			$J_{\varepsilon_z, T}/J_{SSY}$			$K_{\varepsilon_z, T}/K_{SSY}$		
	$\varepsilon_z/\varepsilon_o$ = –0.56	$\varepsilon_z/\varepsilon_o$ = –0.45	$\varepsilon_z/\varepsilon_o$ = –0.38	(–0.56)	(–0.45)	(–0.38)	(–0.56)	(–0.45)	(–0.38)
σ_c/σ_o	T/σ_o = –0.45	T/σ_o = –0.36	T/σ_o = –0.30	(–0.45)	(–0.36)	(–0.30)	(–0.45)	(–0.36)	(–0.30)
2.5	2.80	3.40	3.95	3.07	2.53	2.18	1.75	1.59	1.48
2.6	2.35	2.75	3.25	2.92	2.49	2.11	1.71	1.58	1.45
2.7	1.80	2.30	2.65	3.03	2.37	2.06	1.74	1.54	1.43
2.8	1.60	1.85	2.15	2.59	2.24	1.93	1.61	1.50	1.39
2.9	1.45	1.65	1.80	2.21	1.94	1.78	1.49	1.39	1.33
3.0	1.35	1.50	1.60	1.85	1.67	1.56	1.36	1.29	1.25

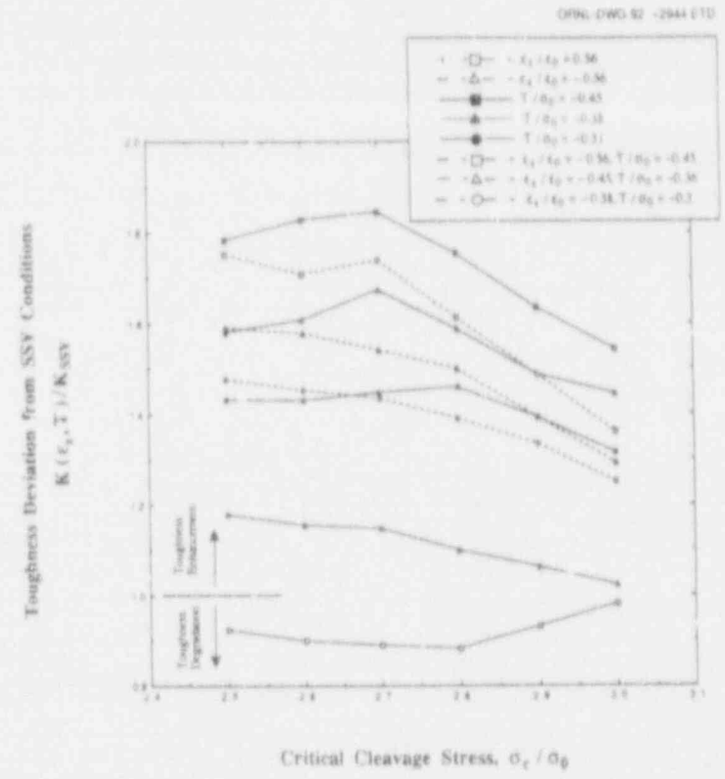

Figure C.18 Estimates of toughness deviation, from reference plane strain, K-dominant (ε_z = T = 0) value, based on RKR model and range of assumed cleavage fracture stress. Estimates are obtained based on results from Figs. C.8, C.11, and C.15, for irradiation-degraded (simulated) material. Predicted toughness deviations are relatively insensitive to range of assumed critical cleavage stress. These results suggest that toughness deviations under negative T-stress conditions can be significant

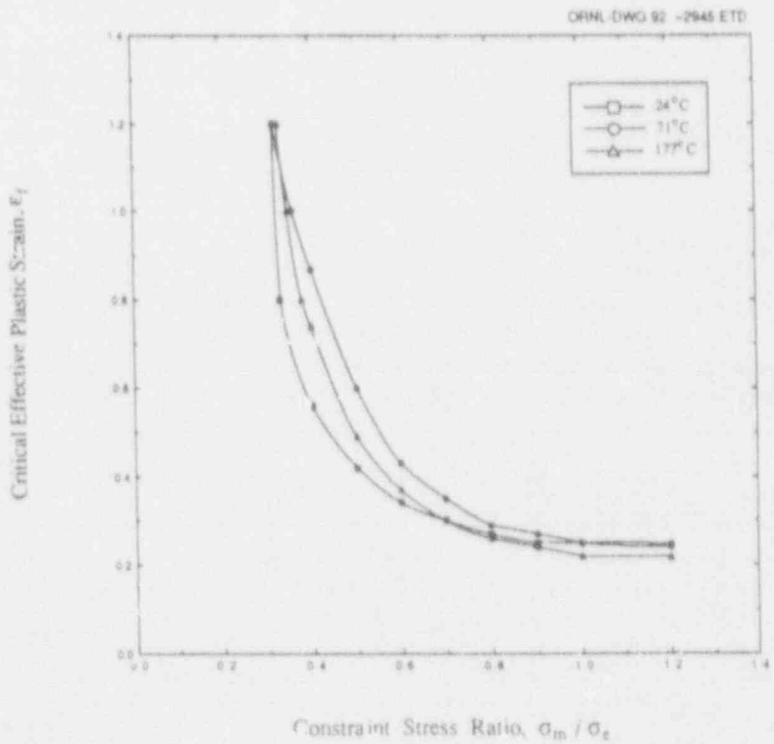

Figure C.19 Material failure curves for unirradiated A 533 B appropriate to MHM ductile fracture model for three upper-shelf temperatures of 24, 77, and 177°C (taken from Ref. 7)

magnitude of the effective plastic strain ε_e exceeding ~25%. From Figs. C.9, C.12, and C.16, it is observed that this magnitude of ε_e is exceeded over a distance approximately $<0.5\ J/\sigma_0$ for all cases considered. The effective plastic strain distributions in these figures are essentially invariant with respect to the range of transverse strain up to a distance of $0.5\ J/\sigma_0$. This invariance implies that minimal ductile toughness deviation due to positive out-of-plane straining is expected. The observation of minimal toughness deviation due to positive out-of-plane straining under ductile fracture conditions is consistent with the near-term estimates provided in the first phase of this work.

As noted previously in the discussion on cleavage fracture, the results in Figs. C.13 and C.17 indicate that where $T < 0$ and $\varepsilon_z \neq 0$ it is the T-stress effects that are primarily responsible for the observed deviations from the plane strain K-dominant distributions. While T-stress effects are seen to dominate over the transverse strain effects, the effective strain distributions in Figs. C.13 and C.17 are also nearly invariant with respect to the range of T-stress considered up to a distance of $0.5\ J/\sigma_0$. The deviation from the plane strain K-dominant distribution due to the range of T-stress considered results in <10% elevation in toughness in terms of J.

The above results suggest that the range of positive out-of-plane straining considered in this study, which is assumed to be representative of the degree of positive out-of-plane strain encountered during the normal operations of an RPV, is not expected to result in significant toughness degradation relative to plane strain ductile fracture and only on the order of 10% degradation (in terms of K) relative to plane strain values for cleavage crack initiation. On the other hand, these results suggest that a greater degree of toughness enhancement is associated with the range of negative out-of-plane strain and negative T-stress considered. For the range of negative transverse strain considered, the toughness cleavage toughness enhancement can be up to 20% in terms of K. Recall that the near-crack-tip fields associated with a short circumferential flaw within an RPV appear to exhibit negative T-stress effects. For the range of negative T-stress considered the toughness enhancement can be up to 85% in terms of K. For the range of combined negative transverse strain and T-stress considered, the toughness enhancement can be up to 75% in terms of K.

It is emphasized that these observations are based on the assumption that the introduction of out-of-plane strain and/or T-stress does not alter the micromechanics governing cleavage or ductile fracture. In addition, the level of toughness degradation or enhancement that can be achieved is dependent on the loading and geometry conditions being considered. Comparison of present analytical findings with limited experimental data obtained for an unirradiated A 533 B steel obtained by The Welding Institute (TWI) is discussed in the next section.

C.7 Comparison of Model Predictions with TWI Data

The TWI tests are believed to be load-controlled, uniaxially and biaxially loaded fracture tests involving wide-plate specimens of unirradiated A 533 B material.[8,9] The test temperatures span the transition region from lower-shelf (< –130°C), transition (–70°C) to the upper-shelf regime (+70°C). However, no duplication of wide-plate tests at a particular combination of test temperature and biaxiality ratio is reported. The plate thickness varies from 25 to 50 mm depending on test temperature. For the case of biaxial loading, equal biaxiality is maintained over an area of in-plane dimensions 500 × 500 mm. Various flaw geometries have been considered, but the primary flaw geometry is an elongated, part-through surface flaw centrally located with respect to the plate's in-plane dimensions. The maximum crack depth is ~40% of the plate's thickness, and the flaw length is 135 to 150 mm. Detailed finite-element analyses of these biaxial tests have not been reported.

Reported values of CTOD at fracture for the wide-plate specimens,[9] as inferred from a double clip-gage arrangement, under various degrees of [illegible]v are indicated in Fig. C.20, along with small-specimen [illegible]s obtained for material characterization purposes. The large differences in CTOD at failure in the transition region (–70°C) for the wide-plate data are related to the large differences in stable crack growth prior to cleavage fracture. On the other hand, the reported differences in CTOD at failure in the lower-shelf region (–160°C) occurred with no previous stable crack growth. It is significant to note that values of the nominal remote stress at failure at a given test temperature do not differ by more than 20%, regardless of the biaxiality ratio considered.

The analytical predictions presented in this appendix assume either pure cleavage or pure ductile failure. A failure mode that involves significant stable crack growth prior to cleavage fracture is not immediately amendable to the analytical treatment presented here. Nevertheless, comparisons of the TWI experimental results with the analytical results presented in this section are accomplished in the following fashion. Under plane strain LEFM conditions and assuming Poisson's ratio = 0.3, the magnitude of the out-of-plane stress parallel to the crack front is ~60% of the in-plane maximum principal stress along the crack plane. As a first estimate, the loading conditions corresponding to $k = 1$ in Fig. C.20 can be associated with positive out-of-plane strain, while $k = 1/2$ and $k = 0$ can be associated with negative out-of-plane strain.

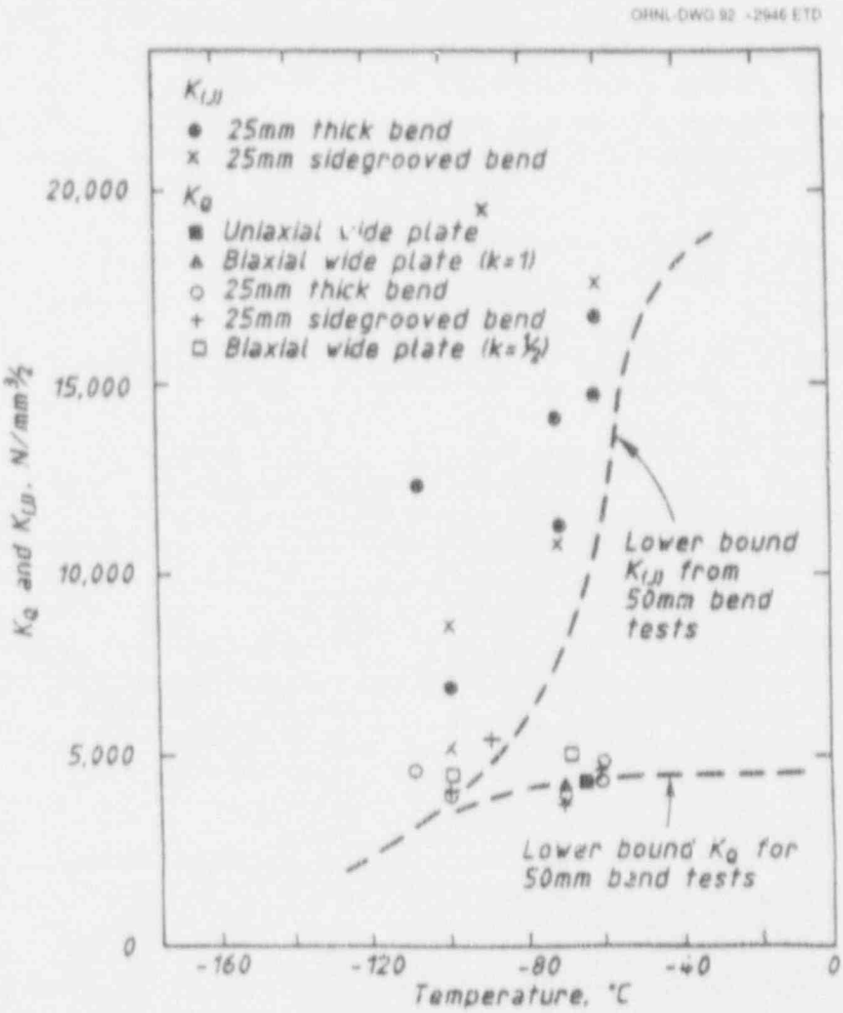

Figure C.20 Reported values of CTOD at fracture for TWI wide-plate specimens, as inferred from double clip-gage arrangement, under various degrees of biaxiality, along with small-specimen results obtained for material characterization purposes (taken from Ref. 9)

A cursory examination of the TWI results would suggest partial agreement with the analytical findings of the previous sections. The TWI results indicate that critical values of CTOD under equal biaxial loading (k = 1) fall within the lower scatter band of the small-specimen data. The experimental observation that positive out-of-plane straining has no effect on fracture toughness is in agreement with the analytical findings presented here.

As the degree of biaxiality decreases from k = 1/2 to k = 0 (uniaxial loading), the critical values of CTOD for the plate specimens become higher than the k = 1 results and the small-specimen data. At the test temperature of –70°C, the critical CTOD value for the uniaxially loaded plate specimen is approximately twice the k = 1 result, while at –160°C the k = 0 result is approximately four times the k = 1 result. In contrast, the TWI results in terms of K, where K is calculated based on the failure load, indicate a modest level of toughness enhancement.

While negative out-of-plane straining is predicted to result in modest toughness enhancement in the previous section, the predicted level of enhancement is much lower than the TWI results in terms of CTOD at failure. A more detailed examination of the TWI results is undertaken to ascertain the apparent discrepancy between analytical predictions and the TWI results. Such an examination reveals a number of experimental features of the TWI tests that appear to prevent a more definitive assessment of the reported data and, therefore, precludes further comparison of analytical predictions with the TWI data.

Specifically, a value of CTOD at failure of magnitude δ = 1.5 mm is reported in Fig. C.20 at a test temperature of –90°C for a 25-mm-thick side-grooved specimen. This value of CTOD at failure is more than four times the lower bound curve for the 50-mm bend specimens at the same temperature. Similar to the TWI small-specimen results, experimental data for HSST plate 13A made of A 533 B

material also indicate that fracture toughness values obtained from 4T-CT specimens at –70°C can differ by up to a factor of 2 in K or a factor of 4 in J or CTOD.[10] (However, note that the fracture toughness in terms of K for the TWI A 533 B material is approximately four times that of HSST plate 13A at –70°C.) The flaw length of 135 mm employed for the –70°C wide-plate specimens corresponds roughly to the flaw length of, for example, a 5T-CT specimen. Consequently, the wide-plate results at –70°C are likely to be still within the scatter band of small-specimen data. That is, the relatively short flaw length in the TWI tests may not be sufficient to exclude statistical variation in fracture toughness. The statistical scatter in toughness associated with the flaw length may mask any out-of-plane strain effects.

The lower-shelf wide-plate results involve cleavage fracture with no prior stable crack growth. Analytical results such as those to be presented in Appendix G suggest that the TWI plate specimen is associated with some degree of negative T-stress. From Table C.1 positive out-of-plane strain (k = 1) is not expected to result in significant toughness degradation, and negative out-of-plane strain (k = 0) is expected to result in modest toughness elevation. From Tables C.2 and C.3 and Fig. C.18, negative T-stress is expected to result in toughness enhancement; as previously noted, negative T-stress effects tend to dominate over positive out-of-plane strain effects. However, any attempt to attribute the observed higher CTOD values at failure for the case of k = 0 to T-stress effects needs to be reconciled with the lack of enhanced CTOD values at failure for the case of k = 1.

A perplexing aspect of the TWI results, when toughness is assumed to be represented by the reported CTOD values, is the apparent lack of correlation between the nominal remote stress and CTOD at failure. As indicated earlier, values of the nominal remote stress at failure at a given test temperature do not differ by more than 20% regardless of the biaxiality ratio considered. For the case of –160°C, this difference is on the order of 10% between the two cases of k = 1 and k = 0. Without commenting on the validity of the TWI K-estimation scheme, it appears reasonable to assume that a limited range of nominal remote stress state would translate into a limited range of crack-tip parameters such as K or J. Exception to this assumption is recognized for the case of gross yielding of the remaining net ligament ahead of the crack front. Gross yielding of the net ligament for the –160°C tests has not been reported and, based on the analysis results from Appendix G, is not expected.

Analytical results presented in Fig. C.4(*a*) and (*b*) indicate that the reference SSY J-CTOD relation is not substantially affected by a range of out-of-plane strain up to 5/9 the yield strain, nor is it substantially affected by a modest value of T-stress down to $T/\sigma_0 = -0.45$ as indicated in Fig. C.14(*a*) and (*b*). Analytical results to be presented in Appendix G for a single-edge-notch-tension (SENT) approximation to a biaxially loaded wide-plate geometry suggest a similar lack of dependence of the J-CTOD relation on out-of-plane strain that is on the order of the yield strain.

In summary, examination of the TWI results reveals a number of perplexing experimental features that prevent a more definitive assessment of the reported data and precludes further comparison of analytical predictions with the TWI data. The lack of confirmatory experimental data provides the motivation for the proposed large-scale biaxial fracture testing program discussed in Appendix G.

C.8 References

1. D. K. M. Shum et al., Martin Marietta Energy Systems, Inc., Oak Ridge Natl. Lab., "Analytical Studies of Transverse Strain Effects on Fracture Toughness for Circumferentially Oriented Cracks," USNRC Report NUREG/CR-5592 (ORNL/TM-11581), April 1991.*

2. *ABAQUS Theory Manual*, version 4-8, Hibbitt, Karlson and Sorensen, Inc., Providence, R.I., 1989.

3. J. W. Hutchinson, "Fundamentals of the Phenomenological Theory of Nonlinear Fracture Mechanics," *J. App. Mech.* 50, 1042–1051 (1983).†

4. R. M. McMeeking, "Finite Deformation Analysis of Crack-Tip Opening in Elastic-Plastic Materials and Implications for Fracture," *J. Mech. Phys. Solids* 25, 357–381 (1977).†

5. N. P. O'Dowd and C. F. Shih, "Family of Crack-Tip Fields Characterized by a Triaxiality Parameter: Part I –Structure of Fields," *J. Mech. Phys. Solids* 39, 989–1015 (1991).†

6. R. O. Ritchie, J. F. Knott, and J. R. Rice, "On the Relationship Between Critical Tensile Stress and Fracture Toughness in Mild Steel," *J. Mech. Phys. Solids* 21, 395–410 (1973).†

7. R. O. Ritchie, W. L. Server, and R. A. Wullaert, "Critical Fracture Stress and Fracture Strain Models

for the Prediction of Lower and Upper Shelf Toughness in Nuclear Pressure Vessel Steels," *Met. Trans. A* 10(A), 1557–1570 (1979).†

8. S. J. Garwood, T. G. Davey, and S. L. Creswell, "Behavior of A533B Under Biaxial Loading at +70°C," *Int. J. Press. Vess. Piping* 36, 199–224 (1989).†

9. S. J. Garwood, "The Significance of Biaxial Loading on the Fracture Performance of a Pressure Vessel Steel," *ASME Pressure Vessel and Piping Division Conference*, PVP-Vol 213/MPC-Vol 32, 113–123, 1991.†

10. D. F. M. Case, "A Comparison of Weibull and β_{Ic} Analyses of Transition Range Data," paper presented at the *23rd National Symposium on Fracture Mechanics, College Station, Tex.*, 1991.*

---

*Available for purchase from National Technical Information Service, Springfield, VA 22161.
†Available in public technical libraries.

Appendix D

Fracture Analysis of Compact Tension Specimen Subjected to Generalized Plane-Strain Loading

B. R. Bass J. Keeney-Walker

D.1 Introduction

The focus of this appendix is on a second approach being developed to investigate the effect of prescribed transverse and in-plane stress states on fracture toughness. The methodology employed here is based on a correlation procedure constructed by Anderson and Dodds[1] to remove the geometry dependence of cleavage fracture toughness values for single-edge-notched bend (SENB) specimens of A 36 steel for a range of crack depths. This procedure uses a local stress-based criterion for cleavage fracture and detailed finite-element analysis. From Ref. 1, dimensional analysis for small-scale yielding (SSY) implies that the principal stress ahead of the crack tip can be written as

$$\frac{\sigma_{p1}}{\sigma_o} = f\left(\frac{J^2}{\sigma_o^2 A}\right) , \qquad (D.1)$$

where σ_o is the 0.2% offset yield strength, σ_{p1} is the maximum principal stress at a point, and A is the area enclosed by the contour on which σ_{p1} is a constant. The strategy employed in Ref. 1 utilizes a fracture criterion dependent upon achieving a critical volume V_{CR} within which the principal stress is greater than σ_{p1}. For a specimen subjected to generalized plane-strain (GPS) conditions, the volume is equal to the specimen thickness B times the area within the σ_{p1} contour on the midplane ($V_{CR} = B \cdot A_{CR}$). Equation (D.1) is the appropriate normalization for SSY solutions when using the latter fracture criterion based on volume or area. This technique was successfully employed by Keeney-Walker et al.[2] to correlate cleavage-initiation toughness data from compact tension (CT) specimens with data from the large-scale WP-1 series of Heavy-Section Steel Technology (HSST) wide-plate specimens.[3]

In the following, the technique is used to investigate the effects of negative and positive out-of-plane strain on local crack-tip fields in a model of a 1T-CT specimen. Results presented here are an extension of the studies previously performed on the same specimen and reported in Chap. 7 of Shum et al.[4] In both cases, analyses were carried out on a three-dimensional (3-D) finite-element model of a CT specimen that assumed an incremental elastic-plastic constitutive formulation and GPS loading conditions. The present study utilized a finite-element model having substantially greater crack-tip mesh refinement when compared with the model described in Ref. 4. The more refined model was employed in the present study to generate improved estimates of the crack-tip stress and strain fields corresponding to cleavage-initiation conditions. The parameter based on the area A_{CR} enclosed within a contour of critical maximum principal stress σ_{p1} ahead of the crack tip was used to correlate these local crack-tip fields with applied loading at initiation. Results of correlations from the improved model are presented for a range of imposed out-of-plane strain values.

As described below, the correlations for the 1T-CT specimen illustrate that development of the methodology depends on establishing the existence of critical σ_{p1} stress values that correlate fracture toughness behavior over a range of transverse strain values. The following sections describe applications of the methodology to fracture toughness data for A 533 B steel from McCabe and Landes[5] that were designed to validate and calibrate the model in the plane stress-to-plane strain domain. Analyses of 3-D finite-element models of compact specimens having a common planform of a 4T specimen and thicknesses ranging from 10.16 to 101.6 mm were performed in an attempt to estimate critical σ_{p1} stress values in the negative transverse strain domain. These estimates of a critical σ_{p1} value are necessary to provide input to toughness correlations in the positive transverse strain domain and, thereby, to provide estimates of reductions in fracture toughness associated with these strains

D.2 Analytical Study of 1T Compact Specimens

D.2.1 Analysis Methods

A 3-D finite-element model of a geometry having the planform of a 1T-CT specimen was generated with the ORMGEN[6] mesh generating program. From symmetry conditions, only one-fourth of the specimen is included in the finite-element model (Fig. D.1). The specimen in Fig. D.1 has a thickness of 1.016 mm and was analyzed with the ADINA[7] finite-element program using special constraints on the nodal displacements to approximate GPS conditions. At any planform location in the model, the nodes (through the thickness) are constrained to have the same in-plane displacements. To model the effects of

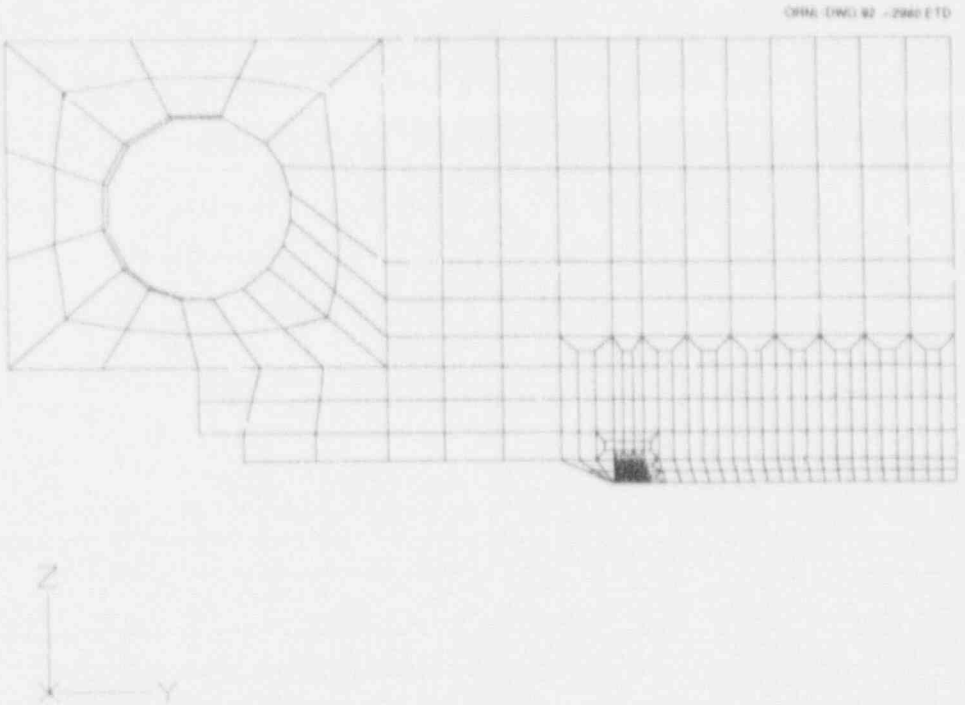

Figure D.1 3-D finite-element model of 1T-CT specimen subjected to GPS conditions

positive or negative out-of-plane strain, the nodes on the outer surface of the specimen are displaced uniformly in the direction normal to the surface; nodes midway between the midthickness symmetry plane and the outer surface are displaced by half that amount. The model depicted in Fig. D.1 consists of 5033 nodes and 674 20-noded isoparametric elements. Collapsed-prism elements surround the crack tip to allow for blunting and for a $1/r$ singularity in the strains at the crack front. The radial dimension of the collapsed-prism elements at the crack tip is r = 0.01524 mm ($r/w = 3 \times 10^{-4}$). Detailed plots of the crack-tip region are given in Fig. D.2. By comparison, the radial dimension of the collapsed-prism elements at the crack tip in the finite-element model of Ref. 4 was r = 0.11 mm ($r/w = 0.00215$).

The 3-D model of the 1T-CT specimen was analyzed using material properties taken from Ref. 3 for A 533 B steel at –75°C. An incremental elastic-plastic constitutive model (Model 8 in ADINA) was used for these analyses. For all cases, Young's modulus is E = 206.9 GPa, Poisson's ratio $\nu = 0.3$, and thermal expansion coefficient $\alpha = 11 \times 10^{-6}$/°C. The multilinear true stress–true strain curves for the material are given in Fig. D.3. The temperature-dependent yield stress for the multilinear representation in this figure is given by the function

$$\sigma_y = 374.866 + 59.894e^{-0.0079328T} , \qquad (D.2)$$

where σ_y and T are in megapascals and degrees Celsius, respectively. The stress-plastic-strain modulus H′(T) as a function of temperature is presented in Table D.1. A material-nonlinear-only (MNLO) formulation (small-strain theory) was used to model the strain response to deformation. A $2 \times 2 \times 2$ Gauss point rule was employed to compute the global stiffness matrix. Incremental loading was applied to the load pin hole of the model in the form of a cosine function with a resultant maximum load of 35 kN. (In tests of 1T-CT specimens K51C, K52B, and K54A described in Ref. 3 and in Table D.2, cleavage initiation was achieved at loads of 29, 35, and 50 kN; the specimens were not side-grooved.) Equilibrium iterations were performed in each load step of the ADINA calculations, using a convergence tolerance of 1×10^{-4} on an energy norm and 1×10^{-6} on a Euclidian norm of the displacement vector. For each load step of the calculations, energy release rates were determined along the crack front using a virtual crack-extension technique developed by deLorenzi[8] and implemented in the ORVIRT[9] program. (The ORVIRT program functions as a postprocessor of a conventional finite-element solution obtained from the ADINA program.)

D.2.2 Analysis Results

The 3-D model of the 1T-CT specimen depicted in Fig. D.1 was analyzed for the load cases given in Table D.3. In each load case, the mechanical loading at the load pin hole and the uniform out-of-plane strains were applied simultaneously and monotonically in 35 equal increments up to the maximum/minimum values indicated in Table D.3. The out-of-plane strains were imposed via equivalent out-of-plane nodal-point displacements. In Table D.3, the normalized out-of-plane strain for case 1 ($\varepsilon_z/\varepsilon_o = -1.05$)

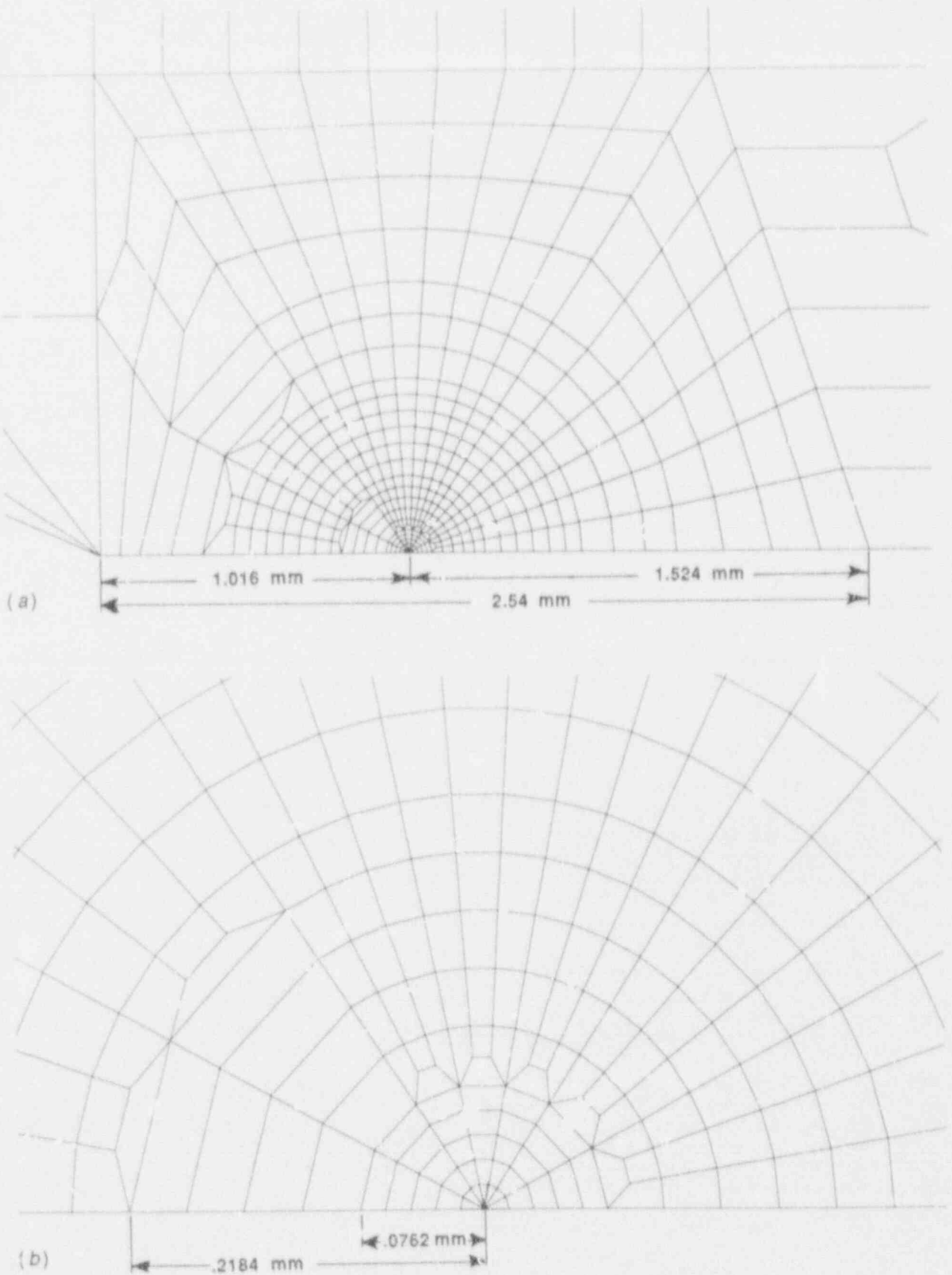

Figure D.2 Detail of crack-tip region of finite-element model of 1T-CT specimen

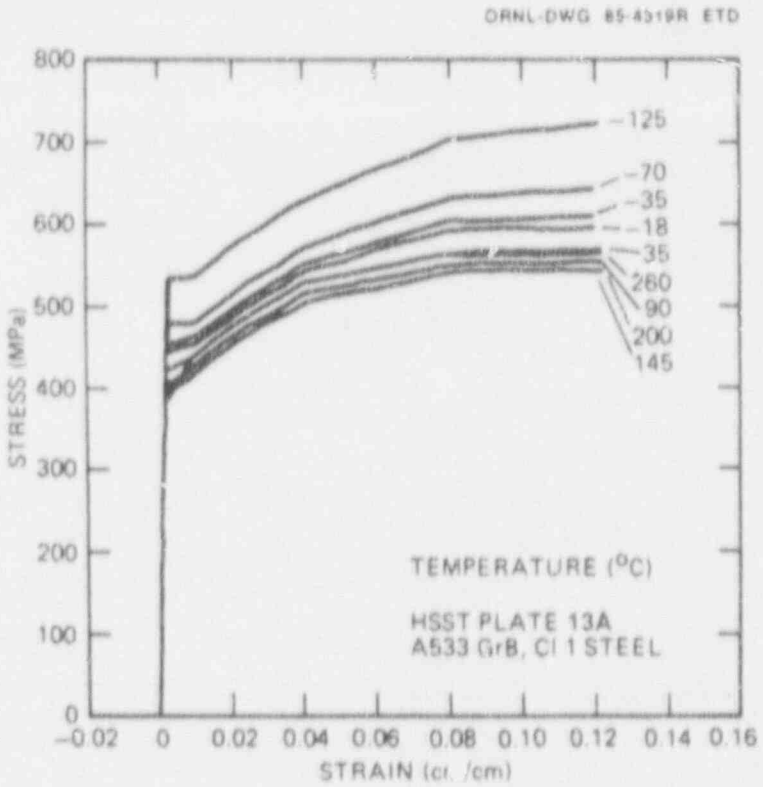

Figure D.3 Multilinear representations of uniaxial stress-strain behavior of HSST plate 13 A of A 533 B steel

Table D.1 Stress-plastic-strain modulus H′ for HSST wide-plate material (HSST plate 13A of A 533 B steel)

Plastic strain interval (%)	Temperature interval (°C)	$H' = \Delta\sigma/\Delta\varepsilon^P$ (MPa/%)
<1	$-125.00 \leq T < -72.78$	0.345
	$-72.78 \leq T < 37.78$	16.044 + 0.214 T
	$37.78 \leq T < 148.89$	21.787 + 0.062 T
	$148.89 \leq T < 260.00$	-24.407 + 0.372 T
1–2	$-125.00 < T < 260.00$	37.23
2–4	$-125.00 < T < 260.00$	26.579 - 0.00776 T
4–8	$-125.00 < T < 37.78$	11.228 - 0.0599 T
	$37.78 \leq T < 260.00$	8.96
8–12	$-125.00 < T < -17.78$	-0.0276 - 0.0403 T
	$-17.78 \leq T < 260.00$	0.0689

was selected to yield a computed J_I value equal to the experimentally determined J_I value (J_I = 26.3 kJ/m^2) reported for specimen K52B in Table D.2 at the initiation load of 35 kN.

The relationship between the area A_{CR} enclosed within the critical maximum principal stress contour defined by σ_{p1} = σ_{CRIT} and the applied J_I as a function of out-of-plane strain for the GPS model of the 1T-CT specimen is shown in Figs. D.4–D.7 for σ_{CRIT} = 1350, 1375, 1400, and 1425 MPa, respectively. These results may provide an estimate of the elevation or reduction of critical load (or J) required for achieving a critical area for cleavage initiation A_{CR} as a function of the out-of-plane strain. Comparison of the refined mesh results in Fig. D.6 for σ_{CRIT} = 1400 MPa with the corresponding results in Fig. 7.5 of Ref. 4 indicates that mesh refinement did not substantially alter the J vs A_{CR} relations expressed as a function of out-of-plane strain.

The J vs A_{CR} correlations depicted in Figs. D.4–D.7 exhibit a decreasing sensitivity to the magnitude of out-of-plane strain as the critical principal stress is increased from σ_{p1} = 1350 MPa to σ_{p1} = 1425 MPa. If the estimate of Hahn, Gilbert, and Reid[10] for the cleavage microcrack propagation stress for individual grains of ferrite (σ_{CRIT} = 1380 MPa) is employed as the critical value, then the J vs A_{CR} correlations of Fig. D.5 imply a reduction from the plane-strain K_I values [$K_I = \sqrt{EJ/(1-\nu^2)}$] of <9% to achieve a critical area A_{CR} for cleavage initiation for the case of positive out-of-plane strain given by $\varepsilon_{zmax}/\varepsilon_o$ = 0.5. With increasing values of positive out-of-plane strain satisfying $\varepsilon_{zmax}/\varepsilon_o > 0.5$, the J vs A_{CR} relation no longer follows the monotonic trend of Figs. D.4–D.7 as a function

Table D.2 Fracture toughness results for wide-plate specimen (WP-1) material (HSST plate 13A, A 533 B steel)

Specimen	Test temperature (°C)	Thickness (mm)	a/W_1	Ductile Δa (mm)	J_{max} (kJ/m^2)	J_{cleave} (kJ/m^2)	K_{Jc} (MPa $\sqrt{m}$)	$K_{Jcleave}$ (MPa $\sqrt{m}$)	Beta-corrected $K_{Jcleave}$ (MPa $\sqrt{m}$)
K33A	−150	50.8	0.554	<0.020	9.2	9.2	44.6	44.6	44.2
K33B	−150	50.8	0.555	<0.200	15.8	15.8	58.4	58.4	57.0
K34A	−75	50.8	0.556	0.071	97.5	97.5	143.6	143.6	102.7
K34B	−18	50.8	0.562	0.366	242.7	242.7	203.8[a]	224.8	119.9
K35A	−150	50.8	0.555	<0.020	10.2	10.1	46.7	46.7	46.2
K35B	−150	50.8	0.543	<0.020	7.5	7.5	40.2	40.2	40.0
K41B	−18	50.8	0.563	0.221	195.9	195.9	202.0	202.0	114.7
K42B	−75	50.8	0.563	<0.020	49.1	49.1	101.9	101.9	84.8
K41A	−75	50.8	0.557	<0.020	64.3	64.3	116.6	116.6	92.1
K42A	−75	50.8	0.554	<0.020	63.8	63.8	116.2	116.2	91.9
K51C	−75	25.4	0.554	<0.020	14.4	14.4	55.2	55.2	50.7
K52B	−75	25.4	0.576	<0.020	26.3	26.3	74.6	74.6	62.5
K53B	−18	25.4	0.562	0.196	177.6	177.6	192.3	192.	91.5
K53F	−18	25.4	0.572	0.064	64.5	64.5	115.9	115.9	74.0
K54A	−75	25.4	0.573	<0.02[illegible]	74.1	74.1	125.2	125.2	82.6
K54F	−18	25.4	0.568	1.122	124.4	124.4	160.9	160.9	85.2

[a] J_{1c} used to calculate K_{Jc}; otherwise J_{max} load used.

Table D.3 Out-of-plane strain conditions imposed on GPS model of IT-CT specimen

Load case	Normalized out-of-plane strain[a] ($\varepsilon_{zz}/\varepsilon_o$)	J at max load (kJ/m^2)	CTOD (δ_t) at max load (mm)	$d = \delta \cdot J/\sigma_o$ at max load
1	−1.05	26.412	0.02732	0.4954
2	−0.5	22.703	0.02512	0.5311
3	0.0	22.594	0.02503	0.5317
	Plane strain			
4	+0.5	22.679	0.02486	0.5262
5	+0.7	24.170		

[a] Maximum/minimum imposed uniform strains; maximum load of 35 kN applied at load pin hole; $\varepsilon_o = \sigma_o/E$; σ_o = 480 MPa; E = 206.9 GPa.

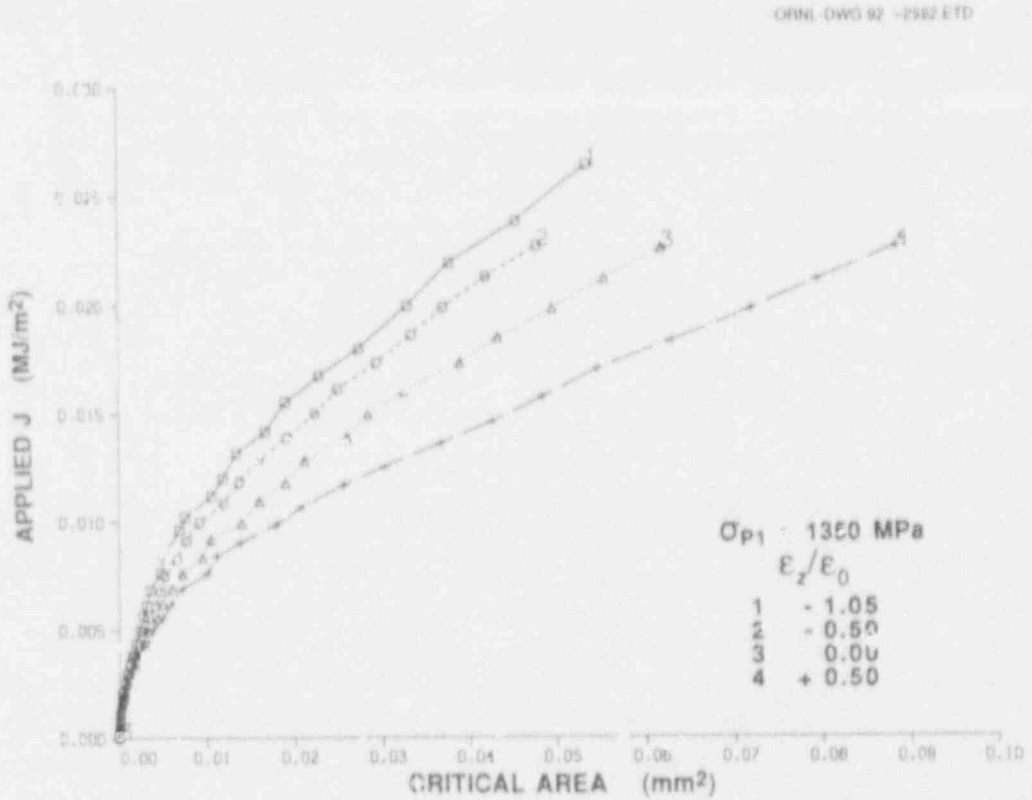

Figure D.4 Applied J vs area A within maximum principal stress contour of σ_{p1} = 1350 MPa for 1T-CT specimen subjected to four load cases of out-of-plane strain

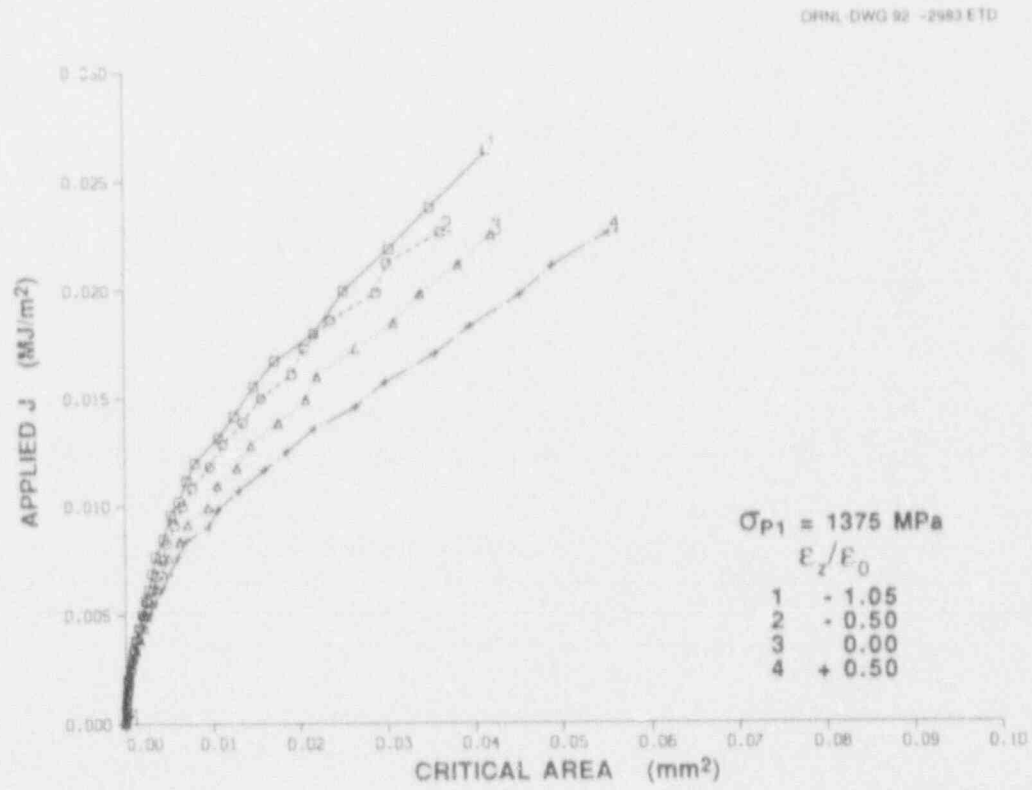

Figure D.5 Applied J vs area A within maximum principal stress contour of σ_{p1} = 1375 MPa for 1T-CT specimen subjected to four cases of out-of-plane strain

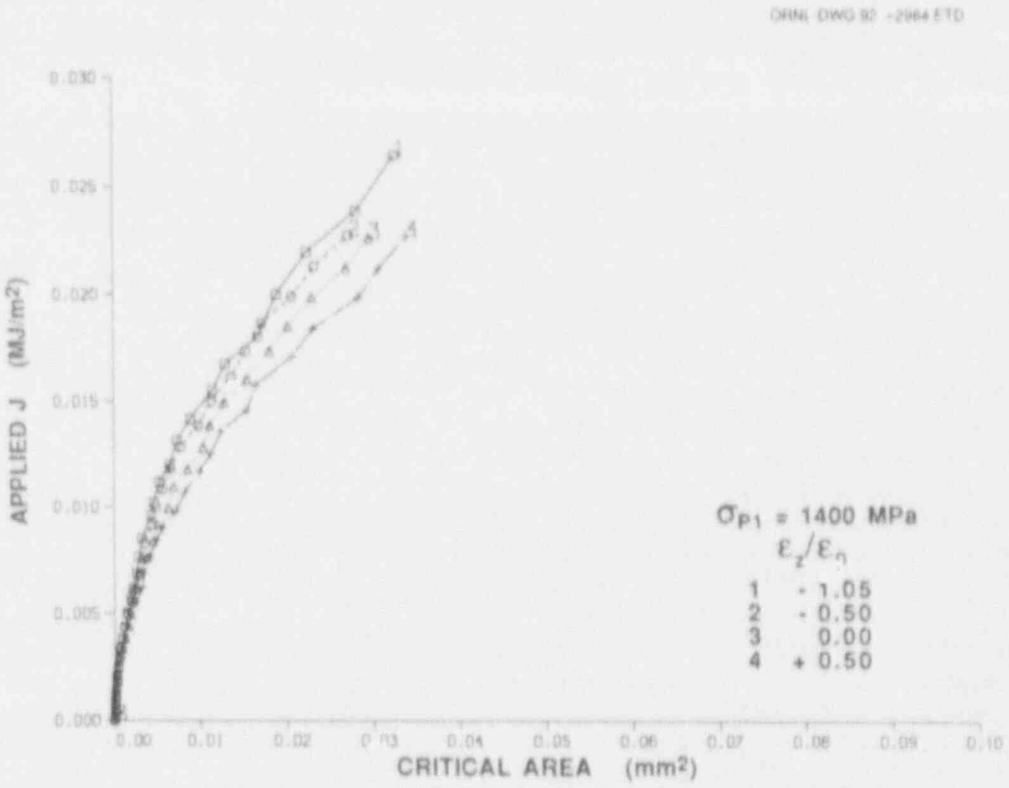

Figure D.6 Applied J vs area A within maximum principal stress contour of σ_{p1} = 1400 MPa for 1T-CT specimen subjected to four cases of out-of-plane strain

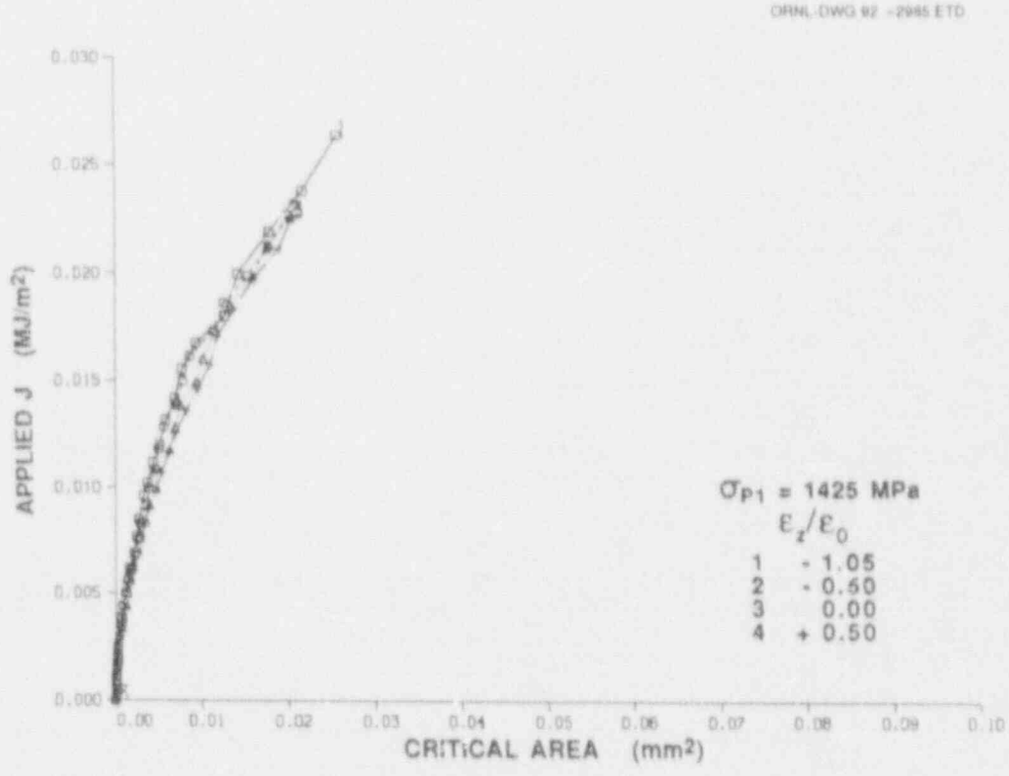

Figure D.7 Applied J vs area A within maximum principal stress contour of σ_{p1} = 1425 MPa for 1T-CT specimen subjected to four cases of out-of-plane strain

of the parameter $\varepsilon_z/\varepsilon_0$. This is illustrated in Fig. D.8, where results for the case $\varepsilon_{zmax}/\varepsilon_0 = 0.7$ are given for a critical maximum principal stress value of $\sigma_{p1} = 1400$ MPa. This onset of nonmonotonic behavior in the J vs A_{CR} relations coincides with the development of a plastic zone at the back face of the CT specimen, as depicted in Fig. D.9. With increasing development of this plastic zone in the ligament, a correlation based on J vs A_{CR} ceases to be viable for the 1T-CT specimen under conditions corresponding to $\varepsilon_{zmax}/\varepsilon_0 > 0.5$.

For the load cases defined in Table D.3, contour plots are given in Figs. D.10–D.13 for selected values of critical maximum principal stress and in Figs. D.14–D.17 for the effective stress function; included in these contours is the value (480 MPa) corresponding to initial yield. These results correspond to the maximum loading conditions given in Table D.3 for load cases 2–5, respectively. Figures D.14–D.17 illustrate the highly nonsymmetric development of the crack-tip plastic zone in the 1T-CT specimens with respect to positive and negative out-of-plane strains. For negative out-of-plane strain conditions (Fig. D.14), there is a substantial increase in enclosed area of the plastic zone and in the extent of yielding in the crack plane ahead of the tip, when compared with the plane strain condition (Fig. D.15). However, for increasing values of positive out-of-plane strain (Figs. D.16 and D.17), there is relatively little change in the size or shape of the yielded region, except for the reduced extent of yielding in the crack plane ahead of the crack tip.

D.3 Analytical Study of 4T Compact Specimens

D.3.1 Analysis Methods

Analyses of fracture toughness data for A 533 B steel[5] obtained from compact specimens having a common planform of a 4T specimen and thicknesses varying from 10.16 to 101.6 mm were carried out to provide critical σ_{p1} values for correlating toughness in the negative transverse strain domain. The 3-D finite-element models of the 4T-CT specimens used in these analyses are similar to the 1T-CT model in Fig. D.1, but with planform dimensions defining the 4T geometry. The characteristic dimension of the elements at the crack tip in Fig. D.18 is 0.44 mm. Four specimen thicknesses were analyzed: (1) Model A—101.6 mm, (2) Model B—50.8 mm, (3) Model C—25.4 mm, and (4) Model D—10.16 mm. Models A and B have 5 elements through the thickness with 8394 nodes and 1640 elements, and Models C and D have 4 elements through the thickness with 6932 nodes and 1312 elements. The analyses used an

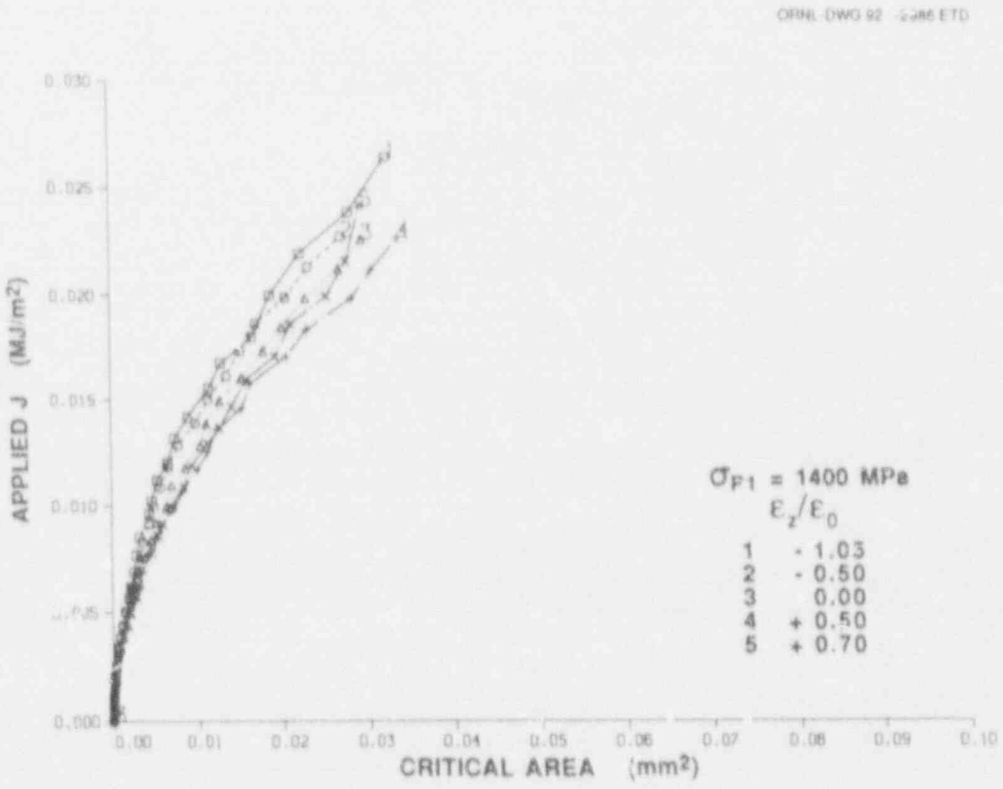

Figure D.8 Applied J vs area A within maximum principal stress contour of σ_{p1} = 1400 MPa for 1T-CT specimen subjected to five cases of out-of-plane strain

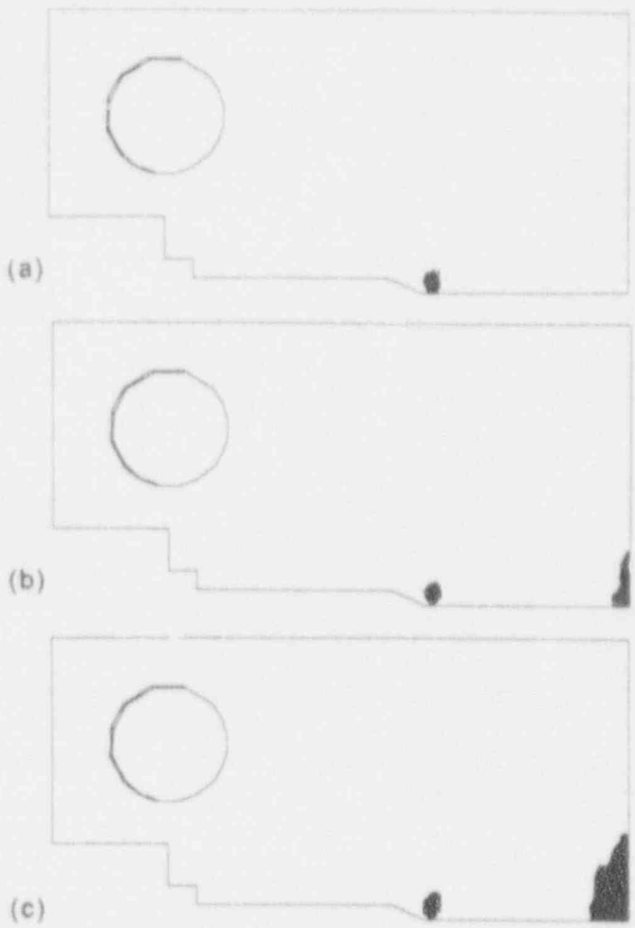

Figure D.9 Region of plasticity in GPS model of 1T-CT specimen corresponding to maximum pin load of 35 kN and three values of out-of-plane strain: (*a*) $\varepsilon_Z/\varepsilon_0 = 0.0$, (*b*) $\varepsilon_Z/\varepsilon_0 = 0.5$, (*c*) $\varepsilon_Z/\varepsilon_0 = 0.7$

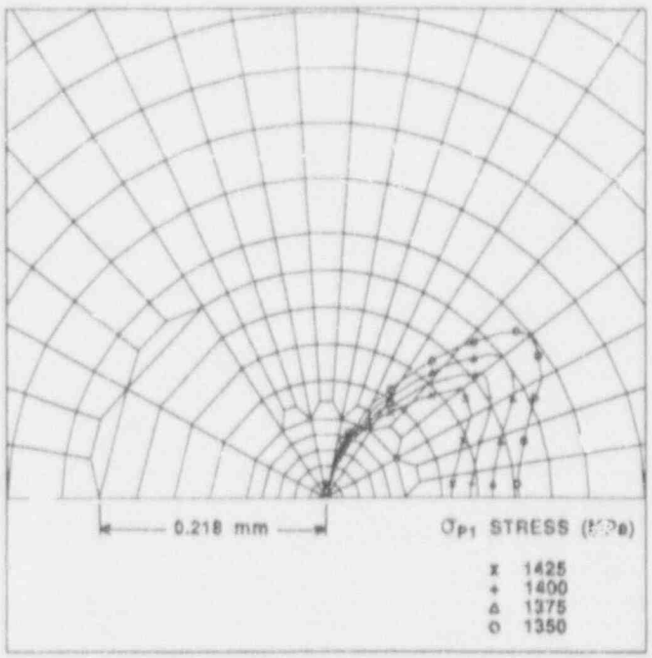

Figure D.10 Contours of maximum principal stress in GPS model of 1T-CT specimen subjected to applied pin load of 35 kN and out-of-plane strain of $\varepsilon_Z/\varepsilon_0 = -0.5$

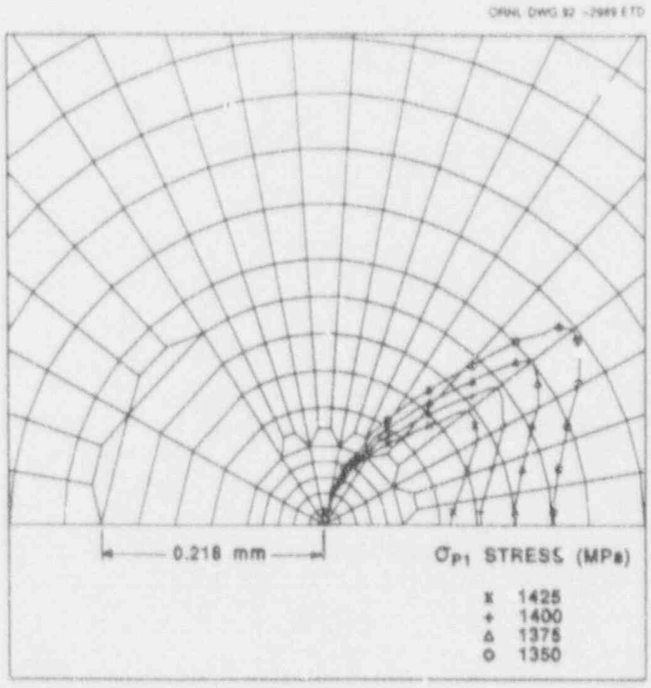

Figure D.11 Contours of maximum principal stress in GPS model of 1T-CT specimen subjected to applied pin load of 35 kN and out-of-plane strain of $\varepsilon_Z/\varepsilon_0 = 0.0$

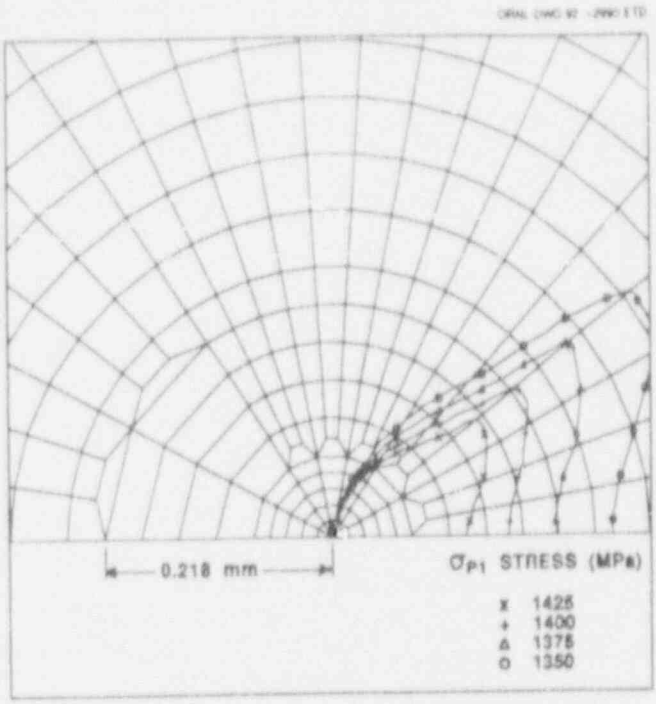

Figure D.12 Contours of maximum principal stress in GPS model of 1T-CT specimen subjected to applied pin load of 35 kN and out-of-plane strain of $\varepsilon_Z/\varepsilon_0 = 0.5$

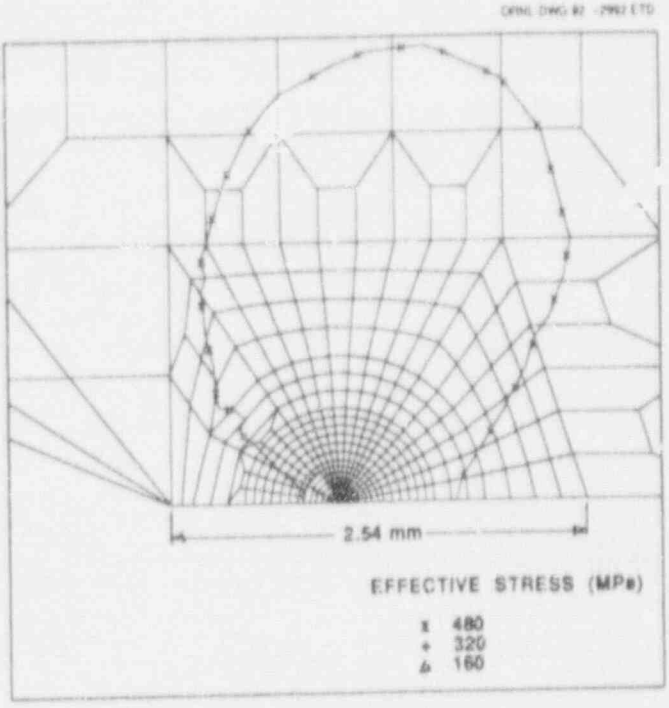

Figure D.14 Contours of effective stress in GPS model of 1T-CT specimen subjected to applied pin load of 35 kN and out-of-plane strain of $\varepsilon_Z/\varepsilon_0 = -0.5$

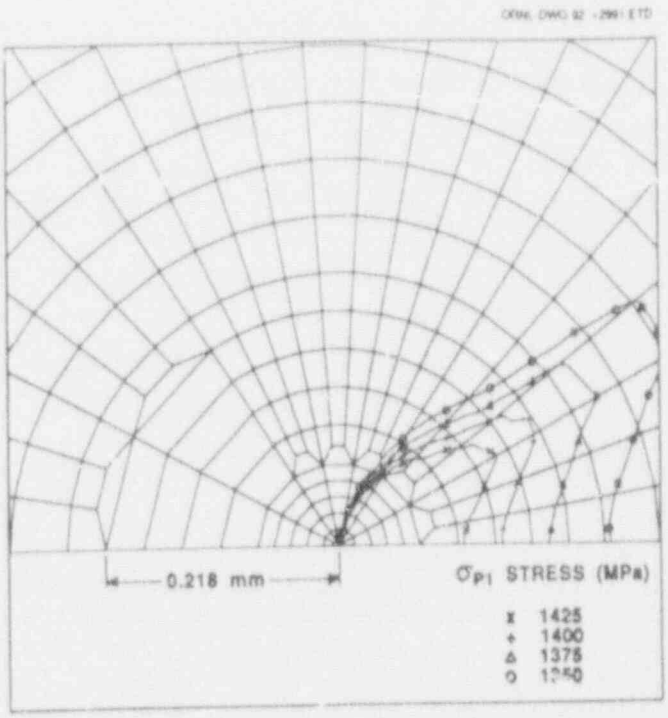

Figure D.13 Contours of maximum principal stress in GPS model of 1T-CT specimen subjected to applied pin load of 35 kN and out-of-plane strain $\varepsilon_Z/\varepsilon_0 = 0.7$

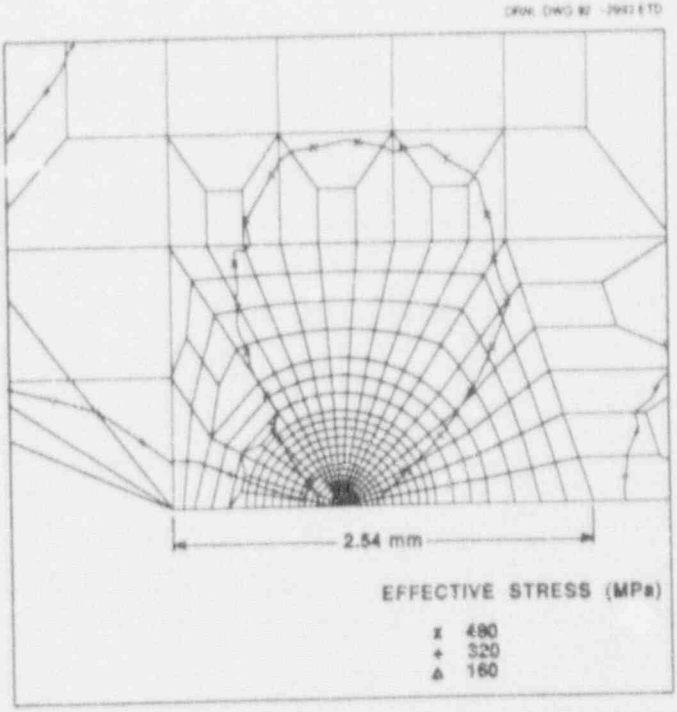

Figure D.15 Contours of effective stress in GPS model of 1T-CT specimen subjected to applied pin load of 35 kN and out-of-plane strain of $\varepsilon_Z/\varepsilon_0 = 0.0$

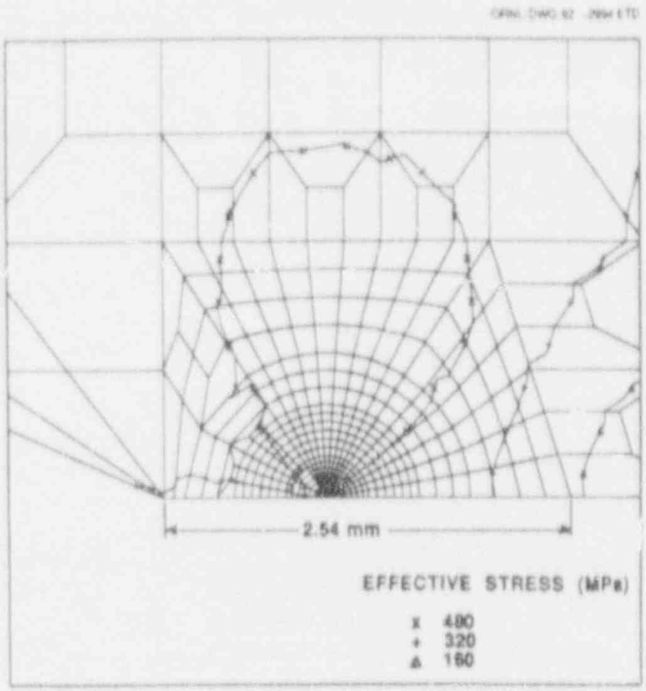

Figure D.16 Contours of effective stress in GPS model of 1T-CT specimen subjected to applied pin load of 35 kN and out-of-plane strain of $\varepsilon_z/\varepsilon_0 = 0.5$

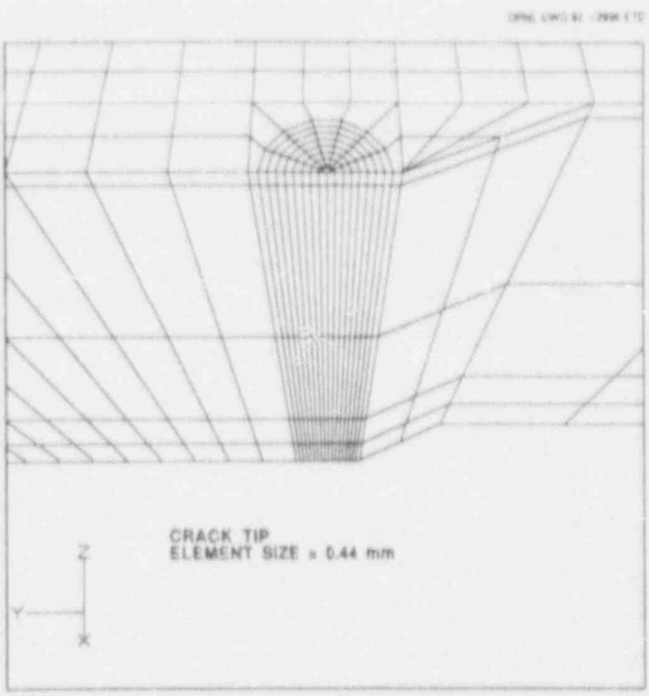

Figure D.18 Crack-tip region of 3-D finite-element model of 4T-CT specimen

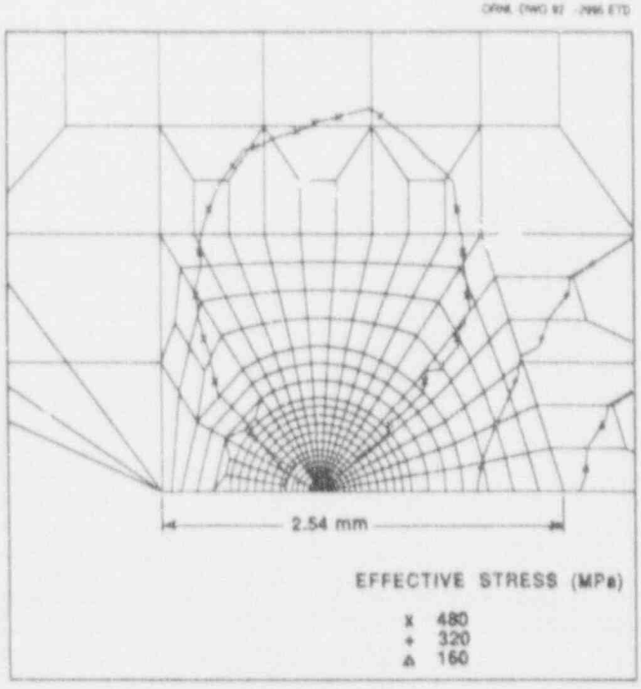

Figure D.17 Contours of effective stress in GPS model of 1T-CT specimen subjected to applied pin load of 35 kN and out-of-plane strain of $\varepsilon_z/\varepsilon_0 = 0.7$

incremental elastic-plastic constitutive model, with a 2 × 2 × 2 Gauss point rule, and an MNLO (small-strain) formulation. A multilinear stress-strain curve was generated from the wide-plate data (see Fig. D.3) corresponding to a temperature of 0°C (yield stress of 434.8 MPa); the curve was then elevated to match the yield stress of 482.6 MPa reported in Ref. 5. Because Young's modulus was not given in Ref. 5, a value of 207.2 GPa was used from the wide-plate data at 0°C. The load was applied incrementally (with equilibrium iterations performed at each load step) up to the load where the calculated applied K value approximated that of the experimental K reported in Ref. 5 for cleavage initiation. These values are recorded in Table D.4.

D.3.2 Analysis Results

In Fig. D.19, the applied J values generated from the analyses of the four models are plotted as a function of the load normalized by each specimen thickness. Figure D.19 indicates that, as the specimen thickness decreases, the degree of nonlinearity increases substantially. This is also evident from Fig. D.20 where the yielded regions are shown for each model at the time of initiation. All of the models have yielded in the crack-tip region at initiation, and Model D is almost completely yielded on the crack plane. The load vs load-line displacements (normalized by specimen width W) from the finite-element analysis of Model D were compared with experimental data[5] in Fig. D.21 to determine if the structural response could be

Table D.4 Critical areas within maximum principal stress contours for planform 4T specimens with varying thicknesses

Specimen thickness (mm)	Experimental K value (MPa$\sqrt{m}$)	Calculated K value (MPa$\sqrt{m}$)	Critical area (A_{CR}) (mm^2) for maximum principal stress values of											
			1200	1250	1300	1350	1375	1400	1425	1450	1475	1500	1550	1600
101.6	151	152	6.57	3.97	2.35	1.31	0.96	0.66	0.38	0.36	0.22	0.14	0.04	0.04
50.8	191	192	9.29	5.55	3.36	2.12	1.64	1.27	0.95	0.78	0.58	0.42	0.25	0.09
25.4	226	221	5.60	4.04	2.88	1.99	1.69	1.28	1.13	0.90	0.69	0.58	0.36	0.18
10.16	629	630	3.39	2.45	2.00	1.39	1.04	0.91	0.78	0.58	0.46	0.42	0.26	0.14

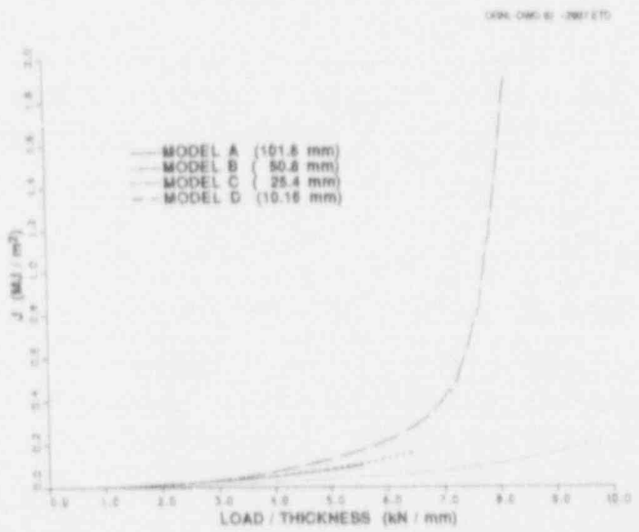

Figure D.19 Applied J vs load normalized by thickness for 4T-CT models with differing thicknesses

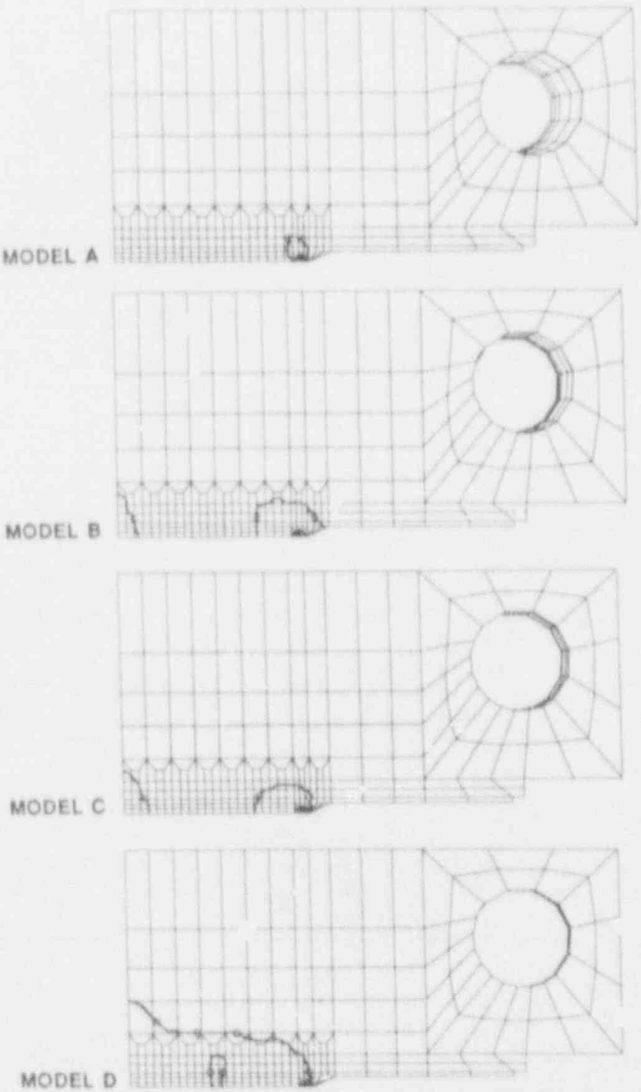

Figure D.20 Yielded regions (σ_y = 482.6 MPa) of four 4T-CT models at initiation

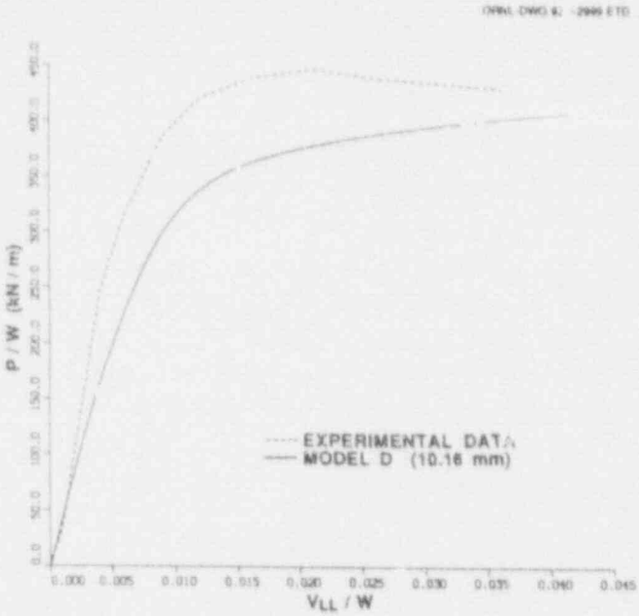

Figure D.21 Load vs load-line displacement (both normalized by W) for Model D, which is 10.16 mm thick, and experimental data

reproduced in the model. From the analysis, the model yielded and became nonlinear at a lower load than that implied by the experimental data. To reproduce the linear part of the load and displacement curve in Fig. D.21, an artificially high yield stress of 610 MPa (determined from a parametric study) was required.

The contours of maximum principal stress, ranging from 1200 to 1600 MPa, at K values corresponding to cleavage initiation are shown in Fig. D.22 for each model. In general, the contours decrease as the specimen thickness decreases and the amount of plasticity increases, except for Model B where the contours are slightly larger than Model A. The critical area parameter A_{CR} was evaluated at initiation for each model over a range of σ_{p1} values. From Fig. D.23, the correlations for Models A and B do not intersect; Model C intersects Model A at ~1250 MPa and coincides with Model B between 1360 and 1400 MPa. Model D intersects Model A at about 1340 MPa and Model B at 1500 MPa. A variation of this correlation is given in Fig. D.24 where the distance L_{CR} measured from the crack tip to the intersection of the maximum principal stress contour with the crack plane is plotted as a function of stress. This correlation also proved to be inconclusive in establishing a critical σ_{p1} parameter.

The analysis results are compared with the SSY solution in Fig. D.25 to investigate Q-stress effects. It can be observed that when the opening-mode stress, normalized by the yield stress, is plotted vs the normalized distance from the crack tip $[r/(J/\sigma_c)]$, Model A is close to the SSY solution as expected, but Model B begins to diverge at a value of $r/(J/\sigma_o) \approx 3$; Models C and D are even more divergent. The normalized stress is also plotted as function of distance (r) from the crack tip in Fig. D.26.

D.4 Conclusions

If a criterion for cleavage fracture is adopted that requires a critical volume of material be stressed to a critical value of maximum principal stress σ_{CRIT}, then the predicted cleavage-initiation load in the 1T-CT specimen is dependent upon the value of σ_{CRIT} and the normalized out-of-plane strain ratio $\varepsilon_{zz}/\varepsilon_o$. For values of σ_{CRIT} = 1680 MPa and $\varepsilon_{zz}/\varepsilon_o = 0.5$, the model predicts a reduction in the K_I value at initiation of ~9% relative to plane strain conditions. The correlation between driving force (J) and stressed volume (A_{CR}) is not viable in the specimen for $\varepsilon_{zz}/\varepsilon_o > 0.5$ due to developing plasticity in the model.

The methodology was applied to fracture-toughness data from compact specimens having a common planform of 4T specimens and varying thicknesses to provide estimates of critical σ_{p1} stress values in the plane stress-to-plane strain domain. The results were inconclusive in that a critical σ_{p1} value common to three (thickness of 25.4, 50.8, and 101.6 mm) of the specimens could not be established. However, it should be noted that the data set in Ref. 5 included only one cleavage-initiation toughness value for each specimen thickness. Additional material properties and load vs load-line displacement from Ref. 5 were not sufficient to permit adequate modeling of the structural response of the test specimens. Because of these difficulties with the experimental data, the viability of the stress contour methodology for correlating fracture toughness in the plane stress-to-plane strain domain cannot be judged on the basis of the above application. Further study of this methodology is warranted, based partly on successful correlations reported[1,2] previously from applications that focussed on in-plane stress effects.

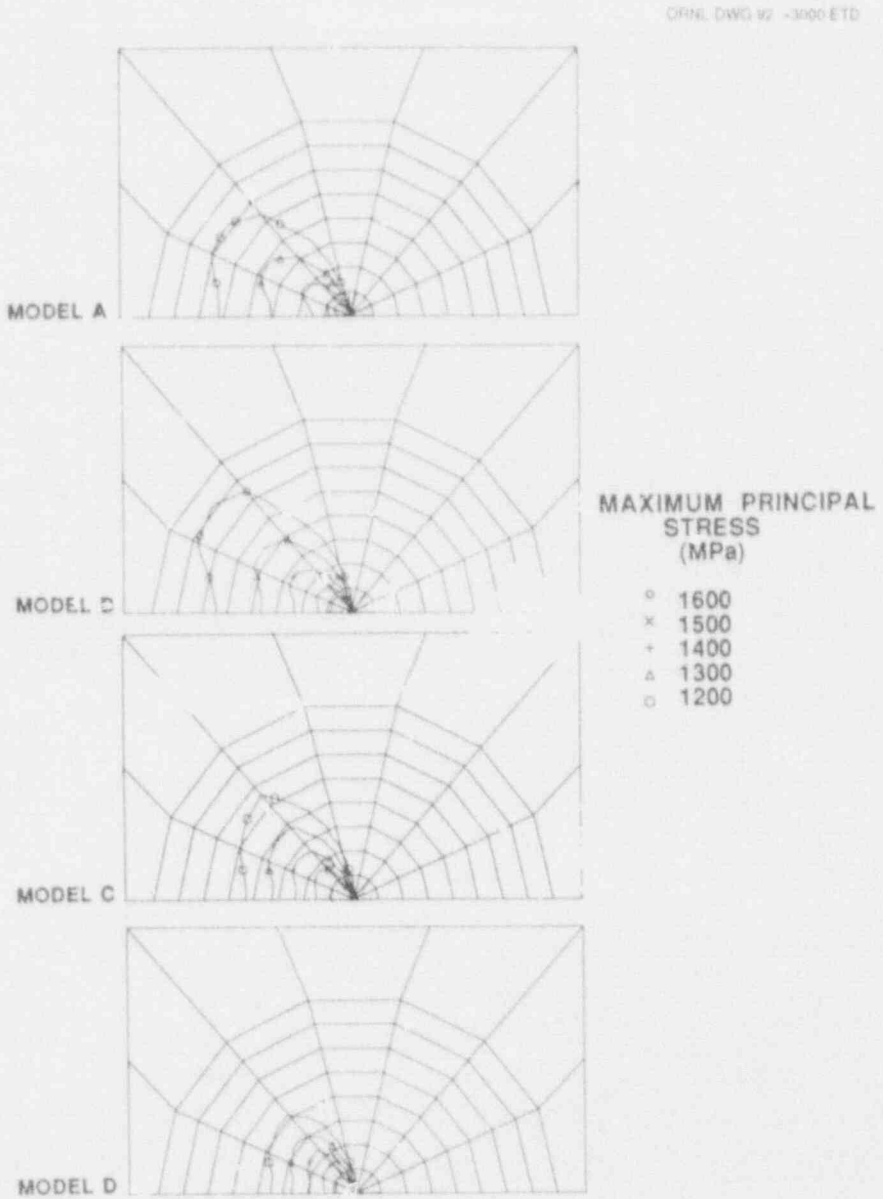

Figure D.22 Contours of maximum principal stress for four 4T-CT models at initiation

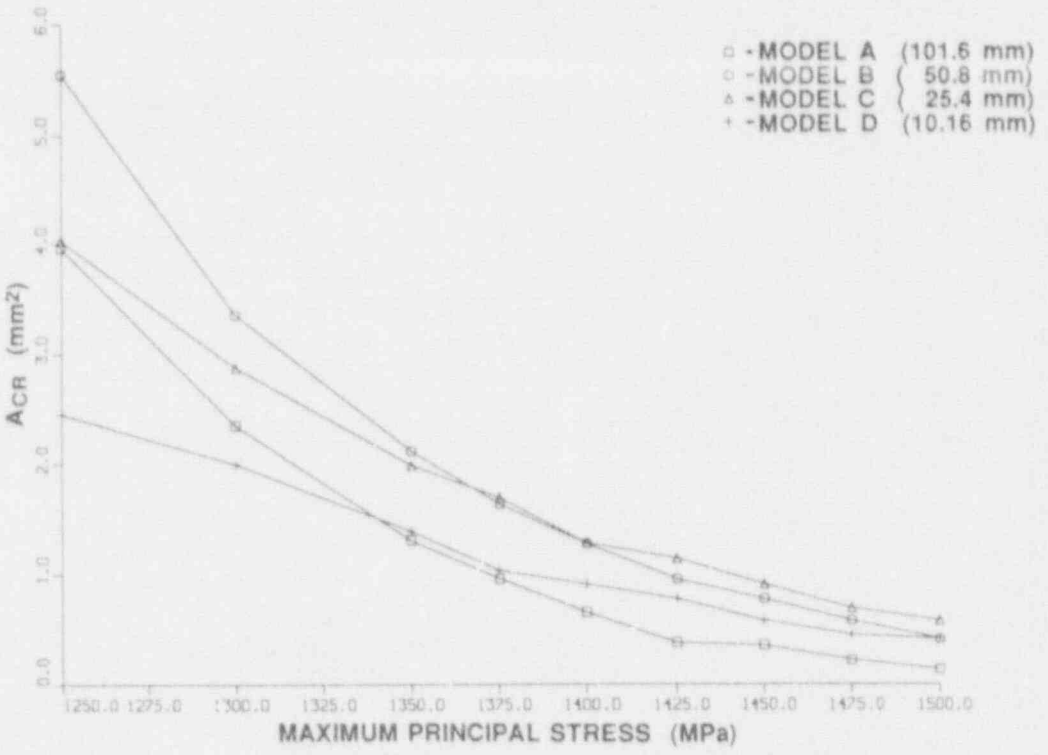

Figure D.23 A_{CR} vs maximum principal stress for four 4T-CT models at initiation

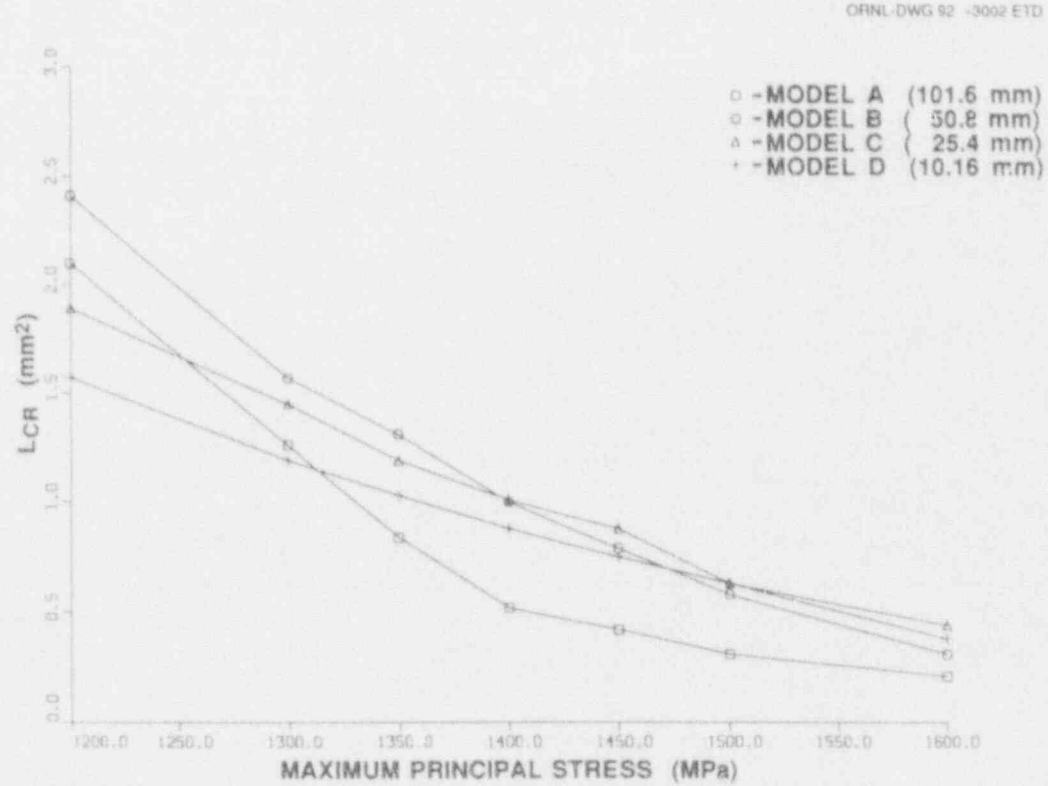

Figure D.24 L_{CR} vs maximum principal stress for four 4T-CT models at initiation

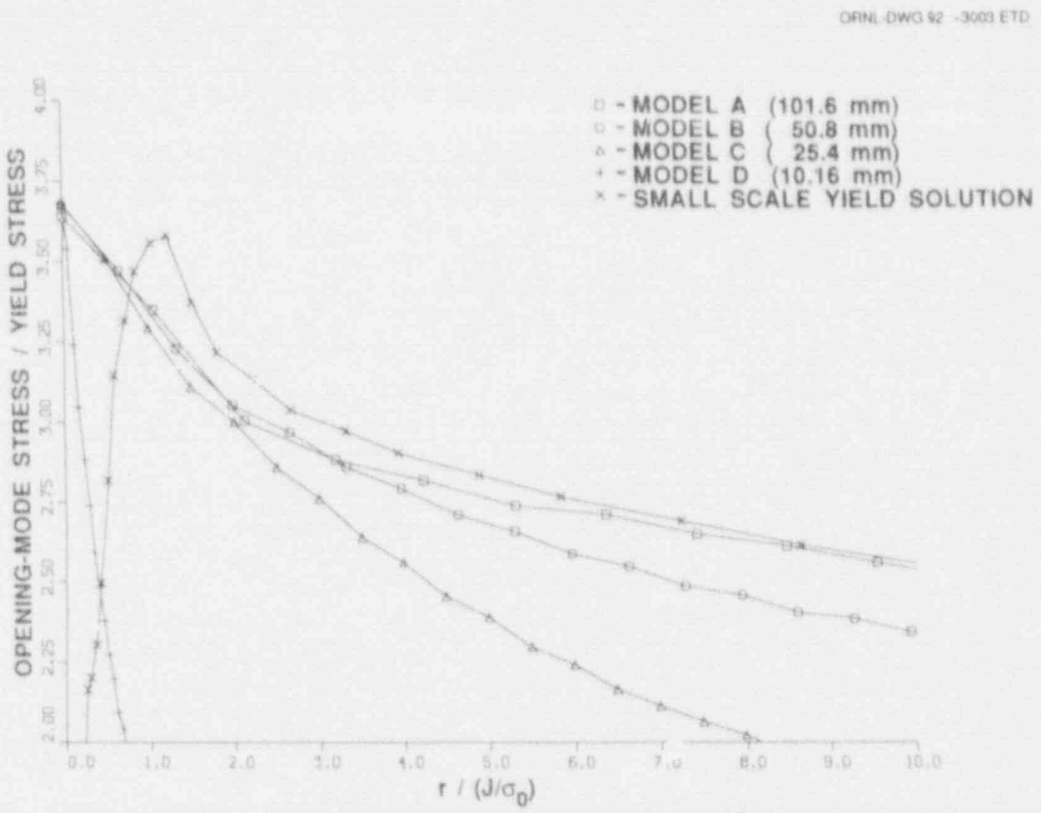

Figure D.25 Comparison of normalized stress vs normalized distance from crack-tip for 4T-CT models and SSY solution

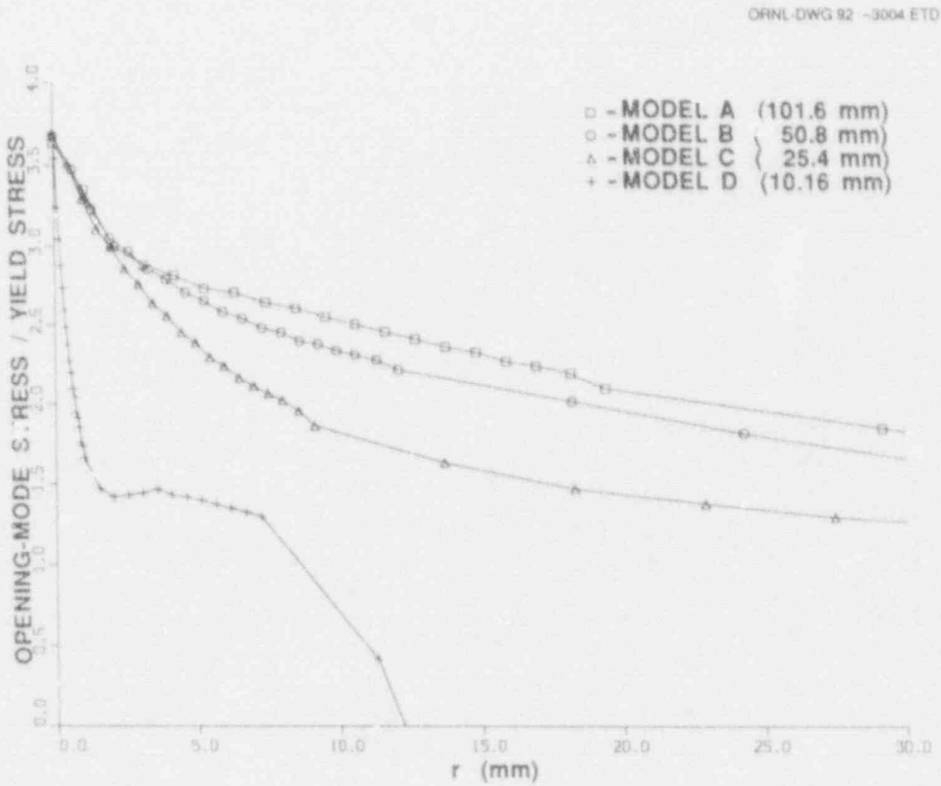

Figure D.26 Normalized stress vs distance from crack-tip for 4T-CT models

D.5 References

1. T. L. Anderson and R. H. Dodds Jr., Mechanics and Materials Center, Texas A&M University, College Station, Texas, "Specimen Size Requirements for Fracture Toughness Testing in the Transition Region," Report MM-6586-90-5, May 1990.*

2. J. Keeney-Walker, B. R. Bass, and J. D. Landes, Martin Marietta Energy Systems, Inc., Oak Ridge Natl. Lab., "An Investigation of Crack-Tip Stress-Field Criteria for Predicting Cleavage-Crack Initiation," USNRC Report NUREG/CR-5651 (ORNL/TM-11692), September 1991.*

3. D. J. Naus et al., Martin Marietta Energy Systems, Inc., Oak Ridge Natl. Lab., "Crack-Arrest Behavior in SEN Wide Plates of Quenched and Tempered A 533 Grade B Steel Tested Under Nonisothermal Conditions," USNRC Report NUREG/CR-4930 (ORNL-6388), August 1987.*

4. D. K. M. Shum et al., Martin Marietta Energy Systems, Inc., Oak Ridge Natl. Lab., "Analytical Studies of Transverse Strain Effects on Fracture Toughness for Circumferentially Oriented Cracks," USNRC Report NUREG/CR-5592 (ORNL/TM-11581), February 1991.*

5. D. E. McCabe and J. D. Landes, Westinghouse R&D Center, "The Effect of Specimen Plan View Size and Material Thickness on the Transition Temperature Behavior of A533B Steel," Research Report 80-1D3-REVEM-R2, November 1980.*

6. B. R. Bass and J. W. Bryson, Union Carbide Corp. Nuclear Div., Oak Ridge Natl. Lab., "Applications of Energy Release Rate Techniques to Part-Through Cracks in Plates and Cylinders, Volume 1, ORMGEN-3D: A Finite Element Mesh Generator for 3-Dimensional Crack Geometries," USNRC Report NUREG/CR-2997/V1 (ORNL/TM-8527), December 1982.*

7. K. J. Bathe, Massachusetts Institute of Technology, "ADINA—A Finite Element Program for Automatic Dynamic Incremental Nonlinear Analysis," Report 82448-1, 1975, revised 1978.*

8. H. G. DeLorenzi, General Electric Company, "On the Energy Release Rate and the J-Integral for 3-D Crack Configurations," TIS Report 80CRD 113, 1980.*

9. B. R. Bass and J. W. Bryson, Union Carbide Corp. Nuclear Div., Oak Ridge Natl. Lab., "Applications of Energy Release Rate Techniques to Part-Through Cracks in Plates and Cylinders, Volume 2, ORVIRT: A Finite Element Program for Energy Release Rate Calculations for 2-D and 3-D Crack Models," USNRC Report NUREG/CR-2997/V2 (ORNL/TM-8527), February 1983.*

10. G. T. Hahn, A. Gilbert, and C. N. Reid, "Model for Crack Propagation in Steel," *J. Iron Steel Inst. (London)* 202, 677–684 (August 1964).†

*Available for purchase from National Technical Information Service, Springfield, VA 22161.

†Available in public technical libraries.

Appendix E

Three-Dimensional Finite-Element Analysis of 1T-CT Specimens

J. Keeney-Walker

E.1 Introduction

This appendix describes analyses of a compact tension (CT) specimen that were performed for the investigation described in Appendix F concerning correlations between measured thickness reduction and fracture toughness for large- and small-scale specimens. Results from these analyses were also considered in selecting input conditions for the sliver model calculations described in Appendix D.

The material properties and fracture toughness data used in these analyses were taken from the same plate of A 533 B steel (HSST plate 13A) described in Appendix D and in Ref. 1. The following sections summarize the finite-element models of 1T-CT specimens analyzed in this study, as well as results of the calculations.

E.2 Analysis Methods

Two-dimensional (2-D) plane strain, and fully three-dimensional (3-D) finite-element models were employed to generate the displacements, stresses, and strains for the 1T-CT specimens. The numerical analysis techniques utilized both small- and large-strain formulations and the elastic-plastic constitutive model representation for A 533 B steel described in Appendix D.

The 2-D finite-element model of the 1T-CT configuration used in the nonlinear elastic-plastic analyses consists of 1738 nodes and 538 8-noded isoparametric elements as shown in Fig. E.1. Collapsed-prism elements surround the crack tip to allow for blunting and for a 1/r singularity in the strains at the crack front. The radial dimension of the collapsed-prism elements at the crack tip is r = 0.015 mm.

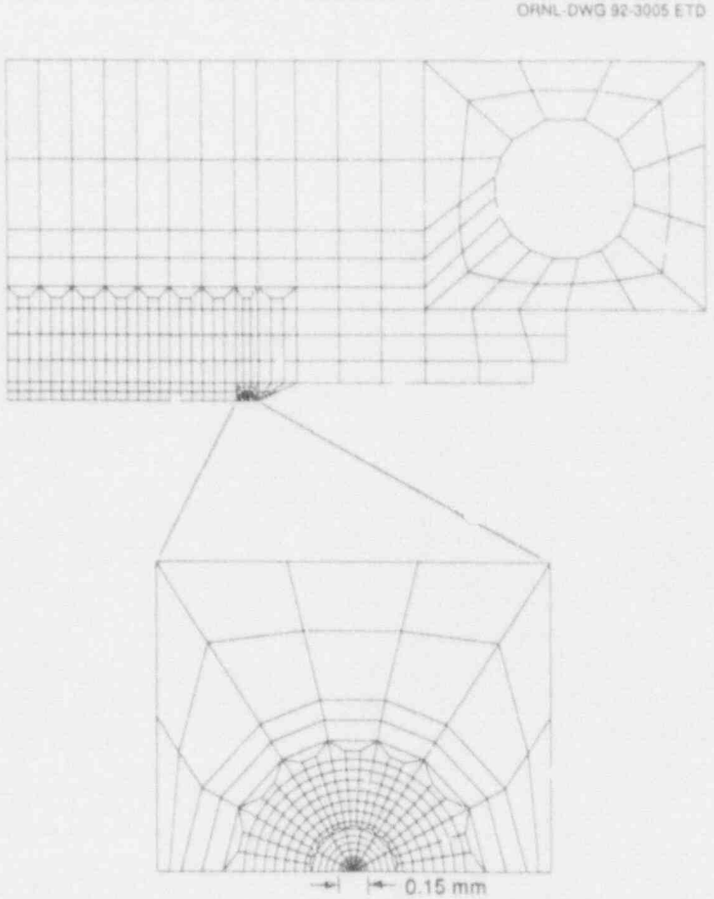

Figure E.1 2-D finite-element model for 1T-CT specimens

Analysis

The 3-D finite-element model of the 1T-CT specimen (Fig. E.2) was generated with the ORMGEN[2] mesh generating program by projecting the planform of a 2-D mesh for the specimen through the thickness, using five elements in the thickness direction. The 3-D model of the 1T-CT specimen consists of 8572 nodes, 1675 20-noded isoparametric brick elements, with collapsed prism elements at the crack front. The radial dimension of the collapsed-prism elements at the crack tip is $r = 0.11$ mm. One-fourth of the specimen is modeled due to symmetry.

The finite-element analyses employed an incremental elastic-plastic constitutive model (Model 8 in ADINA[3]), with a $2 \times 2 \times 2$ Gauss point rule to compute the global stiffness matrix. A 2-D plane strain analysis was performed using the 1T-CT specimen model of Fig. E.1 and the multilinear true stress–true strain curve from Fig. D.3, assuming a uniform temperature of –75°C. A material-nonlinear-only (MNLO) formulation (small-strain theory) was used in this analysis. Two separate 3-D analyses were performed, the first of which was based on an MNLO formulation with a multilinear true stress–true strain curve, and the other on an updated Lagrangian (UL) (large-strain theory) formulation with a bilinear engineering stress-strain curve. In all analyses, the load was applied incrementally to the load pin hole in the form of a cosine distribution function, up to the load where crack initiation took place for each 1T-CT test. Iterations were performed in each load step to establish global equilibrium within a specified tolerance. The 2-D analysis was carried out using the Oak Ridge National Laboratory (ORNL) modified ADINA[3,4] fracture mechanics program, while the 3-D analyses used the ADINA/ORVIRT[3,5,6] fracture analysis system.

E.3 Analysis Results and Evaluations of Transverse Strain

The analysis results are reported in Table E.1, which includes experimental data as well as calculated values of J

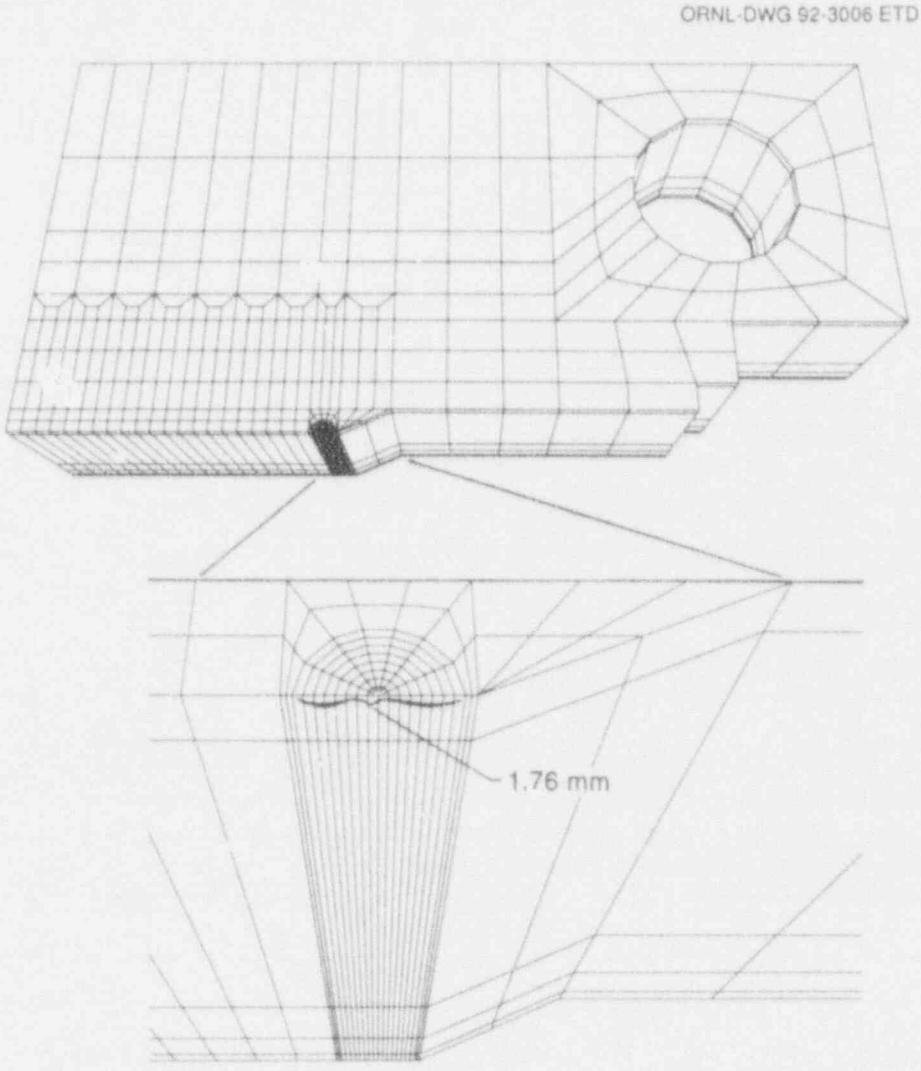

Figure E.2 3-D finite-element model for 1T-CT specimens

Table E.1 Experimental and calculated fracture toughness and COD results for 1T-CT specimens at –75°C

Specimen	Load at fracture (kN)	COD (mm)				J (kJ/m^2)			
		Exp.	2-D plane strain	3-D MNLO	3-D UL	Exp.	2-D plane strain	3-D MNLO	3-D UL
K51C	29	0.21	0.26	0.30	0.28	14.4	14.8	16.9	15.7
K52B	35	0.31	0.32	0.37	0.35	26.3	22.6	25.5	23.7
K54A	50	0.58	0.51	0.75	0.62	74.1	63.5	83.6	67.3

and crack-opening displacement (COD). The load vs COD curves and applied J vs COD curves are plotted in Figs. E.3 and E.4 and compared with experimental data. When the calculated J-values from Fig. E.4 are compared with the experimental data from Table D.2 (Specimens K51C, K52B, and K54A), the differences range between 9 and 10%. The experimental data are anticipated to fall between the 2-D plane-strain analysis and the 3-D analysis; however, this is true only for the specimen that failed at 50 kN (see Fig. E.3). The test records indicate that none of these three specimens were valid K_{JC} tests based on the ASTM E399 criteria. In Fig. E.4, the scatter in toughness is typical of this material at temperatures in the lower-transition region.

In Fig. E.5(*a*)–(*c*), the transverse displacement for the UL analysis is plotted through the thickness for the initiation loads of 29, 35, and 50 kN at increasing distances from the crack tip. As expected, the transverse displacement increases with load at the same distance from the crack tip; for the same load, transverse displacement decreases with increasing radial distance. This is also seen in Fig. E.6, where transverse strain is plotted vs ligament distance at the center plane of the specimen. The values of percent transverse strain for the analyses are reported in Table E.2, where strain is evaluated from the transverse displacement (displacement/specimen width).

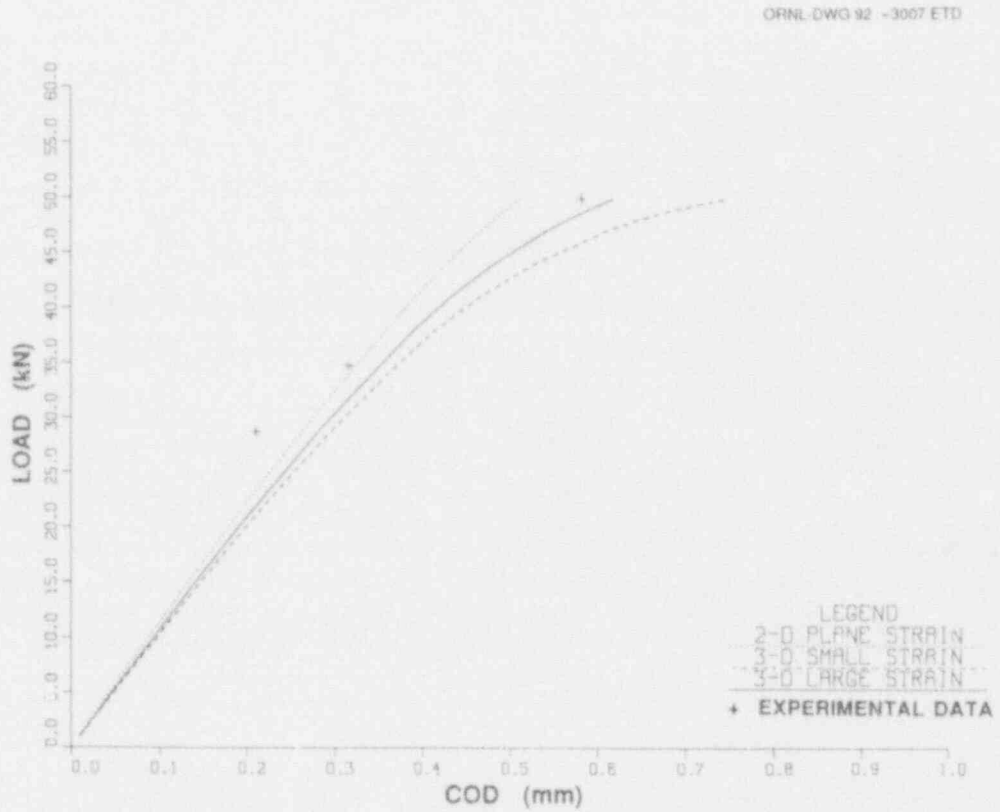

Figure E.3 Results of elastic-plastic analyses for 1T-CT specimens at –75°C showing load vs COD

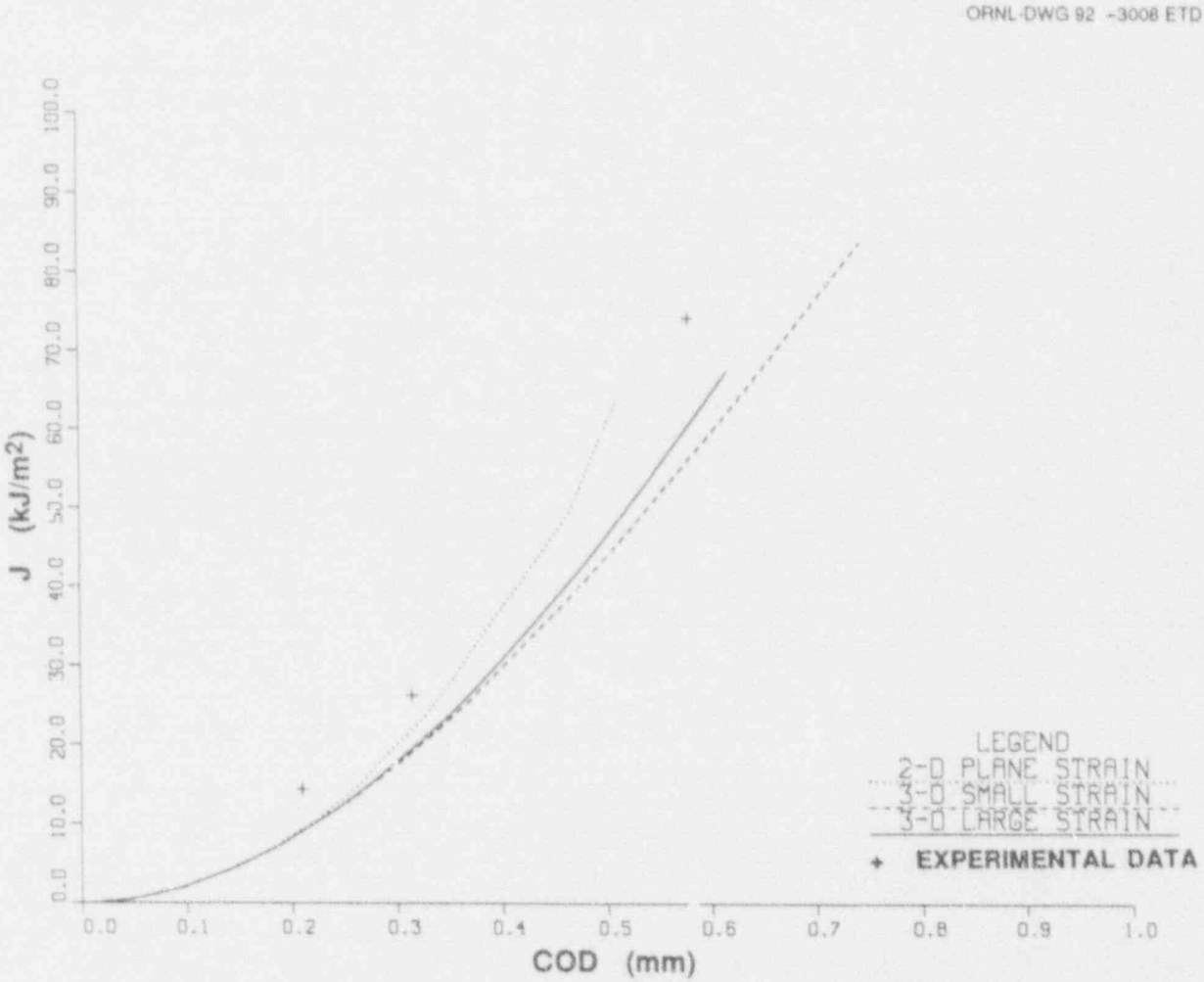

Figure E.4 Results of elastic-plastic analyses for 1T-CT specimens at –75°C showing J vs COD

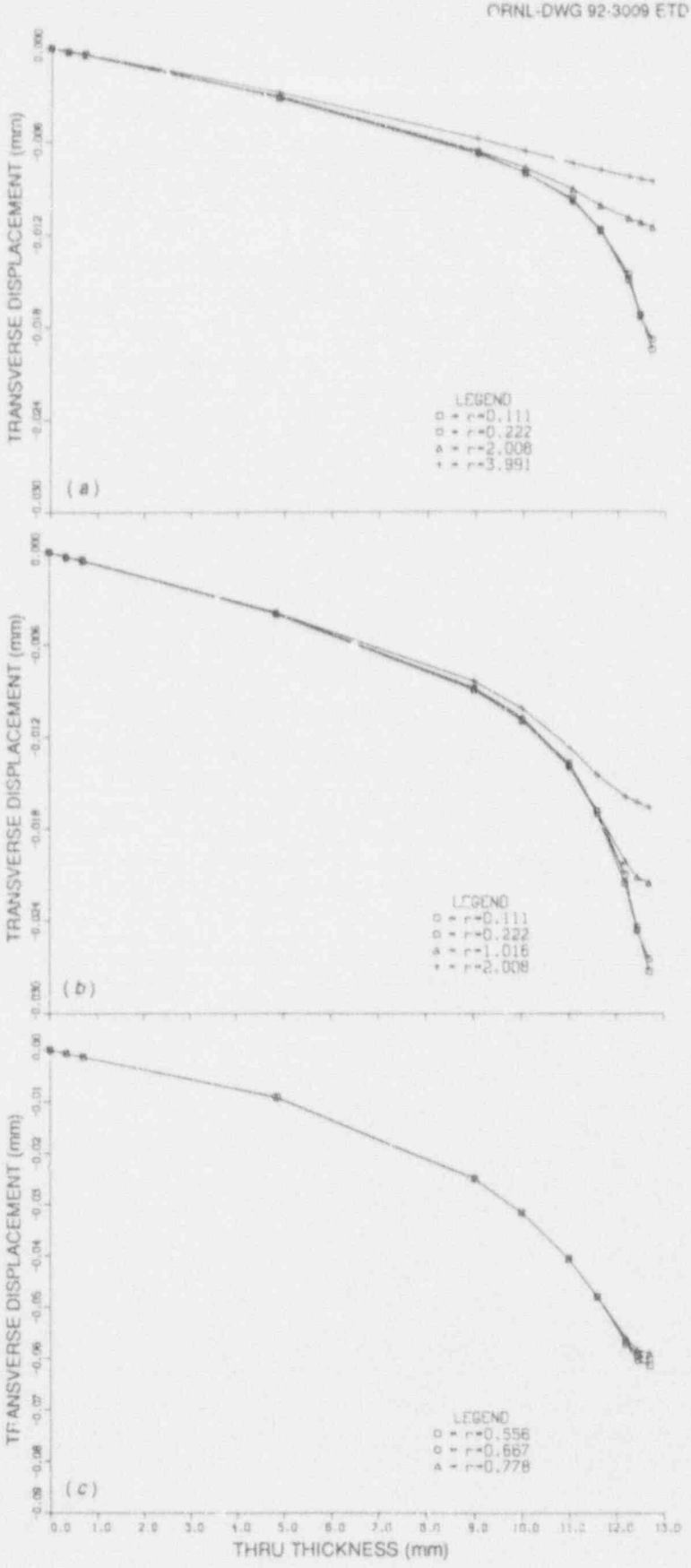

Figure E.5 Comparison of transverse displacement vs through-thickness location for UL analysis for three loading conditions: (*a*) 29 kN, (*b*) 35 kN, and (c) 50 kN

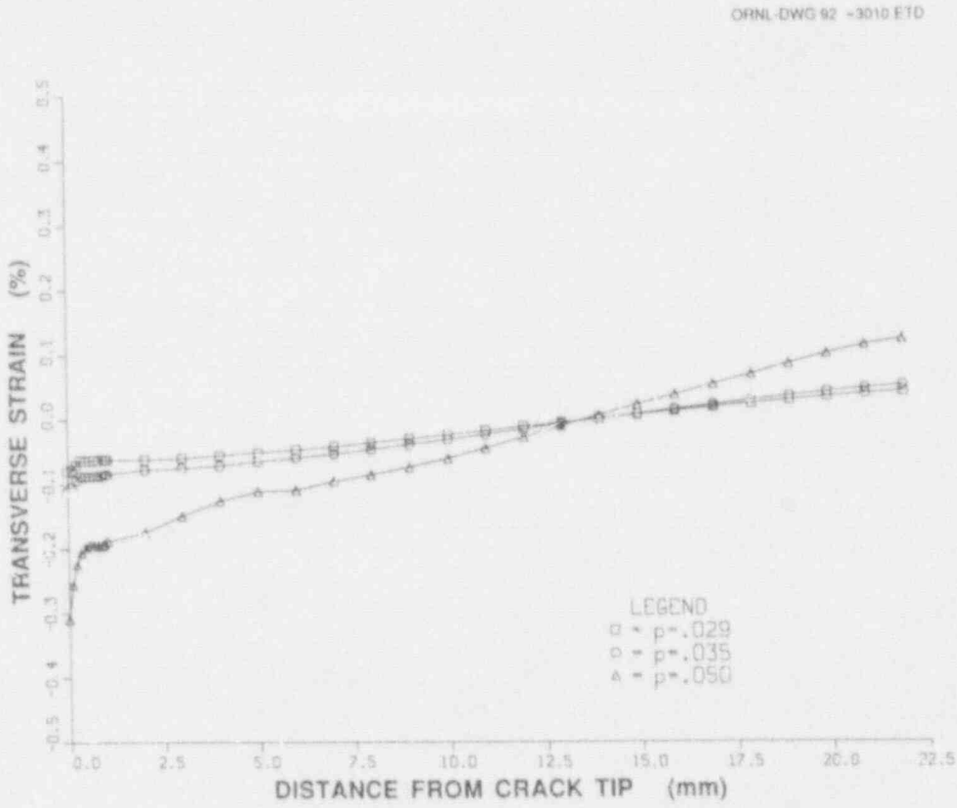

Figure E.6 Transverse strain vs distance from crack tip for UL analysis evaluated at center plane

Table E.2 Calculated transverse strain for 1T-CT specimens at –75°C

Load (kN)	Distance from crack tip (mm)	UL	Percentage of strain (from transverse displacement) MNLO	MNLO[a]
29	0.119	0.15	0.16	0.05
	2.934	0.08	0.08	0.01
35	0.218	0.21	0.22	0.08
	1.382	0.16	0.18	0.07
50	0.622	0.48	0.62	0.42
	0.762	0.46	0.61	0.42

[a]Unloaded (load = 0.0 kN) from each initiation load.

To provide information regarding what may be a "posttest" condition in the CT specimen, the 3-D analysis (MNLO formulation) was restarted at each initiation load (29, 35, and 50 kN) and unloaded to zero load in three separate analyses. The transverse displacement for the specimens in a loaded and unloaded condition is compared in Figs. E.7(*a*)–(*c*) and E.8(a)–(c). The percent transverse strain for these analyses, reported in Table E.2, decreases by 31% to 88% for the unloaded condition.

E.4 Conclusions

Elastic-plastic 2- and 3-D finite-element analyses were performed using data generated from testing of 1T-CT specimens of A 533 B steel. Transverse displacement through the thickness of the specimen at various distances ahead of the crack tip were determined for the three measured fracture loads corresponding to specimens K51C, K52B, and K54A in Table D.2. Residual transverse

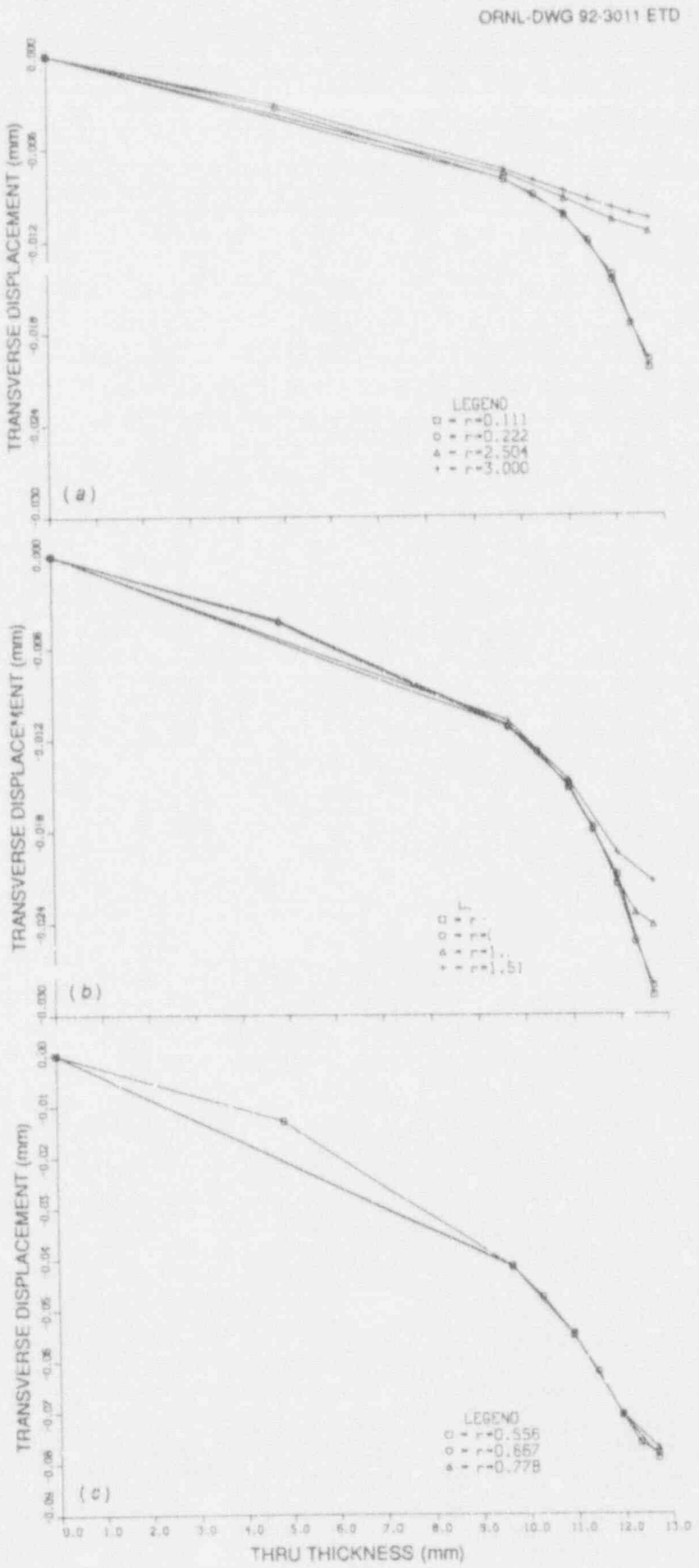

Figure E.7 Comparison of transverse displacement vs through-thickness location for MNLO analysis for three loading conditions: (*a*) 29 kN, (*b*) 35 kN, and (*c*) 50 kN

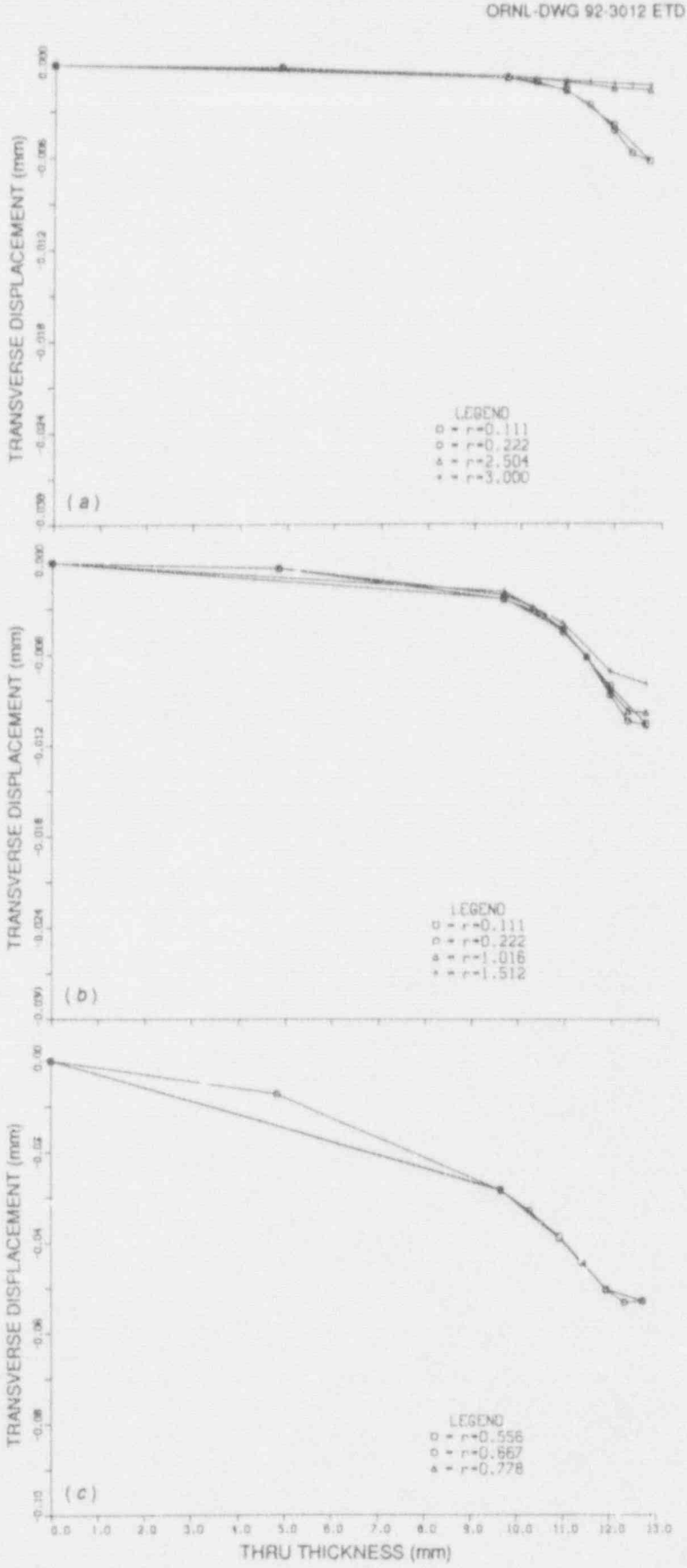

Figure E.8 Comparison of transverse displacement vs through-thickness location for MNLO analysis for three unloaded conditions: (*a*) unloaded from 29 kN, (*b*) unloaded from 35 kN, and (*c*) unloaded from 50 kN

displacements in the unloaded condition for each of these cases were also determined. In Appendix F, these numerical predictions for transverse displacements, summarized in Figs. E.5–E.8, are compared with postfracture thickness reduction (TR) measurements recorded at selected points on the CT specimens. Results from these comparisons are used to address questions concerning to what extent postfracture TR measurements of test specimens can be related to the amount of TR just prior to crack initiation and to the amount of residual TR subsequent to crack initiation.

E.5 References

1. D. J. Naus et al., Martin Marietta Energy Systems, Inc., Oak Ridge Natl. Lab., "Crack-Arrest Behavior in SEN Wide Plates of Quenched and Tempered A 533 Grade B Steel Tested Under Nonisothermal Conditions," USNRC Report NUREG/CR-4930 (ORNL-6338), August 1987.*

2. B. R. Bass and J. W. Bryson, Union Carbide Corp. Nuclear Div., Oak Ridge Natl. Lab., "Applications of Energy Released Rate Techniques to Part-Through Cracks in Plates and Cylinders, Volume 1, ORMGEN-3D: A Finite Element Mesh Generator for 3-Dimensional Crack Geometries," USNRC Report NUREG/CR-2997, Vol. 1 (ORNL/TM-8527/V1), December 1982.*

3. K. H. Bathe, Massachusetts Institute of Technology, "ADINA—A Finite Element Program for Automatic Dynamic Incremental Nonlinear Analysis," Report 82448-1, 1975, revised 1978.*

4. B. R. Bass et al., "Applications of ADINA to Viscoplastic-Dynamic Fracture Mechanics Analysis," *Comp. Struct.* 32(3/4), 815–824 (1989).†

5. H. G. DeLorenzi, General Electric Company, "On the Energy Release Rate and the J-Integral for 3-D Crack Configurations," TIS Report 80CRD113, 1980.*

6. B. R. Bass and J. W. Bryson, Union Carbide Corp. Nuclear Div., Oak Ridge Natl. Lab., "Applications of Energy Release Rate Techniques to Part-Through Cracks in Plates and Cylinders, Vol. 2, ORVIRT: A Finite Element Program for Energy Release Rate Calculations for 2-D and 3-D Crack Models," USNRC Report NUREG/CR-2997, Vol. 2 (ORNL/TM-8527/V2), February 1983.*

*Available for purchase from National Technical Information Service, Springfield, VA 22161.
†Available in public technical libraries.

Appendix F

Correlation Between Induced Thickness Reduction and Fracture Toughness

D. K. M. Shum

F.1 Introduction

The development of various analytical methods to estimate the potential decrease in crack-initiation toughness, from a reference plane strain value, due to positive straining along the crack front of a circumferential flaw in a reactor pressure vessel (RPV) has been detailed in previous appendixes. Validation and modification of these analytical methods rely upon the availability of experimental data on both the magnitude of the *prescribed* transverse strain (positive or negative) along a crack front and the associated fracture toughness at crack initiation. However, there have been very few experiments performed to date in which both the transverse strain and the in-plane loading have been independently prescribed test variables. The two exceptions known to the authors are uniaxially and biaxially loaded fracture experiments involving (1) large-scale surface-cracked plate specimens[1,2] and (2) miniature three-point-bend (TPB) specimens.* The large-scale surface-cracked plate experiments have been reviewed in Appendix C. Insufficient information in the open literature concerning various experimental and analytical aspects of the miniature TPB experiments prevents an informed evaluation of the reported results.

On the other hand, it has recently been proposed that fracture-toughness results obtained from plate-type fracture specimens, in which only the in-plane loading is prescribed, can be correlated with postfracture measurements of thickness reduction (TR) *induced* along the crack front by the in-plane loading.[3,4] The question arose as to whether the proposed correlation and supporting data between induced TR and fracture toughness can be used to verify the various analytical models developed in this report in the negative prescribed transverse strain regime.

The objective of this appendix is to evaluate the proposal that postfracture measurements of TR induced by in-plane loading can be correlated with fracture toughness. The scope of work carried out in this study is as follows. First, formulation of the proposed correlation is presented, and experimental evidence in support of this correlation is reviewed. In particular, recent attempts to use the proposed correlation to examine crack initiation, arrest, and reinitiation results from large-scale fracture experiments are analyzed. Second, the general validity of the proposal is further examined by applying the correlation to newly obtained postfracture TR measurements of a select group of compact (CT) specimens for which the associated crack-initiation-toughness data are available. Third, general observations concerning correlations between induced TR measurements and fracture toughness are noted. Finally, the utility of a correlation based on induced TR for estimating the effects of prescribed transverse displacement on fracture toughness is discussed.

F.2 Formulation of TR Correlation

The TR correlation to be examined was originally formulated for plate-type fracture specimens for which the loading is in-plane in nature and which results in Mode I, or opening-mode, separation of the crack faces under the applied load.[3] For the specified in-plane loading conditions the transverse displacement along the crack front must necessarily be negative, and the term thickness reduction is identified with this type of transverse displacement.

The premise of the TR correlation is simply that TR can be used as an approximate measure of the crack-tip-opening displacement (CTOD) under the prescribed in-plane loading conditions. This premise does not imply that TR influences toughness in any way but merely that TR, like CTOD, is a consequence of in-plane loading and constraint. It is important to note that the appropriate location ahead of the crack front at which TR measurement should be taken is not specified in the formulation.

The starting point of the TR correlation is a CTOD vs J-integral relation of the form

$$\text{CTOD} = J / \sigma_{fl}, \qquad \text{(F.1)}$$

where the flow properties of the material are specified via the parameter σ_{fl}, which is the average value of the uniaxial yield and ultimate stress in tension. By equating the numerical value of TR with CTOD, a correlation

*M. P. Manahan, "Plane-Strain Fracture Toughness Determination Using Stress Field Modified Miniature Specimens," The Pennsylvania State University, July 1990.

between TR and toughness follows by substituting TR for CTOD in Eq. (F.1), resulting in the relation

$$TR = J / \sigma_{fl} . \qquad (F.2)$$

Equation (F.2) is the form of the correlation originally proposed in Ref. 3. Adjustment of Eq. (F.2) for effects related to dynamic crack initiation is accomplished by applying a correction factor to σ_{fl} to account for rate effects.

While not explicitly stated in the original formulation, use of Eq. (F.2) appears to imply the limitation that the TR correlation is not suitable for plane strainlike conditions. First, this limitation is deduced based on the observation that the supporting data cited (to be discussed shortly) for the correlation are for plate-type fracture specimens with stress-free sides. While the extent of plasticity in those tests was not reported, the usual implication associated with plate-type specimens is that a plane stresslike stress state exists along the crack front. Second, this limitation is deduced based on the observation that while a counterpart to Eq. (F.1) is known to exist in the idealized limit of plane strain, TR in that idealized limit is by definition zero.

In reality, of course, testing of a conventional fracture specimen with stress-free sides in a Mode I manner always results in negative straining along at least a portion of the crack front, even for a very thick specimen with a long crack front. Recognition of this apparent limitation to the TR correlation is believed to be essential toward a proper understanding of the applicability of the correlation, a point that will be further elaborated upon later in this appendix.

For the present purpose of evaluating the general merits of a correlation of the type indicated in Eq. (F.2), this correlation is generalized to take the form

$$TR = J/(m \sigma_y) , \qquad (F.3)$$

where the factor m should be regarded as an empirical adjustment factor. Use of this empirical factor m formalizes the ad hoc adjustments assumed in the formulation of Eq. (F.2) in the following fashion. The requirement that the numerical value of TR be nearly identical to CTOD is relaxed. Indeed, Eq. (F.3) merely requires that the relationship between TR and CTOD be linear in nature. The need to provide a quantitative adjustment for rate effects and flow properties in Eq. (F.2) is no longer present. In addition, Eq. (F.3) formalizes considerations of constraint effects associated with the TR correlation under plane strain-to-plane stresslike conditions. The extent to which Eq. (F.3) can be demonstrated to hold at some yet-to-be-determined distance ahead of the crack front, for a relatively constant value of the factor m under nominally constant loading and constraint conditions, would demonstrate the merits of the proposed TR correlation for the determination of toughness.

F.3 Experimental Evidence in Support of TR Correlation

Experimental data cited in Ref. 3 in support of the TR correlation include CTOD and TR measurements obtained for an air-cooled mild steel plate in the form of single-edge-notch-bend (SENB) specimens,[5] for which a near equality between CTOD and TR values close to the notch root was observed. The location ahead of the notch root at which TR values were obtained was not specified.

Unpublished TR measurements for a high-strength aluminum alloy tested in the form of center-cracked-plate (CCP) specimens were also mentioned in Ref. 3, for which a near equality between measured TR values and CTOD values inferred from calculated stress-intensity factors K was reported. The location ahead of the sharp crack front in the aluminum specimens was not specified.

Unpublished experimental data for TR measurements and CTOD values inferred from fracture surface topography for A 710 steel was also cited in Ref. 3, where again a near equality was reported between TR measurements and the topographic estimates of CTOD.

Finally, it has been reported that postfracture TR measurements have been successfully correlated with cleavage-crack initiation, arrest, and reinitiation toughness values for a number of fracture specimens commonly referred to as the Oak Ridge National Laboratory/National Institute of Standards and Technology (ORNL/NIST) Wide-Plate (WP) specimens.[3,4] Application of the proposed correlation to these specimens has been detailed in Refs. 3 and 4, thus permitting a critical evaluation of the proposed correlation. This evaluation is presented in the next section.

F.4 TR Correlation with Crack-Arrest Toughness for ORNL/NIST WP Specimens

The WP specimens were large-scale, single-edge-notched-tension (SENT) crack-arrest specimens. The primary objective of these WP tests is the determination of crack-

arrest toughness values for three RPV-grade materials that simulate unirradiated and irradiated material behavior.[6–10] Eight specimens were prepared from HSST plate 13A of A 533 grade B class 1 steel (WP-1 series), two specimens were prepared from a second heat of A 533 grade B class 1 steel (WP-CE series), and six specimens were prepared from a 2 1/4 Cr-1 Mo steel simulating low-upper-shelf behavior due to neutron irradiation (WP-2 series). The WP specimens were 1 m wide, ~10.8 m long, and 0.1 to 0.15 m thick. Each side of the specimen was side-grooved to a depth equal to 12.5% of the specimen's thickness. In all cases except WP-1.1, WP-1.2, WP-2.3, and WP-2.6, the crack front was further cut into a truncated chevron configuration. The initial crack depth was ~0.2 m, and there was a positive linear temperature gradient in the direction of crack extension. All of the WP specimens experienced at least one crack-arrest and reinitiation event during test. Fracture toughness values in terms of the stress-intensity factor K were determined from J-integral values using the conventional *plane stress* conversion formula. The J-integral values were determined using the finite-element method assuming linear-elastic fracture mechanics (LEFM) conditions.

In the WP studies postfracture thickness-average transverse strain contours for each of the WP specimens are reported, along with specimen thicknesses, temperature-dependent material properties, and the temperature distributions ahead of the crack front for each of the specimens. The transverse strain contours are produced based on postfracture TR measurements taken along the surfaces of the two broken halves of the WP specimens with a deep-throat micrometer. The resolution of the micrometer is ±0.025 mm. The WP specimens are machined to a dimensional tolerance of ±0.13 to ±0.25 mm (±0.005 to ±0.01 in.). Based on the above information and the proposed TR correlation, crack-arrest and reinitiation toughness values have been calculated and reported in Ref. 3 for WP-2 series and in Ref. 4 for WP-1, WP-CE, and WP-2 series of experiments.

The results from Ref. 4 will be taken as representative of toughness predictions based on the TR correlations for WP specimens. In Figs. F.1 and F.2 the crack-arrest and reinitiation toughness values are plotted based on Eq. (F.2) (solid and dotted lines) for the WP-1, WP-CE, and WP-2 series of experiments, along with finite-element calculations based on the load-time and crack position-time history of the specimens (filled and open symbols).[6-10] The reference nil-ductility temperature RT_{NDT} for the three series of specimens are –23°C for WP-1, –34°C for WP-CE, and 60°C for WP-2.

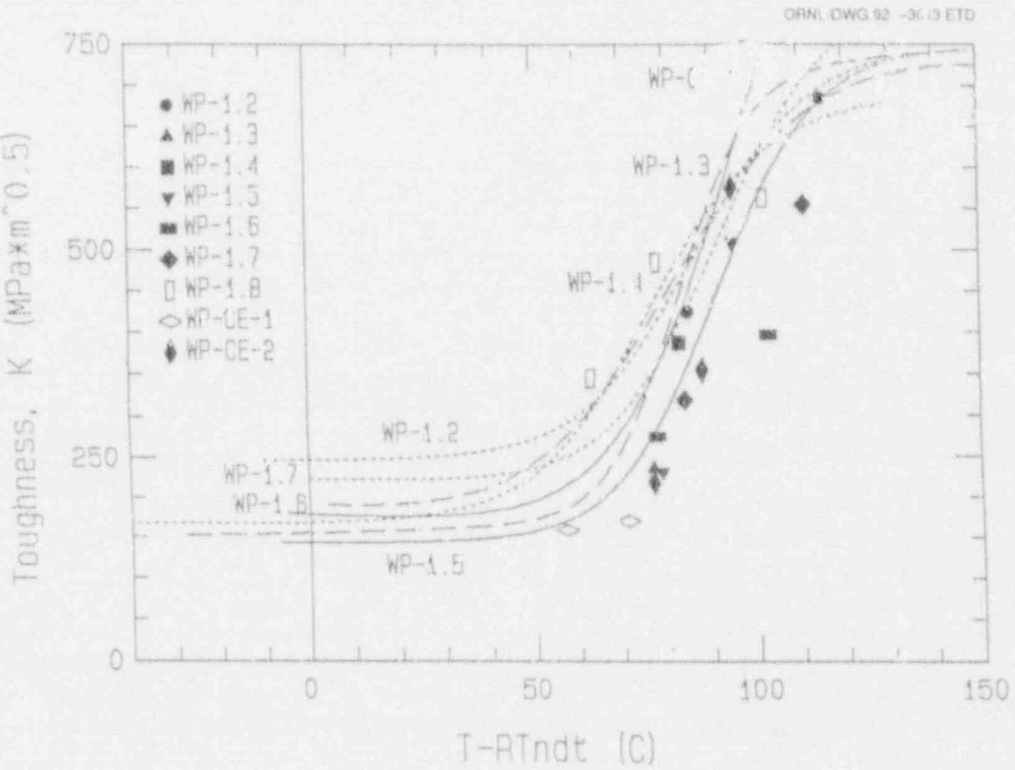

Figure F.1 Crack-arrest and reinitiation toughness predictions (solids and dotted lines) based on TR correlation Eq. (F.2) for WP-1 and WP-CE series of experiments (taken from Ref. 4), along with finite-element calculations based on the load-time and crack position-time history of specimens (filled and open symbols). The references nil-ductility temperature RT_{NDT} is –23°C for WP-1 and –34°C for WP-CE

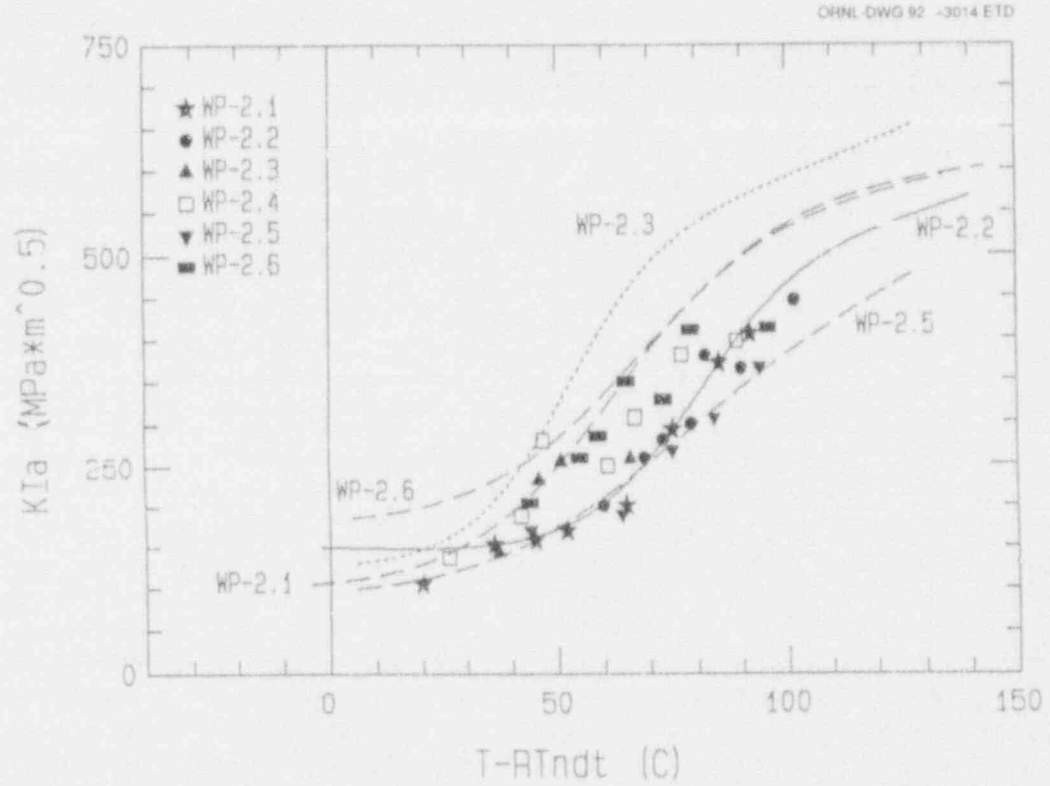

Figure F.2 Crack-arrest and reinitiation toughness predictions (solids and dotted lines) based on TR correlation Eq. (F.2) for WP-2 series of experiments (taken from Ref. 4), along with finite-element calculations based on load–time and crack position-time history of specimens (filled and open symbols). Reference nil-ductility temperature RT_{NDT} is –60°C for WP-2

The proposed TR correlation is reported to be validated for the WP specimens on the basis of an apparent agreement between toughness calculations based on the TR correlation and the finite-element method indicated in Figs. F.1 and F.2. However, note that except for the WP-2 series of tests, validation was based on comparison of TR calculations with either one or two finite-element calculations per WP test. Furthermore, the results in Figs. F.1 and F.2 employ temperature as the independent variable such that the comparison is made across a temperature range, whereas Eq. (F.2) is formulated for isothermal conditions.

It is believed that validation of the TR correlation for the WP tests can be better accomplished by presenting TR-toughness results at a fixed temperature with toughness expressed in terms of J-integral values. The motivation for presenting the TR calculations for a fixed temperature is that by fixing the test temperature of interest, the temperature dependence of various constraint effects in the WP tests is eliminated. For the WP-1 series of tests, at least one crack-arrest event occurred in each specimen within a relatively narrow temperature range of 53 to 62°C. The associated crack-tip locations also fall within a narrow range between 49 and 56 cm. Consequently, it is possible to evaluate the TR correlation for the WP-1 specimens with six data points obtained at essentially the same temperature and crack length.

The motivation for presenting toughness values in terms of J-integral values is as follows. If Eq. (F.3) provides an appropriate description of the correlation between TR and toughness, then experimental values of TR and toughness expressed in terms of J should result in an essentially linear relationship under isothermal conditions. That is, while varying degrees of constraint, in terms of temperature dependence of flow properties, rate effects on flow properties, and plane-strain- or plane-stresslike conditions, would be manifested in terms of different values of the slope at different temperatures, the underlying relationship between TR and J would still be linear in nature at a given temperature.

The results of such a comparison are presented in Fig. F.3, along with three straight lines that correspond to the predicted relationship between TR and J as indicated by Eq. (F.3). The experimental data and finite-element results[6,7] used to generate Fig. F.3 are presented in Table F.1. The predicted TR-J relations are for WP-1 material at 60°C with an associated yield stress σ_y = 412 MPa. The three straight lines are based on three values of the

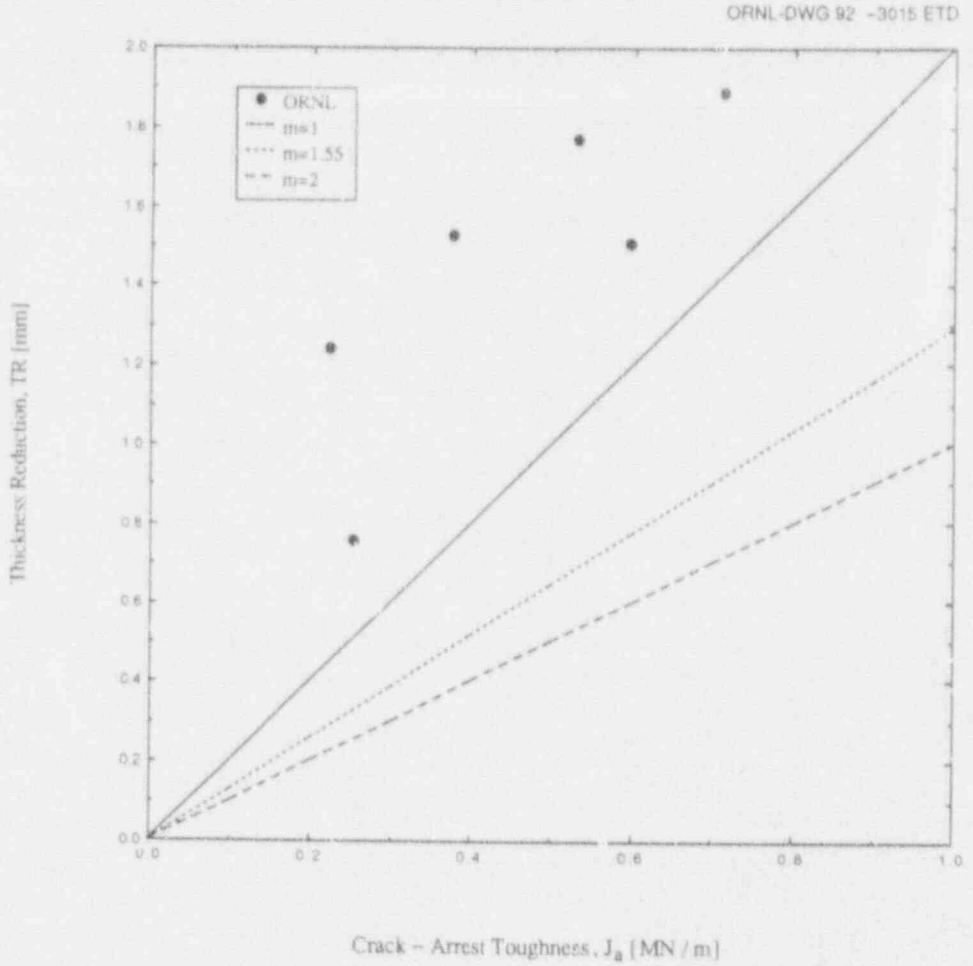

Figure F.3 Comparison of measured and predicted crack-arrest toughness values based on Eq. (F.3) for six of WP-1 specimens. Crack arrest for these six specimens occurred at essentially same temperature and crack length. Three straight lines correspond to predicted relationship between TR and J based on three values of empirical adjustment factor m. The m = 1 line is taken as indicative of lowest constraint conditions, while m = 2 line is taken as indicative of plane strain constraint conditions. (See Table F.1 for details)

Table F.1 Experimental data relevant to TR measurements for six of the WP-1 specimens, along with the ORNL finite-element results on crack-arrest toughness. Crack arrest for these six specimens occurred at essentially the same temperature and crack length

WP tests	Crack-tip relative temperature $T - RT_{NDT}$ (°C)	Crack-tip temperature (°C)	Crack-tip location (cm)	Specimen thickness (mm)	Transverse strain from strain contours ε_z (%)	Thickness reduction (mm)	Crack-arrest toughness from ORNL analysis K ($MPa\sqrt{m}$)	Crack-arrest toughness from ORNL analysis $J = K^2/E$ (MN/m)
WP1.2A	85	62	55.5	101.8	1.86	1.89	384	0.713
WP1.3	77	54	48.5	99.5	1.25	1.24	215	0.223
WP1.4B	83	52.7	52.7	101.6	1.75	1.77	331	0.530
WP1.5A	79	56	52.1	101.7	0.75	0.76	225	0.253
WP1.6A	77	54	49.3	101.8	1.50	1.53	279	0.376
WP1.7A	84	61	52.8	152.4	0.99	1.51	351	0.595

empirical adjustment factor m. If values of TR are indeed identical to values of CTOD, then the straight line denoted as m = 1 corresponds to the limiting nonhardening, plane stress CTOD vs J relation.* Similarly, the line denoted as m = 2 corresponds to the plane strain relation for a Ramberg-Osgood material with a hardening exponent of 10. In Ref. 4 validation of the the TR correlation for the WP tests was performed based on a value of σ_{η} adjusted for rate effects by an elevation of 138 MPa. In the context of Eq. (F.2), the value of σ_{η} at 60°C for WP-1 material is ~500 MPa, so that the adjustment corresponds to m = 1.55.

In this study the m = 1 line will be taken as indicative of the lowest constraint condition possible in the WP-1 tests, while the m = 2 line is taken as indicative of the constraint conditions associated with an RPV-grade material (without rate effects and irradiation adjustments of the uniaxial yield stress).

When comparison of TR predictions and the WP-1 results are cast in the form shown in Fig. F.3, the validity of the proposed TR correlation for the WP-1 tests is not readily apparent. This interpretation is based on the observation that the existence of a TR correlation involves not only a linear relationship between TR and toughness, but also that this linear relationship needs to be anchored at the origin of the plot in Fig. F.3. In addition, the TR-J data need to be to the right of the m = 1 line due to the assumption of minimum constraint associated with the static, plane stress condition.

F.4.1 TR Correlation with Crack-Initiation Toughness for ORNL/NIST WP Specimens

While much attention has been focused on the application of the TR correlation to crack-arrest and reinitiation toughness values obtained in the WP series of tests,[3,4] application of this correlation to the WP crack-initiation toughness values has been largely ignored. Presumably, this lack of interest is a consequence of the observation that of the 16 WP specimens examined in Ref. 4, 11 of them experienced no measurable postfracture TR in the neighborhood of the fatigue crack front where the crack-initiation event took place. As explained in Ref. 4, the lower asymptotes in Figs. F.1 and F.2 associated with all the WP specimens are determined using an approximate analytical procedure and are not based on the TR correlation for obvious reasons. While not explicitly stated, it would appear that the upper asymptotes in these figures are also determined independently of the TR correlation.

Attention will again be focused on the WP-1 series of tests. The aforementioned lack of measurable TR values at initiation is observed for WP-1.2 to -1.7 tests. Resolution of the TR micrometer and the WP specimen thickness tolerances reported previously suggest that the micrometer is capable of providing measurements of overall transverse strain on the order of the yield strain. Consequently, the absence of measurable values of TR at crack initiation implies that a state of nearly plane strain conditions existed along the crack front at initiation. As indicated in Table F.1, the magnitude of the transverse strain associated with the first crack-arrest location is on the order of 1 to 2%, or 5 to 10 times the yield strain. Perhaps crack initiation in the WP tests occurred under conditions outside the range of applicability of the TR correlation as discussed earlier. However, the apparent lack of correlation between TR and crack-arrest-toughness values shown in Fig. F.3 may not be amendable to a similar explanation.

F.5 Postfracture TR Measurements for Compact Specimens

Postfracture TR measurements from three sizes of compact (CT) specimens have been obtained for the purpose of correlating with the associated crack-initiation fracture toughness values. These specimens are standard CT specimens (1/2T, 1T, and 2T) with a crack length-to-width ratio a/W of 0.5. These specimens were also taken from HSST plate 13A. Some of these specimens were tested a number of years ago to provide small-specimen fracture toughness characterization in support of the ORNL/NIST Wide-Plate studies.[6,7] The remainder were tested in a subsequent effort to characterize the statistical nature of the fracture toughness measurements.[11] In the following discussion a total of 17 specimens that were tested at a lower-shelf temperature of –75°C are considered.

Various 4T-CT specimens were also tested as part of the WP characterization effort. These specimens were machined to a larger dimensional tolerance than the smaller CT specimens. These specimens have a nominal crack front dimension of 0.1 m (4 in.) that closely resembles that of the WP specimens. TR measurements have been obtained for five of these 4T-CT specimens. Unfortunately, the magnitudes of these TR measurements are within the specimens' dimensional tolerances so that a meaningful interpretation of the TR and toughness results is not possible. In the following discussion only the fracture toughness data, not the TR data, for these 4T-CT specimens are included.

*C. F. Shih, "Table of Hutchinson-Rice-Rosengren Singular Field Quantities," Brown University Report MRL E-147, June 1983.

F.5.1 Fracture Toughness Data

All CT specimens considered in this section failed in an unstable cleavage manner. The majority of these toughness results could not be identified as valid K_{Ic} or J_{Ic} values.[6,7] The critical values of the J-integral correspond to the value of J at maximum load. The critical values of the stress-intensity factor K_{Jc}, are derived from $J_{cleavage}$ via the relation

$$K^2_{Jc} = E\, J_{cleavage} \quad . \qquad (F.4)$$

Distribution of K_{Jc} values for all the CT specimens considered are shown in Fig. F.4. Within each specimen size the toughness values are arranged in an ascending order. The 1T-CT specimen with the lowest value of K_{Jc} in Fig. F.4 failed after an initial pop-in event; the indicated K_{Jc} value is based on maximum load. In Fig. F.5 average values of K_{Jc} for each specimen size are indicated. While the variation in toughness values within each specimen size is substantial, the observed scatter is typical of A 533 B in the lower-transition temperature range. In Fig. F.5, average values of K_{Jc} for each specimen size are indicated. It is observed that the average toughness values are relatively specimen size independent at –75°C.

F.5.2 TR Measurements

The broken halves of each of the CT specimens considered in this study were archived subsequent to the WP test program, and they have been retrieved for the present purpose of providing TR measurements. Recall that the proposed TR correlation does not provide guidance on an appropriate measurement location. However, the identification of CTOD with TR, and the forms of Eqs. (F.2) and (F.3), imply that the measurement location should reflect the response of the specimen material without explicit contributions from the geometry of the specimen.

In this study, postfracture TR measurements have been taken along the specimen surfaces at two locations ahead

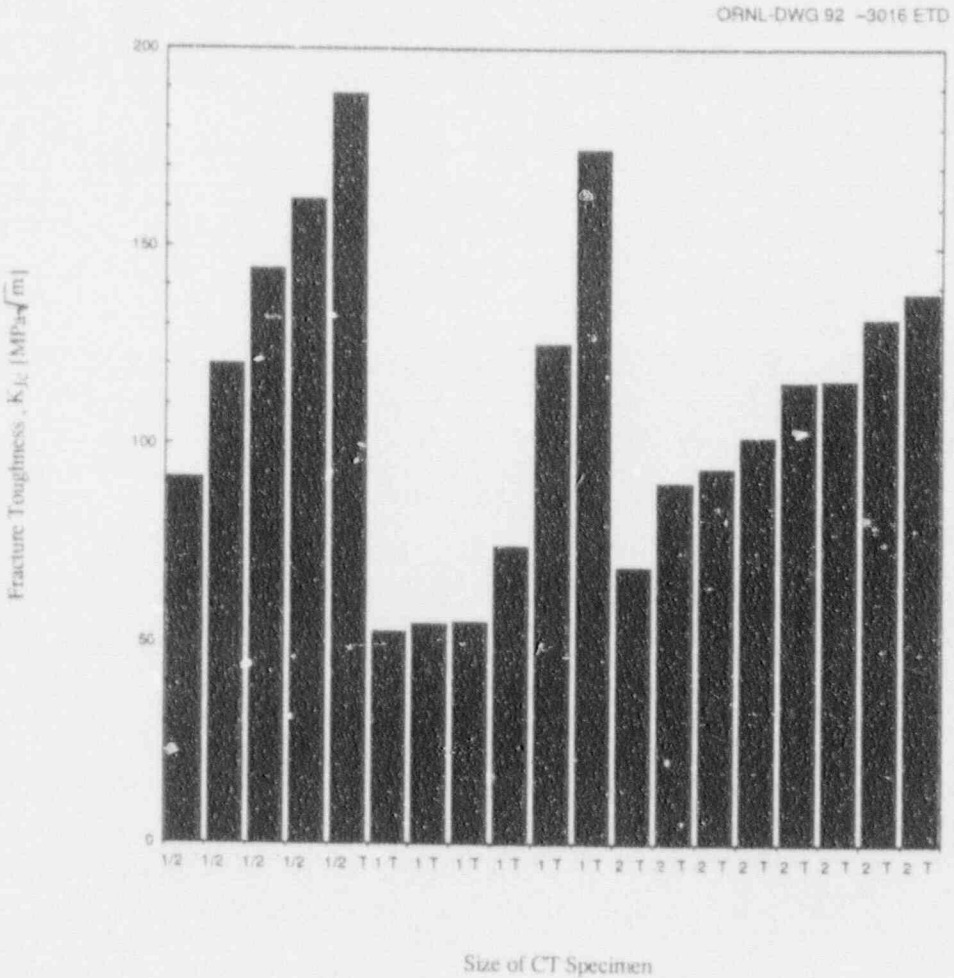

Figure F.4 Distribution of K_{Jc} values for CT specimens. Within each specimen size, toughness values are arranged in ascending order.While variation in toughness values within each specimen size is substantial, observed scatter is typical of A 533 in lower-transition temperature range

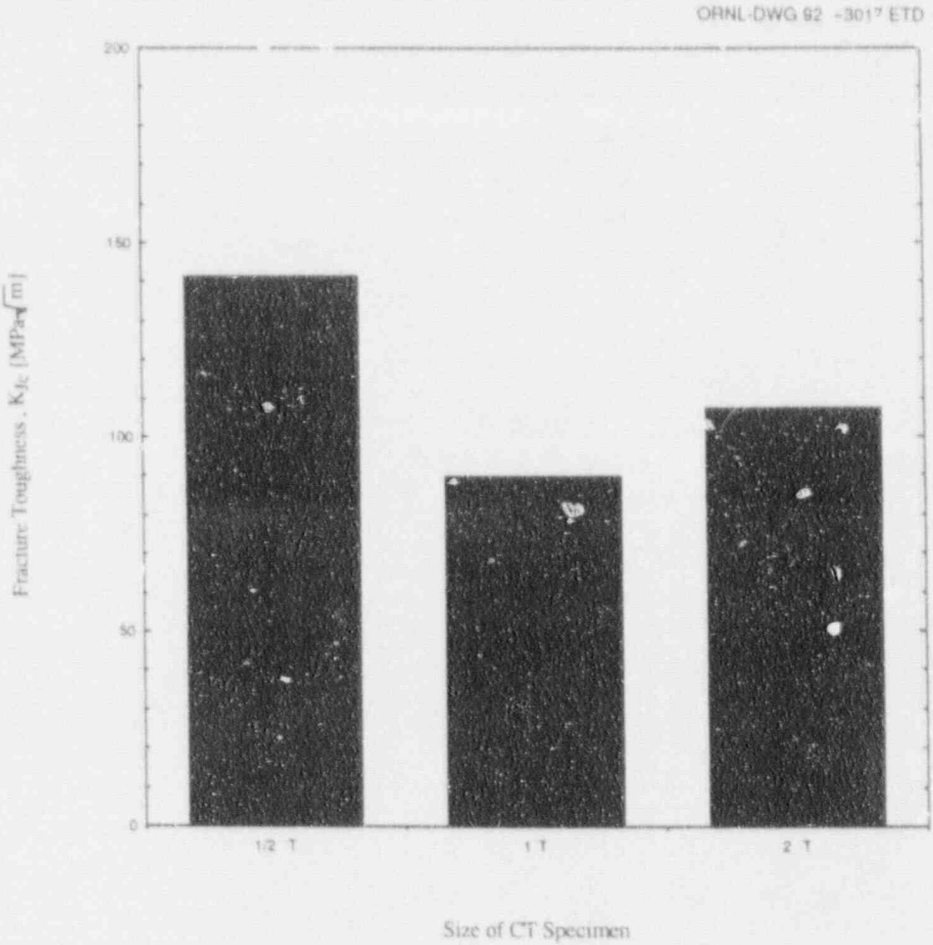

Figure F.5 Average values of K_{Jc} for each CT specimen size. In contrast to Fig. F.4, the average toughness values are relatively specimen size-independent at –75°C

of the fatigue crack front using a microscope-micrometer setup as schematically indicated in Fig. F.6. The measurement location is denoted as t_o. The two choices of t_o are (1) a distance of 5 J/σ_o ahead of the crack front, where J is equal to $J_{cleavage}$ and σ_o is the uniaxial yield stress in tension at the test temperature, and (2) a location denoted as t_{max} that appears to have the most TR based on visual examination of the specimen using the microscope.

The first measurement location corresponds to a constant normalized distance, with respect to the applied load, ahead of the crack front. It is believed that this distance is sufficiently close to the crack tip to provide indications of near-crack-tip behavior. The second measurement location is chosen to give some indication of the maximum TR value and its location within a specimen. The present definition of t_{max} is necessarily approximate because there is no attempt to explicitly establish the variation of TR ahead of the crack front.

Distributions of the t_o locations based on these two definitions adopted in this study are indicated in Fig. F.7 for the 17 specimens (excluding 4T-CT). The specimens within each specimen size are again arranged in ascending order of toughness. Association of toughness and t_o values for each specimen indicated in Figs. F.4 and F.7 can thus be straightforwardly accomplished. (This format for presenting results related to individual specimens is employed in all subsequent plots.) Measurement locations denoted as $t_o = 5\ J/\sigma_o$ necessarily follow an ascending order within each specimen size because the toughness values are so ordered. On the other hand, there does not appear to be an obvious ordering of $t_o = t_{max}$ locations within or among the specimen sizes.

At TR measurement location t_o, negative transverse displacement associated with the two free surfaces is taken and is arbitrarily denoted as dt1 and dt2, as indicated in Fig. F.6. For each specimen the broken halves are labelled high or low based on comparison of total TR = |dt1+dt2| for the two halves of a given specimen. A given specimen

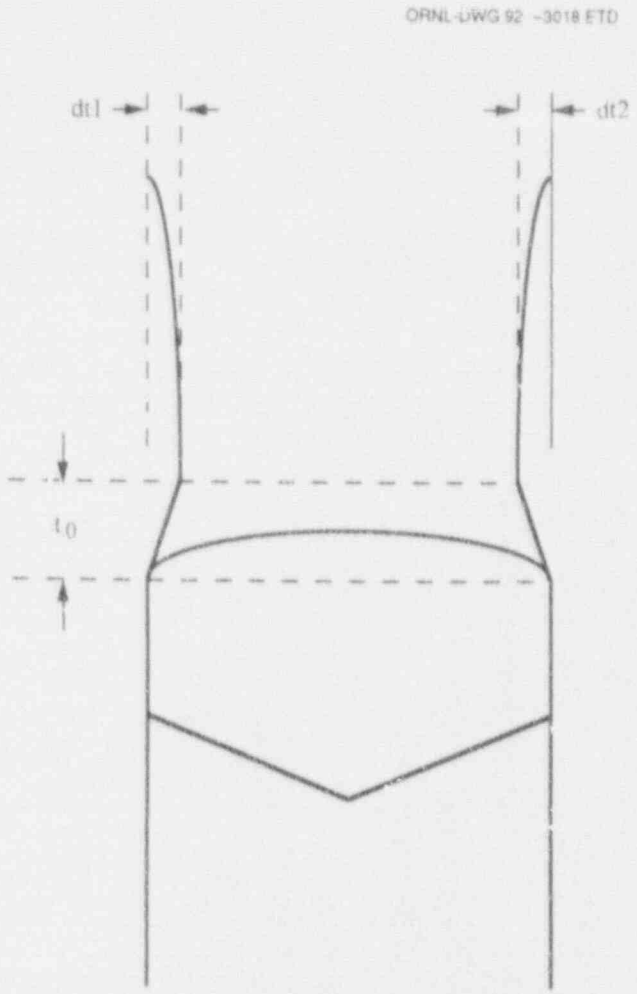

Figure F.6 Schematic indicating the location (t_0) along a specimen's surface from which postfracture TR measurement is taken. Two choices of (t_0) are as follows: (1) a distance of 5 J/σ_0 ahead of the crack front, where J is equal to $J_{cleavage}$ and σ_0 is uniaxial yield stress in tension at test temperature, and (2) location denoted as t_{max} that appears to have most TR based on visual examination of specimen using microscope

half may therefore be labeled high with respect to t_0 = 5 J/σ_0 and low with respect to $t_0 = t_{max}$.

Distributions of transverse displacement values associated with the two sides of the specimens are shown in Figs. F.8 and F.9 for the two definitions of t_0. Agreements between values of dt1 and dt2 at a given location of t_0 for each specimen are perhaps indicative of the test conditions in terms of material homogeneity, the degree of symmetry of load application, and of unstable crack growth subsequent to crack initiation.

Distributions of TR measurements averaged from both halves of the specimens at the two t_0 locations are indicated in Fig. F.10. It is seen that TR values generally increase with increasing toughness within each specimen size. Recall that the measurement location $t_0 = t_{max}$ is chosen for each specimen because it appears to correspond to maximum thickness reduction. Results from Fig. F.10 indicate that the $t_0 = t_{max}$ locations thus chosen do in fact correspond to TR values that are larger than those for t_0 = 5 J/σ_0 for almost all cases considered. Exception is noted for one 1T specimen for which TR values from $t_0 = t_{max}$ are slightly lower than the value obtained from the t_0 = 5 J/σ_0 location. While the TR values show marked variation within each specimen size, the average values for each specimen size appear to be much more uniform as indicated in Fig. F.11.

F.5.3 Correlation Between TR and Crack-Initiation Toughness

Data shown in Fig. F.4 and Figs. F.7 to F.10 indicate that significant variability in measured quantities, both in terms of t_0, TR, and toughness values, exists within a given specimen size and among the specimen sizes. The scatter associated with the toughness values is typical of that associated with A 533 B in the lower-transition temperature range. However, it is emphasized that the validity of Eq. (F.3) requires that the proposed TR correlation be insensitive to scatter in toughness values. That is, while scatter in toughness values is to be expected, the proposal that TR is related to CTOD in a relatively constant manner is by its nature not subject to scatter.

In Fig. F.12 the average values of TR are plotted at the two measurement locations t_0 for each specimen against the reported toughness values based on results from Fig. F.4. The toughness values are reported in terms of their J-integral values for reasons indicated earlier in the discussion on WP results. In Fig. F.12 three straight lines are drawn for three values of the empirical adjustment factor m that corresponds to the predicted relationship between TR and J, as indicated by Eq. (F.3) and discussed previously. Rate adjustment of the type employed in Ref. 4 corresponds to m = 1.47, based on yield stress σ_y = 500 MPa and flow stress σ_{fl} = 598 MPa at –75°C, and a rate-adjusted flow stress elevation of 138 MPa. The m = 1 line will be taken as indicative of the lowest constraint conditions, while the m = 2 line is taken as indicative of plane strain constraint conditions.

Results shown in Fig. F.12 indicate that aside from the 1/2T specimens, it does not appear that a correlation of the type suggested by Eq. (F.3) applies to the 1T and 2T

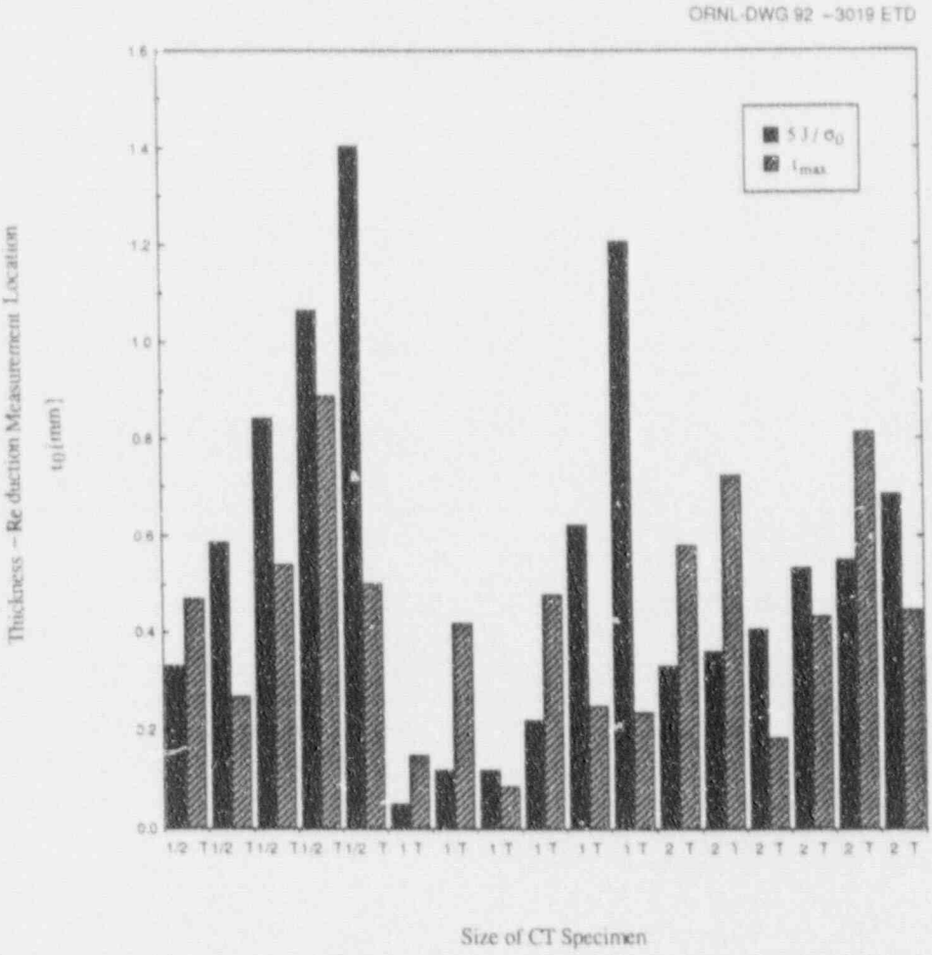

Figure F.7 Distributions of t_0 locations based on two definitions adopted in this study indicated for 17 specimens (excluding 4T-CT). Measurement locations denoted as $t_0 = 5\ J/\sigma_0$ necessarily follow ascending order within each specimen size since toughness values are so ordered. In contrast there does not appear to be an obvious ordering of $t_0 = t_{max}$ locations within or among specimen sizes

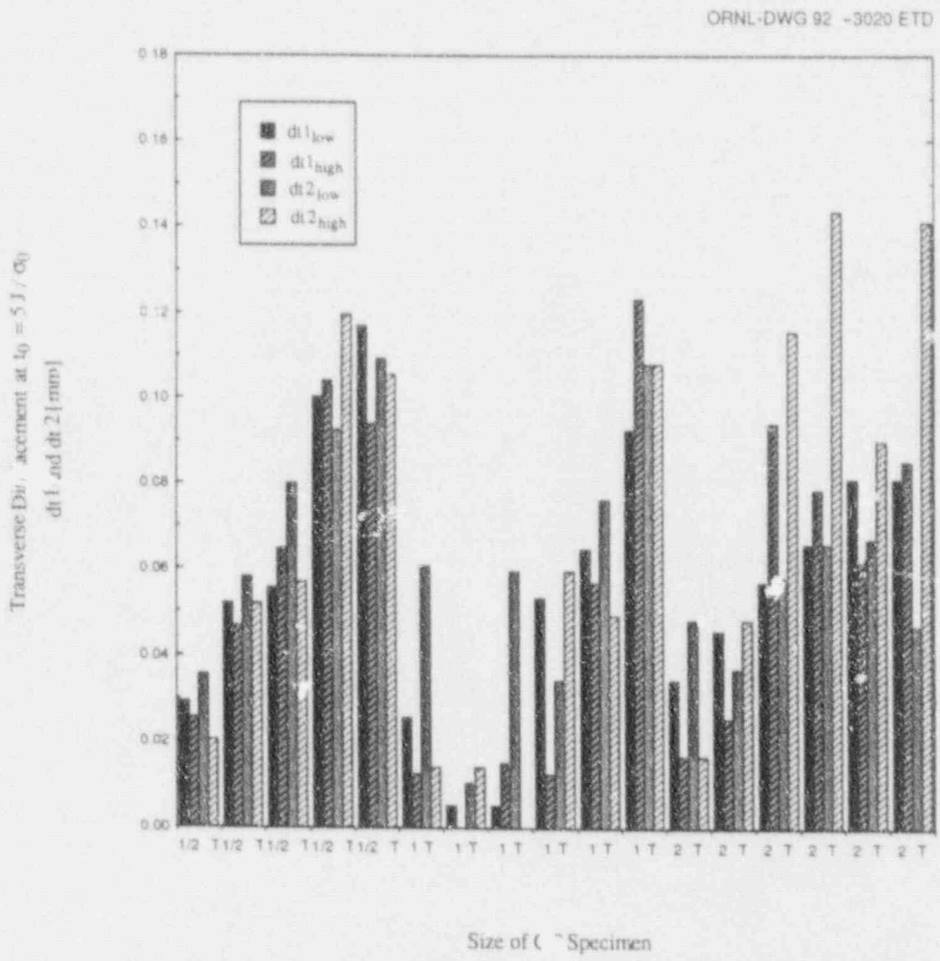

Figure F.8 Distributions of transverse displacement values associated with two sides of specimens for t_o = 5 J/σ_o. For each specimen the broken halves are labelled "high" or "low" based on comparison of total TR = |dt1 + dt2| for two halves of given specimen

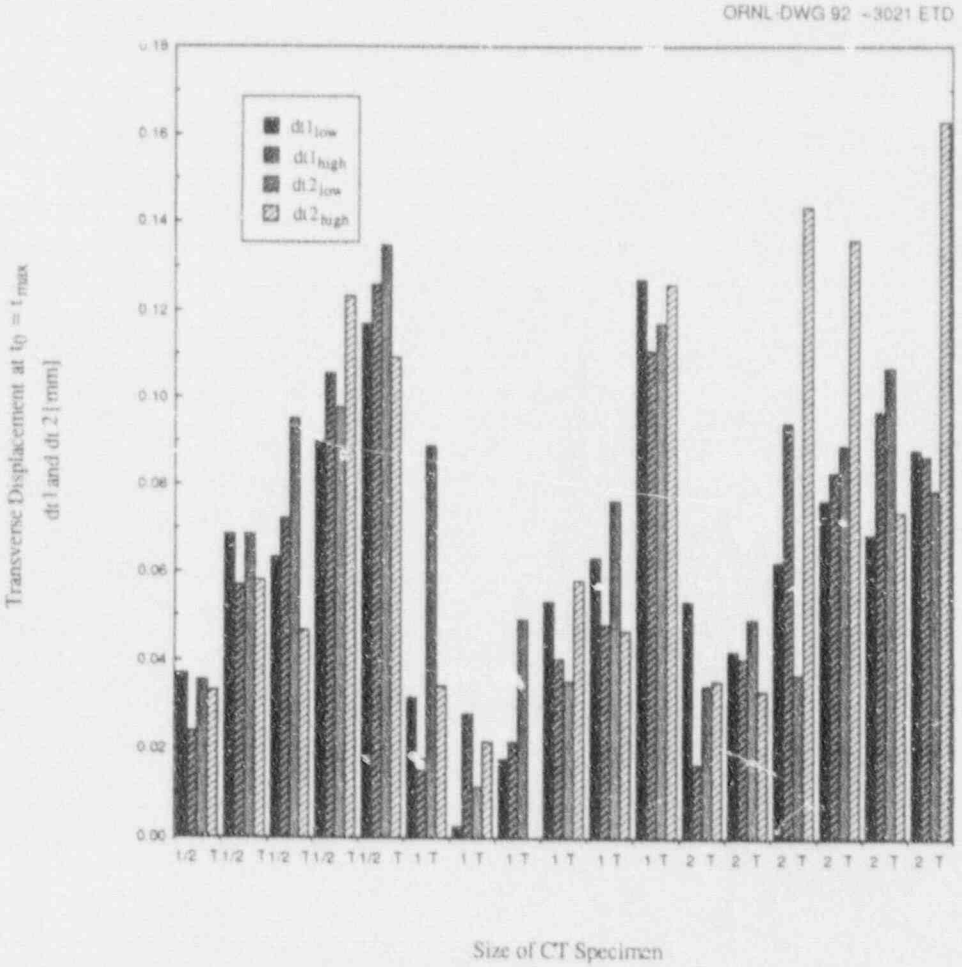

Figure F.9 Distributions of transverse displacement values associated with two sides of specimens for $t_o = t_{max}$. A given specimen half may be labeled "high" with respect to $t_o = 5\ J/\sigma_o$ and "low" with respect to $t_o = t_{max}$

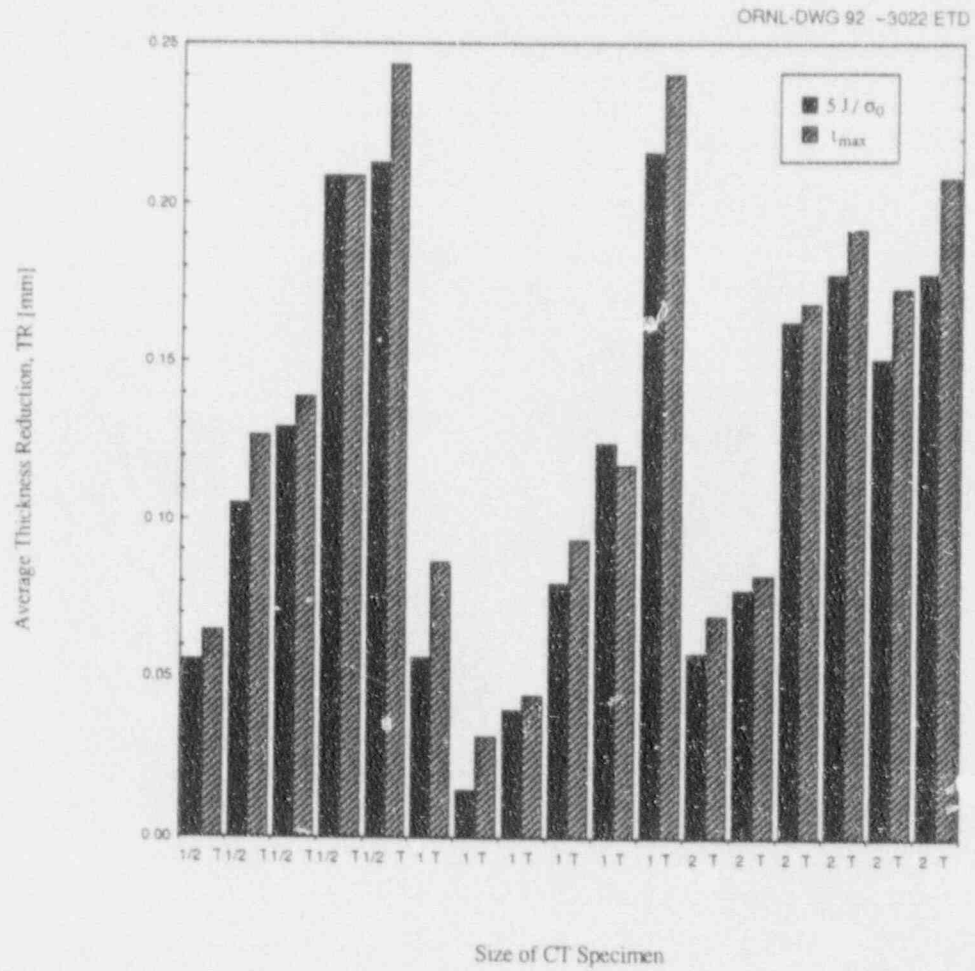

Figure F.10 Distributions of TR measurements averaged from both halves of specimens at two t_0 locations. TR values generally increase with increasing toughness within each specimen size

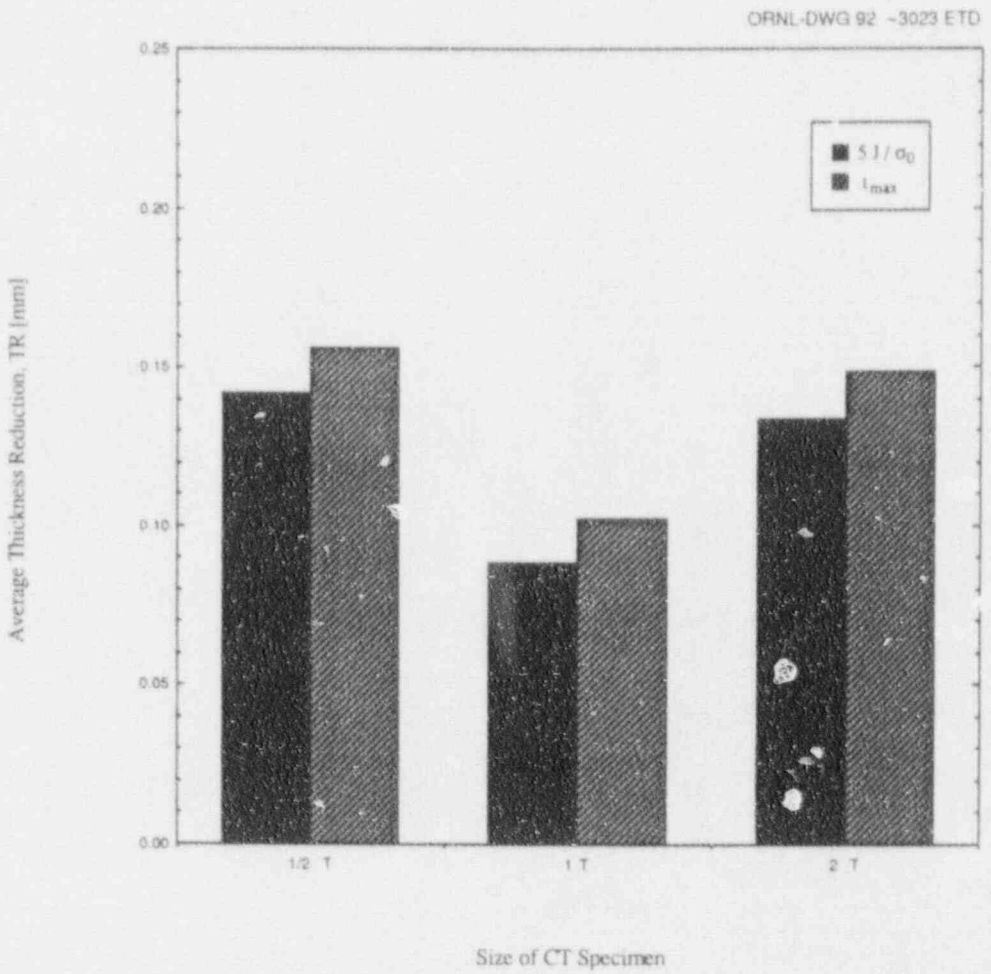

Figure F.11 Average values of TR for each specimen size. While TR values show marked variation within each specimen size (see Fig. F.10), average values for each specimen size appear to be much more uniform

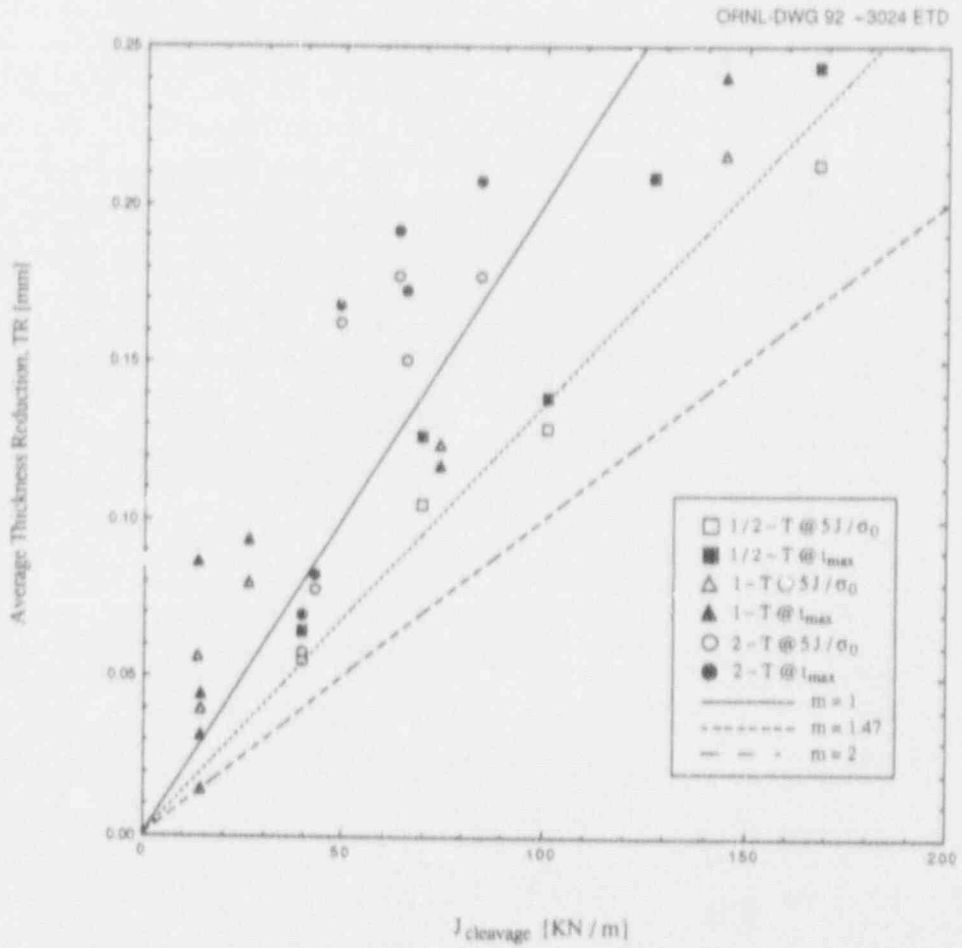

Figure F.12 Comparison of measured and predicted toughness based on Eq (F.3) for CT specimens. Measured toughness for each specimen is plotted against TR values obtained at two measurement locations. Three straight lines correspond to predicted relationship between TR and J based on three values of empirical adjustment factor m. The m = 1 line is taken as indicative of lowest constraint conditions, while m = 2 line is taken as indicative of plane strain constraint conditions

specimens. Again, this interpretation is based upon the observation that the existence of a TR correlation involves not only a linear relationship between TR and J, but also that this linear relationship needs to be anchored at the origin of the plot in Fig. F.12. In addition, the TR-J data need to be to the right of the m = 1 line due to the assumption of minimum constraint associated with the static, plane stress condition. The magnitudes of the transverse strain for the various specimens are 0.4 to 1.6% for the 1/2-CT , 0.2 to 1% for the 1T-CT, and 0.1 to 0.4% for the 2T-CT specimens. For the 1/2T specimens, the TR correlation appears to be validated for both large and small values of induced thickness reduction if an adjustment factor less than that suggested in Ref. 4 is assumed.

F.5.4 Numerical Predictions of In-Situ TR

Recall that the TR correlation in Eq. (F.2) is premised upon TR being an approximate measure of CTOD at failure, where both quantities must necessarily be in-situ prefracture values. The generalization of this correlation in the form of Eq. (F.3) still requires a constant relationship between TR and CTOD. In view of the apparent lack of correlation between the measured TR and toughness values for the CT specimens, analyses were performed for a three-dimensional (3-D) finite-element model of a 1T-CT specimen in an attempt to gain further insights. Specifically, the question to be addressed concerns to what extent postfracture TR measurements can be related to the amount of TR just before crack initiation and to the amount of residual TR subsequent to crack initiation.

Details of these finite-element analyses have been described in Appendix E of this report. Specifically, the load histories for three of the 1T-CT specimens considered in Fig. F.12 were examined. These specimens failed at values of the maximum applied load P_{max} equal to 29, 35, and 50 kN, respectively. Relevant experimental data on these three specimens are presented in Table F.2 to facilitate the following discussion.

Finite-element calculations of the transverse displacement distribution across these specimens at P_{max} are presented in Fig. E.7(*a*)–(*c*). In these figures the negative transverse displacement results indicated on the vertical axis correspond to those experienced by one-half of the specimen, with the origin of the horizontal axis denoting the midplane of the specimen. TR values are thus obtained by doubling the displacement values indicated in these figures, with proper accounting for the negative sign of the finite-element results. These TR values are presented in Table F.2.

Transverse displacement distributions for the three 1T-CT specimens after unloading from peak load to zero applied load are presented in Fig. E.8 (*a*)–(*c*); the associated TR values are presented in Table F.2. Note that while these residual TR values may be indicative of the effects due to removal of the applied load, they do not account for the TR contributions due to unstable crack initiation and propagation, especially tensile necking in shear lips. Comparisons of the results presented in Table F.2 indicate that the numerically determined residual TR values are on the order of one-third their measured values at P_{max} for K51C and K52B and that they are nearly identical for specimen K54A.

The first observation is that the finite-element results indicate that the distribution of TR is a decreasing function of distance from the crack front. Based on elementary crack-tip-field considerations, one would indeed anticipate this to be the case. On the other hand, the experimental data presented in Table F.2 suggest an opposite trend for two of the three specimens (K52B and K54A). Furthermore, the results presented in Fig. F.7 suggest no definite trends with respect to the two measurement locations.

The second observation is that the finite-element analyses predict substantially lower values of residual TR than those determined experimentally for K51C and K52B, while the finite-element prediction for K54A is nearly identical to

Table F.2 Experimental data relevant to TR measurements for three 1T-CT specimens, along with finite-element calculations of TR at maximum fracture load and after unloading from peak load to zero applied load

							From 3-D model			
					From TR measurements		$P = P_{max}$		After unloading	
Specimen No.	P_{max} (kN)	$J_{cleavage}$ (kN/m)	$t_o = 5\ J/\sigma_o$ (mm)	$t_o = t_{max}$ (mm)	Average TR at $5\ J/\sigma_o$ (mm)	Average TR at t_{max} (mm)	TR at $5\ J/\sigma_o$ (mm)	TR at t_{max} (mm)	TR at $5\ J/\sigma_o$ (mm)	TR at t_{max} (mm)
K51C	29	14.4	0.12	0.084	0.040	0.044	0.041		0.013	
K52B	35	26.3	0.22	0.48	0.080	0.094	0.056	0.046	0.020	0.019
K54A	50	74.3	0.62	0.25	0.124	0.117	0.157		0.127	

the corresponding experimental measurement. It is believed that this observation can be understood by recognizing that the experimental postfracture TR measurements represent the total contribution from crack-initiation and crack-propagation effects. On the other hand, the finite-element results represent in-situ predictions of TR values due to the application of maximum load and subsequent unloading. Consequently, it would appear that the contribution to TR resulting from shear-lip formation due to crack propagation may at times overwhelm the contribution due to crack initiation.

The third observation is that the numerically determined TR values at maximum load are similar to measured post-fracture values. However, it is not possible to conclude whether the numerically determined TR values at maximum load are either consistently higher or lower than measured values. Clearly, the amount of TR at fracture can be correlated with the applied fracture load or alternately with the fracture toughness. However, the apparent lack of correlation between TR and J for the 1T-CT, as indicated in Fig. F.12, appears to rule out the premise that the amount of TR prior to crack initiation can be correlated with fracture toughness in the manner described by Eq. (F.3), at least for some of the 1T-CT specimens.

F.6 General Observations on Correlation Between Induced TR and Fracture Toughness

The first observation concerns the functional form of the proposed TR correlation as indicated in Eq. (F.3). In view of the apparent nonlinear nature of the results when TR is plotted against the J-integral in Figs. F.3 and F.12, it might be tempting to suggest a nonlinear relationship between TR and CTOD and to incorporate this nonlinearity into Eq (F.3). However, if a nonlinear TR-CTOD relationship is adopted, the empirical factor m would no longer be an empirical constant but a nondimensional function involving some nondimensional load parameter. The problem with this proposal is that there does not appear to be any theoretical basis for such a dependence on load that is in addition to the contribution via J/σ_0 that has already been assumed in Eq. (F.3). The dependence on material parameters would appear as a constant at a given test temperature and strain rate. This dependence has already been implicitly assumed in the definition of the factor m in Eq. (F.3).

The second observation concerns the uncertainty related to the practical limitations associated with use of Eq. (F.3). As indicated in Sect. F.2, the proposed TR correlation is strictly not applicable near plane strainlike conditions. However, it should be recognized that even for sufficiently thick test specimens that satisfy standard plane strain validity requirements, the magnitude of the TR or transverse *displacement*, as opposed to transverse *strain*, may be appreciable. This comment is based on the observation that displacement is the product between strain and specimen thickness integrated along the crack front. It is not possible to establish, a priori, the relative contribution to this product from the interior of the specimen (small strain but large thickness) as compared to the two surface-layer regions (large strain but small thickness). It is unclear to what degree the proposed TR correlation is sensitive to the relative contribution to TR from the interior and surface-layer regions. Perhaps this uncertainty is related to the varying degree of success in applying the proposed TR correlation to the CT and WP specimens and to the experimental data cited in Ref. 3.

The third observation concerns the effects of higher-order T- or Q-stress on the proposed TR correlation. To the extent that the proposed correlation is premised upon the J-CTOD relation associated with a given material, the effects of T- or Q-stress on this correlation are expected to be directly related to the effects of T- or Q-stress on the J-CTOD relation.*

The fourth observation is that while the proposed correlation implies a nearly constant relation between the degree of induced TR and J in a manner similar to the nearly constant relation between CTOD and J, this implication of constancy does not contradict the commonly observed scatter in fracture toughness values. Recall that while the magnitude of fracture toughness at the lower-shelf and transition temperature range is known to show a large degree of variability under nominally identical testing conditions, the relation between critical values of fracture toughness and the independently measurable CTOD is fairly constant. Similarly, on the basis of Eq. (F.3), the relation between critical values of toughness and TR, should one exist, would be fairly constant.

F.7 Induced vs Prescribed Transverse Strain

The utility of a correlation based on induced TR toward determination of the effects of prescribed transverse displacement on fracture toughness is limited. That is, even if the validity of a correlation between induced TR and toughness [such as Eq. (F.3)] can be established, it does not follow that this correlation can be used to determine toughness as a function of TR, nor that this correlation can

*N. P. O'Dowd and C. F. Shih, "Family of Crack-Tip Fields Characterized by a Triaxiality Parameter: Part II—Fracture Applications," submitted for publication in *J. Mech. Phys. Solids*, August 1991.

be extrapolated into the positive straining regime, whether the positive straining is induced or prescribed. The toughness data presented in Fig. F.13 will now be used to emphasize this idea.

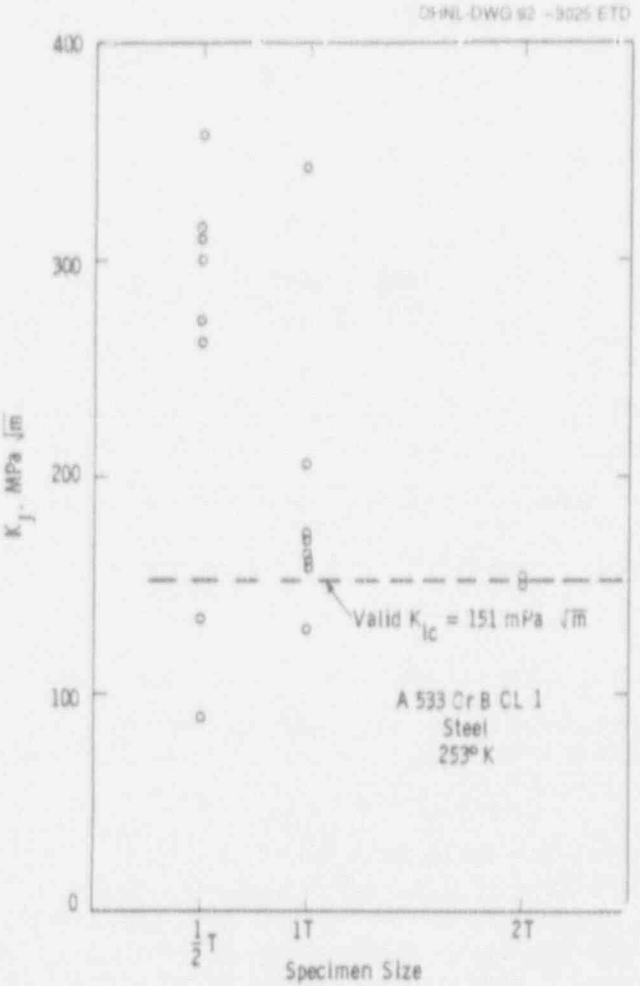

Figure F.13 Variation of critical K values (converted from critical J values at instability) for a number of CT specimens of various planforms and thicknesses

Critical K values (converted from critical J values in instability) for a number of CT specimens of various planforms and thicknesses are presented in Fig. F.13.* While there are only two data points for the 2T specimens, these data do appear to support the observation that the average value of toughness decreases with increasing specimen width. However, it would be incorrect to suggest that the decrease in average thickness reduction or induced transverse strain at fracture with increasing specimen thickness is responsible for the observed trend in toughness. An interpretation is that inhomogeneity in a given heat of material results in a distribution of critical conditions necessary to initiate fracture. As specimen size is increased, a specimen will sample a larger volume of material and exhibit lower fracture toughness.[12] Indeed, such an explanation is compatible with both the observation that the minimum toughness is lower for the 1/2T than the 2T specimens and that the reverse is true for the average toughness value.

While it may be possible to establish a correlation that relates the variation in toughness, both among specimen sizes and within a given specimen size, with the magnitude of the induced transverse strain, experimental results of the type indicated in Fig. F.13 simply give no information on the role of prescribed transverse strain on toughness. The effects of prescribed transverse strain on fracture toughness can, however, be evaluated in the following manner. Fracture toughness tests need to be performed for a suitable number of specimens under nominally identical in-plane conditions but various degrees of prescribed out-of-plane straining. The influence of transverse strain on toughness can be established, based on the extent that the prescribed transverse strain influences the scatter in toughness data, such as that indicated in Fig. F.13.

F.8 References

1. S. J. Garwood, T. F. Davey, and S. L. Cresswell, "Behavior of A533B under Biaxial Loading at +70°C," *Int. J. Pres. Vessel and Piping* 36, 199–224 (1989).*

2. S. J. Garwood, "The Significance of Biaxial Loading on the Fracture Performance of a Pressure Vessel Steel," *ASME Pressure Vessel and Piping Division Conference*, PVP-Vol 213/MPC-Vol 32, 113–123, 1991.†

3. G. R. Irwin., University of Maryland for Martin Marietta Energy Systems, Inc., Oak Ridge Natl. Lab., "Use of Thickness Reduction to Estimate Values of K," USNRC Report NUREG/CR-5697 (ORNL/TM-11581), October 1991.†

4. R. deWit, R. J. Fields, and G. R. Irwin, "Use of Thickness Reduction to Estimate Fracture Toughness," paper presented at the *ASTM Symposium on Constraint Effects in Fracture, Indianapolis, IN*, May 8–9, 1991.†

5. F. M. Burdekin, "Initiation of Brittle Fracture in Structural Steels," *Weld. Eng.*, 74–82 (October 1967).†

*D. E. McCabe and J. D. Landes, "The Effect of Specimen Plan View Size and Material Thickness on the Transition Temperature Behavior of A533B Steel," Research Report 80-1D3-REVEM-R2, Westinghouse R&D Center, November 1980.

6. D. J. Naus et al., Martin Marietta Energy Systems, Inc., Oak Ridge Natl. Lab., "Crack-Arrest Behavior in SEN Wide Plates of Quenched and Tempered A 533 Grade B Steel Tested Under Nonisothermal Conditions," USNRC Report NUREG/CR-4930 (ORNL-6388), August 1987.†

7. D. J. Naus et al., Martin Marietta Energy Systems, Inc., Oak Ridge Natl. Lab., "High-Temperature Crack-Arrest Behavior in 152-mm-Thick SEN Wide Plates of Quenched and Tempered A 533 Grade B Class 1 Steel," USNRC Report NUREG/CR-5330 (ORNL/TM-11083), April 1989.†

8. D. J. Naus et al., Martin Marietta Energy Systems, Inc., Oak Ridge Natl. Lab., "SEN Wide-Plate Crack-Arrest Tests Using A 533 Grade B Class 1 Material: WP-CE Test Series," USNRC Report NUREG/CR-5408 (ORNL/TM-11269), November 1989.†

9. D. J. Naus et al., Martin Marietta Energy Systems, Inc., Oak Ridge Natl. Lab., "High-Temperature Crack-Arrest Tests Using 152-mm-Thick SEN Wide Plates of Low-Upper-Shelf Base Material: Tests WP-2.2 and WP-2.6," USNRC Report NUREG/CR-5450 (ORNL/TM-11352), February 1990.†

10. D. J. Naus et al., Martin Marietta Energy Systems, Inc., Oak Ridge Natl. Lab., "Crack-Arrest Behavior in SEN Wide Plates of Low-Upper-Shelf Base Material Tested Under Nonisothermal Conditions: WP-2 Series," USNRC Report NUREG/CR-5451 (ORNL/TM-6584), August 1990.†

11. D. E. McCabe, "A Comparison of Weibull and β_{Ic} Analyses of Transition Range Data," paper presented at the *23rd National Symposium on Fracture Mechanics, College Station, TX*, 1991.†

12. J. D. Landes and D. E. McCabe, "Effects of Section Size on Transition Temperature Behavior of Structural Steels," pp. 378–392 in *Fracture Mechanics: Fifteen Symposium, ASTM STP 833*, American Society of Testing and Materials, Philadelphia, 1984.†

---

*Available in public technical libraries.

†Available for purchase from National Technical Information Service, Springfield, VA 22161.

Appendix G

Detailed Crack-Tip Analysis of Proposed Large-Scale Biaxial Fracture Specimen

D. K. M. Shum

G.1 Introduction

This appendix describes the application of the analytical fracture prediction methods discussed in Appendix B to predict the fracture response of a candidate large-scale biaxial fracture specimen. The candidate large-scale biaxial fracture specimen is schematically illustrated in Fig. G.1. The plate specimen is 76 mm (3 in.) thick, with planar dimensions measuring 1220 by 1220 mm (48 by 48 in.). The proposed flaw geometry is an elongated elliptical surface flaw with a length of 813 mm (32 in.) and a maximum flaw depth of 19 mm (0.75 in.).

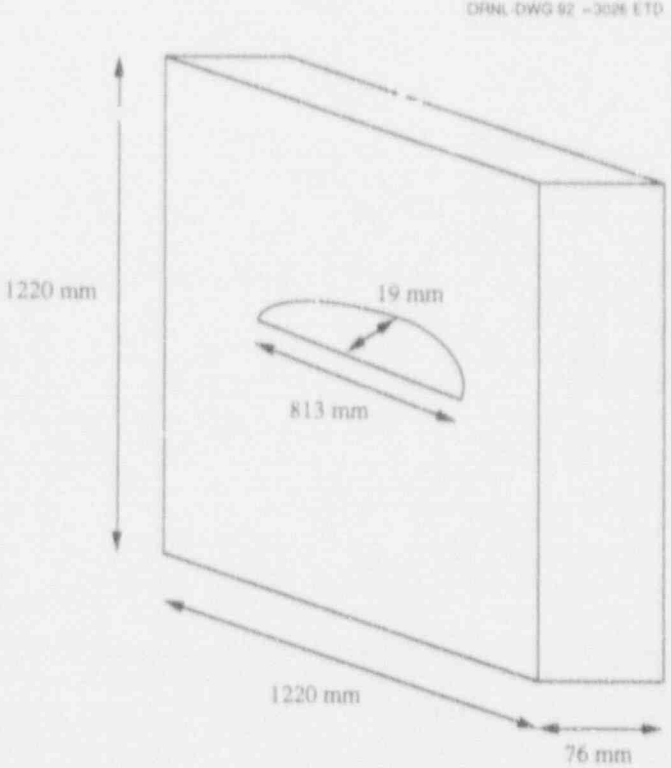

Figure G.1 Schematic of candidate large-scale biaxial fracture specimen. The plate specimen is 76 mm (3 in.) thick with planar dimensions measuring 1220 by 1220 mm (48 by 48 in.). The flaw geometry is an elongated elliptical surface flaw with length of 813 mm (32 in.) and a maximum flaw depth of 19 mm (0.75 in.)

G.2 Correspondence Between 3-D and 2-D Generalized-Plane-Strain Description of Biaxial Specimen

As discussed in Chaps. 3 and 5, quantitative determination of crack-tip stress and strain fields under generalized plane-strain (GPS) conditions is a necessary first step toward estimating the potential decrease in fracture toughness, from a reference plane strain value, due to positive straining along the crack front. The methodology demonstrated in Appendixes A and B can, in principle, be applied to a three-dimensional (3-D) model of the proposed biaxial fracture specimen. However, the computational efforts associated with an elastic-plastic analysis of the near-crack-tip fields of a 3-D crack front, involving elements with minimum dimensions on the order of the crack-tip-opening displacement (CTOD), is extremely prohibitive.

Fortunately, the experimental requirement of an elongated flaw geometry to ensure near uniformity of transverse strain is expected to result in crack-tip fields with variations along the crack front that are much less severe than their variation in directions perpendicular to the crack front. That is, along the central portions of the crack front, the crack-tip fields are expected to be essentially 2-D in nature in a manner characteristic of a state of GPS. The validity of the GPS assumption, and the extent along the 3-D crack front over which this assumption is approximately valid, are examined by comparing the distribution of the stress-intensity factor K along the 3-D crack front with the associated 2-D fracture problem assuming linear-elastic material response.

G.2.1 Comparison of 3-D and 2-D Results

The 3-D finite-element model of the proposed biaxial specimen is shown in Fig. G.2(*a*) and (*b*). From symmetry considerations only one-quarter of the specimen is modeled. The loading condition considered is uniaxial loading in the direction perpendicular to the crack plane. This loading condition is imposed in the finite-element model as a uniform load of 6.89 MPa (1 ksi) applied along the remote edge of the specimen. In a linear-elastic analysis the imposition of transverse strain along the crack front would not affect the value of the stress-intensity factor K; hence, transverse loading is not considered. The finite-element program ABAQUS[1] is used to examine this

ORNL-DWG 92-3027 ETD

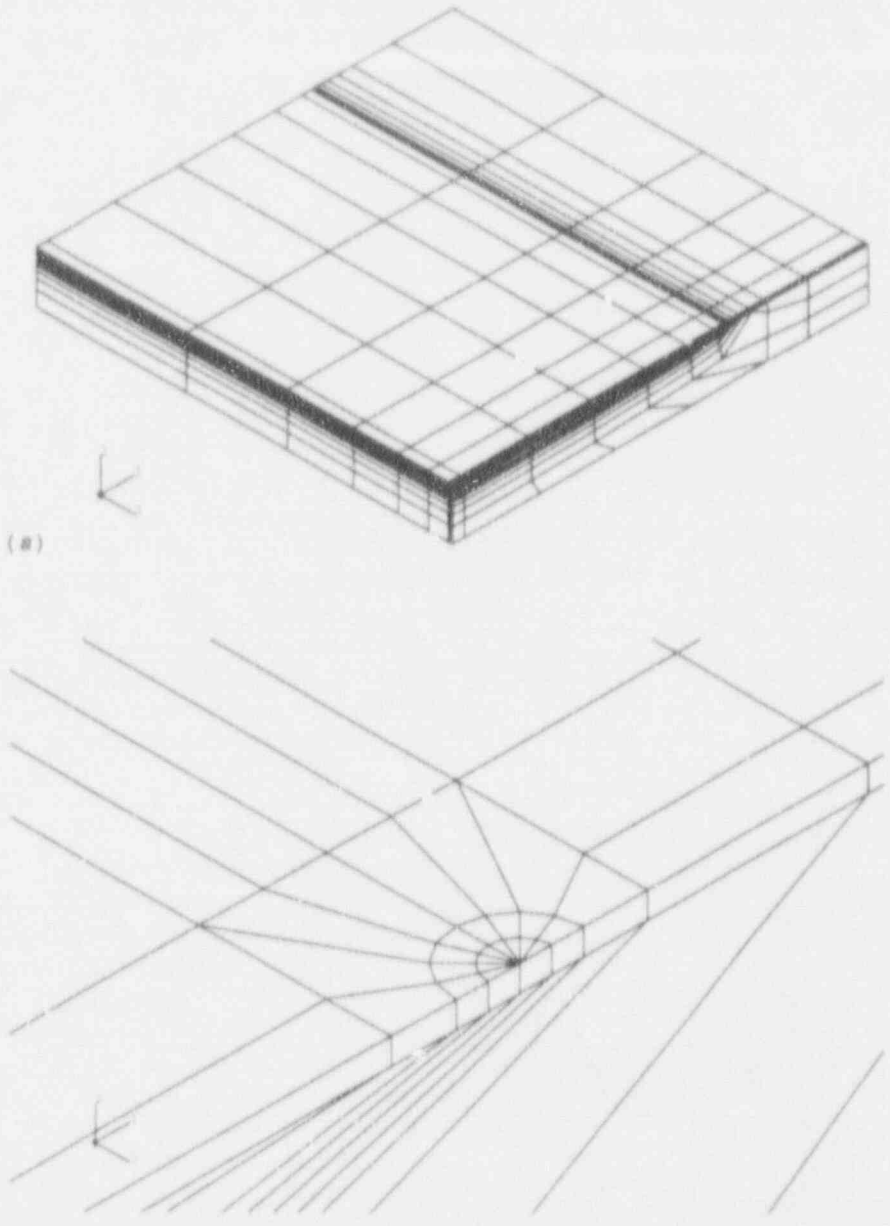

Figure G.2 **(*a*) 3-D finite-element of candidate biaxial specimen. From symmetry considerations only one-quarter of the specimen is modeled. (*b*) Crack tip region of 3-D finite-element model of candidate biaxial specimen. J-integral values are evaluated along two semicircular contours shown here**

3-D linear-elastic problem. The 3-D K values are obtained based on the J-integral values evaluated along the two semicircular contours shown in Fig. G.2(*b*). Path independence of the calculated J-integral values is observed.

The 2-D GPS geometry associated with the central portion of the biaxial specimen is a single-edge-notch (SEN) geometry as schematically illustrated in Fig. G.3. The crack length to specimen width ratio is a/W = 0.25. The linear-elastic K value for the SEN geometry subject to a uniform remote tensile load is available in the literature. Specifically, for the SEN geometry indicated in Fig. G.3 subject to uniform remote tensile load of 6.89 MPa (1 ksi), the K value is reported to be 2.535 MPa•$\sqrt{m}$ (2.307 ksi•$\sqrt{in.}$) with an error of 0.5%.[2]

The distribution of K values along the 3-D crack front is shown in Fig. G.4. The crack front location is expressed in terms of the associated surface location. In Fig. G.4, x = 0 mm corresponds to the deepest part of the 3-D flaw, and x

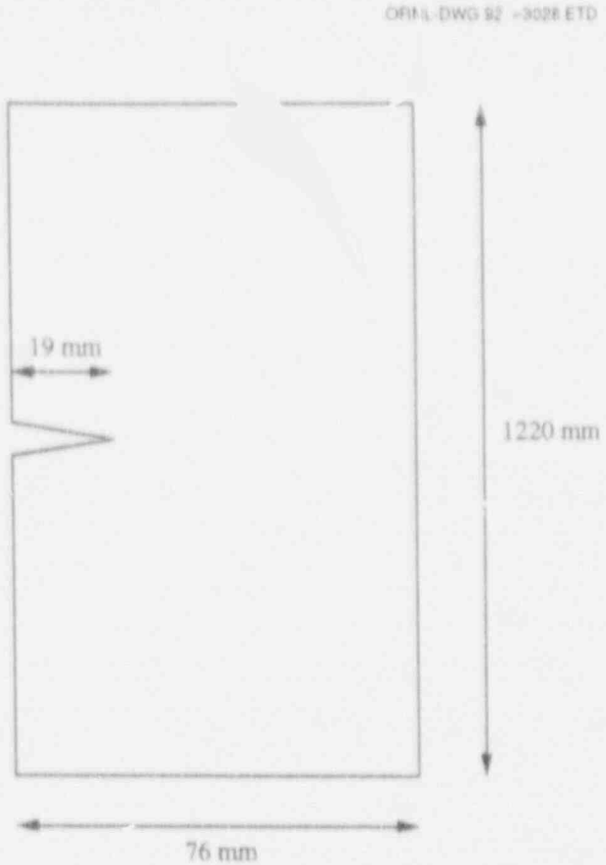

Figure G.3 Schematic of the 2-D SEN geometry associated with central, GPS portion of biaxial specimen

= 406 mm corresponds to the intersection of the crack front with the specimen's free surface. The K values are expressed as the ratio of the 3-D K values to the associated 2-D value. As indicated in Fig. G.4, the K value at the center plane of the biaxial specimen is ~84% of the SEN value. However, the feature of the 3-D K values that is relevant to the present discussion is that, along the central 406-mm (16-in.) portion of the crack front, the 3-D K values are within 88.5% of the center-plane value. The results in Fig. G.4 suggest that the near-crack-tip fields along a substantial central portion of the 3-D crack front can indeed be adequately determined via a 2-D, GPS, SEN approximation.

G.3 Detailed 2-D Finite-Element Model

Based on the findings of the previous section, the fracture response of the candidate large-scale biaxial fracture specimen is examined via the associated GPS SEN geometry illustrated schematically in Fig. G.3. The detailed 2-D finite-element model for one-half of the SEN geometry is shown in Fig. G 5(*a*)–(*c*). A unique feature of the finite-element mesh indicated in Fig. G.5(*a*) is the highly refined crack-tip region indicated in Fig. G.5(*a*) and (*b*). The outer extent of the crack-tip mesh is rectangular with dimensions 19 by 38 mm (0.75 by 1.5 in.). Within this rectangular region reside 32 rings of elements placed concentrically about the crack tip. The crack tip in its unloaded state is a semicircular notch with an approximate radius of 6×10^{-5} mm as indicated in Fig. G.5(*c*). The unloaded notch radius is ~1/300,000 of the shorter dimension of the rectangular crack-tip mesh indicated in Fig. G.5(*b*). The high degree of refinement is necessary to obtain an accurate determination of the crack-tip fields within a distance of a few CTODs ahead of the blunting-notch tip. The similarity of the present crack-tip mesh with the modified-boundary-layer (MBL), finite-element mesh presented in Appendix B is noted.

The material model considered in this study is one that simulates the uniaxial stress-strain response in tension of a reactor pressure vessel (RPV) grade material subject to irradiation effects. This material model was employed in the MBL analyses in Appendix C. The elastic portion of the true stress–true strain curve is characterized by a yield strain of magnitude $\varepsilon_0 = \sigma_0/E = 1/311$, where E is Young's modulus, $\sigma_0 = 623$ MPa (90.3 ksi) denotes the yield stress, and Poisson's ratio is 0.3. The uniaxial true stress–true plastic strain curve in tension is bilinear. The plastic portion of the uniaxial stress-strain curve becomes nonhardening at a normalized stress level of $\sigma/\sigma_0 = 1.3$ with an associated true plastic strain of 0.075.

The finite-strain, elastic-plastic, GPS nature of the present problem is examined using the finite-element code ABAQUS.[1] The analyses assume a rate-independent J_2 (isotropic-hardening) incremental plasticity theory as implemented in ABAQUS. The finite-element mesh in Fig. G.5(*a*) is made up of 963 GPS elements and 3032 nodes. These elements behave as conventional 8-node isoparametric elements except for an extra degree-of-freedom that allows for uniform straining in a direction perpendicular to the plane of the mesh.[1] The integration order of the elements is 2 by 2. J-integral values are determined from up to 32 paths surrounding the crack tip to ensure path independence. A measure of the refinement of the mesh indicated in Fig. G.5(*a*) is that the elastically determined K value using this mesh is within 99.5% of the closed-form value reported previously. Convergence requirements of the elastic-plastic, finite-element values to be presented are specified by means of limiting the maximum value of the residual nodal force per unit thickness at any node. Specifically, the maximum value is required to be <0.1% of the product between the yield stress and the smallest element dimension in the finite-element mesh.

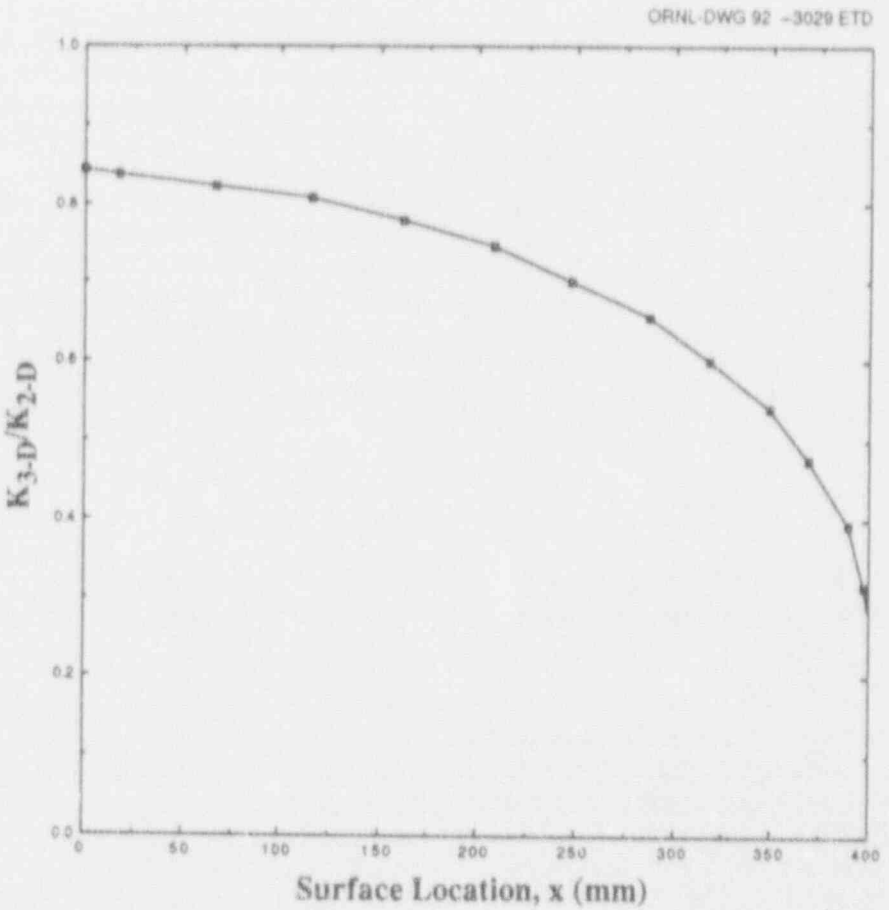

Figure G.4 Distribution of K values along 3-D crack front. Crack front location is expressed in terms of associated surface location: x = 0 mm corresponds to deepest part of the 3-D flaw and x = 406 mm corresponds to intersection of crack front with specimen's free surface. K values are expressed as ratio of 3-D K values to associated 2-D value. These results suggest that near-crack-tip fields along substantial central portion of 3-D crack front can indeed be adequately determined via 2-D, GPS SEN approximation

ORNL-DWG 97-3030 ETD

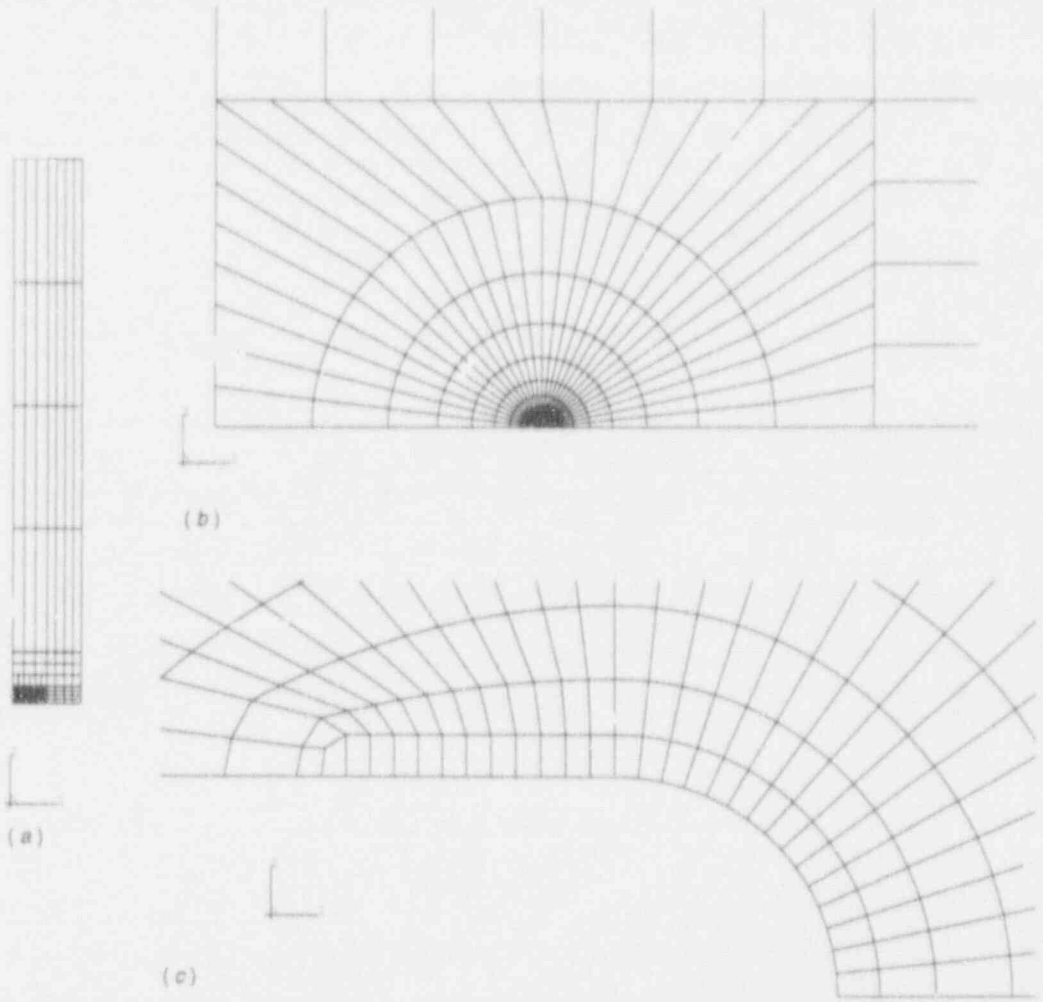

Figure G.5 **(*a*) Detailed 2-D finite-element model for one-half of SEN geometry. A unique feature of finite-element mesh is highly refined crack-tip region indicated in (*a*) and (*b*). (*b*) Finite-element model of crack-tip region for SEN geometry. Outer extent of crack-tip mesh is rectangular with dimensions 19 by 38 mm (0.75 by1.5 in.). Within this rectangular region are 32 rings of elements placed concentrically about the "crack-tip." (*c*) Finite-element model of crack tip for SEN geometry. Crack tip in its unloaded state is semicircular notch with approximate radius of 6×10^{-5} mm. Unloaded notch radius is ~1/300,00 of shorter dimension of rectangular crack-tip mesh indicated in (*b*). High degree of refinement is necessary to obtain accurate determination of crack-tip fields within distance of few CTODs ahead of blunting notch tip**

The in-plane loading conditions correspond to a distributed tensile load applied at the top edge of the SEN geometry. This distributed load increases monotonically from zero up to a maximum value 207 MPa (30 ksi) . The maximum distributed tensile load of 207 MPa corresponds to an integrated load of 19.2 MN. Two types of transverse loading are considered. The prescribed transverse strain considered is either $\varepsilon_z = 0$ (plane strain) or positive out-of-plane strain. Consideration of these two cases of out-of-plane straining allows the isolation of the effects of out-of-plane straining on crack initiation in the proposed biaxial specimen.

For the case of GPS, the magnitude of the prescribed transverse strain increases monotonically and concurrently with the in-plane distributed tensile load from zero to a maximum magnitude of $\varepsilon_z/\varepsilon_0 = 0.56$. The degree of out-of-plane straining is considered to be severe with respect to the normal operations of an RPV. These loading conditions simulate a load-controlled biaxial test, in a manner similar to the displacement boundary conditions considered in Appendix C. The maximum transverse load can be estimated from linear elasticity based on the magnitude of the prescribed transverse strain and the in-plane distributed tensile load. The maximum transverse load is ~38 MN. The

axial and transverse loading parameters are within the anticipated capacity of the biaxial test fixture.

G.4 Detailed 2-D Finite-Element Results

The plane strain ($\varepsilon_z = 0$) opening-mode stress distribution directly ahead of the blunting notch is presented in Fig. G.6 at two stages of the uniaxially applied load up to the maximum value of 19.2 MN. The distance ahead of the blunting notch is normalized by the parameter J/σ_0, where J is the value of the J-integral corresponding to the applied loading conditions. In Fig. G.7 the distribution of effective plastic strain ε_e directly ahead of the blunting notch is indicated. In Fig. G.8 the distribution of effective plastic strain and the associated stress state, as characterized by the ratio of hydrostatic stress to effective stress σ_m/σ_e, directly ahead of the blunting notch is presented. Note that ε_e is not a unique function of σ_m/σ_e as indicated by the elbows in the figure. As will be discussed shortly, it is that portion of the ε_e distribution that decreases with increasing value of σ_m/σ_e that is relevant to the ductile failure model to be presented. In addition, the reference plane strain K-dominant small-scale yielding (SSY) distributions for this material, obtained using the boundary-layer approach described in Appendixes B and C are also presented in Figs. G.6–G.8. The plane strain SSY distributions are assumed to represent the crack-tip fields associated with a standard ASTM fracture specimen, such as the compact (CT) or the three-point-bend (TPB) specimen, within the loading and geometry regime considered valid within the specifications of the testing standard.

In Figs. G.9–G.11 results analogous to those presented in Figs. G.6–G.8, except now for the case of GPS loading up to $\varepsilon_z/\varepsilon_0 = 0.56$, are presented. The parameter values indicated in these figures correspond to the magnitudes of the applied out-of-plane strain and in-plane distributed load, respectively. In Figs. G.12–G.14 the plane strain and GPS results are indicated for the case of maximum in-plane loading of 19.2 MN and, where appropriate, out-of-plane loading of magnitude $\varepsilon_z/\varepsilon_0 = 0.56$. Similar to the findings in Appendix C, results in Figs. G.9–G.14 indicate that the effects of transverse strain on the crack-tip fields increase with either increasing distance from the crack tip or increase in the magnitude of the applied transverse strain.

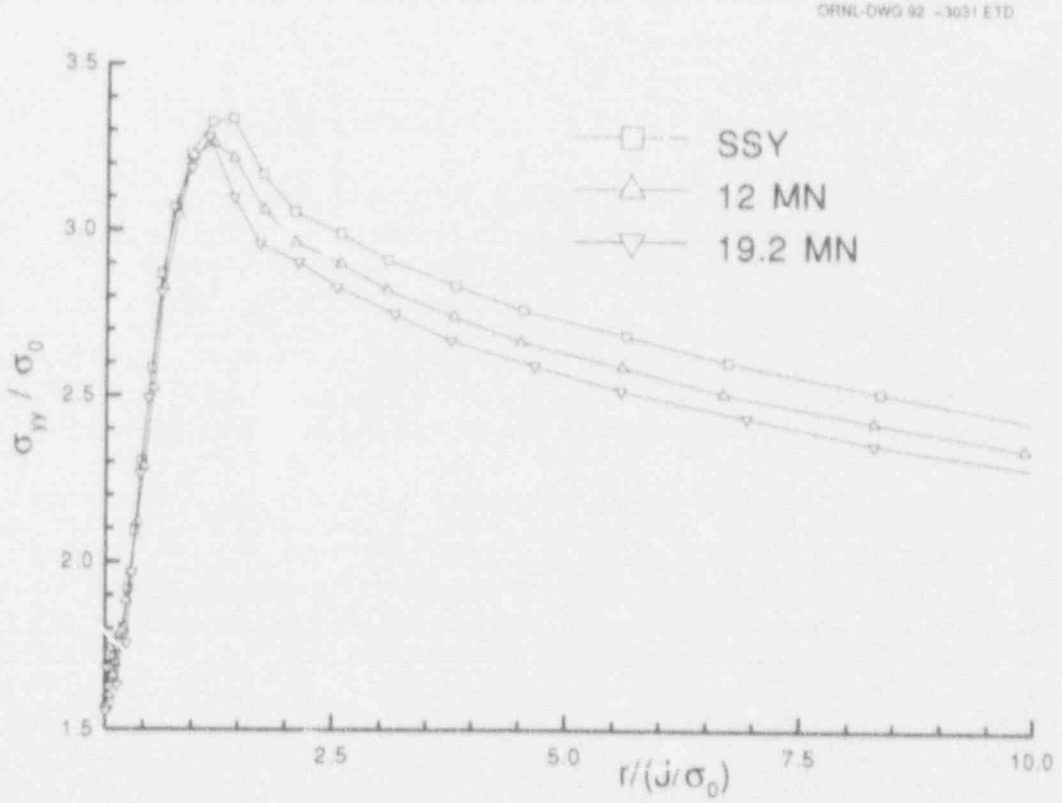

Figure G.6 Plane strain ($\varepsilon_z = 0$) opening-mode stress distribution directly ahead of blunting notch SEN geometry at two stages of uniaxially applied load to maximum value of 19.2 MN. Material model considered is one that simulates uniaxial stress-strain response in tension of RPV-grade material subject to irradiation effects with $\sigma_0 = 623$ MPa. Distribution identified as SSY is reference plane strain K-dominant distribution for this material obtained using boundary-layer approach described in Appendix C

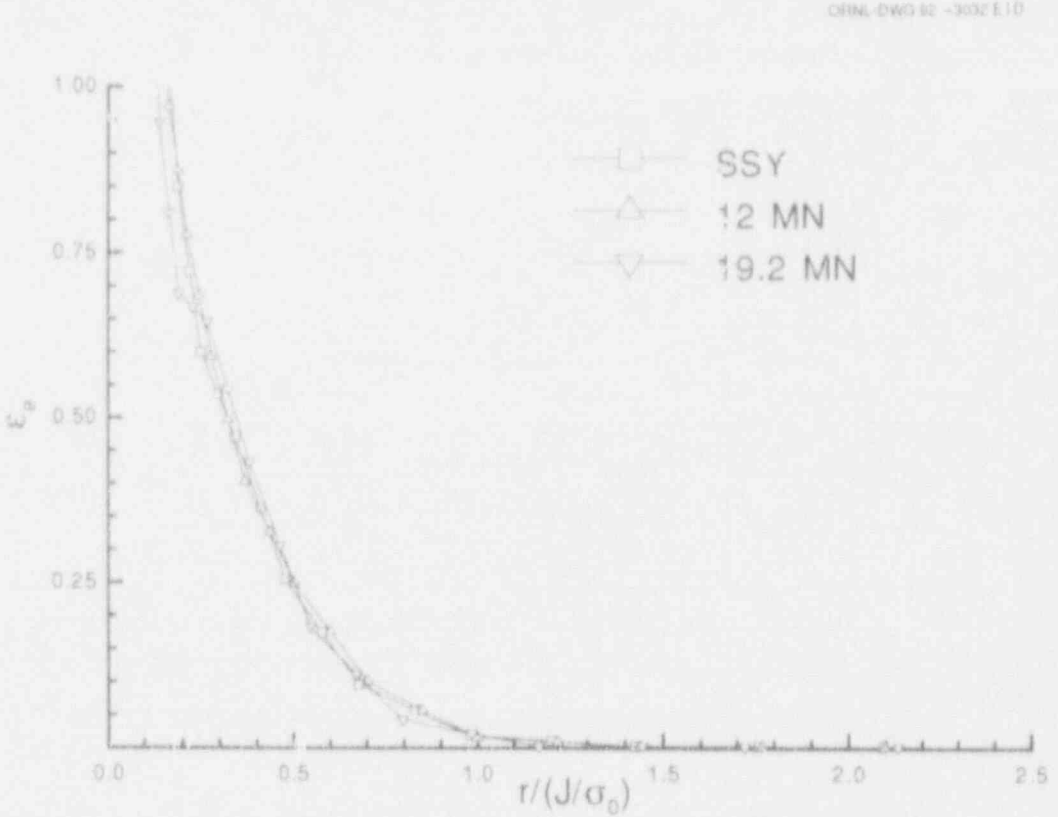

Figure G.7 Distribution of effective plastic strain directly ahead of blunting notch for SEN geometry at two stages of uniaxially applied load up to maximum value of 19.2 MN, along with reference SSY distribution

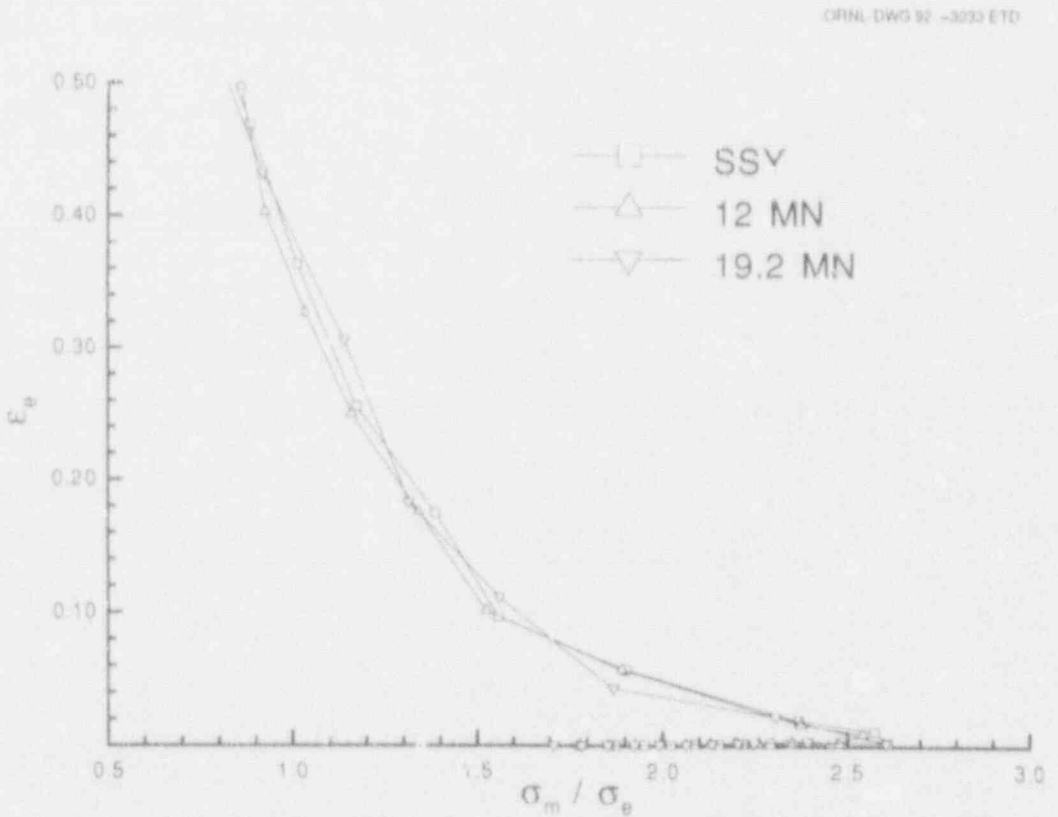

Figure G.8 Distribution of effective plastic strain as function of stress ratio σ_m/σ_e for SEN geometry at two stages of uniaxially applied load up to maximum value of 19.2 MN, along with reference SSY distribution

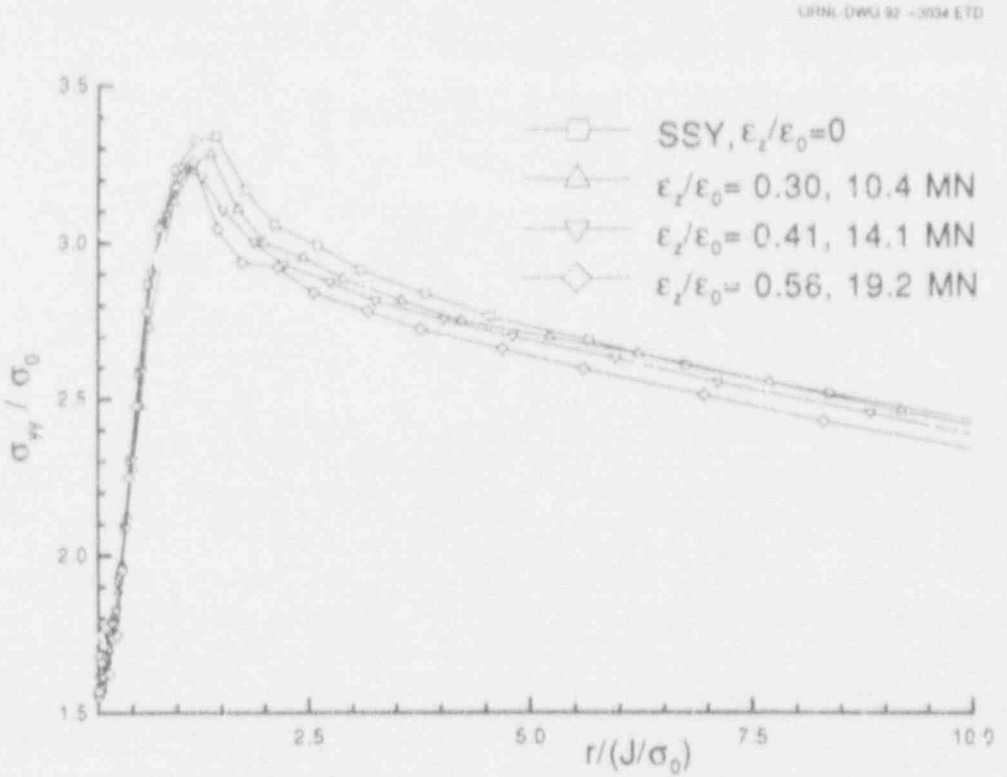

Figure G.9 Distribution of opening-mode stress directly ahead of blunting notch for SEN geometry with out-of-plane loading up to $\varepsilon_z/\varepsilon_0$ = 0.56 and in-plane loading up to 19.2 MN, along with reference SSY distribution. Parameter values indicated in this figure correspond to magnitudes of applied out-of-plane strain and in-plane distributed load, respectively

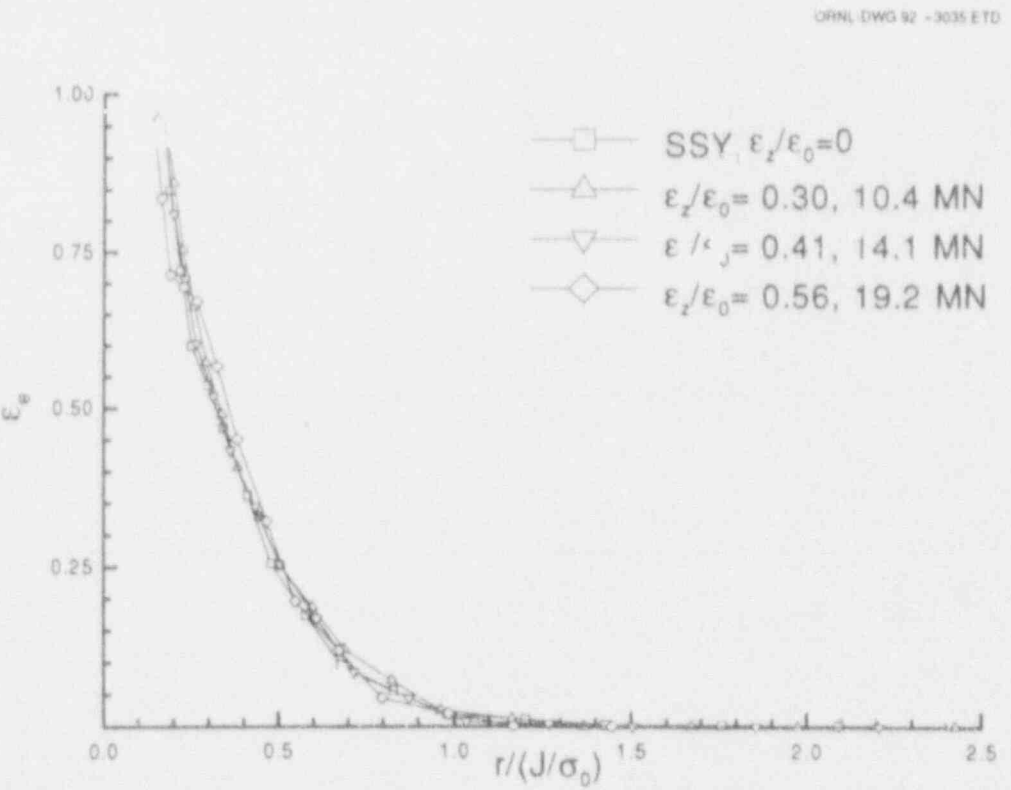

Figure G.10 Distribution of effective plastic strain directly ahead of blunting notch for SEN geometry with out-of-plane loading up to $\varepsilon_z/\varepsilon_0$ = 0.56 and in-plane loading up to 19.2 MN, along with reference SSY distribution

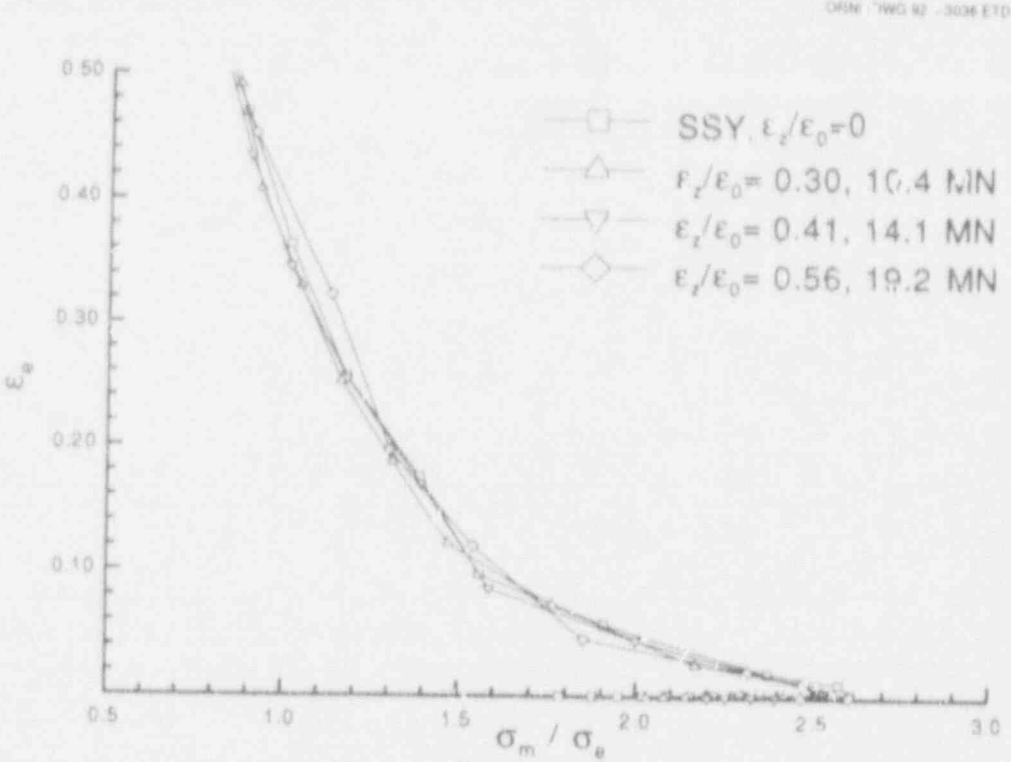

Figure G.11 Distribution of effective plastic strain as function of stress ratio σ_m/σ_e for SEN geometry with out-of-plane loading up to $\varepsilon_z/\varepsilon_0 = 0.56$ and in-plane loading up to 19.2 MN, along with reference SSY distribution

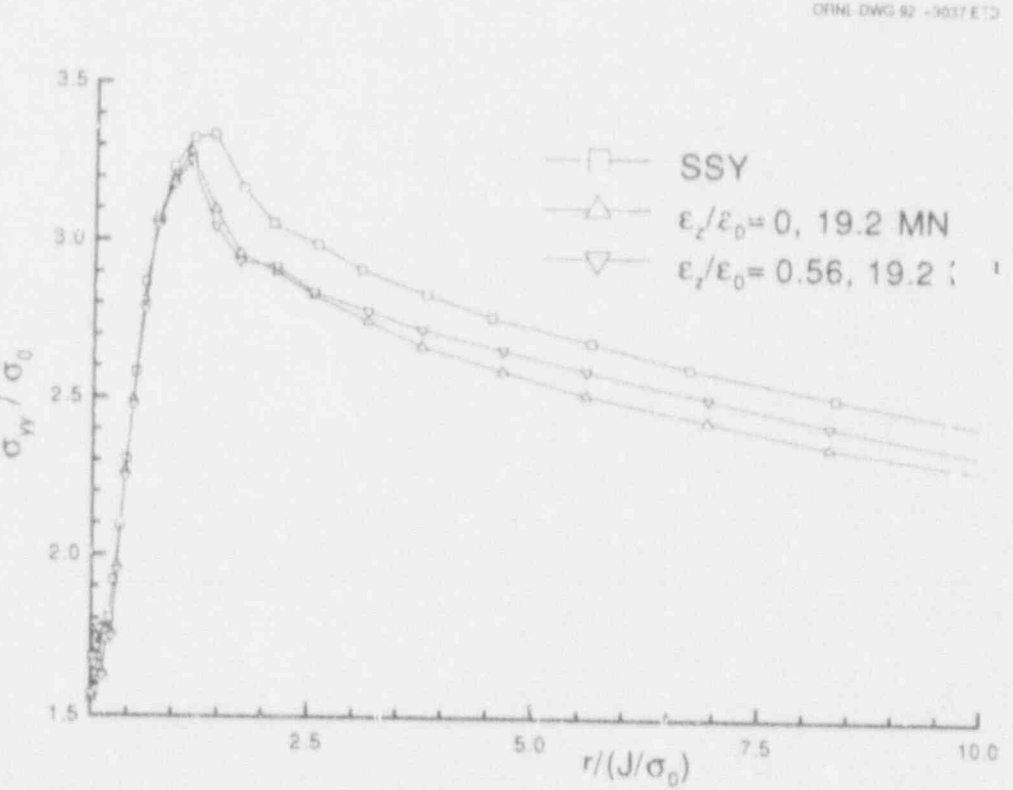

Figure G.12 Distribution of opening-mode stress directly ahead of blunting notch for SEN geometry at maximum in-plane loading of 19.2 MN. Out-of-plane loading condition is either plane strain ($\varepsilon_z/\varepsilon_0 = 0$) or at maximum out-of-plane loading ($\varepsilon_z/\varepsilon_0 = 0.56$). SSY distribution is also indicated

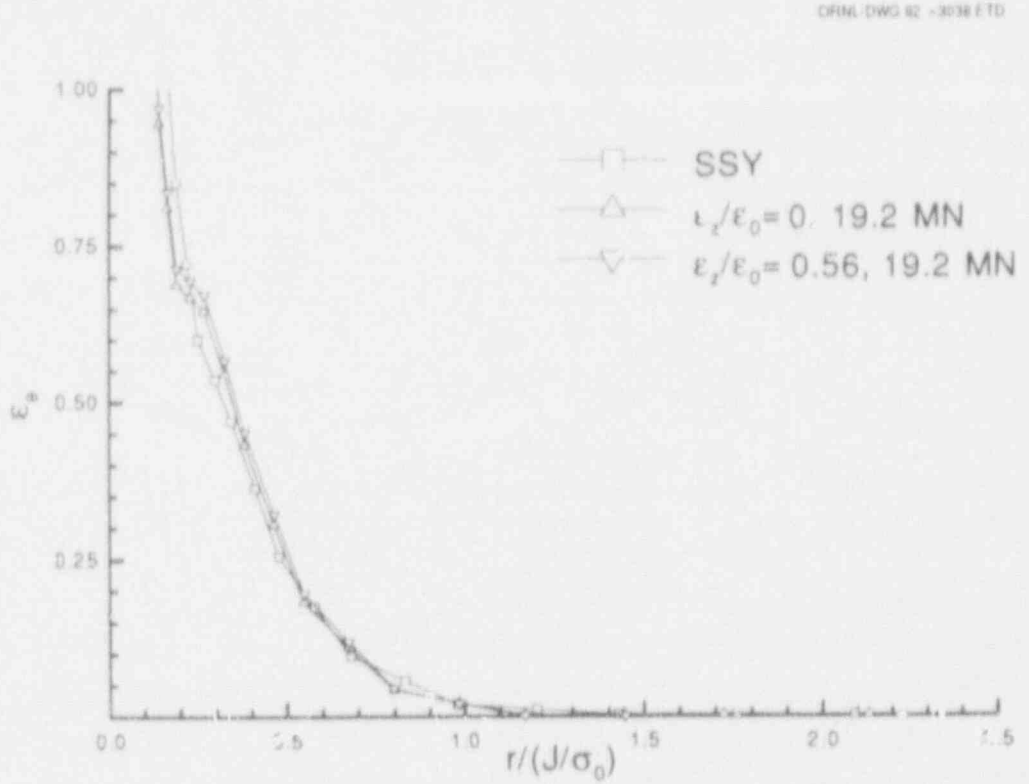

Figure G.13 Distribution of effective plastic strain directly ahead of blunting notch for SEN geometry at maximum in-plane loading of 19.2 MN. Out-of-plane loading condition is either plane strain ($\varepsilon_z/\varepsilon_0 = 0$) or at maximum out-of-plane loading ($\varepsilon_z/\varepsilon_0 = 0.56$). SSY distribution is also indicated

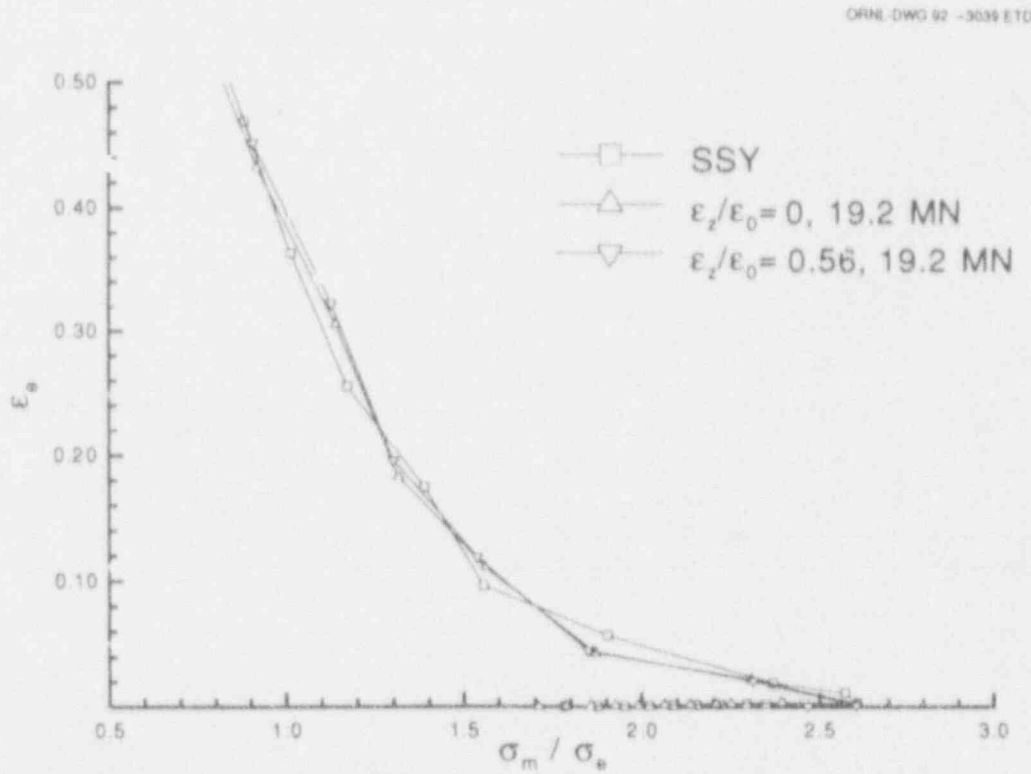

Figure G.14 Distribution of effective plastic strain as function of stress ratio σ_m/σ_e for SEN geometry at maximum in-plane loading of 19.2 MN. Out-of-plane loading condition is either plane strain ($\varepsilon_z/\varepsilon_0 = 0$) or at maximum out-of-plane loading ($\varepsilon_z/\varepsilon_0 = 0.56$). SSY distribution is also indicated

In Fig. G.15(*a*) and (*b*) the J-CTOD relations, based on the two definitions of CTOD discussed in Appendix C, are presented for the SEN geometry under plane strain and GPS conditions. The terminus of these curves corresponds to maximum in-plane and out-of-plane loading. The SSY relations are also indicated in these figures.

G.5 Analytical Predictions of Crack Initiation Under GPS Conditions

A simplified view is adopted here when the biaxial specimen, as characterized by the present material model, is expected to fail either in a cleavage or in a ductile manner in response to the loading conditions. In addition, a deterministic rather than statistical approach is adopted for simplicity. In the following discussion the Ritchie-Knott-Rice (RKR) model[3] is adopted for the prediction of cleavage fracture, and the McClintock-Hancock-MacKenzie (MHM) model[4,5] is adopted for the prediction of ductile fracture. As discussed in Appendix B, these two models are chosen because they have been applied to A 533 B material, in the lower-transition and upper-shelf regions, respectively, with some success under nonirradiated and irradiated conditions.

Within the context of the stated assumptions, it is possible to analytically predict whether the biaxial specimen would fail in either a cleavage or ductile manner. Accordingly, sample calculations to predict the failure mode are presented based on the GPS results. However, the prediction of failure mode should not be viewed as definitive, due to both the simplicity of the failure models adopted and the uncertainty regarding various critical material parameters, as will be evident shortly. Instead, the primary focus in the following sections is to determine the magnitude of toughness deviation from the reference plane strain, SSY condition that can be expected under GPS conditions, assuming alternately that the failure mechanism is cleavage or ductile in nature.

G.5.1 Sample Calculations Illustrating Analytical Prediction of Failure Mode

The GPS, finite-element results for the biaxial specimen presented in Figs. G.9–G.11 will now be taken as input to the two predictive fracture models. As will be evident shortly, however, the predicted failure mode for the biaxial specimen under GPS conditions applies equally well to the case assuming the biaxial specimen to be under plane strain conditions and to the case of a typical laboratory-size small specimen as characterized by the reference plane strain, SSY condition.

Attention will be focused first on the prediction of cleavage fracture. For simplicity, the present application of the RKR model for fracture prediction involves tracking the loading history of a material point located at a critical distance ahead of the blunting crack tip. Crack initiation is assumed to be a consequence of the opening-mode stress component associated with that material point reaching a critical stress level. Limited experimental data for HSST plate 02 (A 533 B) suggest that the critical cleavage stress is on the order of 1700 to 1800 MPa as discussed in Appendix B. The corresponding critical distance to cleavage initiation sites that best fit small-specimen data is taken to be on the order of 50 to 100 μm. A more sophisticated treatment of cleavage fracture in the spirit of the RKR model would involve treating both the critical distance parameter and the critical failure stress as statistical variables.

The variation of J-integral values with axial load up to a maximum value of 19.2 MN is presented in Fig. G.16 for both the plane strain and GPS conditions. As expected, the application of transverse strain does not influence the magnitude of J for a given value of the axial load. Variation of the opening-mode stress component with the axial load, where the magnitude of the axial load is expressed via J-integral values, is presented in Fig. G.17 for the case of GPS conditions. In Fig. G.17 the variations are presented at two locations ahead of the crack tip corresponding to r = 45 and 143 μm. These two locations span the range of critical distances to cleavage-initiation sites discussed previously. Also indicated in this figure are the corresponding variation for the biaxial specimen, assuming plane strain conditions, and the variation corresponding to the reference plane strain SSY condition.

Attention will be focused on the GPS variations for the moment. From Fig. G.17, it is observed that an assumed critical cleavage stress of 1744 MPa ($\sigma_c/\sigma_0 = 2.8$) is exceeded at location r = 45 μm for loading exceeding J = 8 kN/m. This same level of opening-mode stress is reached at location r = 143 μm at maximum in-plane and out-of-plane loading corresponding to J = 27.9 kN/m. For an assumed critical cleavage stress of magnitude <1744 MPa, the critical cleavage stress is maintained over a distance >143 μm. Therefore, within the range of critical distances associated with small-specimen toughness data the critical condition for cleavage fracture is satisfied within the anticipated capacity of the proposed biaxial test frame. Consequently, cleavage fracture is a *possible* failure mode for the flaw embedded in the biaxial specimen, as modeled by the SEN geometry, at or prior to the attainment of maximum in-plane and out-of-plane loads.

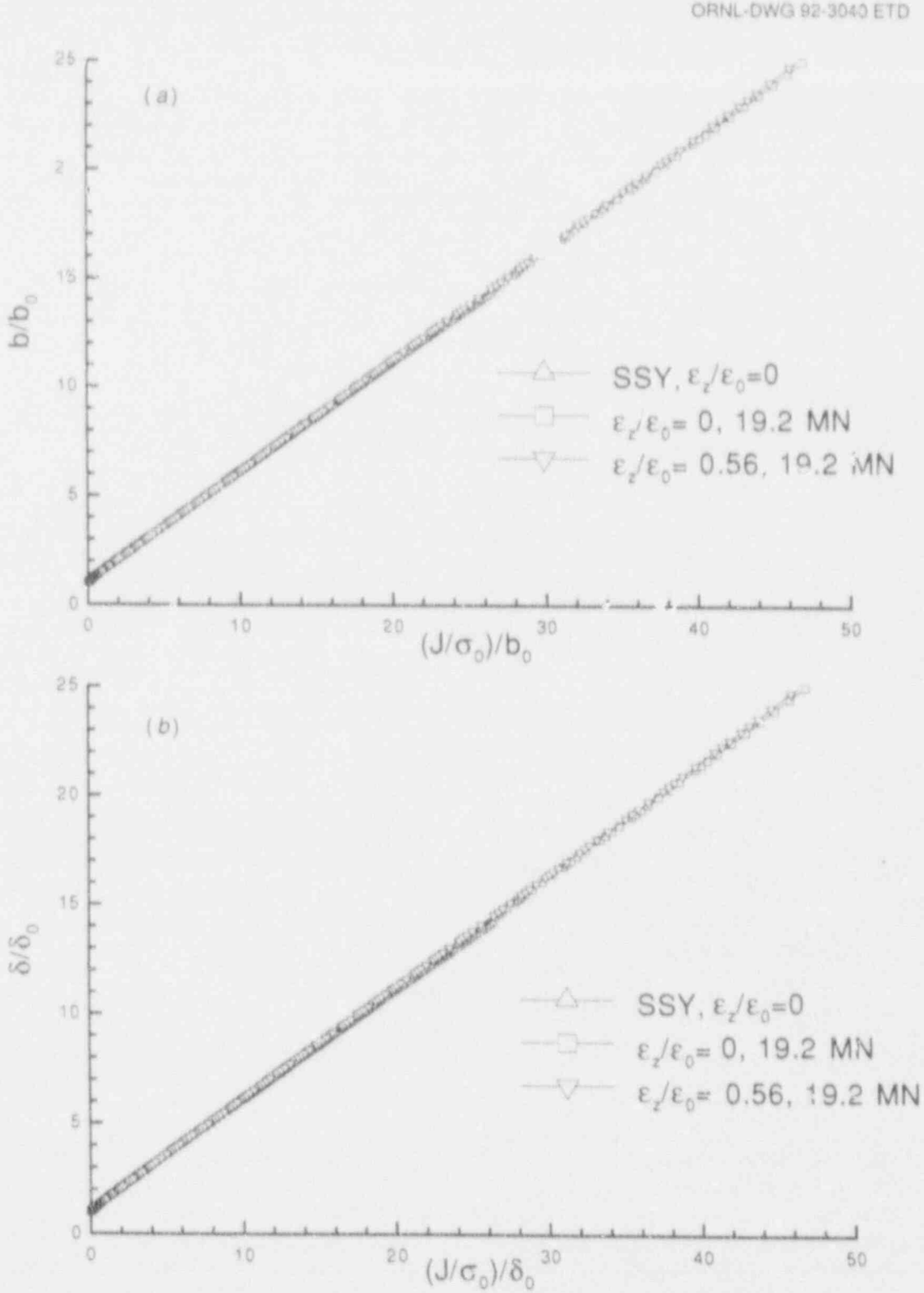

Figure G.15 (*a*) J-CTOD relation for SEN geometry with out-of-plane loading up to $\varepsilon_z/\varepsilon_0 = 0.56$ and in-plane loading up to 19.2 MN, along with reference SSY relation. Definition of CTOD is based on Mode I displacement at point B indicated in Fig. C.2. These results suggest that J-CTOD relation is not very sensitive to range of positive out-of-plane loading considered. (*b*) J-CTOD relations for SEN geometry with out-of-plane loading up to $\varepsilon_z/\varepsilon_0 = 0.56$ and in-plane loading up to 19.2 MN, along with reference SSY relation. Definition of CTOD is based on 45° intercept definition indicated in Fig. C.2

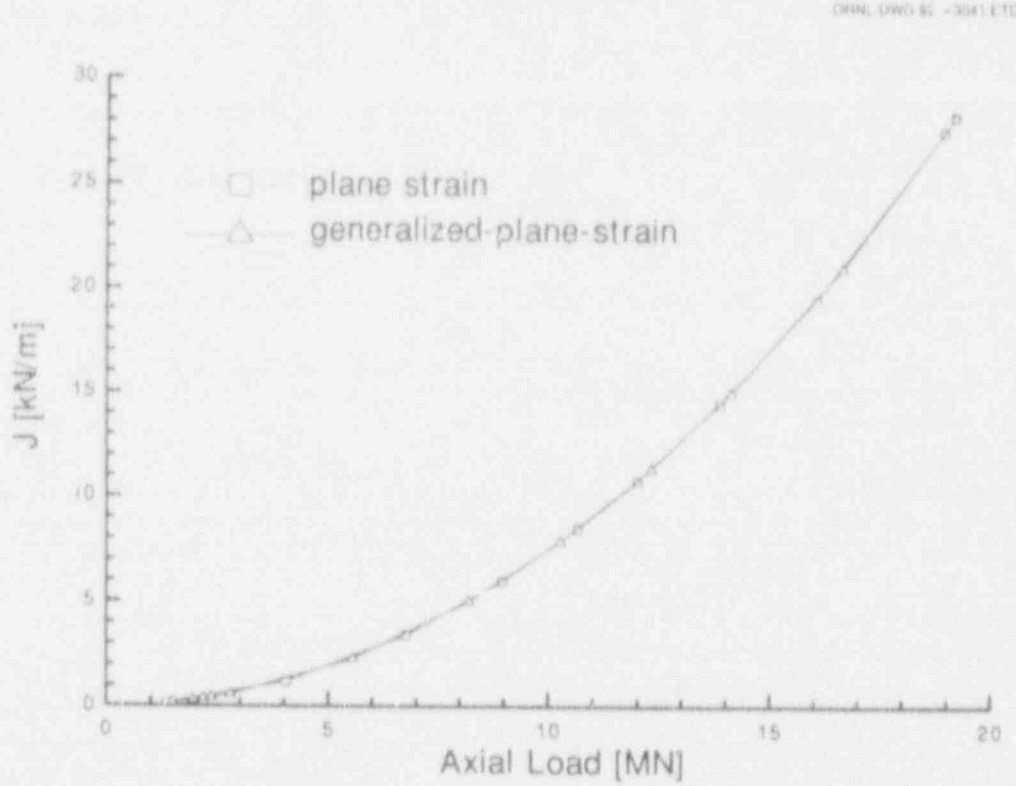

Figure G.16 Variation of J-integral values with axial load up to maximum value of 19.2 MN for biaxial specimen. Variation is indicated for both plane strain and GPS conditions

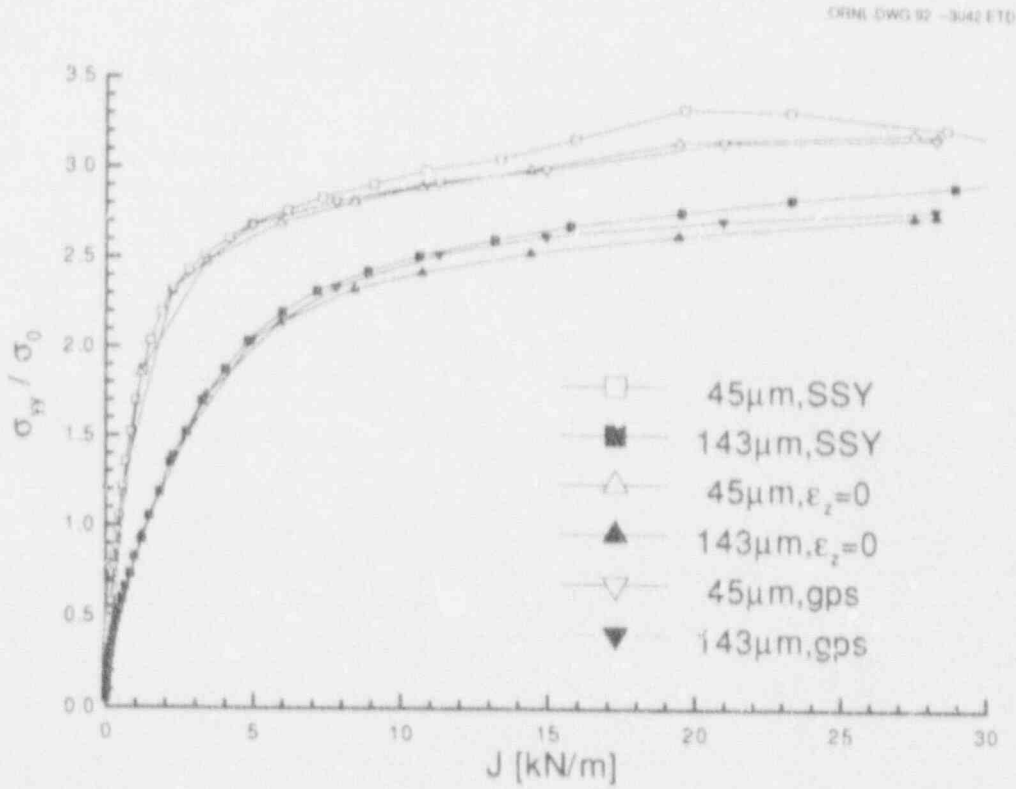

Figure G.17 Variation of opening-mode stress component with axial load expressed via J-integral values for both plane strain and GPS biaxial specimen at two locations ahead of the crack tip r = 45 μm and 143 μm. Variation corresponding to the reference SSY condition is also indicated

Prediction of ductile failure is based on the ductile failure data presented in Fig. C.19 in Appendix C. From Ref. 6, the minimum size of a region necessary to accommodate ductile fracture or plastic-flow localization, as determined from best fit to small-specimen toughness data, is on the order of 300 to 350 μm. It is observed that the MHM failure criterion (see Fig. C.19) is exceeded by the results indicated in Fig. G.11 for magnitude of the effective plastic strain $\varepsilon_e \geq 25\%$. From Fig. G.10 it is observed that, even under maximum in-plane and out-of-plane loading, this magnitude of ε_e is exceeded only over a distance $r \leq 0.5\ J/\sigma_0$. A distance of $0.5\ J/\sigma_0$ corresponds approximately to 22 μm based on a calculated J-integral value of 27.9 kN/m at maximum load. Because the calculated distance of 22 μm is much smaller than the reported minimum size necessary to accommodate ductile failure, ductile failure is not expected to be the failure mode upon reaching the maximum in-plane and out-of-plane loads.

Consequently, cleavage crack initiation is anticipated for the proposed biaxial specimen configuration. However, it is emphasized that this prediction is dependent on the stress-strain curve of the biaxial specimen material, along with the validity of the various critical material parameters assumed in this prediction.

G.5.2 Analytical Prediction of Fracture Toughness Assuming Cleavage Failure Mode

Estimates of the potential toughness deviation relative to a reference plane strain, SSY condition for the biaxial specimen follows the approach illustrated previously. From Fig. G.17, it is observed that the magnitude of the opening-mode stress component for the SEN geometry, assuming either plane strain or GPS conditions, is consistently below that associated with the SSY condition at either value of the critical distance parameter $r = 45$ or 143 μm. In Table G.1 estimates of toughness deviation are presented for a range of assumed cleavage fracture stress. These toughness estimates are plotted in Fig. G.18.

Results in Table G.1 and Fig. G.18 indicate that the biaxial specimen, as modeled by the SEN geometry, is expected to exhibit a small amount of toughness enhancement relative to the small-specimen value. With regard to transverse straining, minimal toughness deviation due to positive out-of-plane straining is expected for the assumed set of analysis conditions. Therefore, it is anticipated that the proposed biaxial test specimen would fail at essentially the same level of axial load under uniaxial or biaxial loading condition.

G.5.3 T-Stress Effects

Results from Figs. G.12–G.14, along with the toughness-deviation predictions presented in Fig. G.18, suggest that the fracture response of the proposed biaxial specimen can be readily understood within the context of the two-parameter approaches discussed in Appendixes A–C. That is, the gradual deviation of the near-tip fields of the proposed biaxial specimen from the SSY distributions with increasing in-plane and out-of-plane loading can, to a good approximation, be correlated with increasing negative T-stress values. In Figs. C.11–C.17 in Appendix C, the MBL distributions for the biaxial specimen material are presented. The MBL analyses are performed for the indicated minimum values of T-stress and, where appropriate, positive transverse strain. The similarity between the MBL and the biaxial full-field distributions are noted.

Table G.1 Estimates of toughness deviation from a reference plane strain, SSY ($\varepsilon_z = T = 0$) value, based on the RKR model and a range of assumed cleavage fracture stress. The critical material distance parameter is taken to be 45 and 143 μm. These estimates are obtained based on results from Fig. G.18 for the SEN geometry with out-of-plane loading up to $\varepsilon_z/\varepsilon_0 = 0.56$ and in-plane loading up to 19.2 MN. Magnitude of the yield stress $\sigma_0 = 623$ MPa

	$r_c = 45$ μm							$r_c = 143$ μm						
	J at r_c			J_{PS}	K_{PS}	J_{GPS}	K_{GPS}	J at r_c			J_{PS}	K_{PS}	J_{GPS}	K_{GPS}
σ_c/σ_0	SSY	PS	GPS	J_{SSY}	K_{SSY}	J_{SSY}	K_{SSY}	SSY	PS	GPS	J_{SSY}	K_{SSY}	J_{SSY}	K_{SSY}
2.3	2.2	2.2	2.2	1	1	1	1	7.0	8	7.4	1.14	1.07	1.06	1.03
2.4	2.6	2.8	3.1	1.08	1.04	1.19	1.09	8.4	10.2	9.0	1.21	1.10	1.07	1.04
2.5	3.2	3.6	3.6	1.13	1.06	1.13	1.06	10.4	13.3	10.8	1.28	1.13	1.04	1.02
2.6	4.1	4.8	4.4	1.17	1.08	1.07	1.03	13.0	17.8	14.0	1.37	1.17	1.08	1.04
2.7	5.2	6.1	5.4	1.17	1.08	1.04	1.02	16.5	24.6	19.8	1.49	1.22	1.20	1.10
2.8	6.8	8.2	7.5	1.21	1.10	1.10	1.05							
2.9	8.8	10.7	10.5	1.22	1.10	1.19	1.09							

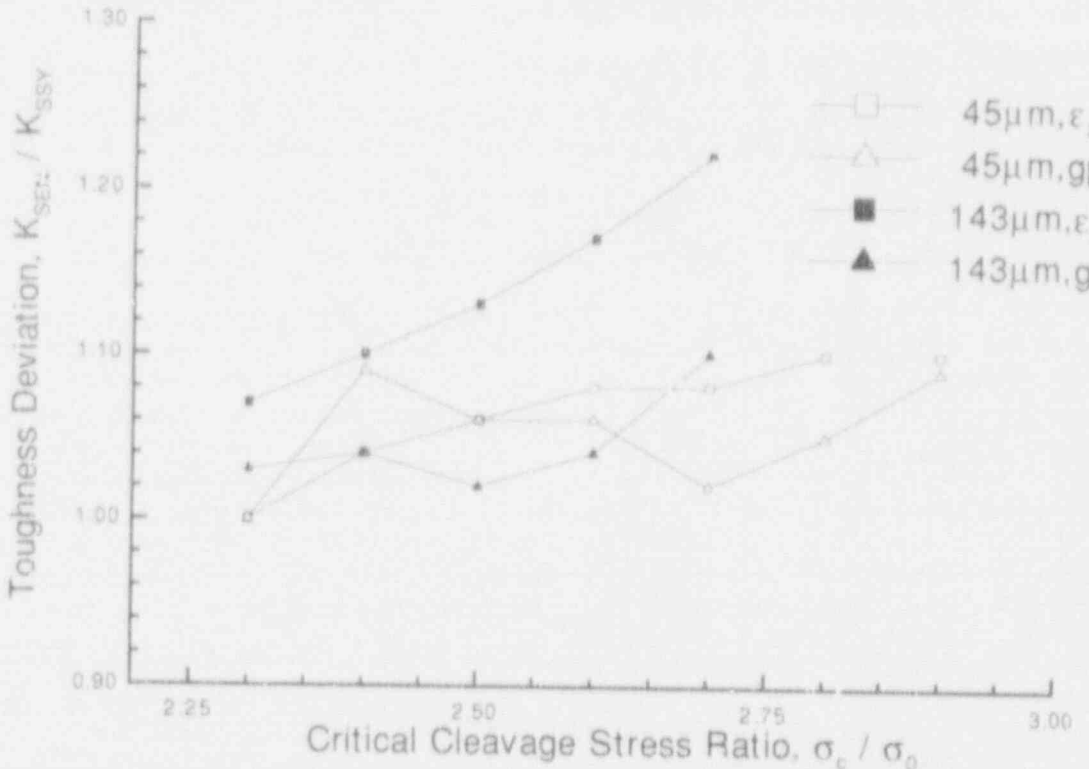

Figure G.18 **Estimates of toughness deviation, from reference plane strain K-dominant (ε_z = T = 0) value, based on RKR model and range of assumed cleavage fracture stress. Critical material distance parameter is taken alternatively to be 45 μm and 143 μm. These estimates are obtained based on results from Fig. G.17 for SEN geometry with out-of-plane loading up to $\varepsilon_z/\varepsilon_0$ = 0.56 and in-plane loading up to 19.2 MN. These results suggest that the biaxial specimen, as modeled by the SEN geometry, is expected to exhibit a small amount of toughness enhancement relative to small-specimen value. With regard to transverse straining, minimal toughness deviation due to positive out-of-plane straining is expected for assumed set of analysis conditions**

G.6 Comparison of Analytical Predictions with Available Experimental Data

Comparisons of analytical predictions of crack initiation under GPS conditions with limited large-scale biaxial experimental data have been presented in Appendix C. As discussed in Appendix C, a perplexing aspect of The Welding Institute (TWI) results[7,8] is the apparent lack of correlation between the nominal remote stress and CTOD at failure. Large variations in CTOD at failure, as a consequence of uniaxial and biaxial loading, are reported in the TWI studies even though the nominal remote stress state at failure is nearly constant.

The J-CTOD relations for the present biaxial geometry up to the maximum axial load are presented in Fig. G.15(*a*) and (*b*) for both plane strain and GPS conditions. The two definitions of CTOD employed in these figures are discussed in Appendix C. The J-CTOD relations under SSY conditions are also included in these figures. These results suggest that the J-CTOD relation is not very sensitive to the range of positive out-of-plane loading considered in this study and do not reflect the sensitivity reported in the TWI studies.

G.7 Limitations on Applicability of Fracture Prediction Models

Analytical predictions of crack initiation, such as those presented in Appendix C and in this appendix, involve interpretation of detailed results of the near-crack-tip fields in the context of a postulated fracture model. The accuracy of the near-crack-tip results, assuming the applicability of continuum theory, appears more than adequate. As discussed in Appendix B, utility of these continuum results requires that the size of the annular region characterized by the near-tip parameters such as K, J, T, or Q be sufficiently large, in comparison to relevant microstructural parameters

such as the grain size, to ensure that a continuum, homogeneous description using these parameters is physically meaningful.

However, the fracture models considered in this report are phenomenological in nature, and empirically determined material parameters are needed to render these models complete. The uncertainty concerning prediction of crack initiation is, in large measure, related to the uncertainty concerning the general validity of the proposed fracture model. In cases where the fracture model is reasonably sound, the uncertainty is related to values of the critical material parameters associated with the fracture model.

G.7.1 Limitations on Cleavage Fracture Prediction

The validity of the WKR approach for the prediction of cleavage fracture of RPV-grade materials has received limited acceptance based on both theoretical considerations and supporting experimental data. As demonstrated in Appendixes B and C and in this appendix, the underlying uncertainty associated with a quantitative prediction of cleavage toughness using the RKR model resides with (1) the magnitude of the critical cleavage stress and (2) the range of minimum distances over which this critical cleavage stress needs to be maintained.

G.7.2 Limitations on Ductile Fracture Predictions

The general validity of the MHM model for the prediction of ductile failure of RPV-grade materials has not been similarly established, due to the fewer number of investigations focusing on this model. Extra caution must thus be applied when invoking this model, guided in part by the following observation. The MHM model was developed to describe material failure conditions in which plastic straining is an integral part of the failure process. Therefore, expression of the MHM failure criterion in terms of effective plastic strain is self-explanatory. At the same time, the associated stress measure, namely the hydrostatic to effective stress ratio, is chosen based on analytical investigations that indicate that the growth rate of voids is sensitive to this stress measure.[4,9]

Consequently, interpretation of near-crack-tip results based on the MHM model is, at most, meaningful only within the numerically calculated plastic zone surrounding the crack tip. This has been the approach adopted in this work. In this study, the MHM ductile failure criterion has been determined to be exceeded at a near-tip location that experiences a level of effective plastic strain in excess of 25%. Thus, the corresponding critical material location is located well within the plastic zone and inside the region of finite strain.

G.7.3 Examples of Questionable Interpretations

Application of a phenomenological failure model without due consideration of its underlying premises can, at times, lead to paradoxical or erroneous observations. Extra caution must be applied when invoking a given model in a regime for which confirmatory data are not available. Two related examples will now be given to emphasize this point. Both of these examples involve a questionable interpretation of the distribution of hydrostatic to effective stress ratio ahead of the crack tip for the purpose of ductile failure prediction. The fracture problem considered is the SEN geometry in this appendix at maximum in-plane loading. The stress ratio distribution is indicated in Fig. G.19

In the first example, the hypothesis that ductile failure can be somewhat related to the maximum value of the hydrostatic to effective stress ratio distribution is examined. From Fig. G.19 it is seen that the maximum value of this ratio is substantially higher for the positive out-of-plane strain SEN geometry than either the corresponding plane strain or SSY value. In Fig. G.20 the variation of this stress ratio for only the GPS SEN geometry, as a function of the transverse strain, is indicated. It is seen that the maximum value of this stress ratio associated with positive out-of-plane strain *increases* with *decreasing* value of the out-of-plane strain and in-plane loading (recall that the in-plane and out-of-plane loadings are applied concurrently). A discontinuity is implied by these results with the paradox, if one adopts the proposed hypothesis, that toughness deviation is highest for infinitesimal loading.

An explanation for the observed paradox is as follows. From the definitions of effective and hydrostatic stress, and denoting Poisson's ratio as ν, this stress ratio under linear-elastic fracture mechanics (LEFM) K-dominant in-plane conditions takes the form

$$\frac{\sigma_m}{\sigma_e} = \frac{\dfrac{2(1+\nu)}{\sqrt{2\pi}} + \left(\dfrac{\varepsilon_z}{\varepsilon_o}\right)\sqrt{\varepsilon_o}\sqrt{\dfrac{r}{J/\sigma_o}}}{\sqrt{\left[\dfrac{1-2\nu}{\sqrt{2\pi}} - \left(\dfrac{\varepsilon_z}{\varepsilon_o}\right)\sqrt{\varepsilon_o}\sqrt{\dfrac{r}{J/\sigma_o}}\right]}} \quad . \qquad (G.1)$$

From Eq. (G.1) it is observed that this ratio becomes unbounded at some distance ahead of the crack tip for *any* positive values of the out-of-plane strain. However, this singularity is not physically meaningful. This singularity results from extending the definition of effective stress,

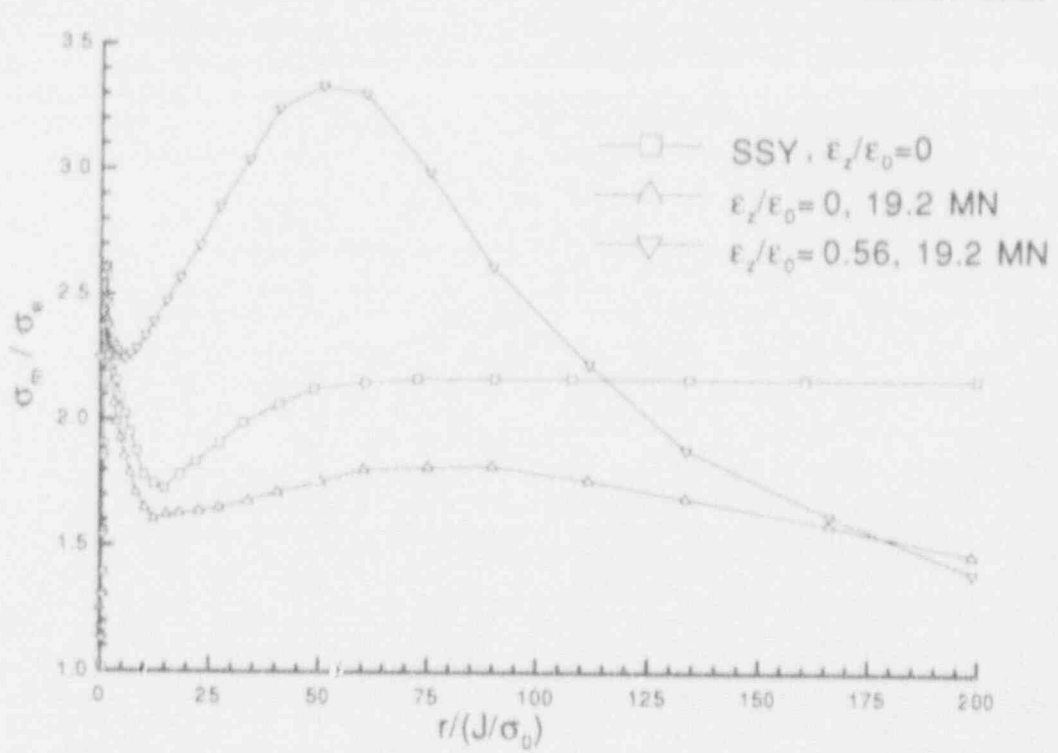

Figure G.19 Distribution of stress ratio σ_m/σ_e for SEN geometry at maximum in-plane loading of 19.2 MN. Out-of-plane loading condition is either plane strain ($\varepsilon_z/\varepsilon_0 = 0$) or at maximum out-of-plane loading $\varepsilon_z/\varepsilon_0 = 0.56$. SSY distribution is also indicated

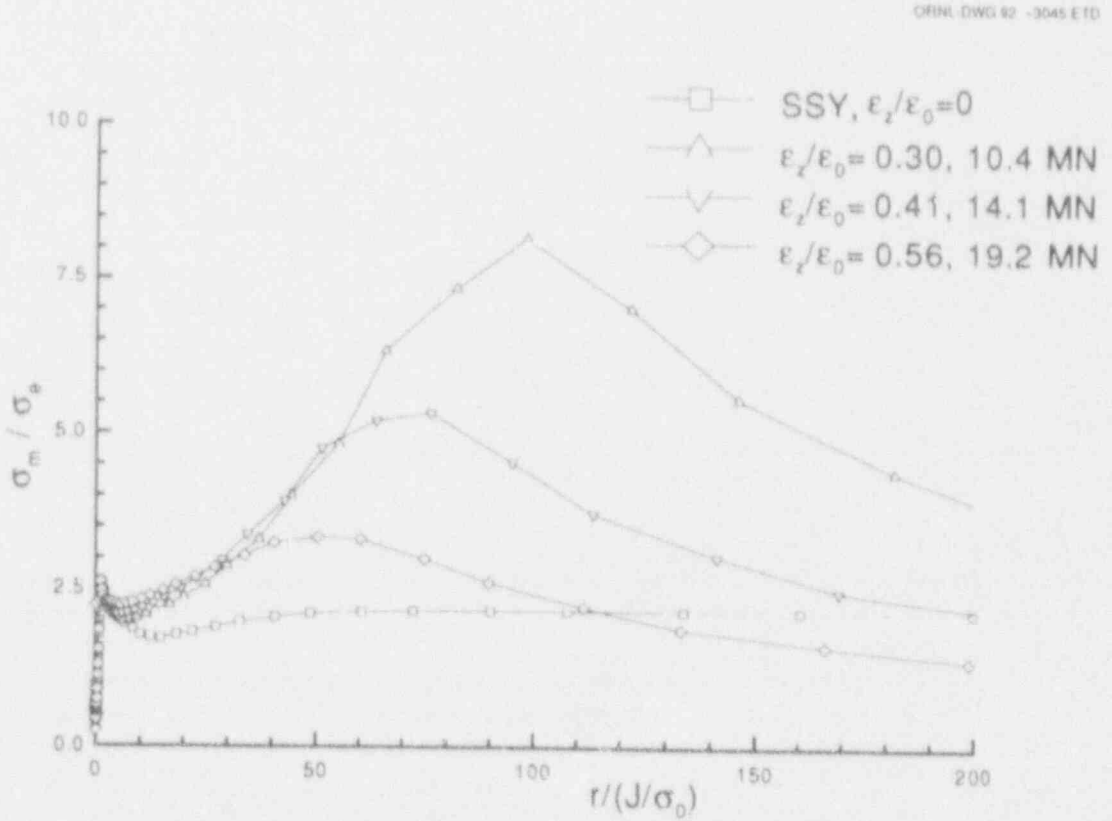

Figure G.20 Distribution of the stress ratio σ_m/σ_e for SEN geometry with out-of-plane loading up to $\varepsilon_z/\varepsilon_0 = 0.56$ and in-plane loading up to 19.2 MN, along with reference SSY distribution

originally formulated as an invariant stress measure in *plasticity* theory, into an *elastic* stress analysis. The singular nature of Eq. (G.1) is demonstrated in Fig. G.21 for parameter values $\varepsilon_o = 1/311$, $\nu = 0.3$, and three values of positive out-of-plane strain. In the case of the elastic-plastic distributions indicated in Figs. G.19 and G.20, evidently the onset of plasticity results in a maximum in the distributions outside of the plastic zone. Use of the MHM model in previous sections involves plastic strains on the order of 25% at a location well within the finite-strain region. Within the finite-strain region, the distribution of the stress ratio is evidently not affected by the mathematical singularity outside of the plastic zone.

In the second example, an alternate hypothesis that ductile failure can be related somewhat to the distribution of the stress ratio indicated in Fig. G.19 in the neighborhood of the elastic-plastic boundary ahead of the crack tip is examined. The magnitude of this stress ratio for the plane strain SEN problem is ~1.6 at the elastic-plastic boundary, which is located at a distance of ~12 J/σ_o. At the same location the stress ratio for the case of positive out-of-plane strain is ~ 2.4. On the other hand, the magnitude of this stress ratio at the elastic-plastic boundary for the positive out-of-plane strain SEN problem, which is located at a distance of ~2.5 J/σ_o, is ~2.3. At this location the stress ratio for the case of plane strain is ~2.1.

At this point it is unclear how, in accordance with the stated hypothesis, one would estimate the toughness deviation due to positive out-of-plane strain in a manner consistent with what is known about ductile failure. It may be tempting to take the ratio of the stress measure at the elastic-plastic boundary under plane strain and GPS conditions as indicative of toughness deviation. However, adoption of this viewpoint does not readily offer a method to quantify the magnitude of the toughness deviation. More importantly, the distribution of stress ratio for the GPS SEN problem, in the neighborhood of the elastic-plastic boundary, appears to be strongly influenced by the singular nature of this distribution in the elastic region. The apparent paradox discussed in the first example strongly discourages use of this stress ratio in the vicinity of the elastic-plastic boundary as a failure criterion.

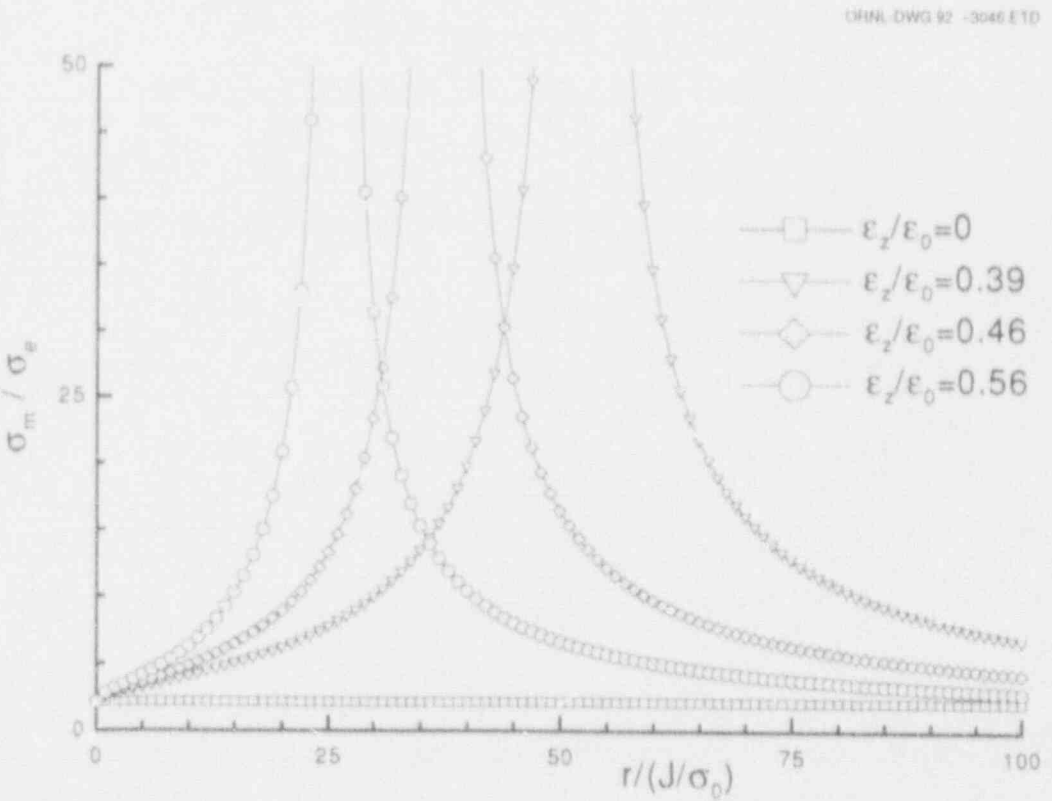

Figure G.21 Distribution of stress ratio σ_m/σ_e under K-dominant in-plane conditions with out-of-plane loading up to $\varepsilon_z/\varepsilon_o = 0.56$, along with reference SSY distribution, based on LEFM assumptions. Singular nature of distributions under positive out-of-plane loading results from extending definition of effective stress, originally formulated as an invariant stress measure in *plasticity* theory, into an *elastic* stress analysis

G.8 References

1. ABAQUS *Theory Manual*, version 4-8, Hibbitt, Karlson and Sorensen, Inc., Providence, R.I., 1989.

2. H. Tada, P. C. Paris, and G. R. Irwin, *The Stress Analysis of Cracks Handbook*, Del Research Corporation, Hellertown, Pa., 1973.*

3. R. O. Ritchie, J. F. Knott, and J. R. Rice, "On the Relationship Between Critical Tensile Stress and Fracture Toughness in Mild Steel," *J. Mech. Phys. Solids* 21, 395–410 (1973).*

4. F. A. McClintock, "A Criterion for Ductile Fracture by the Growth of Holes," *J. Appl. Mech.* 35, 363–371 (1968).*

5. J. W. Hancock and A. C. MacKenzie, "On the Mechanisms of Ductile Failure in High-Strength Steels Subjected to Multi-Axial Stress-States," *J. Mech. Phys. Solids* 24, 147–169 (1976).*

6. R. O. Ritchie, W. L. Server, and R. A. Wullaert, "Critical Fracture Stress and Fracture Strain Models for the Prediction of Lower and Upper Shelf Toughness in Nuclear Pressure Vessel Steels," *Met. Trans. A*, 10A, 1557–1570 (1979).*

7. S. J. Garwood, T. G. Davey, and S. L. Creswell, "Behavior of A533B under Biaxial Loading at +70°C," *Int. J. Pres. Ves. and Piping* 36, 199–224 (1989).*

8. S. J. Garwood, "The Significance of Biaxial Loading on the Fracture Performance of a Pressure Vessel Steel," *ASME Pressure Vessel and Piping Division Conference*, PVP-Vol 213/MPC-Vol 32, 113–123, 1991.*

9. J. R. Rice and D. M. Tracey, "On the Ductile Enlargement of Voids in Triaxial Stress Fields," *J. Mech. Phys. Solids* 17, 201–217 (1969).*

* Available in public technical libraries.

NUREG/CR-6008
ORNL/TM-12131
Dist.Category RF

Internal Distribution

1. D. J. Alexander
2–4. B. R. Bass
5. J. W. Bryson
6. E. W. Carver
7–8. R. D. Cheverton
9. J. M. Corum
10. W. R. Corwin
11. J. S. Crowell
12. T. L. Dickson
13. F. M. Haggag
14. W. F. Jackson
15. J. E. Jones Jr.
16. S. K. Iskander
17–19. J. Keeney-Walker
20. W. J. McAfee
21. D. E. McCabe
22. J. G. Merkle
23. R. K. Nanstad
24. D. J. Naus
25–29. W. E. Pennell
30. C. B. Oland
31. C. E. Pugh
32. G. C. Robinson
33–35. D. K. M. Shum
36. R. L. Swain
37. T. J. Theiss
38. G. E. Whitesides
39. E. W. Whitfield
40. ORNL Patent Section
41. Central Research Library
42. Document Reference Section
43–44. Laboratory Records
45. Laboratory Records (RC)

External Distribution

46. L. C. Shao, Director, Division of Engineering, U.S. Nuclear Regulatory Commission, Washington, DC 20555
47. C. Z. Serpan, Jr., Division of Engineering, U.S. Nuclear Regulatory Commission, Washington, DC 20555
48. E. M. Hackett, Division of Engineering, U.S. Nuclear Regulatory Commission, Washington, DC 20555
49. A. L. Hiser, Division of Engineering, U.S. Nuclear Regulatory Commission, Washington, DC 20555
50–51. S. N. M. Malik, Division of Engineering, U.S. Nuclear Regulatory Commission, Washington, DC 20555
52. M. E. Mayfield, Division of Engineering, U.S. Nuclear Regulatory Commission, Washington, DC 20555
53. A. Taboada, Division of Engineering, U.S. Nuclear Regulatory Commission, Washington, DC 20555
54. W. L. Fourney, Department of Mechanical Engineering, University of Maryland, College Park, MD 20742
55. J. D. Landes, The University of Tennessee, Knoxville, TN 37996-2030
56. S. T. Rolfe, The University of Kansas, Lawrence, KS 66045-2235
57. A. R. Rosenfield, Battelle Columbus Division, Columbus, OH 43201
58. C. W. Schwartz, Department of Civil Engineering, University of Maryland, College Park, MD 20742
59. E. T. Wessel, 312 Wolverine, Haines City, FL 33844
60. Office of Assistant Manager for Energy Research and Development, DOE–OR, Oak Ridge, TN 37831
61–62. Office of Scientific and Technical Information, P. O. Box 62, Oak Ridge, TN 37831

NRC FORM 335 (2.89) NRCM 1102, 3201, 3202

U.S. NUCLEAR REGULATORY COMMISSION

BIBLIOGRAPHIC DATA SHEET

(See instructions on the reverse)

1. REPORT NUMBER (Assigned by NRC, Add Vol., Supp., Rev., and Addendum Numbers, if any.)

NUREG/CR-6008
ORNL/TM-12131

2. TITLE AND SUBTITLE

Constraint Effects on Fracture Toughness for Circumferentially Oriented Cracks in Reactor Pressure Vessels

3. DATE REPORT PUBLISHED

MONTH: August YEAR: 1992

4. FIN OR GRANT NUMBER

B0119

5. AUTHOR(S)

B. R. Bass, D. K. M. Shum, J. Keeney-Walker

6. TYPE OF REPORT

Technical

7. PERIOD COVERED (Inclusive Dates)

8. PERFORMING ORGANIZATION – NAME AND ADDRESS (If NRC, provide Division, Office or Region, U.S. Nuclear Regulatory Commission, and mailing address; if contractor, provide name and mailing address.)

Oak Ridge National Laboratory
Oak Ridge, TN 37831-6285

9. SPONSORING ORGANIZATION – NAME AND ADDRESS (If NRC, type "Same as above"; if contractor, provide NRC Division, Office or Region, U.S. Nuclear Regulatory Commission, and mailing address.)

Division of Engineering
Office of Nuclear Regulatory Commission
U. S. Nuclear Regulatory Commission
Washington, DC 20555

10. SUPPLEMENTARY NOTES

11. ABSTRACT

Pressurized-thermal-shock (PTS) loading produces biaxial stress fields in a reactor pressure vessel (RPV) wall with one of the principal stresses aligned parallel to postulated surface cracks in either longitudinal or circumferential welds. The limited quantity of existing biaxial test data suggests a significant decrease of fracture toughness under out-of-plane (i.e., parallel to the crack front) biaxial loading conditions when compared with toughness values obtained under uniaxial conditions. Any increase in crack-tip constraint resulting from these out-of-plane biaxial stresses would act in opposition to the in-plane constraint relaxation that has been previously demonstrated for shallow cracks. Consequently, understanding of both in-plane and out-of-plane crack-tip constraint effects is necessary to a refined analysis of fracture initiation from shallow cracks under PTS transient loading. This report is the second in a series investigating the potential impact of far-field out-of-plane stresses and strains on fracture initiation toughness. Selected fracture prediction models, previously validated for small-scale fracture specimens under nearly plane strain conditions, were applied to additional large-scale data with the objective of validating models in the plane stress-to-plane strain domain before applying them to positive out-of-plane strain conditions. The general finding was that applications of the models resulted in predictions of fracture behavior that conflicted with existing experimental data considered relevant to the problem. Because of the conflicting results, it is apparent that testing of RPV steels is required (1) to determine the magnitude of out-of-plane biaxial loading effects on fracture toughness and (2) to provide a basis for development of predictive models. This course of action is necessary to support a refined treatment of in-plane and out-of-plane constraint effects in PTS analysis. Proposed in this report are criteria for a biaxial specimen that would form the basis of a testing program designed to provide data to explain differences between theoretical predictions and measured material behavior. Results of design studies on the biaxial specimen will be presented in a future report from the Heavy-Section Steel Technology Program.

12. KEY WORDS/DESCRIPTORS (List words or phrases that will assist researchers in locating the report.)

pressurized-thermal-shock (PTS)
biaxial stress
reactor pressure vessel (RPV)
shallow cracks
crack-tip
fracture toughness
out-of-plane
in-plane
prediction models
welds

13. AVAILABILITY STATEMENT

Unlimited

14. SECURITY CLASSIFICATION

(This Page) Unclassified

(This Report) Unclassified

15. NUMBER OF PAGES

16. PRICE

THIS DOCUMENT WAS PRINTED USING RECYCLED PAPER

UNITED STATES
NUCLEAR REGULATORY COMMISSION
WASHINGTON, D.C. 20555-0001

OFFICIAL BUSINESS
PENALTY FOR PRIVATE USE, $300

SPECIAL FOURTH-CLASS RATE
POSTAGE AND FEES PAID
USNRC
PERMIT NO. G-67

120555139531 1 1AN1RF
US NRC-OADM
DIV FOIA & PUBLICATIONS SVCS
TPS-PDR-SUPER
P-211
WASHINGTON DC 20555